

DESIGN AND FABRICATION OF NOVEL REACTIVE HYDROGELS  
FOR DELIVERY OF THERAPEUTIC AGENTS AND  
BIOMOLECULAR IMMOBILIZATION

by

Laura Chambre

B.Sc. Chemical Management, Florida Institute of Technology & SKEMA, 2009

M.Sc. Chemistry, Florida Institute of Technology, 2012

Submitted to the Institute for Graduate Studies in  
Science and Engineering in partial fulfillment of  
the requirement for the degree of  
Doctor of Philosophy

Graduate Program in Chemistry

Boğaziçi University

## ACKNOWLEDGEMENTS

I would like to express my sincere gratitude to my thesis supervisor Prof. Amitav Sanyal. I am truly thankful for his motivation, enthusiasm, and endless support during my graduate studies. I appreciate his patience, mentoring and academic guidance which led me to improve my scientific skills and enabled me to achieve my current level. I am also very grateful to him for helping me pursue collaborations with other research groups for my PhD thesis.

I would like to extend my thanks to my thesis jury, Prof. Rana Sanyal, Assoc. Prof. Fabienne Dumoulin, Assist. Prof. Oktay Demircan and Assist. Prof. Ozgul Gok for taking the time to review and evaluate my work.

I appreciate our scientific collaborations with Prof. Sabine Szunerits and Assoc. Prof. Fabienne Dumoulin, for sharing their precious knowledge with me and the scientific research that we conducted together. I would like to thank Yann Bretonniere and Hong Boon Lee for their collaborations.

I would like to thank all my fellow labmates of the Sanyal group (present and past members).

I would like to thank the Boğaziçi University Foundation (BUVAK), TÜBİTAK (Project No. 114Z307), Bogazici University Research Funds (Project No. 17B05D3), and RS Research for financial assistance for the work reported in this thesis. This project has also received funding from the European Union's Horizon 2020 research and innovation program under grant agreement No 690836.

Finally, I would like to thank my family and friends for their personal support throughout my studies.

## ABSTRACT

### DESIGN AND FABRICATION OF NOVEL REACTIVE HYDROGELS FOR DELIVERY OF THERAPEUTIC AGENTS AND BIOMOLECULAR IMMOBILIZATION

Polymers have been widely used for the past decades as drug delivery systems owing to their attractive physical, chemical and mechanical properties. In this thesis, nanosized drug delivery systems were developed for the treatment of cancer, owing to their size and ability to target cancer cells via the enhanced permeability and retention effect. Also, cryogels were fabricated as an antibacterial patch and bio-immobilization support by virtue of their macroporous structure. In the first part, nanogels containing hydroxyl and maleimide groups were fabricated using an *in-situ* polymerization. Nanogels were decorated with doxorubicin, and a thiol-based dye, to act as a marker for imaging. As an improved version, in the subsequent chapter, multifunctional nanogels were fabricated by crosslinking copolymers using their thermo-responsive self-assembly in aqueous media. Obtained theranostic constructs were modified with doxorubicin, a dye and a targeting ligand, and they demonstrated enhanced internalization in breast cancer cells. In the third part, a porphyrin photosensitizer used for photodynamic and photothermal therapy in cancer was used as a crosslinker for fabricating nanogels. Obtained constructs generated singlet oxygen and killed breast cancer cells when excited at certain wavelengths. In the fourth part, furan-containing cryogels were utilized as a wound healing patch for the eradication of bacteria via release of a small molecule antibiotic and anti-microbial peptide, where the former was encapsulated and the latter was attached using the Diels-Alder reaction. Reduced graphene oxide incorporated into cryogels enabled photothermal heating. Upon heating drugs released by desorption from graphene oxide or through retro Diels-Alder reaction eradicated *E. Coli* and *S. Aureus* bacterial strains. As a final part of this thesis, novel thiol-reactive cryogels were fabricated and utilized as a platform for bio-immobilization and detection of proteins. In conclusion, various polymeric systems were fabricated and their possible application in different therapeutic areas was demonstrated.

## ÖZET

# İLAÇ TAŞIMA VE BİYOMOLEKÜLER İMMOBİLİZASYON İÇİN YENİ REAKTİF HİDROJELLERİN TASARIMI VE SENTEZLENMESİ

Polimerler ilgi çekici fiziksel, kimyasal ve mekanik özelliklerinden dolayı son yıllarda yaygın olarak ilaç taşıma sistemi olarak kullanılmaktadır. Bu tezde, kanser tedavisi için, nano boyutlarından dolayı artırılmış geçirgenlik ve tutulma etkisi sayesinde kanser hücrelerini hedefleme yeteneği olan ilaç taşıma sistemleri geliştirilmiştir. Aynı zamanda, makro gözenekli yapıları sayesinde antibakteriyel bandaj ve biyomolekül sabitleme amacıyla kullanılabilen kriyo jeller hazırlanmıştır. İlk kısımda, hidroksil ve maleimit gruplarıyla fonksiyonlandırılmış nano jeller in situ polimerleşme ile sentezlenmiştir. Nanojellere kemoterapi ilacı doksorubisin ve görüntüleme için tiyol içeren boya bağlanmıştır. Bu sistemin geliştirilmiş bir uyarlaması tezin ikinci bölümünde, kopolimerlerin sulu ortamda ısıya duyarlı olarak kendi kendilerine biraraya gelerek çapraz bağlanması ile çok fonksiyonlu nanojeller elde edilmiştir. Hem teşhis hem tedavi için kullanılan bu yapılara doksorubisin, boya ve hedefleyici ligand bağlanmış ve meme kanseri hücrelerine artan girişi gösterilmiştir. Tezin üçüncü bölümünde, kanserde fotodinamik ve fototermal terapi için kullanılan ışığa duyarlı porfirin nanojellerin sentezinde çapraz bağlayıcı olarak kullanıldı. Bu nanojeller, belirli dalga boylarında uyarıldığında başarılı bir şekilde tekli (singlet) oksijen üretmiş ve meme kanseri hücrelerini öldürmüştür. Dördüncü bölümde ise, furan içeren makro gözenekli kriyojeller, enkapsüle edilen antibiyotik moleküllerin ve Diels-Alder reaksiyonu ile kovalent olarak bağlanmış antimikrobiyal peptitlerin salımı ile bakterileri yok etmek için kullanılmıştır. Bu kriyojellerin içerisine eklenen indirgenmiş grafen oksit fototermal olarak ısıtılmasını mümkün kılmıştır. İlaçlar, fototermal ısıtma uygulandığında grafen oksitten desorpsiyon yoluyla ya da retro Diels-Alder reaksiyonu sonucunda ayrılarak *E. Coli* ve *S. Aureus* bakteri suşlarını başarılı bir şekilde öldürmüştür. Tezin beşinci ve son bölümünde, tiyol reaktif makro gözenekli kriyojeller sentezlenmiş ve protein tespiti ve sabitleme platformu olarak kullanılmıştır. Sonuç olarak, çeşitli polimerik yapılar hazırlanmış ve farklı terapötik alanlarındaki muhtemel uygulamaları gösterilmiştir.

## TABLE OF CONTENTS

ACKNOWLEDGEMENTS .....	iii
ABSTRACT .....	iv
ÖZET.....	v
LIST OF FIGURES.....	xi
LIST OF ACRONYMS/ABBREVIATIONS .....	xix
1. INTRODUCTION.....	1
1.1. Polymeric Materials for Drug Delivery.....	1
1.1.1. Drug delivery system for cancer .....	1
1.1.2. Drug Delivery Systems to treat microbial infections.....	6
1.1.3. Nanogels.....	8
1.1.4. Bulk Gels.....	13
2. RESEARCH OVERVIEW.....	19
3. FABRICATION OF IN SITU NANOGELS FOR DRUG DELIVERY AND IMAGING .....	20
3.1. Introduction .....	20
3.2. Experimental .....	22
3.2.1. Materials.....	22
3.2.2. Methods.....	23
3.2.3. Synthesis of NG-DEGMA Nanogels. ....	23
3.2.4. Synthesis of NG-OH Nanogels. ....	24
3.2.5. NHS Activation of Nanogels.....	24
3.2.6. Conjugation of DOX to NHS Nanogels. ....	24
3.2.7. Synthesis of NG-FuMa Nanogels. ....	24
3.2.8. Synthesis of PEGFuMaMA.....	25
3.2.9. Synthesis of NG-PEGFuMa.....	25
3.2.10. Activation of Maleimide Groups of NG-PEGFuMa via the Retro Diels–Alder Reaction.....	25

3.2.11. Conjugation of BODIPY-SH to Nanogels. ....	25
3.3. Results and discussion.....	26
3.3.1. Synthesis of peg macro-CTA .....	26
3.3.2. Synthesis of DEGMA nanogel.....	26
3.3.3. Synthesis of HEMA nanogel.....	28
3.3.4. Conjugation of NHS to Nanogels.....	30
3.3.5. Conjugation of DOX to Nanogels.....	30
3.3.6. Release of doxorubicin.....	31
3.3.7. Synthesis of PEGFuMa nanogel .....	32
3.3.7.1 Synthesis of hydrophilic PEGFuMaMA monomer.....	33
3.3.7.2 Synthesis of PEGFuMA nanogels.....	35
3.3.8. Activation of Maleimide Functional Group.....	37
3.3.9. Attachment of Bodipy thiol to the maleimide.....	39
3.4. Conclusion.....	41
4. MULTIFUNCTIONAL NANOGELS AS THERANOSTICS PLATFORMS: EXPLOITING REVERSIBLE AND NON-REVERSIBLE LINKAGES FOR TARGETING, IMAGING AND DRUG DELIVERY .....	42
4.1. Introduction .....	42
4.2. Experimental .....	47
4.2.1. Materials.....	47
4.2.2. Methods.....	47
4.2.3. Synthesis of Furan-Protected Maleimide-Containing Copolymer.....	48
4.2.4. Activation of Maleimide Groups of Copolymer via the Retro Diels–Alder Reaction.....	49
4.2.5. Synthesis of Nanogels.....	49
4.2.6. NHS Activation of Nanogel.....	50
4.2.7. Conjugation of DOX to NHS Nanogels.....	50
4.2.8. Conjugation of BODIPY-SH to Nanogels.....	50
4.2.9. Conjugation of N-Ethyl Maleimide to Nanogels.....	50
4.2.10. Conjugation of 2-Mercaptoethanol to Nanogels.....	51
4.2.11. Conjugation of cRGDfC to Nanogels.....	51

4.2.12.	Conjugation of Cy5 Maleimide to Nanogels.....	51
4.2.13.	Release of Doxorubicin.....	51
4.2.14.	Cytotoxicity Experiments with L929 Fibroblast Cells.....	52
4.2.15.	Cytotoxicity Experiments with MDA-MB-231 Cells.....	52
4.2.16.	Internalization Experiments.....	53
4.3.	Results and Discussion.....	53
4.3.1.	Synthesis of Reactive Copolymers.....	53
4.3.2.	Synthesis of Multi-Functionalizable Nanogels .....	55
4.3.3.	Functionalization of Nanogels.....	58
4.3.3.1	Conjugation of NHS to Nanogels.....	59
4.3.3.2	Conjugation of DOX to Nanogels.....	59
4.3.3.3	Conjugation of BODIPY-SH to Nanogels.....	60
4.3.3.4	Conjugation of cRGDfC to Nanogels.....	62
4.3.3.5	Conjugation of Cy5 Maleimide Dye to Nanogels.....	63
4.3.4.	Drug Release Experiments.....	64
4.3.5.	In Vitro Experiments.....	65
4.3.6.	In Vitro Internalization Assays.....	66
4.3.7.	In Vitro Cytotoxicity Assay of NG-DOX and NG-DOX-RGD Nanogels.....	68
4.4.	Conclusions .....	69
5.	A SURFACTANT-FREE DIRECT ACCESS TO PORPHYRIN-CROSSLINKED NANO GELS FOR PHOTODYNAMIC AND PHOTOTHERMAL THERAPY .....	70
5.1.	Introduction .....	70
5.2.	Experimental .....	74
5.2.1.	Materials.....	74
5.2.2.	Preparation of azido-containing copolymer.....	75
5.2.3.	Preparation of the nanogels.....	75
5.2.4.	Photophysics and photochemistry.....	75
5.2.5.	In vitro studies.....	76
5.2.6.	Photothermal properties of nanogels.....	78
5.3.	Results and Discussion.....	78
5.3.1.	Synthesis of reactive azide-functionalized copolymers.....	78

5.3.2. Synthesis of porphyrin-crosslinked nanogels.....	80
5.3.3. Photophysics and photochemistry.....	83
5.3.4. Cellular Internalization.....	88
5.4. Conclusions .....	89
6. STIMULI-RESPONSIVE ANTIBIOTIC RELEASING CRYOGELS .....	90
6.1. Introduction .....	90
6.2. Experimental .....	94
6.2.1. Materials.....	94
6.2.2. Fabrication of Cryogels.....	94
6.2.3. Synthesis of Maleimide-conjugated Peptide.....	95
6.2.4. Synthesis of rGO Loaded Furan-containing Cryogels .....	95
6.2.5. Preparation of Kapton/rGO flexible patch .....	95
6.2.6. Swelling of cryogels.....	95
6.2.7. Antibiotic loading.....	96
6.2.7.1 Non-covalent integration of ampicillin .....	96
6.2.7.2 Diels-Alder Reaction of Maleimide-contain Dye and Peptide.....	96
6.2.8. Quantification of loading and release.....	96
6.2.9. Photothermal release studies .....	97
6.2.10. Characterization .....	97
6.3. Results and Discussion.....	98
6.3.1. Fabrication of rGO loaded furan-modified cryogels.....	98
6.3.2. Loading of anti-bacterial compounds.....	101
6.3.2.1 Loading via absorption.....	101
6.3.2.2 Loading via Diels-Alder reaction.....	102
6.3.3. Release of antibiotic .....	103
6.3.4. Release of Peptide from Cryogels.....	104
6.3.5. In vitro tests .....	107
6.3.6. Activity of released antibiotic and anti-microbial peptide .....	107
6.4. CONCLUSION .....	108
7. THIOL-REACTIVE MACROPOROUS CRYOGEL FOR BIOMOLECULAR IMMOBILIZATION.....	110

7.1. Introduction .....	110
7.2. Experimental .....	112
7.2.1. Materials .....	112
7.2.2. Methods .....	113
7.2.3. Fabrication of Photopolymerized Cryogels.....	113
7.2.4. Swelling Study of Bulk Hydrogel. ....	113
7.2.5. Functionalization of Cryogels with FITC-BSA. ....	114
7.2.6. Biotinylation of the Cryogels .....	114
7.2.7. Immobilization of Streptavidin onto the Biotinylated Cryogels. ....	114
7.3. Results and Discussion.....	115
7.3.1. Synthesis of hydrophilic maleimide monomer.....	115
7.3.2. Functionalization of Cryogels via Thiol–Ene Conjugation. ....	118
7.3.3. Functionalization of Cryogels with Biotin-thiol and Immobilization of Streptavidin. ....	120
7.4. Conclusion.....	121
8. CONCLUSIONS .....	122
REFERENCES .....	124
APPENDIX A: COPYRIGHT NOTICES .....	153

## LIST OF FIGURES

Figure 1.1. Normal vs cancer cell divisions. Image adapted from the National Cancer Institute.....	2
Figure 1.2. Timeline of the development of nanomedicine. Reprinted from [6]. .....	3
Figure 1.3. Enhanced Permeability and retention effect. Reprinted from [13]. .....	4
Figure 1.4. Passive vs active targeting. Reprinted from [15]. .....	4
Figure 1.5. Polymeric drug delivery system. Reprinted from [17]. .....	5
Figure 1.6. Benefits of antibiotics loaded polymeric particles. Reprinted from [26]. .....	7
Figure 1.7. Injectable hydrogel loaded with vancomycin that delivers antibiotic locally suitable for treatment of infections in avascular or necrotic tissues. Reprinted from [29]. .....	8
Figure 1.8. Various Types of Nanogels and their Applications. ....	9
Figure 1.9. Commonly used Approaches for Fabrication of Nanogels.....	9
Figure 1.10. Nanogel formation based on self-assembly of amphiphilic copolymers using di-thiol crosslinker. Reprinted from [37]. .....	11
Figure 1.11. Synthesis of shell click-crosslinked nanoparticles from alkyne-containing micelles and azide-containing dendrimers. Reprinted from [38]. .....	12
Figure 1.12. Schematic Illustration of the Preparation, Surface Modification, Dual-Drug Loading, and Drug Releasing of the Designed PAA-Based Nanogels. Reprinted from [39]. .....	13

Figure 1.13. (A) Illustration of the fabrication of PEGDMA-rGO hydrogels; (B) Photographs of free standing hydrogels without (a) and with rGO (0.8 mg) (b). (C) SEM images of PEGDMA, PEGDMA-rGO (0.8 mg) and insulin loaded PEGDMA-rGO (0.8mg). Reprinted from [59].	15
Figure 1.14. Schematic illustration showing different stages involved during cryogel formation. Reprinted from [80].	17
Figure 1.15. Illustrations of (a) cryogel and (b) hydrogel, and their microstructures using SEM, c) In vitro doxorubicin release profile from cryogels (CH) and bulk gels (BH) in acetate buffer pH=5.4. Reprinted from [84].	18
Figure 3.1. Synthesis of PEG-CTA.	26
Figure 3.2. a) Synthesis of DEGMA in situ nanogel, b) Hydrodynamic radius in water at 25 °C and c) TEM images of the nanogels.	27
Figure 3.3. <sup>1</sup> H NMR of NG-DEGMA nanogels.	28
Figure 3.4. a) Synthesis of HEMA in situ nanogel, b) Hydrodynamic radius in water at 25 °C, c) TEM images of the nanogels.	29
Figure 3.5. <sup>1</sup> H NMR of NG-HEMA.	29
Figure 3.6. Schematic representation of conjugation of NHS to NG-OH.	30
Figure 3.7. Schematic representation of attachment of Doxorubicin to NG-NHS and FTIR spectra.	31
Figure 3.8. Cumulative release of doxorubicin from NG-DOX at pH 7.4 and 5.4.	32
Figure 3.9. Attempted route for synthesis of NG-FuMa nanogels using the EtOH as a cosolvent.	33
Figure 3.10. Synthesis of hydrophilic monomer PEGFuMaMA.	34
Figure 3.11. <sup>1</sup> H NMR of the PEGFuMaMA monomer.	34

Figure 3.12. a) Synthesis of PEGFuMa in situ nanogel, b) Hydrodynamic radius in water at 25 °C obtained using DLS and c) TEM image of the nanogels.....	36
Figure 3.13. <sup>1</sup> H NMR spectrum of NG-FuMaPEGMA nanogels. ....	37
Figure 3.14. Schematic representation of deprotection of NG-PEGFuMa nanogels and <sup>1</sup> H NMR spectrum of NG-PEGMA nanogels.....	38
Figure 3.15. Schematic representation of BODIPY attachment to NG-PEGMA, UV spectra of Bodipy attachment to nanogels, picture of 1) NG-DEGMA+BODIPY-SH, 2) NG-PEGMA+BODIPY-SH, 3) NG-PEGMA+BODIPY-Br, 4) NG-PEGFuMa+BODIPY-SH .....	40
Figure 4.1. Schematic Illustration of Multi-Functionalization of Nanogels .....	46
Figure 4.2. (a) Synthesis of copolymer poly(PEGMEMA-co-MaMA-co-HEMA); <sup>1</sup> H NMR spectra of (1) poly(PEGMEMA-co-FuMaMA-co-HEMA) and (2) poly(PEGMEMA-co-MaMA-co-HEMA) .....	54
Figure 4.3. UV of the polymer before and after retro Diels-Alder reaction.....	55
Figure 4.4. (a) Aggregation of copolymer in aqueous solution above its LCST. (b) Change in hydrodynamic size as determined by DLS at 25 and 70 °C. (c) Change in % transmittance of copolymer poly(PEGMEMA-co-MaMA-co-HEMA) solution at 600nm with temperature. ....	56
Figure 4.5. Schematic presentation of gelation reaction of copolymer poly(PEGMEMA-co-MaMA-co-HEMA), hydrodynamic size of nanogel at 25 °C using DLS and TEM. ....	57
Figure 4.6. Molecular weight of the nanogels determined using static light scattering... ..	58
Figure 4.7. Illustration of activation and FTIR spectra of NG-OH and NG-NHS nanogels. ....	59

Figure 4.8. (a) Attachment of drug to NG-NHS nanogels. (b) UV–vis spectra of NG-DOX and NG-OH+DOX control experiment and (c) FTIR spectra of NG-NHS and NG-DOX nanogels. ....	60
Figure 4.9. Attachment of BODIPY-SH to NG-DOX, UV spectra, and photograph under UV illumination of nanogel solutions after treatment with DOX and BODIPY-SH.....	61
Figure 4.10. UV spectra and UV images of nanogel solution after treatment with Bodipy-SH (left) and Bodipy-Br (right).....	62
Figure 4.11. Conjugation of cyclic peptide cRGDfC to NG-DOX nanogel. ....	63
Figure 4.12. Conjugation of Cy5 maleimide to NG-DOX-RGD nanogels. Fluorescence spectra of NG-DOX-RGD-CY5 and control nanogels .....	64
Figure 4.13. Cumulative release of doxorubicin from NG-DOX at pH 7.4 and pH 5.4. ...	65
Figure 4.14. Cytotoxicity assay of NG-NHS on L 929 fibroblast cells. ....	66
Figure 4.15. (a) Merged fluorescence images of MDA-MB-231 cells treated with nanogels with only doxorubicin (NG-DOX), nanogels conjugated with doxorubicin and cRGDfC (NG-DOX-RGD), and free cRGDfC and NG-DOX-RGD nanogels (NG-DOX-RGD + RGDFK). Cells were incubated at 37 °C for different time periods (3, 6, and 24 h). The scale bar is 100 μm. (b) Normalized fluorescence intensity for NG-DOX, NG-DOX-RGD, and NG-DOX-RGD+RGDFK at 3, 6, and 24 h. ....	67
Figure 4.16. (a) In vitro toxicity of free DOX, NG-DOX, and NG-DOX- RGD on MDA-MB-231 breast cancer cells and (b) their histogram representation. ...	68
Figure 5.1. Synthesis and photo-induced singlet oxygen generation and photothermal heating of the porphyrin-crosslinked nanogels. ....	73
Figure 5.2. <sup>1</sup> H NMR of copolymer poly(PEGMEMA-co-AHMA). ....	79

Figure 5.3 Aggregation of copolymers in aqueous solution above its LCST and change in hydrodynamic size as determined by DLS at 25 and 70 °C. ....	80
Figure 5.4. a) Schematic presentation of gelation reaction of copolymer poly(PEGMEMA-co-AHMA). b) Hydrodynamic size of <b>NG-A</b> , <b>NG-B</b> and <b>NG-C</b> at 25 °C using DLS. c) Size of nanogel <b>NG-A</b> using TEM. d) Size distribution of <b>NG-A</b> from TEM analysis. ....	82
Figure 5.5. UV-visible spectra of <b>NG-A</b> , <b>NG-B</b> and <b>NG-C</b> in ethanol and plots of the absorbance at 425, 570 and 607 nm vs concentration. ....	84
Figure 5.6. Cell viability of MDA-MB-231 after (A) 24 h of incubation in the dark, (B) laser irradiation at 450 nm, 0.4 W.cm <sup>-2</sup> and (C) laser irradiation at 635 nm, 1 W.cm <sup>-2</sup> . ....	86
Figure 5.7. Transient bulk temperature profile of <b>NG-A</b> and <b>NG-C</b> with dispersions in complete DMEM under laser irradiation at (A) 450 nm (0.4 W.cm <sup>-2</sup> ), (B) 635 nm (1 W.cm <sup>-2</sup> ). ....	87
Figure 5.8. Effect of laser irradiation on MDA-MB-231 cell at (A) 435nm and (B) 650nm ....	87
Figure 5.9. Cellular internalization of <b>NG-A</b> and <b>NG-C</b> . Corresponding bright field images merged with fluorescence images were included for clarity. The scale bars correspond to 20 μm. ....	88
Figure 6.1. Illustration of fabrication of furan-containing rGO embedded cryogels .....	98
Figure 6.2. Water uptake of cryogels containing varying amounts of furan (a) with rGO and (b) without rGO in water at 24 °C. ....	99
Figure 6.3. Hydrogel samples prepared using similar amount of monomers and SEM images of cryogels with (left) and without (right) embedded rGO. ....	100
Figure 6.4. Photothermal heating curves of cryogels with different amount of rGO when immersed in PBS (0.1 M, pH 7.4) and exposed to laser light of 980 nm for 10 min. ....	100

Figure 6.5. Loading capacity of cryogel with different concentrations of Ampicillin.....	101
Figure 6.6. Schematic representation of dye loading and microscopy images of CGrGO-0 (control) and CGrGO-40 (CG-Furan) after treatment with maleimide dye.....	102
Figure 6.7. Release of ampicillin in using active and at passive (24°C) modes.....	103
Figure 6.8. Release of fluorescein maleimide dye via retro Diels Alder from CG-rGO in % using laser (active) and at 37 °C (passive). ....	104
Figure 6.9. Schematic representation of loading and release of maleimide containing construct using DA-rDA mechanism. a) Release of the fluorescein maleimide dye and b) anti-microbial peptide at 37 °C (passive) and at 70 °C (active) using NIR laser.....	106
Figure 6.10. Cells viability of Hela after 24h incubation with CGrGO (0-40% furan) and CG (0-40% furan).....	107
Figure 6.11. a) Bacteria <i>E.coli</i> viability in %, b) Bacteria <i>S. aureus</i> viability in % upon treatment with antibiotics released from cryogels.....	108
Figure 7.1. Schematic representation of protein immobilization onto maleimide bearing microporous cryogels. ....	112
Figure 7.4. Schematic representation for the fabrication of thiol-reactive microporous cryogel, and a) top view of dry cryogel, b) top view of wet cryogel, c) side view of dry cryogel and d) side view of wet cryogel. ....	116
Figure 7.5. Comparison of a) morphology from SEM images, b) swelling profile, and c) FTIR spectra of cryogels. ....	117
Figure 7.6. a) Functionalization of cryogel with FITC-BSA, b) Fluorescence images of cryogels after functionalization, c) relative fluorescence intensities of the cryogels after functionalization with FITC-BSA. ....	119

Figure 7.7. Fluorescence images and relative fluorescent intensities of cryogels after their functionalization with FITC-BSA.....	119
Figure 7.8. a) Biotinylation of the cryogels, followed by immobilization of TRITC-streptavidin, b) fluorescence microscopy images of TRITC-streptavidin immobilized cryogels and c) relative fluorescence intensities of cryogels after protein immobilization.....	120
Figure A.1. Copyright licence of [6]. .....	172
Figure A.2. Copyright licence of [13]. .....	173
Figure A.3. Copyright licence of [15]. .....	174
Figure A.4. Copyright licence of [17]. .....	175
Figure A.5. Copyright licence of [26]. .....	176
Figure A.6. Copyright licence of [29]. .....	177
Figure A.7. Copyright licence of [36]. .....	178
Figure A.8. Copyright licence of [37]. .....	179
Figure A.9. Copyright licence of [38]. .....	180
Figure A.10. Copyright licence of [39]. .....	181
Figure A.11. Copyright licence of [59]. .....	182
Figure A.12. Copyright licence of [80]. .....	183
Figure A.13. Copyright licence of [84]. .....	184
Figure A.14. Copyright licence of [192]. .....	185

## LIST OF TABLES

Table 1.2. Free radical polymerization technique for nanogels synthesis. Reprinted from [36].....	10
Table 5.1. UV-vis, fluorescence and singlet oxygen generation values of the nanogels ...	83
Table 6.1. Composition and conversion of cryogels fabricated via photo-crosslinking. ...	99
Table 7.1. Photopolymerization of cryogels in presence of PEGFuMaMA .....	115

**LIST OF ACRONYMS/ABBREVIATIONS**

ACVA	4'4-Azobis(4-cyanovaleric acid)
AIBN	2,2'-azobisisobutyronitrile
AMP	Anti-Microbial Peptide
BODIPY	4,4-difluoro-4-bora-3a,4a-diaza-s-indacene
BSA	Bovine Serum Albumin
CTA	Chain Transfer Agent
DA	Diels-Alder
DCM	Dichloromethane
DDS	Drug Delivery System
DEGMA	Diethylene glycol methacrylate
DLS	Dynamic Light Scattering
DMEM	Dulbecco's Modified Eagle's Medium
DMPA	4-Dimethylaminopyridine
DMSO	Dimethyl sulfoxide
DOX	Doxorubicin
DSC	Disuccinimidyl carbonate
DTT	Dithiothreitol
E. Coli	Escherichia Coli
EPR	Enhanced Permeability and Retention
Et3N	Triethyl amine
FITC	Fluorescein Isothiocyanate
FRET	Fluorescence Resonance Energy Transfer

FT-IR	Fourier-transform infrared
FuMaMA	Furan Maleimide Methacrylate
GPC	Gel Permeation Chromatography
HEMA	Hydroxy-ethyl Methacrylate
HIV	Human Immunodeficiency Virus
HPLC	High-performance liquid chromatography
LCMS	Liquid chromatography–mass spectrometry
LCST	Lower Critical Solution Temperature
MeOH	Methanol
MMP-9	Metalloproteinase-9
NIPAAm	<i>N</i> -isopropylacrylamide
NIR	Near Infra-Red
NMR	Nuclear Magnetic Resonance
OD	Optical Density
PBS	Phosphate-bufferedd saline
PDI	Polydispersity Index
PDT	Photodynamic therapy
PEG	Poly(ethylene glycol)
PEGDMA	Poly(ethylene glycol) dimethacrylate
PEGMA	Poly(ethylene glycol) methyl methacrylate
PISA	Polymerization-Induced Self-Assembly
PS	Photosensitizer
PTT	Photothermal therapy
RAFT	Reversible Addition Fragmentation chain Transfer
rDA	retro Diels-Alder

rGO	reduced graphene oxide
ROS	Reactive oxygen species
S. Aureus	Staphylococcus Aureus
SOG	Singlet oxygen generation
TEM	Transmission Electron Microscopy
THF	Tetrahydrofuran
TRITC	Tetramethylrhodamine-isothiocyanate
UV	Ultra-violet
VGEF	Vascular Endothelial Growth Factor
ZnTPP	Zinc tetraphenylporphyrin

# 1. INTRODUCTION

## 1.1. Polymeric Materials for Drug Delivery

Natural and synthetic drugs have been used for centuries to treat health disorders and prolong lives. Unfortunately, many drugs have serious side effect due to their inherent toxicity and lack of specificity, which leads to harm of healthy organs and tissues. Side effects limit the ability to fabricate optimal treatments for many diseases such as cancer, neurodegenerative and infectious diseases. To circumvent those issues, enormous amount of research have been focused on development of efficient drug delivery systems (DDS). Such systems would help regulate the rate at which the drug is released as well as the location where it is released. This thesis will focus on development of polymeric systems to address such challenges in the area of cancer and anti-microbial infections.

### 1.1.1. Drug delivery system for cancer

According to statistics from the World Health Organization, cancer is one the leading cause of death worldwide, and was responsible for 8.8 million deaths in 2015 and approximately 1 in 6 deaths is due to cancer. It is also projected that, in 2018, approximately 1,735,350 new cases of cancer will be diagnosed in the United States and 609,640 people will die due to it [1]. Cancer occurs when the body's normal control mechanism cease to work and old cells do not die and grow unusually and lead to the formation of a tumor (Figure 1.1). The three main treatments against cancer are surgery, chemotherapy and radiation therapy. During chemotherapy, cytotoxic agents are used, that trigger cell death or inhibit cell growth, generally by preventing microtubule or protein function, or DNA synthesis.

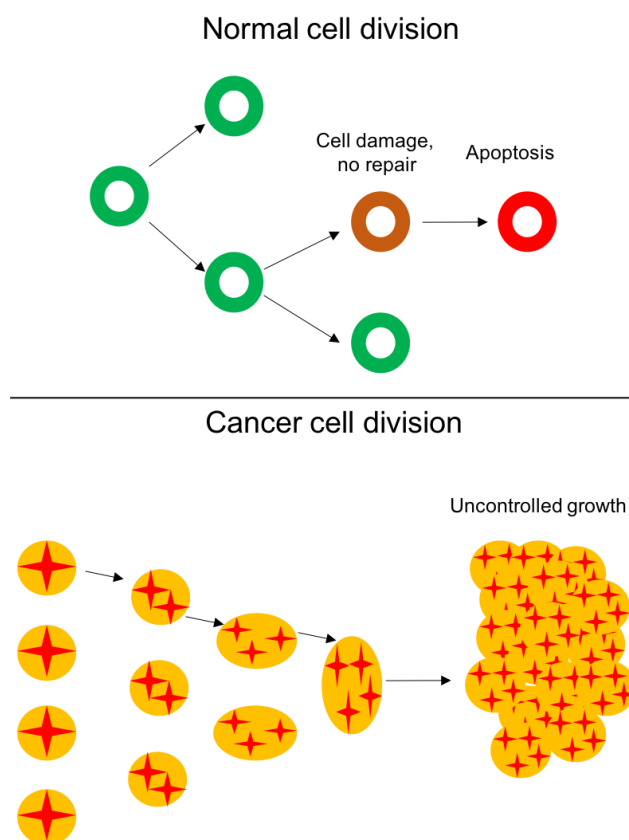


Figure 1.1. Normal vs cancer cell divisions. Adapted from [1].

But due to the small size, poor solubility, rapid clearance and toxicity of conventional small molecule drugs their effect is limited and often accompanied with serious side effects. To circumvent those issues arising with various drugs in multiple diseases, and make the treatment more efficient, drug delivery systems needs to be improved through the enhancement of targeted therapy using macromolecular constructs. The use of nanotechnology as drug delivery vector is anticipated to revolutionize the focus of pharmaceutical and biotechnology industries [2-4]. Utilization of nanosized constructs suggest that poorly water-soluble drugs can be better administered and diseased tissues can be targeted. Furthermore, with suitable targeting groups, macromolecular constructs can be delivered to intracellular site of actions. It also renders possible the simultaneous delivery of multiple drugs to allow combined therapy or theranostic treatment, where it is possible to treat the disease while simultaneously visualize the site of action.

One of the first nanotechnology drug delivery systems to be developed, in 1960s, was liposomes [5]. Afterward, a myriad of other constructs for drug delivery such as dendrimers, micelle, and nanoparticles were discovered (Figure 1.2) [6].

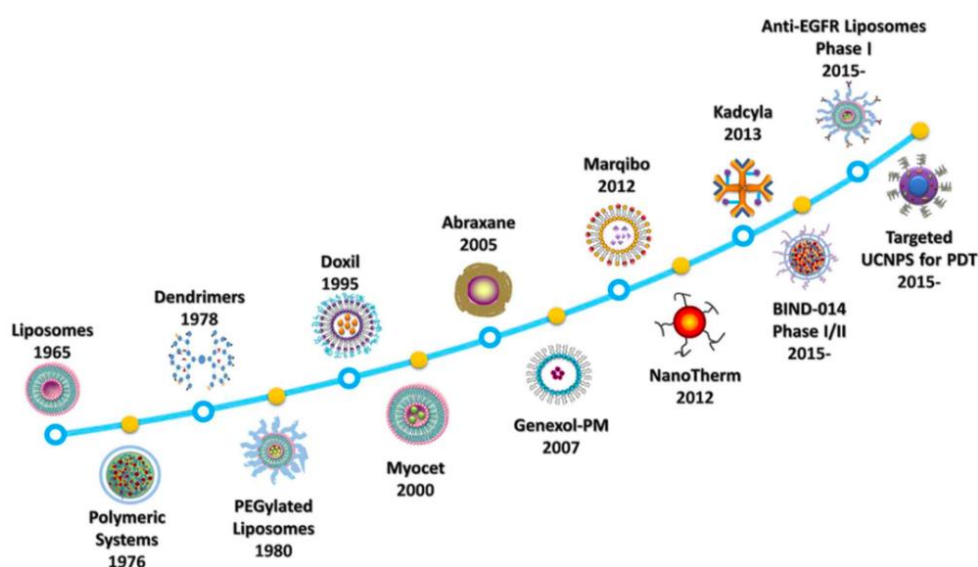


Figure 1.2. Timeline of the development of nanomedicine. Reprinted from [6].

Polymeric system for controlled release for delivery of macromolecules were first introduced in 1976 which led to the use of hydrophilic polymers, thanks to their ability to enhance circulation time for liposomes and polymeric nanoparticles [7]. As of today, there are over twenty nano-therapeutic constructs that have been accepted for clinical use because of their enhanced pharmaceutical efficacy, and liposomal drugs and polymer-drug conjugates are the main two leading categories [8]. The biophysical chemical properties of the vector, such as its size, charge, and the nature of the ligand on its surface can all influence the circulating half-life of the macromolecules as well as their bio-distribution [9,10]. Indeed, the occurrence of targeting moieties on the surface of the vehicle can improve its cellular uptake within the cell of interest via receptor-mediated endocytosis. This process is also known as active targeting. While targeted DDS are developed for numerous diseases, the focus of research has been intense in addressing solid tumors. The present approach in oncology involves effective use of nanosized therapeutic constructs by amassing in cancerous tissues through the enhanced permeability and retention (EPR) effect (Figure 1.3).

Due to the higher vascular density of tumor tissues and their lack of effective lymphatic drainage, macromolecular drugs can accumulate and be retained selectively without dispersing to healthy tissues [11-14].

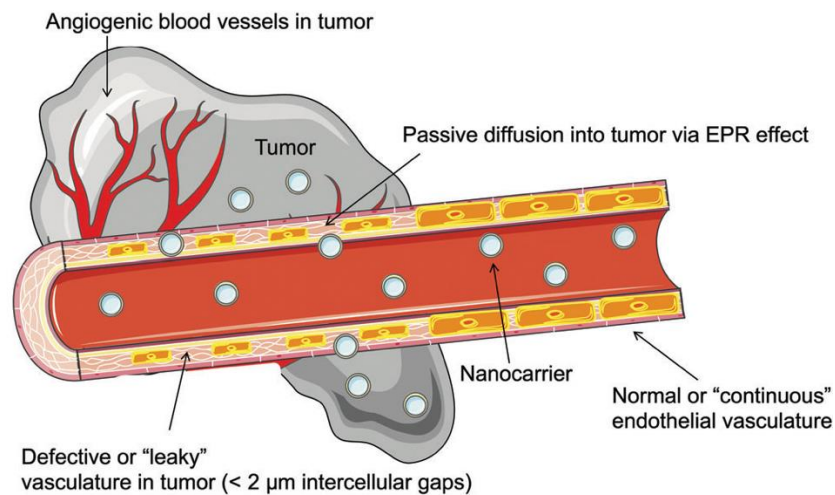


Figure 1.3. Enhanced permeability and retention effect. Reprinted from [13].

Passive targeting occurs when molecular constructs extravagate through the uneven vasculature of tumors and damaged tissue, and accumulate through the EPR effect. After reaching the targeted tissue by extravasation, constructs decorated with ligand will have an enhanced accumulation to the corresponding receptor present on the cells of target leading to endocytosis. This process, called active targeting, increases the therapeutic efficiency of the drug by directly targeting the cells of concern (Figure 1.4).

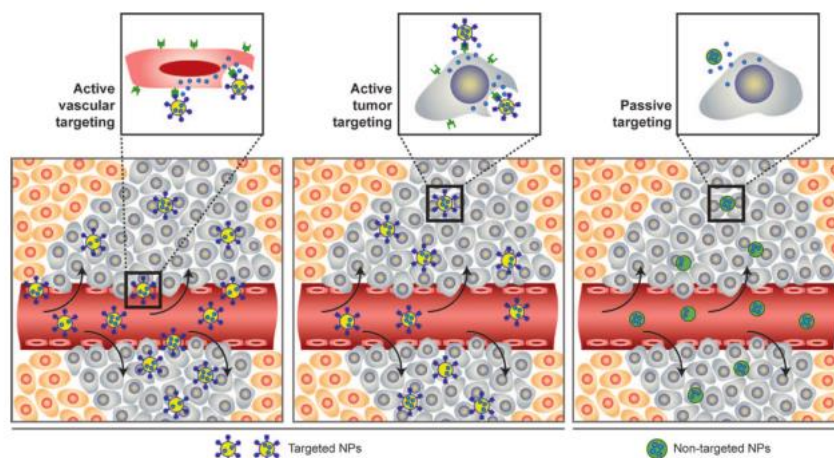


Figure 1.4. Passive vs active targeting. Reprinted from [15].

Polymeric constructs have played a fundamental role in the development of DDS by controlled release of drugs in continuous doses over prolonged period of time, with repeating dosage, and adjustable release of the therapeutic agents. Polymers with linear or branched architectures can be used as the carrier of the therapeutic agent in various forms such as a polymer-drug conjugate, polymeric micelles, and multicomponent polyplexes (Figure 1.5) [16].

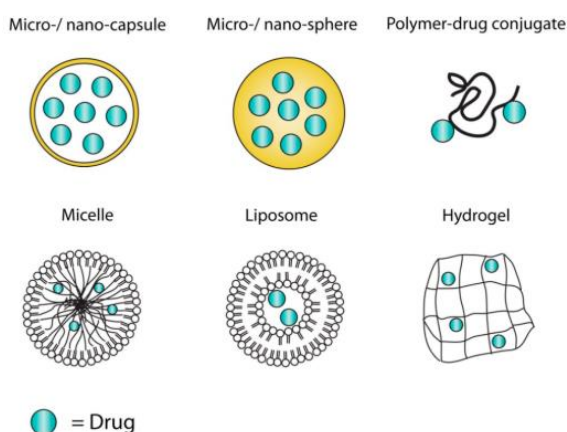


Figure 1.5. Polymeric drug delivery systems. Reprinted from [17].

Among the various polymers used to date, Poly(ethylene glycol) (PEG) has been perhaps the most widely utilized macromolecular component in drug delivery. PEG is a very common component used in DDSs for encapsulation of numerous drugs, offering prolongation of their half-life and reducing their dosage frequency [18]. It is also widely used as a protective coating material for drug delivery vehicles such as liposomes and nanoparticles. Likewise, PEG has been extensively employed to provide stability to biomacromolecules such as proteins under physiological conditions [18-20]. PEG is amphiphilic, therefore soluble in organic solvents as well as in water; they are also nontoxic and are cleared out by a combination of renal and hepatic pathways thus making them ideal for several biomedical applications. They are bio-inert, thus undergo poor protein adsorption, low cell activation and adhesion, poor cellular uptake, and induce negligible degree of inflammation. The anti-biofouling aspect of PEG plays an important role in fabrication of sensing platforms, as well as scaffolds for cell growth, since these materials will have minimal non-specific interactions with other biomolecules and cellular materials.

Using nanosized polymeric constructs, the pharmacokinetic and pharmacodynamics properties of the drugs are remarkably increased. In particular, the plasma half-life of drugs are enhanced, they are protected from proteolytic enzymes, immunogenicity is decreased, and the solubility of hydrophobic drugs is tremendously improved [21-23]. Most of the polymeric constructs are designed for packaging anticancer agents, but other diseases such as rheumatoid arthritis, diabetes, hepatitis B and C, and ischemia have also been of target [24]. It has been demonstrated that the tumor concentration of anti-cancer therapeutics can increase up to 70 folds when combined with macromolecular systems [16], presumably due to EPR effect. In the search of novel strategies to obtain targeted release and decrease unwanted toxicity of conventional drugs, the field of polymer therapeutics has seen a remarkable growth in recent years.

### **1.1.2. Drug Delivery Systems to treat microbial infections**

Infectious diseases, considered as the second leading cause of deaths worldwide, are triggered by pathogenic microbes such as viruses, bacteria and fungi, and are still one of the world's biggest global health issues with constant fear of global epidemics [25]. Due to the recurrent progression of evolving diseases, especially the quickening of the HIV/AIDS contagion throughout developed countries, the impact of infectious diseases will intensify globally. Thanks to the use of penicillin around 1940s, mortality from infections was tremendously reduced, but unfortunately many microorganisms have become resistant to antibiotics making researchers focus on the treatment of infectious diseases a main goal. *Staphylococcus aureus* (*S. Aureus*) and *Escherichia coli* (*E. Coli*) bacteria are the main multi-drug resistant pathogens and principal causes of bacterial infections. In 2011, it was announced that 25,000 patients die yearly in Europe due to infections generated by antibiotic-resistant bacteria, with a majority of them because of Gram-negative pathogens such as *S. Aureus* [25]. The medical failure of antibiotic therapy can be attributed to their poor bioavailability, low penetration to bacterial infection sites, and the side effects of antibiotics, as well as the antibiotic resistance properties of bacteria.

Polymeric constructs provide protection to antibiotics against environmental deactivation and can bypass tissue and cellular barriers to transport antibiotics into otherwise difficult to access tissues and target cells. Polymeric constructs can be also be altered to target or react to bacterial infection microenvironment (Figure 1.6) [26].

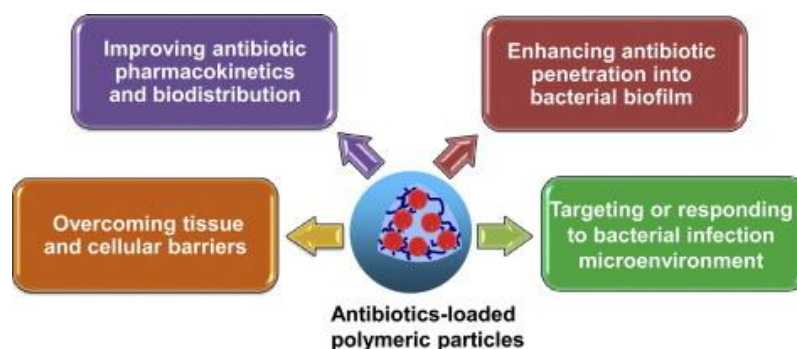


Figure 1.6. Benefits of antibiotics loaded polymeric particles. Reprinted from [26].

Polymeric particles, especially the one in the nanometric range, are well suited for targeting bacterial infections inside the body as the antibiotic-loaded particles allows efficient penetration through the mucus layer around bacteria biofilms, thus increasing the local concentration of antibiotic within the biofilm [26].

In contrast, antibiotic loaded bandages, foams and dressings are favored for external applications such as the management of chronic wounds [27, 28]. For example, Hoque et al. developed an injectable hydrogel loaded with vancomycin that releases the antibiotic locally to eradicate infections in avascular as well as necrotic tissues [29]. The hydrogels were made of polydextran aldehyde acting as a bio-adhesive polymer, along with an antibacterial polymer *N*-(2-hydroxypropyl)-3-trimethylammonium chitosan chloride (Figure 1.7). The antibiotic, Vancomycin, was covalently bonded to the polydextran aldehyde via reversible and pH sensitive imine bonds in the hydrogel which permitted the controlled released the antibiotic over an extended period of time. The hydrogels were therefore able to kill by the bacteria by localized action, on direct contact with the infected site, as well as by releasing the antibiotic to its surrounding upon stimuli.

Upon subcutaneous implantation, the gel was shown to kill methicillin-resistant *S. Aureus* when bacteria were introduced directly into the gel, as well as at a distal site from the gel in a mice model.

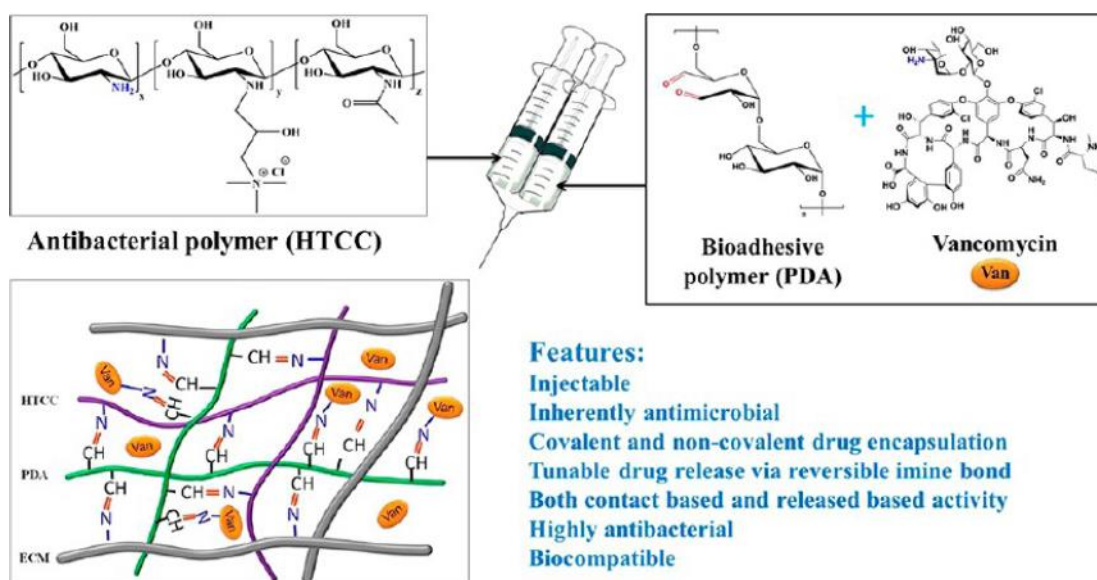


Figure 1.7. Injectable hydrogel loaded with vancomycin that delivers antibiotic locally suitable for treatment of infections in avascular or necrotic tissues. Reprinted from [29].

### 1.1.3. Nanogels

Nanosized hydrophilic gels, formed by physically or chemically crosslinked polymer networks, also called nanogels, have seen growing interest in the past decade. Nanogels have demonstrated appealing potential in the area of drug delivery, tissue engineering, protein encapsulation and bio-imaging platform (Figure 1.8) [30-33]. Nanogel applicable for drug delivery or imaging should be biocompatible, non-toxic and antifouling. In this regard, PEG containing nanogels are an ideal candidate for designing stimuli-responsive nanogels since PEG exhibits excellent biocompatible and antifouling properties [34, 35].

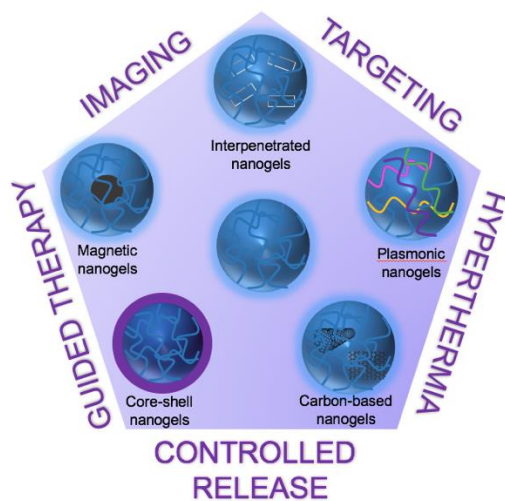


Figure 1.8. Various types of nanogels and their applications.

Nanogels can be synthesized through one of the two main approaches, either fabricating nanogels from polymeric precursors or forming nanogels networks via heterogeneous polymerization of monomers (Figure 1.9). In general, the first method allows for surfactant free conditions, thus decreasing possible toxicity that can be induced by the residual surfactants. Table 1.2 provides a more detailed version of the different techniques and their advantages and limitations in the synthesis of nanogels.

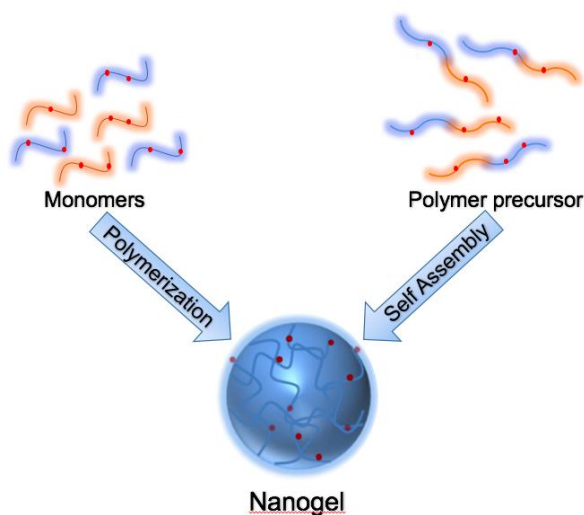


Figure 1.9. Commonly used Approaches for Fabrication of Nanogels.

Table 1.2. Free radical polymerization technique for nanogel synthesis.

Reprinted from [36].

Reaction	Details	Advantages/limitations
Miniemulsion	Nanodroplets formation through high shear stress (ultrasonication) of the mixture of monomers and surfactants	Narrow size distributions for diameters in the 50–500 nm range. Allows <i>in situ</i> encapsulation// Surfactant and co-stabilizer required. Special equipment necessary (ultrasonic device).
Microemulsion	Absence of high shear stress Use of a critical concentration of surfactant Monomer molecules are in micelles	Usually nanogel sizes between 10 and 150 nm can be achieved No shear stress necessary// High surfactant concentration needed. Co-surfactant necessary.
Dispersion	Initially all the reaction ingredients are soluble in the reaction medium Polymerization occurs in a homogeneous phase The polymers are insoluble and form a stable dispersion with an aid of colloidal stabilizers	Simple batch synthesis. Particle size adjusted by monomer and dispersant concentration in the range of 0.1–15 mm Preferably for core-shell particles synthesis// Preferably for vinylic functionalized monomers
Precipitation	Initiation of reaction occurs in homogeneous solution of the monomers in the reaction medium. Polymer is soluble in the reaction medium. Particles separation by crosslinking	Batch synthesis No surfactant required Particle size adjusted by monomer concentration in the range of 100–600 nm// Frequently irregular shape and high polydispersity

Most amphiphilic copolymers self-assemble in solution to form several nanosized structures in the absence of surfactants. Using efficient crosslinking chemistry, such aggregates can easily be crosslinked to obtain stable nanogels.

As a recent example, Sanyal and coworkers fabricated multi-functionalizable nanogels using thermally driven self-assembly of thiol-reactive thermosensitive polymers and crosslinking them using dithiol based linkers [37]. Such nanogels were formed by heating the poly(ethylene glycol) methylether methacrylate (PEGMA)-based maleimide containing polymers above their LCST and crosslinking the nanosized aggregates using dithiol based crosslinkers (Figure 1.10). Remaining thiol and maleimide functional groups were used to conjugate a maleimide-bearing dye and a thiol-containing peptide, respectively, to show its potential usage as an targeted imaging agent in cancer therapy.

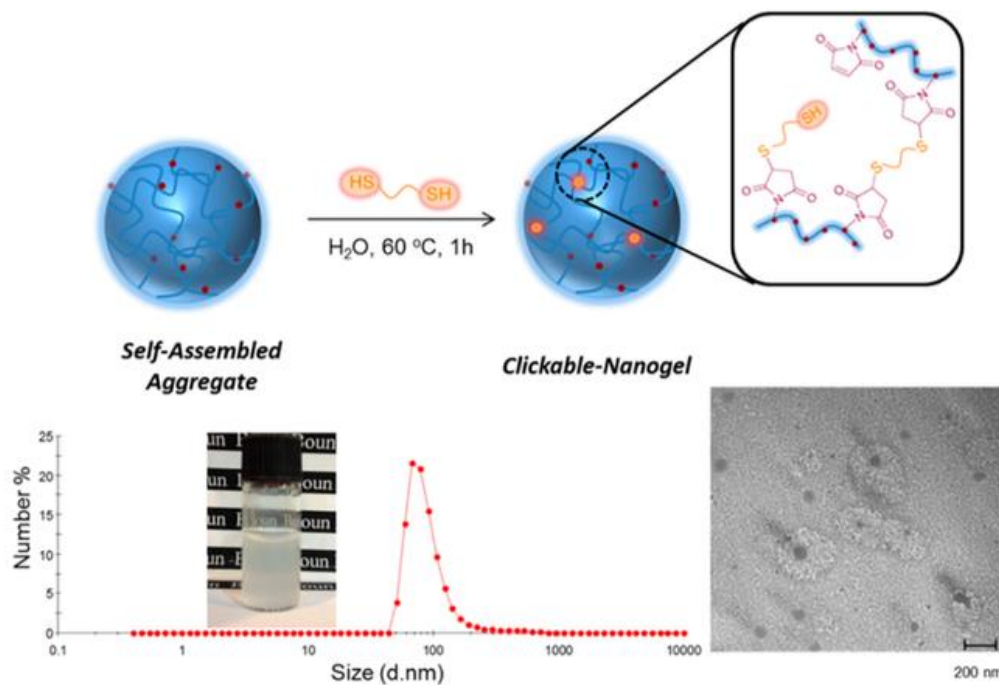


Figure 1.10. Nanogel formation based on self-assembly of amphiphilic copolymers using di-thiol crosslinker. Reprinted from [37].

Click chemistry between an azide and an alkyne is also of used for the design of stable nanogels but usually requires metal catalyst, that can be quite challenging to remove and can lead to systemic toxicity. Wooley and coworkers fabricated shell click-crosslinked nanogels by assembling into micellar structure amphiphilic poly(acrylic acid) and poly(styrene) polymer functionalized with alkyne groups [38]. Dendrimers of the zero, first, second, and third order with increasing numbers of azide terminating groups were utilized as crosslinkers via click reactions with the alkynyl groups of the polymers to obtain crosslinked shell (Figure 1.11). It was shown that only the first generation dendrimer had the adequate balance of polyvalency and water solubility to obtain a crosslinking nanogel. To obtain a fluorescent constructs, the unreacted azide group left on the dendrimeric crosslinker were then functionalized via click reaction with an alkynyl-fluorescein.

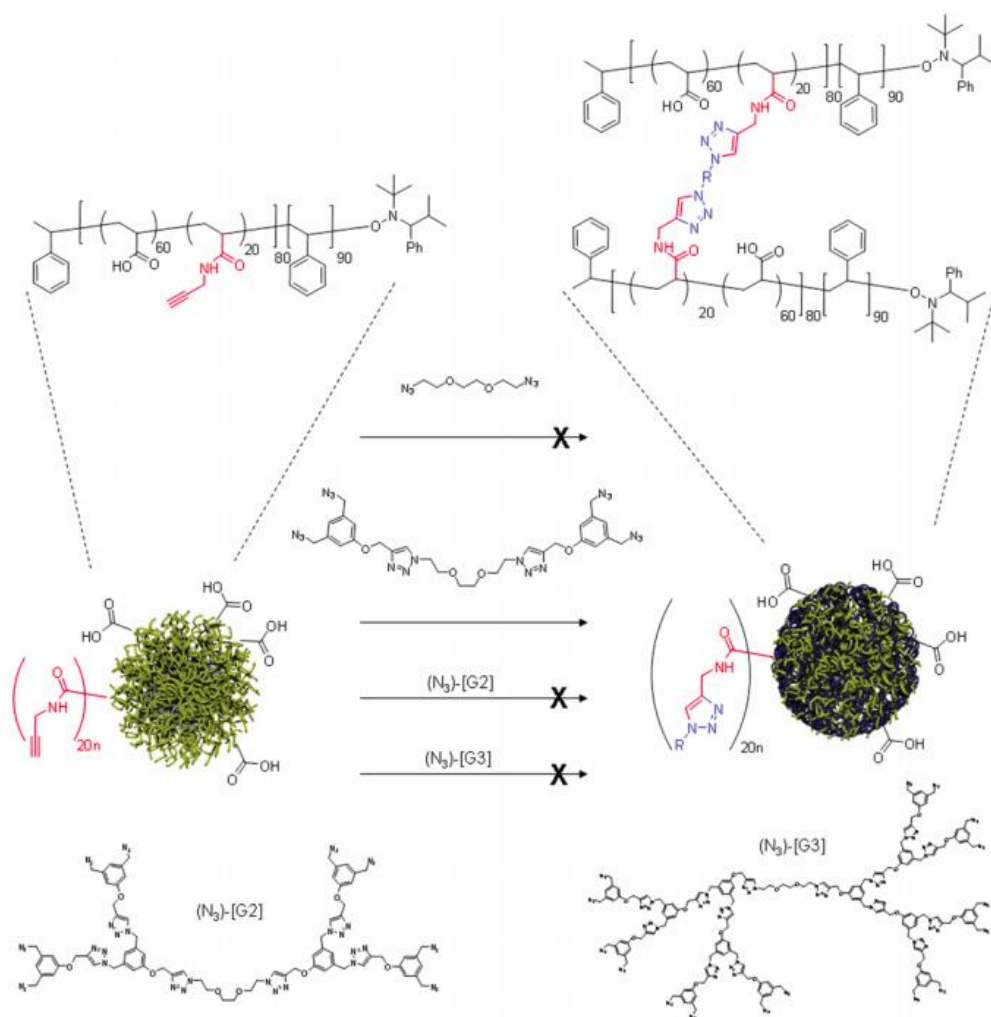


Figure 1.11. Synthesis of shell click-crosslinked nanoparticles from alkyne-containing micelles and azide-containing dendrimers. Reprinted from [38].

In the other approach, nanogels can be fabricated using crosslinking of hydrophilic monomers under appropriate polymerization conditions. Nanogels have been widely used in various area such as sensing, diagnostics, and bioengineering, but its utmost impact has been in the field of drug delivery [31, 33]. Using the monomer based approach, Wang and coworkers designed poly(acrylic acid)-based nanogels with multiple stimuli-responsive properties (Figure 1.12) [39].

Obtained nanogels, after their functionalization with folic acid (FA) targeting group, were employed for co-delivery of doxorubicin and cisplatin for synergistic chemotherapy. Doxorubicin was loaded into the nanogels by strong electrostatic and stacking interactions with high efficiency, while cisplatin was conjugated with the acid group by chelation interactions. Both drugs were released upon decrease in pH with high release content within 24 h. Moreover, both drugs were successfully delivered into MCF-7/ADR cells and demonstrated potent antitumor activity. Additionally, a substantial inhibition of tumor growth and reduced drug-related systemic toxicity were observed.

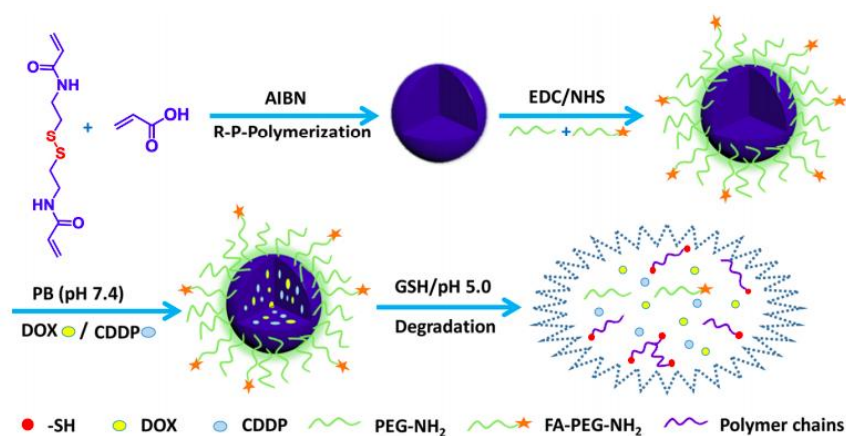


Figure 1.12. Schematic illustration of the preparation, surface modification, dual-drug loading, and drug releasing of the designed PAA-based nanogels. Reprinted from [39].

#### 1.1.4. Bulk Gels

Cross-linked, three dimensional hydrophilic polymeric networks, namely hydrogels, have witnessed increased interest in recent years as potential candidates for applications in areas such as tissue engineering, drug delivery systems, sensors and implant materials.[40-43] Widespread interest in hydrogels arises from their facile fabrication, low cost and ease of interactions with various biological materials. Properties of hydrogels such as their high swelling ratio, their porosity and their soft consistency render them similar to natural living tissue thus making them ideal candidates for the use in biomedical applications.

Hydrogel can be designed to be chemically stable or biodegradable and can be coated on different devices to be used as a reservoir for slow releases of therapeutic agents [44- 46]. They can be in various form such as sheets, or discs and have been used for the release of chemotherapeutic drugs that are implanted post-surgery to eliminate any leftover cancer cells that could lead to the reappearance of tumor [47, 48]. The drug can either be crosslinked or encapsulated inside the hydrogel. Hydrogels that are chemically crosslinked with covalently attached drugs via suitable linkers can offer slow and prolonged release preventing any unwanted burst release that can arise when using physically crosslinked hydrogels with encapsulated drug. Features such as swelling, porosity, and degradability of these hydrogels can be exploited to adapt the release profile of the covalently linked drug [49]. Metal-catalyzed Huisgen-type click cycloaddition reaction between azide and alkyne group is one of the most commonly utilized reaction for synthesis of hydrogels due to its high efficiency under mild reaction conditions [50, 51]. Although, the residual copper catalyst can be expected to pose toxicity, their proper removal can yield non-toxic and biocompatible materials.

In recent years stimuli-responsive polymeric materials have garnered interest since the presence of a trigger to enable on-demand delivery of therapeutic agents widens the difference between passive and active release [52,53]. Among the various triggers that have employed in hydrogels; pH, heat, photochemical, redox-responsive and enzymatic cues are quite common. These triggers can be used either to release the therapeutic agent while maintaining the crosslinked structure of the hydrogel or induce degradation of the hydrogel to facilitate release. In a recent example, Sanyal and coworkers prepared bio-compatible and bio-antifouling redox-responsive hydrogels. The hydrogels were crosslinked using Diels-Alder reaction between a furan-containing hydrophilic copolymer and a disulfide-containing bis-maleimide crosslinker that were successfully degraded using DTT to reduce the disulfide bond [54]. Diels–Alder (DA) cycloaddition takes place between a diene and dienophiles molecules and delivers a stable conjugate without the use of any harsh conditions preventing the use of catalyst that could be potentially toxic. Moreover, cycloadduct obtained from DA reactions are thermosensitive and can reverse to their initial forms via retro Diels-Alder (rDA) upon increase in temperature.

The Diels-Alder connectivity can be used to synthesize the hydrogel as illustrated in example below, but the same chemistry can also be used to release drug molecules from polymeric constructs [55-58]. An example of a thermally-triggered hydrogel for insulin release was reported by Szunerits and coworkers, where they employed photopolymerization to fabricate reduced graphene oxide (rGO)-containing PEG-based hydrogels for insulin release (Figure 1.13) [59]. Reduced graphene oxide (rGO) was used as a near infrared (NIR)-absorbing photothermal agent for light-to-heat conversion under low-power NIR irradiation [60]. In this work, insulin was loaded into the hydrophilic hydrogels through simple immersion of the hydrogel into an insulin solution. Exposition of hydrogel to near-infrared NIR light induced heating of the PEGDMA-rGO hydrogels allowing for release of 6.5–8.7  $\mu\text{M}$  insulin, which is higher than the amount of insulin needed to decrease diabetic blood glucose concentrations. This example utilizes heat as a trigger to increase the diffusion rate of the biomacromolecules from the hydrogel, without altering any bond connectivity in the matrix.

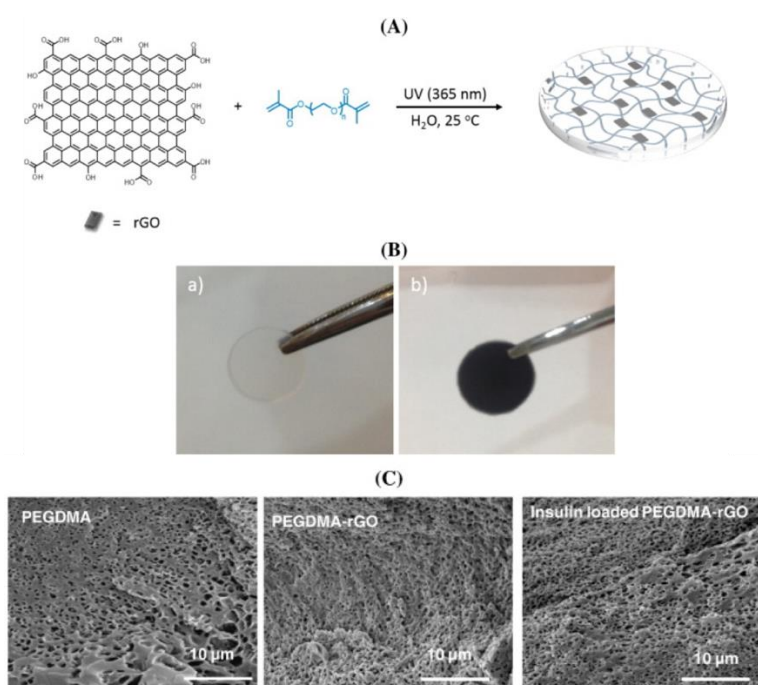


Figure 1.13. (A) Illustration of the fabrication of PEGDMA-rGO hydrogels; (B) hydrogels without (a) and with rGO (0.8 mg) (b). (C) SEM images of PEGDMA, PEGDMA-rGO (0.8 mg) and insulin loaded PEGDMA-rGO (0.8 mg). Reprinted from [59].

Apart from acting as a matrix for delivery of therapeutic agents, hydrogel scaffolds have been extensively used as supports for bio-immobilization for purpose of protein sensing and cellular immobilization [61,62]. In general photo-polymerization based approaches have been used for fabrication of hydrogels since they allow spatial and temporal control over the process [63-73]. Hydrogels with varying porosities in either homogenous or gradient manner can be fabricated using photochemical approaches. For attachment of biologically relevant ligands for protein recognition, as well as direct immobilization of biomolecules, reactive groups are incorporated into the hydrogel matrix [74].

Even though, in general, hydrogels possess a microporous structure, it may not be sufficient to allow efficient diffusion of therapeutic materials or nutrients when these are used as scaffolds. For this purpose a hydrogels with macroporous structure can be obtained using gelation at low temperatures. Such hydrogels, commonly referred to as cryogels, are fabricated by cryotropic gelation at low temperatures through covalent crosslinking of monomers via homogeneous or heterogeneous network formation with physical stability. Cryogels with different morphologies and properties can be obtained by varying the experimental conditions and formulation, and can be adjusted depending on the desired applications [75-77].

Generally, the reaction mixture comprised of polymer precursors, is cooled below the freezing point of the solvent, where the solvent will crystallize and part of the reaction mixture will stay liquid. As the solvent crystallizes, the polymer precursors are concentrated in liquid microphases (Figure 1.14). After gelation has occurred, the cryogel is returned to room temperature, leading to the formation of opaque materials with macropores ranging from 1 to 150  $\mu\text{m}$ . The size and structure of the pores can be controlled by the crystallization, based on the freezing temperature, and the polymerization, based on the concentrations of the monomers, crosslinker and solvent [78-80].

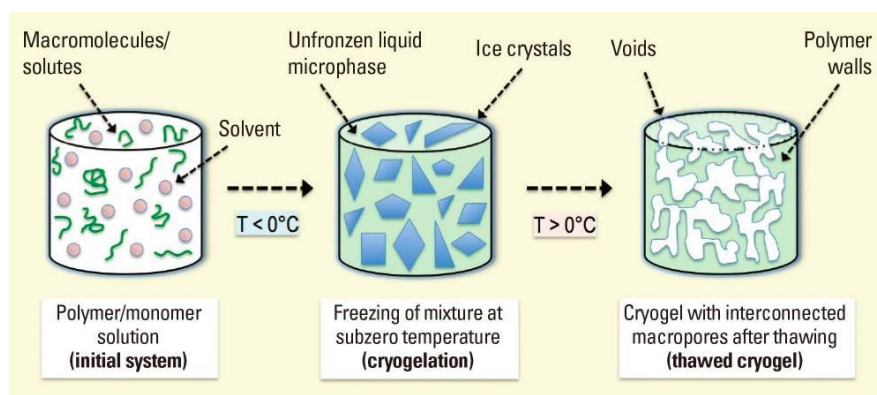


Figure 1.14. Schematic illustration showing different stages involved during cryogel formation. Reprinted from [80].

Cryogels have been widely explored for various biotechnological applications such as tissue engineering and regenerative medicine owing to their macroporous structure, as well as superior mechanical properties [81]. Sanyal et al. fabricated PEG-based bulk hydrogels and cryogels with amine reactive linkage for drug conjugation [84]. The anticancer drug doxorubicin was conjugated through a carbamate linker, and release was studied at neutral and acidic pH. About 7 fold increase in drug release was observed for cryogels compared to hydrogels, due to their high ability to swell and high porosity (Figure 1.15).

Sections above unambiguously demonstrate the powerful role played by crosslinked polymeric materials such as hydrogels in addressing challenges in various biomedical areas ranging from diagnostics to therapy. Furthermore, hydrogel materials span a large dimensional space starting from nanogels to bulk hydrogels. Fabrication of hydrogel materials in each of these dimensions with properties suitable for particular applications necessitates development of novel methodologies and chemistries. In spite of advances to date, as illustrated in the abovementioned examples, the design of smart hydrogel materials is still at its infancy. In this thesis, fabrication of various novel nanogels and cryogels for therapeutic and biomolecular protein sensing applications are undertaken to advance the current state of the art.

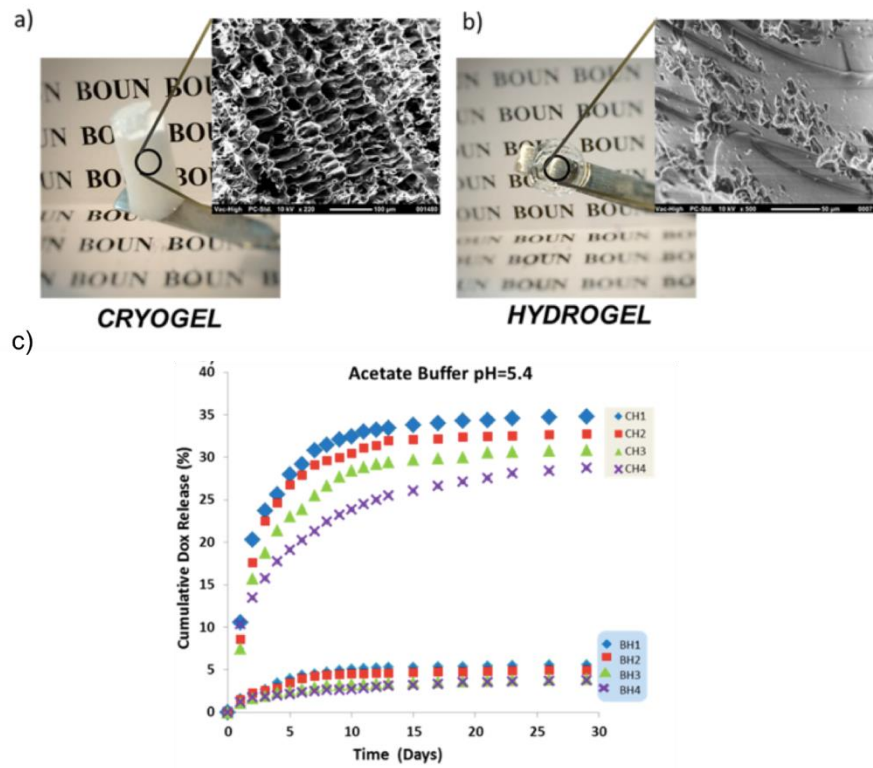


Figure 1.15. Illustrations of (a) cryogel and (b) hydrogel, and their microstructures using SEM, c) In vitro doxorubicin release profile from cryogels (CH) and bulk gels (BH) in acetate buffer pH=5.4. Reprinted from [84].

## 2. RESEARCH OVERVIEW

This thesis encompasses five research projects related to the design and fabrication of polymeric constructs for biomedical applications. The aim has been accomplished through the fabrication of two different kinds of crosslinked polymeric platforms: nanogels and macroporous cryogels.

Approaches involve utilization of functionalizable monomers or copolymers to obtain gels in the range of nanometric to bulk size using different gelation methodologies. Maleimide and hydroxyl-containing nanogels for theranostic applications were obtained using *in-situ* polymerization, as well as self-assembly of amphiphilic copolymers. The nanogel were designed to contain a pH sensitive carbamate bond for the controlled released of chemotherapeutic agent as well as maleimide groups for equipping with a targeting ligand for enhanced cellular internalization. The methodology developed here was adapted to obtain porphyrin-containing nanogels using click-chemistry between an azide-bearing copolymers and a tetra-alkyne bearing porphyrin to obtain constructs applicable toward photodynamic and photothermal therapy. In subsequent part of the thesis, rGO-embedded cryogels capable of undergoing photothermal heating were fabricated. While the hydrogels could be loaded with antibiotics through simple non-covalent encapsulation, these materials were also embedded with furan moieties to provide a handle for covalent conjugation of drugs. Release of conventional small molecule and peptide-based antibiotics under photothermal heating was investigated. Finally, thiol-reactive cryogels were fabricated for the bio-immobilization and detection of proteins. In summary, this dissertation reports on the design and synthesis of novel hydrogel materials with demonstrated applications, using advances in contemporary organic and polymer chemistry.

### 3. FABRICATION OF *IN SITU* NANOGELS FOR DRUG DELIVERY AND IMAGING

#### 3.1. Introduction

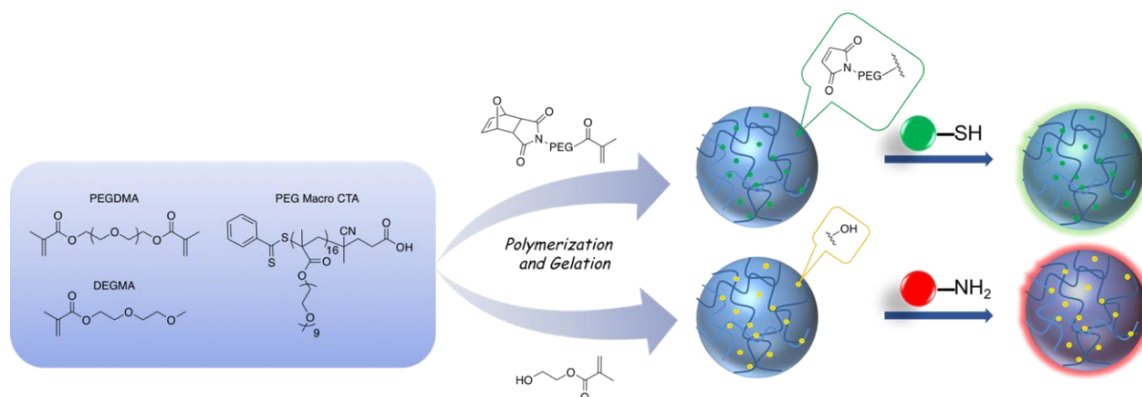
Nanogels can be fabricated following one of the two main approaches. The first method involves heterogeneous polymerization of monomers synthesizing nanogels from polymeric precursors, and the second method uses self-assembly of amphiphilic copolymers while heated above their LCST and crosslinked into nanogels using functional crosslinkers [84, 85]. However, in order to obtain cross-linked gels within the nanometric range, surfactants are often needed, which can be challenging to completely remove after gel formation and can lead to undesirable toxicity [86, 87]. Synthesis of water-dispersible nanogels is often achieved by using polymerization in an inverse microemulsion created using a two phase system and surfactants [88]. Another widely used approach to form nanogels employs crosslinking of polymers in emulsions, instead of monomers thus circumventing any concerns of toxicity from leftover monomers [89]. Despite the advantages of using surfactants to achieve well controlled narrow size distributions, complete removal of surfactants can be challenging. Needless to say, efficient crosslinking chemistry is important for fabrication of nanogels in a controlled manner.

An and coworkers were able to synthesize nanogels that are biocompatible with a thermosensitive core shell using aqueous dispersion polymerization also called *in-situ* polymerization [90]. Di-(ethylene glycol) methyl ether methacrylate (DEGMA) and poly(ethylene glycol) methyl ether methacrylate (PEGMA) were polymerized to form nanogels using reversible addition-fragmentation chain transfer (RAFT) polymerization. Linear PEG chain or grafted PEG chain were utilized and the morphology of the obtained constructs were investigated.

Indeed, RAFT polymerization enables the formation of high molecular weight amphiphilic polymers and when used in aqueous dispersion polymerization, it allows fabrication of nanoparticles using amphiphilic diblock copolymers [91-94]. Recent synthetic advances in polymerization-induced self-assembly (PISA) allow formation of spherical and worm-like micelles or vesicles composed of well-defined block copolymers to be prepared directly in concentrated aqueous solution via either RAFT dispersion or emulsion polymerization [95, 96]. Among the several methods used for the preparation of nanogels, surfactant-free, RAFT-mediated dispersion/precipitation polymerization using hydrophilic macromolecular chain transfer agents (Macro-CTAs) can efficiently generate nanogels with controlled core/shell architecture in water, with high solids content.

In this work, we report our preliminary study on RAFT dispersion copolymerization of PEGMEMA, and a hydroxyl containing monomer HEMA, as well as a thiol-reactive maleimide-containing monomer, namely FuMaMA. Ethanol is selected as the minor solvent to act as a cosolvent, because of its low toxicity, and ability to solubilize various hydrophobic comonomers. As no nanogels could be obtained using the cosolvent system, a hydrophilic PEG-containing furan-protected maleimide monomer (PEGFuMaMA) was synthesized to circumvent the use of solvent mixtures.

Nanogels functionalized with hydroxyl group were fabricated and modified to enable conjugation of a cancer drug, doxorubicin, through formation of a carbamate bond. A second construct was fabricated using the PEGFuMaMA monomer to obtain maleimide-containing nanogels. The later was functionalized with a thiolated fluorescent dye using the thiol-ene reaction (Scheme 3.1).



Scheme 3.1. Polymerization, gelation and functionalization of hydroxyl and maleimide-containing monomers.

## 3.2. Experimental

### 3.2.1. Materials

Poly(ethylene glycol) methyl ether methacrylate ( $M_n = 300 \text{ g mol}^{-1}$ , PEGMEMA, 99%, SigmaAldrich), 2-hydroxyethyl methacrylate (HEMA, 98%, SigmaAldrich), Poly(ethylene glycol) methacrylate ( $M_n = 360 \text{ g mol}^{-1}$ , PEGMA, 99%, SigmaAldrich), di(ethylene glycol) methyl ether methacrylate (DEGMA, 95%, SigmaAldrich), Poly(ethylene glycol) dimethacrylate ( $M_n=550 \text{ g mol}^{-1}$ , PEGDMA, SigmaAldrich) are passed through basic alumina column to remove inhibitor. 2,2'-azobis(2-methylpropionitrile) (AIBN), 4-cyano-4(phenylcarbonothioylthio)pentanoic acid (>97%), 4,4'-Azobis(4-cyanovaleric acid), (ACVA,  $\geq 75\%$ ), 4-aminobutyric acid were from Sigma-Aldrich unless otherwise stated and used as received. The dialysis bags (Spectra/Por Biotech Regenerated Cellulose Dialysis Membranes, MWCO 3.5 kDa) were purchased from Spectrum Laboratories. BODIPY-SH, furan-protected maleimide-containing monomer, furan-protected maleimide acid (FuMaCOOH) and the PEG-CTA were synthesized according to the literature [37, 98, 99, 91]. Column chromatography was performed using Silicagel-60 (43–60  $\mu\text{m}$ ) and thin layer chromatography was performed by using silica gel plates (Kiesel gel 60 F254, 0.2 mm, Merck).

### 3.2.2. Methods

NMR spectra were recorded using a 400 MHz Bruker spectrometer at 25 °C. Measurements were taken in deuterated chloroform (CDCl<sub>3</sub>) or deuterated DMSO (DMSO-d<sub>6</sub>). The molecular weights of the copolymers were estimated by gel permeation chromatography using a PSS-SDV column (Gram linear, length/ID 8 × 300 mm, 10 μm particle size) calibrated with poly(methyl methacrylate) standards (1–175 kDa) using a refractive-index detector. Dimethylacetamide (DMAC) was used as eluent at a flow rate of 1 mLmin<sup>-1</sup> at 30 °C. Fourier transform infrared (FTIR) spectra were obtained using a Thermo Scientific Nicolet 380 FT-IR spectrometer. UV-visible spectra were collected on a Varian Cary 100 Scan UV-vis spectrophotometer. Fluorescence spectra were collected on a Varian Cary Eclipse spectrophotometer. Hydrodynamic radii of nanogels and polymers were determined from 1 mg/mL samples filtrated via 0.2 μm cellulose acetate membrane using an off-line dynamic light scattering analysis (DLS, Malvern, Zetasizer Nano ZS). Images of nanogels were obtained using a LVEM5 electron microscope system (DeLong America) in transmission electron microscopy (TEM) mode.

### 3.2.3. Synthesis of NG-DEGMA Nanogels.

The co-polymerizations of DEGMA were done in water at 70 °C using ACVA as the radical initiator and PEGDMA as the cross-linker. The molar ratio of PEG-CTA, DEGMA, PEGDMA, and ACVA was kept constant (1:150:1.6:0.4). Monomer-containing solution was then cooled down using an ice bath and was bubbled with nitrogen for 30 min to remove oxygen. Then the reaction mixture was heated to 70 °C. After several minute, degassed ACVA solution was added to the reaction mixture. Polymerization was stopped at predetermined time point and quenched by exposing the reaction mixture to air and cooling it in an ice-water bath. A turbid whitish dispersion was obtained.

#### 3.2.4. Synthesis of NG-OH Nanogels.

The copolymerization of HEMA and DEGMA was performed in water at 70 °C with ACVA as the initiator and PEGDMA as the cross-linker. The molar ratio of PEG-CTA, PEGDMA, and ACVA was kept constant (1:150:1.6:0.4) while the ratio of DEGMA and HEMA was varied. The same procedure as above was followed to obtain a turbid whitish nanoparticle solution.

#### 3.2.5. NHS Activation of Nanogels.

For the activation of the hydroxyl group, nanogels (**NG-OH**) were dispersed in THF (5mg/mL). DSC (4.25 mg, 0.0165 mmol) and Et<sub>3</sub>N (0.006 mmol) were added into nanogel solution and the solution was stirred at rt for 24 h. After the reaction, solution was centrifuged at 7000 rpm for 25 min to yield amine-reactive nanogels (**NG-NHS**). Precipitated nanogels were redispersed in THF and centrifuged to remove unreacted reagents.

#### 3.2.6. Conjugation of DOX to NHS Nanogels.

NHS-activated nanogels were dissolved in THF (5 mg/mL) and doxorubicin hydrochloride (9.6 mg, 0.0165 mmol) and Et<sub>3</sub>N (0.022 mmol) were added to this solution and the reaction mixture was stirred at 0 °C for 3 h. After the reaction, any unconjugated DOX was removed by dialysis against methanol (MWCO 3500 Da) to obtain **NG-DOX**.

#### 3.2.7. Synthesis of NG-FuMa Nanogels.

The co-polymerizations of FuMaMA and DEGMA were performed in water at 70 °C with ACVA as the initiator and PEGDMA as the cross-linker. The molar ratio of PEG-CTA, PEGDMA, and ACVA was kept constant (1:1.6:0.4) while the ratio of DEGMA and FuMaMA was varied. The same procedure as previously was followed but no nanogel could be observed.

### 3.2.8. Synthesis of PEGFuMaMA

The esterification between FuMaCOOH and PEGMA-360 was achieved in DCM at room temperature. To a solution of FuMaCOOH (125 mg, 0.498 mmol), EDC (95 mg, 0.498 mmol), DMAP (6 mg, 0.05 mmol) in DCM (5 mL) was added PEGMA-360 (90 mg, 0.249 mmol). The solution was stirred at rt under nitrogen atmosphere for 24 h. The crude was then loaded onto silica column and purified using a mixture of DCM and methanol (90:10) to obtain the compound FuMaPEGMA (100 mg, 67%). <sup>1</sup>H NMR spectrum <sup>13</sup>C NMR (CDCl<sub>3</sub>, δ) 6.52 (s, 2H), 6.13 (s, 1H), 5.55 (s, 1H), 5.26 (s, 2H), 4.30 (t, 2H), 4.22 (t, 2H), 3.75–3.42 (m, 16H), 3.55 (t, 2H), 2.84 (s, 2), 2.33 (t, 2H), 1.98 (s, 3H), 1.94 (t, 2H).

### 3.2.9. Synthesis of NG-PEGFuMa

The copolymerizations of PEGFuMaMA and DEGMA were performed in water at 70 °C with ACVA as the initiator and PEGDMA as the cross-linker. The molar ratio of PEG-CTA, PEGDMA, and ACVA was kept constant (1:150:1.6:0.4) while the ratio of DEGMA and PEGFuMaMA was varied. The same procedure as above was followed to obtain a turbid whitish solution.

### 3.2.10. Activation of Maleimide Groups of NG-PEGFuMa via the Retro Diels–Alder Reaction.

The nanogel **NG-PEGFuMa**(150 mg) was dissolved in anhydrous toluene and heated for 8 h at 110 °C to obtain the thiol-reactive maleimide containing copolymer (130 mg, 87% yield). Complete removal of the oxabicyclic group was confirmed by <sup>1</sup>H NMR analysis.

### 3.2.11. Conjugation of BODIPY-SH to Nanogels.

For the conjugation of the dye BODIPY–SH, nanogels were dispersed in THF (1 mg/mL). BODIPY-SH (0.1 mg, 0.22 μmol) and Et<sub>3</sub>N (0.22 μmol) were added into the nanogel solution and stirred at room temperature for 24 h.

After the reaction, the nanogels (**NG-PEGMa-BODIPY**) were dialyzed using a 25 kD cut-off membrane to remove any excess unreacted dye.

### 3.3. Results and discussion

#### 3.3.1. Synthesis of peg macro-CTA

To perform RAFT polymerization, a chain transfer agent (CTA) is needed. Commercially available CTA are not water soluble, therefore they need to be modified using a hydrophilic molecule such as PEG to render the construct hydrophilic and suitable for the experimental condition. A water soluble macro-CTA was synthesized according to literature protocol (Figure 3.1) [91].

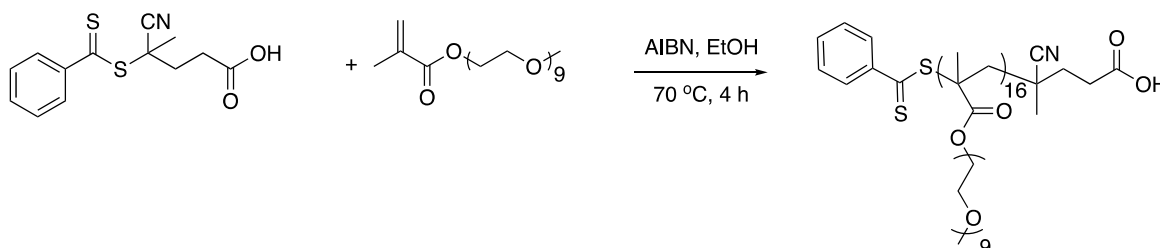


Figure 3.1. Synthesis of PEG-containing hydrophilic macro CTA.

#### 3.3.2. Synthesis of DEGMA nanogel.

In dispersion polymerization, the macro-CTAs, monomers (DEGMA and cross-linker PEGDMA) and initiator (ACVA) form a homogeneous solution in water. DEGMA and PEGMEMA are thermosensitive with the lower critical solution temperature (LCST) being 26 °C for DEGMA and in the range of 26-90 °C for their copolymers, depending on the composition [100].

During polymerization when the chain length increases beyond a critical length, the polymers aggregate and form core-shell nanoparticles at temperatures higher than their LCST. Obtained nanogels are composed of PEG as the shell and poly(DEGMA-co-PEGDMA) as the core. An average size of 63 and 24 nm was deduced from DLS and TEM, respectively (Figure 3.2). From the  $^1\text{H NMR}$  it was expected proton resonances at 4.03 ppm and 3.37 ppm belonging to  $\text{OCH}_2$  ester protons and  $\text{OCH}_3$  protons of DEGMA, respectively, confirmed the presence of both macro-CTA shell and the poly(DEGMA-co-PEGDMA) core (Figure 3.3).

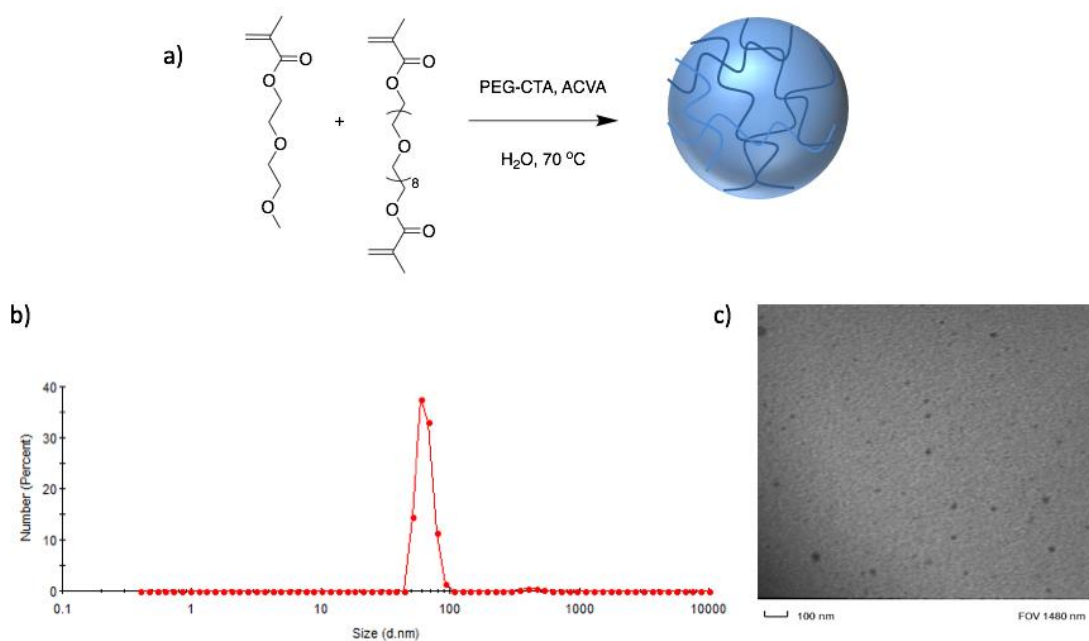


Figure 3.2. a) Synthesis of DEGMA in situ nanogel, b) Hydrodynamic radius in water at 25 °C and c) TEM images of the nanogels.

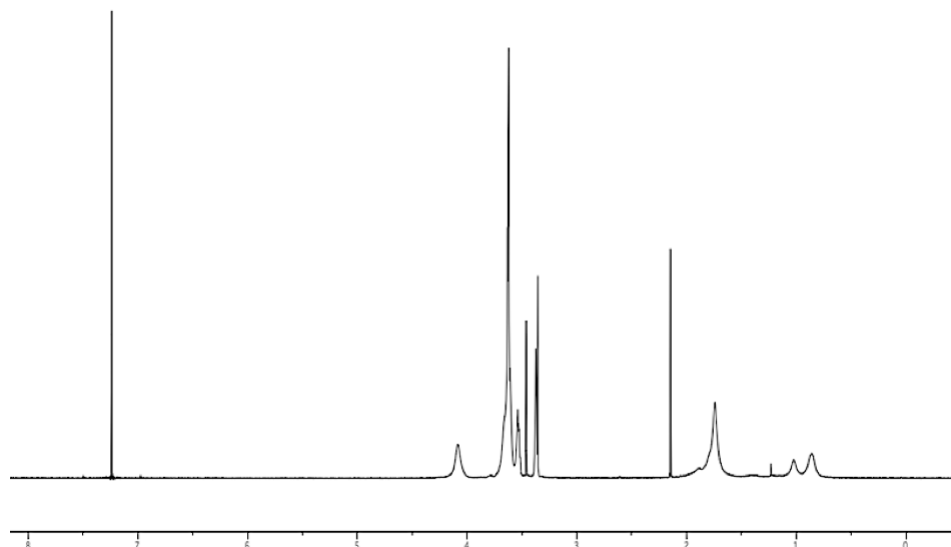


Figure 3.3.  $^1\text{H}$  NMR of NG-DEGMA nanogels.

### 3.3.3. Synthesis of HEMA nanogel

In this part, in order to introduce a functional handle a hydroxyl group containing monomers, hydroxyethyl methacrylate (HEMA) was introduced into nanogels. The hydroxyl group at the end chain will allow post-functionalization in order to add either a therapeutic agent or a dye. Previously established procedure was repeated and monomer were introduced with a predetermined feed ratio of CTA, DEGMA, HEMA and PEGDMA (1:120:40:1.6) to yield nanogels NG-OH20 with a hydrodynamic radius of 55 and 17 nm according to DLS and TEM respectively (Figure 3.4). The same experiment was repeated with a feed ratio of HEMA to DEGMA of 135:15 (NG-OH10) and 105:45 (NG-OH30). No significant change in hydrodynamic size could be observed from the DLS measurement. The presence of the  $\text{CH}_2$  group alpha to the OH group within the nanogel was confirmed using  $^1\text{H}$  NMR (singlet at 3.8 ppm) (Figure 3.5).

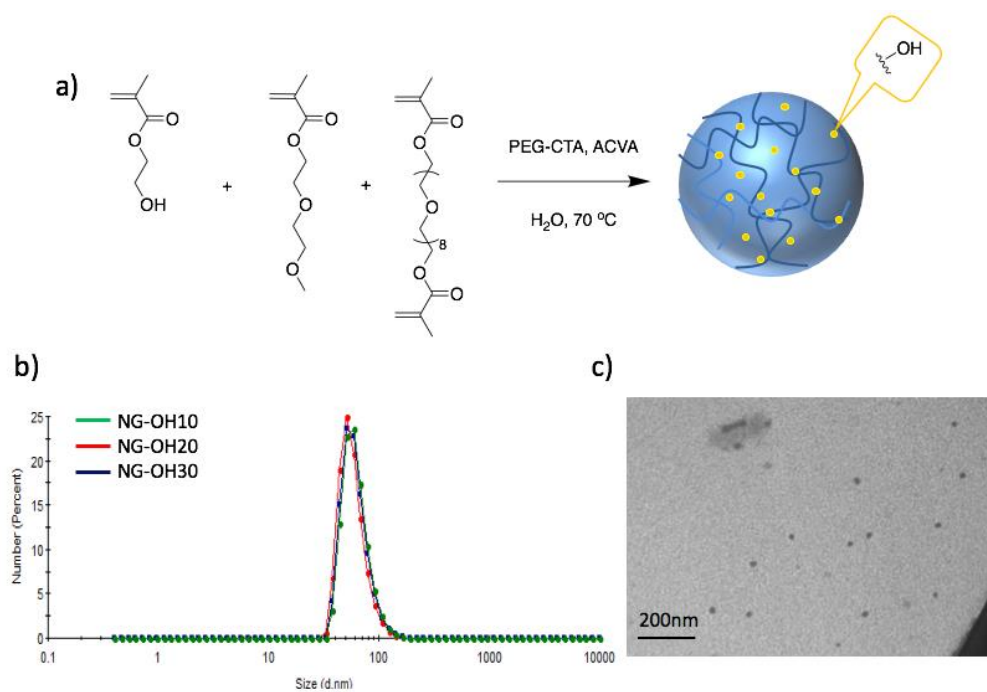


Figure 3.4. a) Synthesis of HEMA in situ nanogel, b) Hydrodynamic radius in water at 25 °C, c) TEM images of the nanogels.

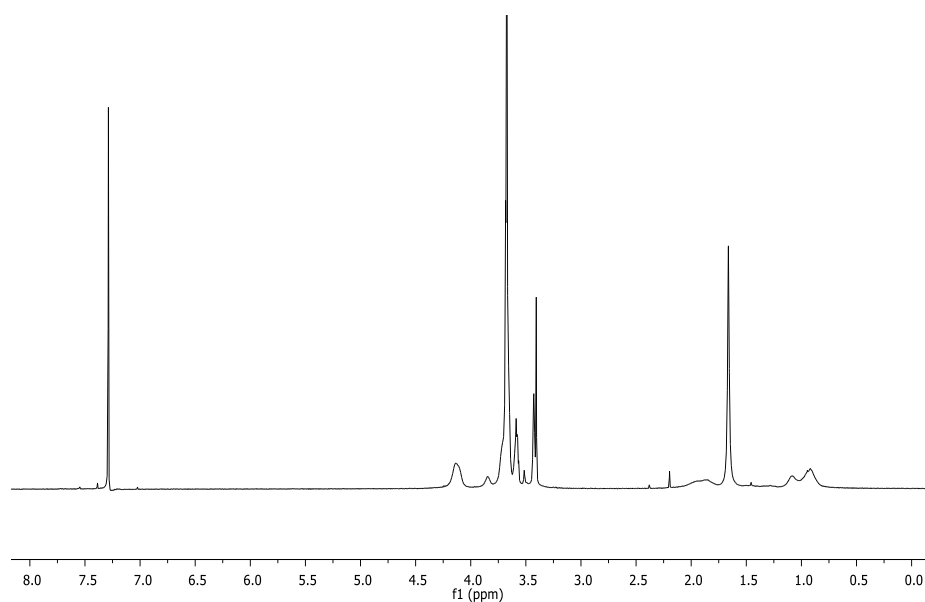


Figure 3.5.  $^1\text{H}$  NMR spectrum of NG-HEMA.

### 3.3.4. Conjugation of NHS to Nanogels.

Prior to further modification, the hydroxyl group in the nanogels was activated using *N,N'*-disuccinimidyl carbonate to obtain activated carbonate groups for facile reaction with amine-containing molecules. Activation of the hydroxyls was performed in THF at room temperature in the presence of triethylamine (Figure 3.6).

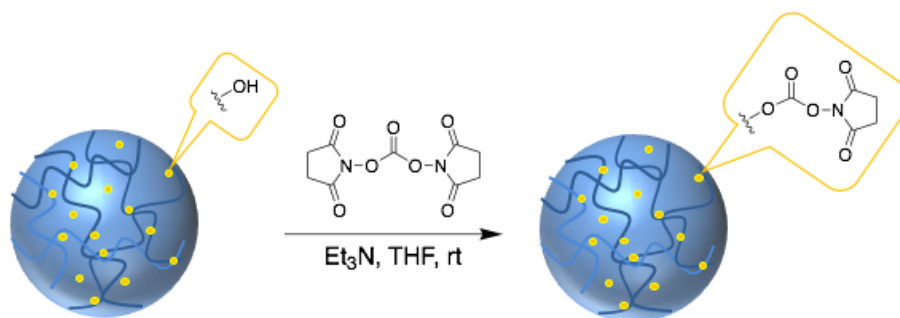


Figure 3.6. Schematic representation of conjugation of NHS to NG-OH.

### 3.3.5. Conjugation of DOX to Nanogels.

NHS-activated nanogels (**NG-NHS**) were conjugated with doxorubicin through carbamate linkages to yield dox-conjugated nanogels (**NG-DOX**). The reaction was carried out in THF at 0 °C for 3 h. The residual non-conjugated drug was removed via dialysis. Attachment of the drug was confirmed using UV-vis spectroscopy, where an absorbance due to the drug was observable at 485 nm. The amount of conjugated dox was determined as 0.118 mg dox/mg nanogels. As a control, the same procedure was repeated with non-activated nanogels (**NG-OH**) and no observable peak at 485 nm in UV-vis spectrum could be detected (Figure 3.7).

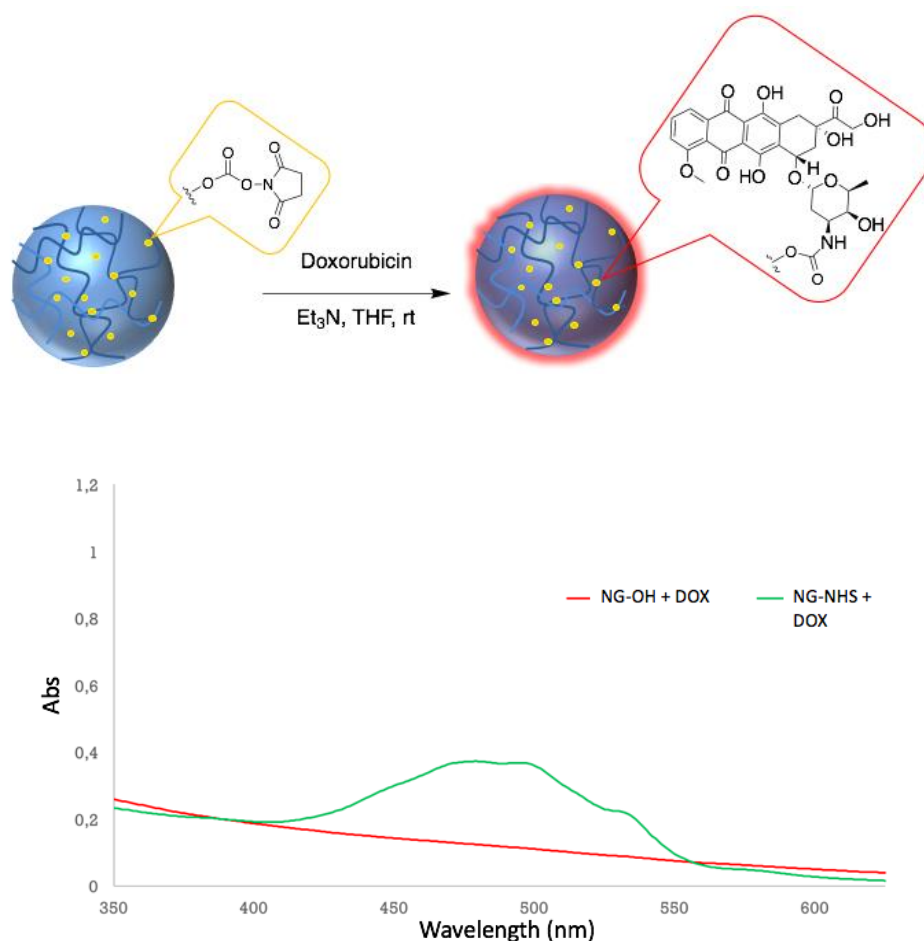


Figure 3.7. Schematic representation of attachment of Doxorubicin to NG-NHS and FTIR spectra.

### 3.3.6. Release of doxorubicin

To show the pH-sensitive nature of the carbamate linker in the nanogels, **NG-DOX** solutions were placed in dialysis bag (3.5 kDa cutoff) and immersed in 25 mL PBS buffer (pH = 7.4), and separately in an acetate buffer (pH = 5.4). At certain time intervals, a buffer aliquot was analyzed with fluorescence spectroscopy to measure the amount of released DOX. As expected, a slower release of drug was observed at neutral pH (18% over 10 days) since the drug is conjugated through a relatively stable, yet hydrolyzable carbamate linker, whereas a higher drug release was observed at lower pH (58% over 10 days) due to enhanced degradation of the carbamate group in acidic medium (Figure 3.8).

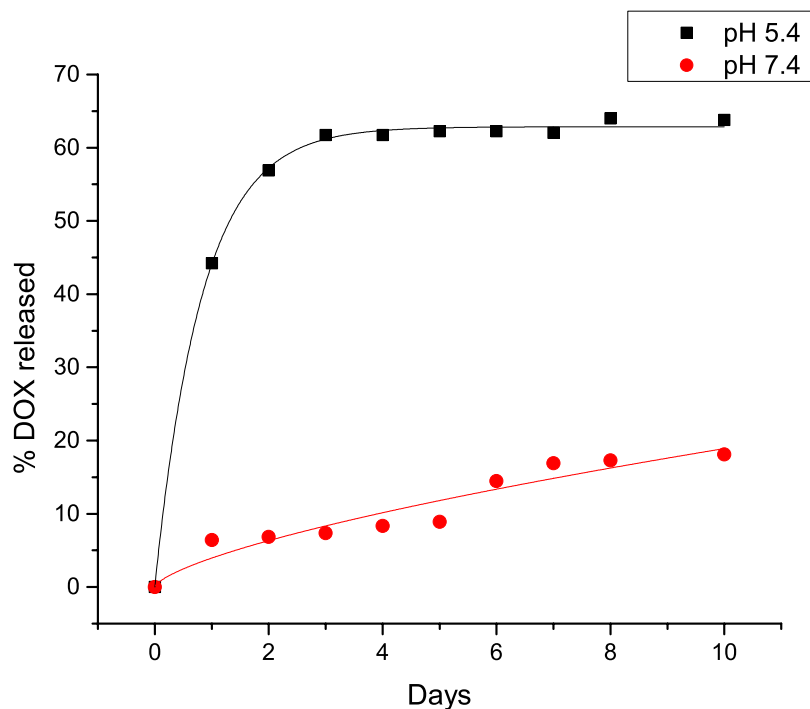


Figure 3.8. Cumulative release of doxorubicin from NG-DOX at pH 7.4 and 5.4

### 3.3.7. Synthesis of PEGFuMa nanogel

To obtain thiol reactive nanogels, incorporation of the organo-soluble furan-protected maleimide monomer, FuMaMA, was attempted. While HEMA would allow the introduction of a cleavable carbamate bond, the FuMaMA monomer after conversion to the maleimide form will provide a non-reversible conjugation handle. It is expected that the maleimide group will provide efficient conjugation of thiol-containing molecules through the thiol-maleimide click reaction. The maleimide monomer was synthesized following literature procedure previously reported by our group [98]. Nanogel formation was attempted using the procedure that was previously used to obtain the HEMA nanogels, but the solvent was changed from water to a mixture of water and ethanol since the FuMaMA monomer was not water soluble (Figure 3.9). The monomer were loaded with a feed ratio of CTA, DEGMA, FuMaMA and PEGDMA of 1:120:38:1.5 and polymerization was attempted in an EtOH/H<sub>2</sub>O mixture by varying EtOH amount from 10-90 % v/v.

Unfortunately, no nanogel could be obtained even with introduction of low amounts of EtOH. Based on our previous experiments, it can be concluded from this part that inclusion of ethanol as a co-solvent disrupts aggregate formation during polymerization.

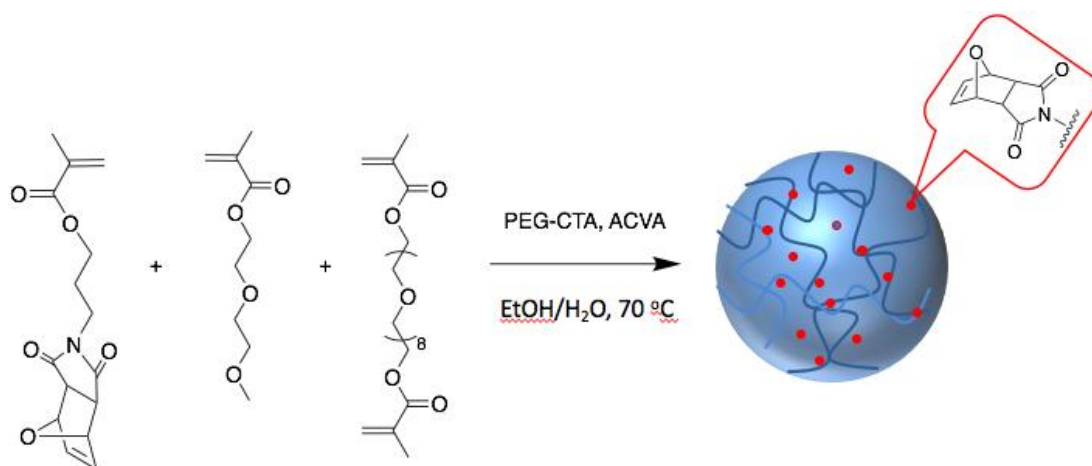


Figure 3.9. Attempted route for synthesis of NG-FuMa nanogels using the EtOH as a cosolvent.

**3.3.7.1 Synthesis of hydrophilic PEGFuMaMA monomer.** To remedy to the issue previously encountered, the maleimide monomer was modified by addition of PEG to be rendered hydrophilic, thus sidestepping the use of any co-solvent. Furan protected maleic anhydride was mixed with 4-amino butyric acid in a mixture of MeOH and THF at 50 °C for 12 h to obtain the furan-protected maleimide functionalized with an acid (FuMaCOOH). The carboxylic acid was then coupled with PEG-360 through esterification using EDC and DMAP in DCM. After purification using column chromatography, the hydrophilic FuMaPEGMA monomer was obtained in 67% yield (Figure 3.10). Peak corresponding to cycloadduct can clearly be seen on <sup>1</sup>HNMR at 6.52 and 5.26 ppm, as well as the peak corresponding to the vinylic protons on the double bond of the methacrylate units are present at 6.13 and 5.55 ppm (Figure 3.11).

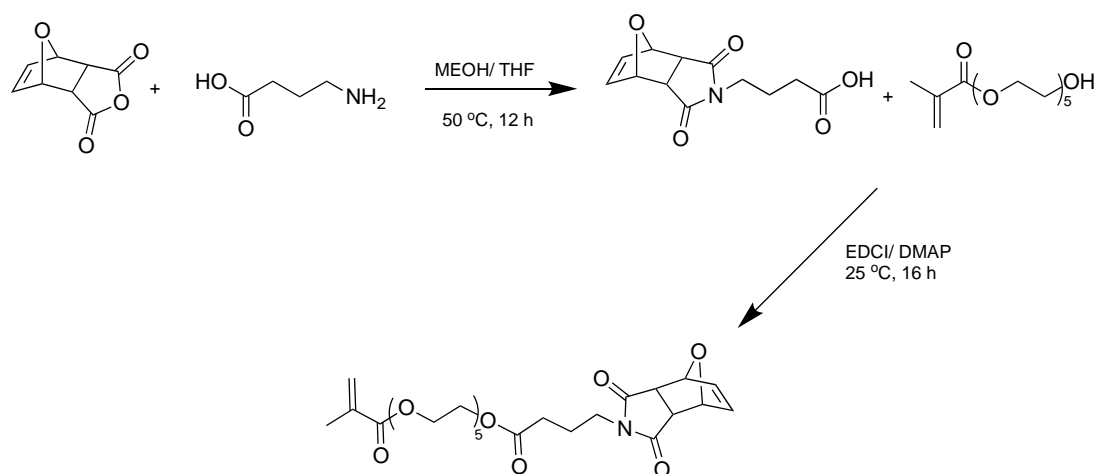
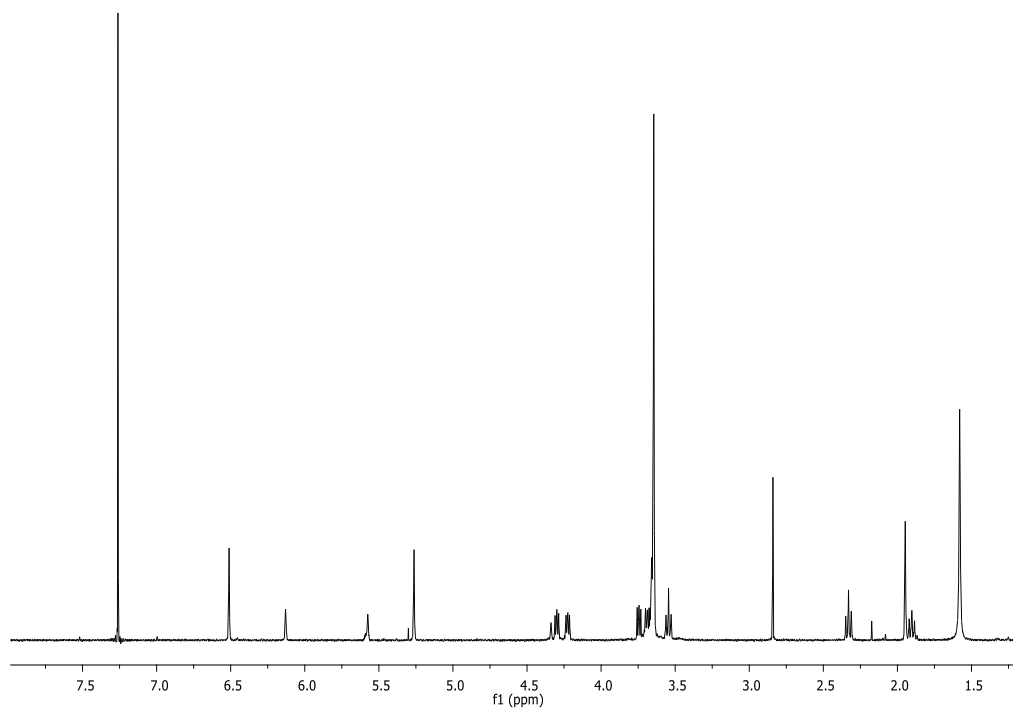


Figure 3.10. Synthesis of hydrophilic monomer PEGFuMaMA.

Figure 3.11.  $^1\text{H}$  NMR spectrum of the PEGFuMaMA monomer.

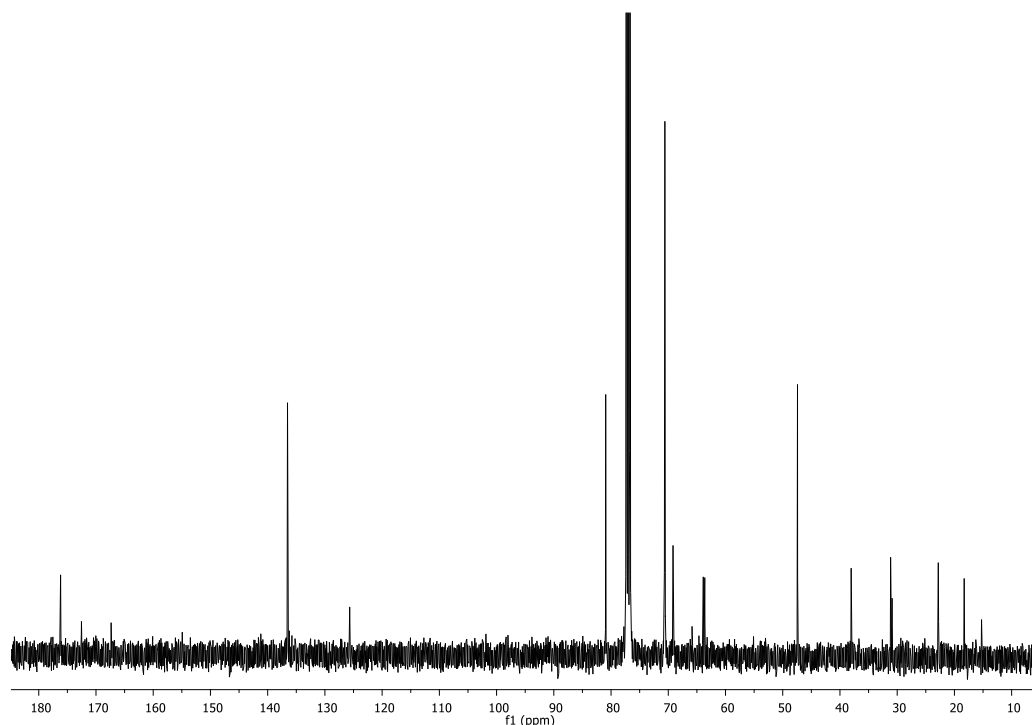


Figure 3.12.  $^{13}\text{C}$  NMR spectrum of the PEGFuMaMA monomer.

3.3.7.2. Synthesis of PEGFuMA nanogels. The same procedure that for other nanogel is repeated using the previously synthesized hydrophilic maleimide monomer PEGFuMaMA. The monomers were loaded with a feed ratio of CTA, DEGMA, PEGFuMaMA and PEGDMA of 1:120:38:1.5. The reaction was stopped after 2 hours and the reaction mixture was dialyzed using 25kD membrane and nanogels with a size of 58 and 23 nm were obtained from DLS and TEM, respectively (Figure 3.13). The peak corresponding to the cycloadduct could be observed by NMR in DMSO d6 at 6.52 and 5.26 ppm (Figure 3.14). Additional peaks that suggested presence of unreacted methacrylate units were present at 6.13 and 5.55 ppm. It is possible that the crosslinker only participates in polymerization through one of its reactive ends, since once it gets entangled in the nanogel, steric hindrances prohibit facile reaction of other end. The possibility that these methacrylate signals may arise from free residual crosslinker is minimal since nanogels were exhaustively purified using dialysis.

Moreover, the incorporation of the hydrophilic **PEGFuMaMA** monomer was not deemed to be efficient, as deduced from HNMR integration of the nanogels (Figure 3.14). Also from integration of proton resonances from PEG, it was deduced that an incorporation of **PEGFuMaMA** to 20% was achieved. Also, the ratio of unreacted methacrylate units to the oxabicyclic unit was calculated to be about 1:1.

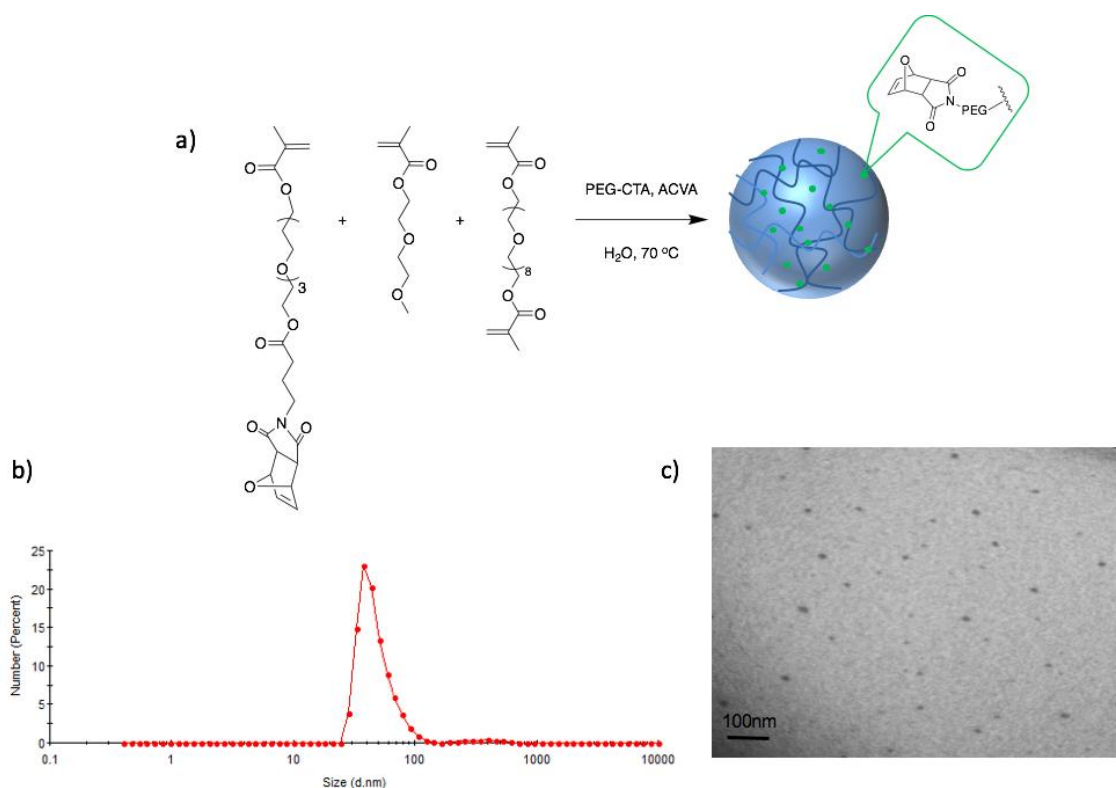


Figure 3.13. a) Synthesis of PEGFuMa in situ nanogel, b) Hydrodynamic radius in water at 25 °C obtained using DLS and c) TEM image of the nanogels.

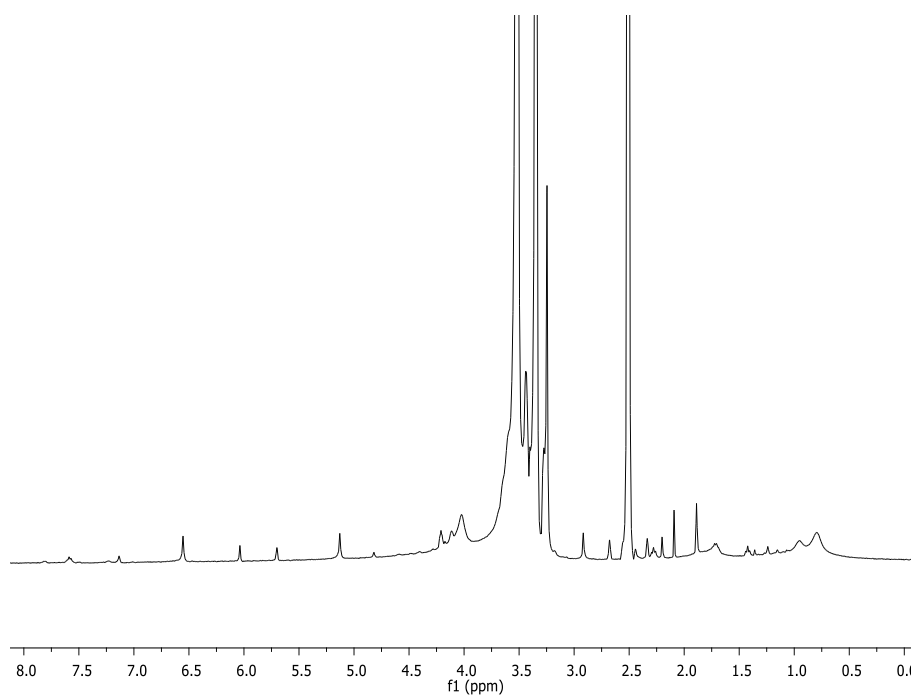


Figure 3.14.  $^1\text{H}$  NMR spectrum of NG-FuMaPEGMA nanogels.

### 3.3.8. Activation of Maleimide Functional Group

As previously mentioned, maleimide can be functionalized using the thiol-maleimide click reaction which will result in conjugation through a non-cleavable bond. In order to do so, the maleimide group must be unmasked by deprotection. The PEGFuMa nanogel was dissolved in anhydrous toluene and refluxed under a  $\text{N}_2$  atmosphere. After 8 h, the solution was cooled to room temperature and the solvent was evaporated *in vacuo* to obtain **NG-PEGMa** nanogels. Thus obtained polymer was characterized using  $^1\text{H}$  NMR. The appearance of a new peak at 6.71 ppm and disappearance of peaks at 5.25 and 6.21 ppm in the  $^1\text{H}$  NMR spectrum suggested successful cycloreversion (Figure 3.15). From the  $^1\text{H}$ NMR it was deduced that ratio of maleimide to methacrylate, stayed unchanged to 1:1, and an overall incorporation of maleimide into nanogels was limited to 20%.

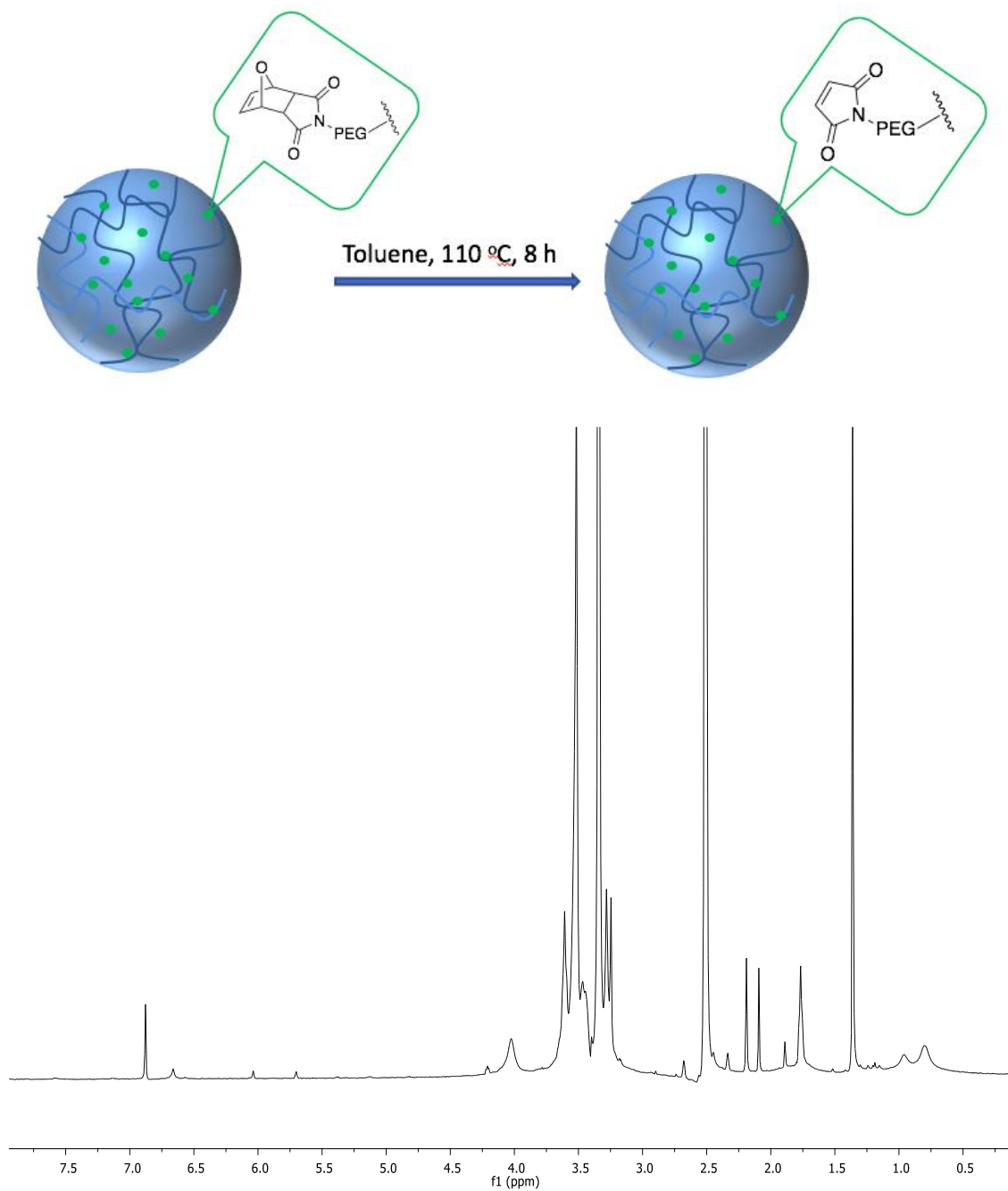


Figure 3.15. Schematic representation of deprotection of NG-PEGFuMa nanogels and <sup>1</sup>H NMR spectrum of NG-PEGMA nanogels.

### 3.3.9. Attachment of Bodipy thiol to the maleimide.

In order demonstrate that these nanogels can be transformed to imaging agents, attachment of a fluorescent dye was undertaken. The thiol-reactive maleimide site will be used for this purpose as it offers non-cleavable conjugation and will ensure the dye is not released during any diagnostic application. A highly fluorescent dye from the BODIPY fluorophore family was chosen as a model dye. A thiol-containing BODIPY dye was synthesized according to literature protocol [37]. The dye conjugation was undertaken at room temperature in THF, in the presence of Et<sub>3</sub>N as a catalyst (Figure 3.16). After removal of residual dye, successful attachment of the dye was confirmed from the presence of the characteristic absorbance of the dye at 525 nm in the UV-vis spectrum. As a control, nanogels were treated with a dye without any thiol functional group, namely, Bodipy-Br, in the presence of Et<sub>3</sub>N. As expected, no absorbance peak from the dye could be observed by UV-vis spectroscopy (Figure 3.16).

As another control, the Bodipy-SH was added to the nanogel with the protected maleimide **NG-PEGFuMa**. It was observed that under UV illumination, fluorescence could be observed for both the control **NG-PEGFuMa** and the **NG-PEGMa**, meaning the dye reacted with the deprotected maleimide as well as the protected one. The reaction between the **NG-PEGFuMa** and the thiolated dye is believed to be happening due to the presence of double bond left from the methacrylate from the **PEGFuMaMA** monomer. Indeed, it can be noticed from the NMR spectra, that there are unreacted methacrylate peak at 6.13 and 5.55 ppm (Figure 3.15). Furthermore, this thiol Michael addition reaction has been widely used in bioengineering, including cell encapsulation, controlled drug delivery, and degradable hydrogels applications.

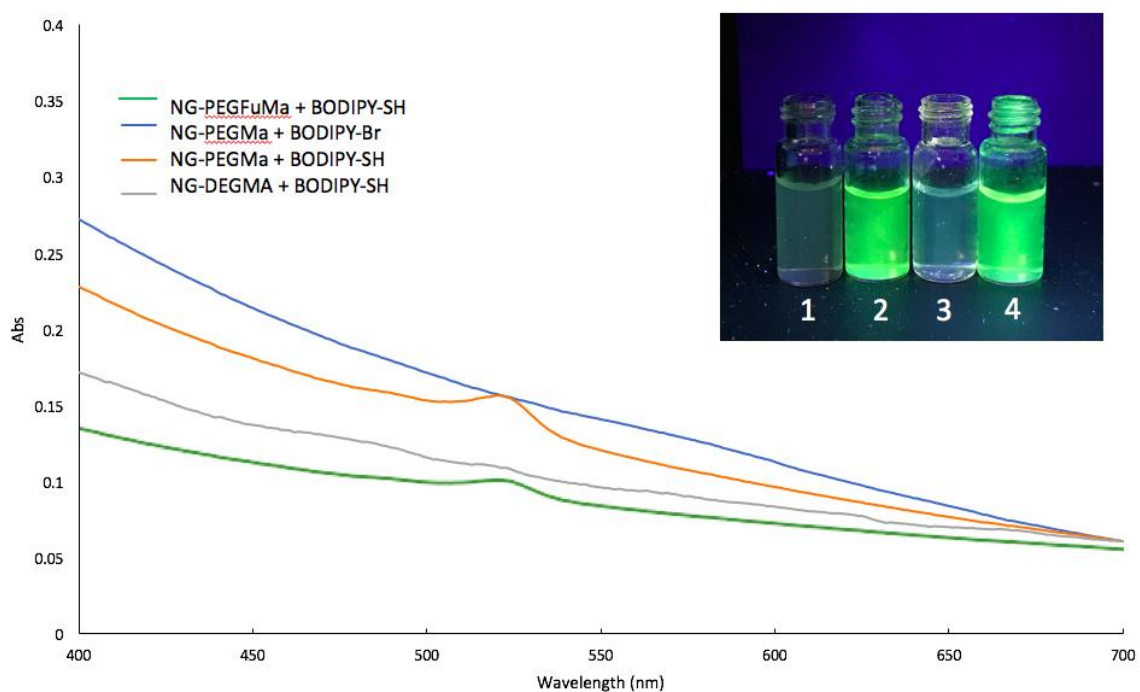
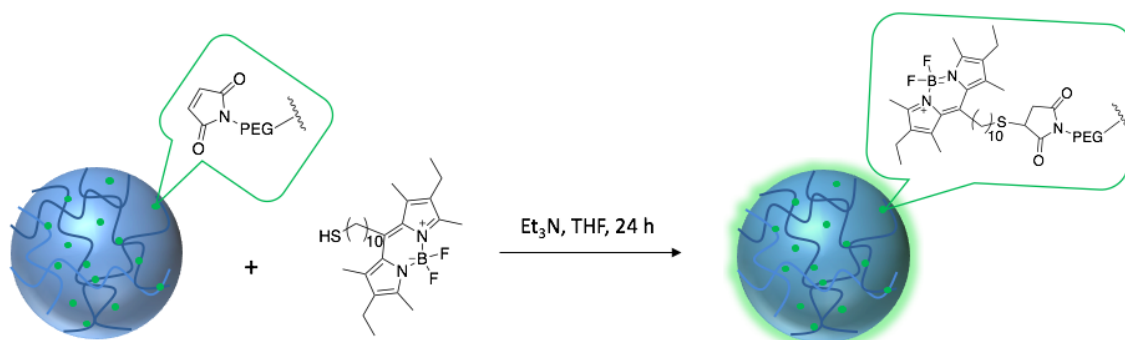


Figure 3.16. Schematic representation of BODIPY attachment to NG-PEGMA, UV spectra of Bodipy attachment to nanogels, picture of 1) NG-DEGMA+BODIPY-SH, 2) NG-PEGMa+BODIPY-SH, 3) NG-PEGMa+BODIPY-Br, 4) NG-PEGFuMa+BODIPY-SH

### 3.4. Conclusion

In conclusion, a variety of nanogels were obtained using aqueous dispersion polymerization. Nanogels containing hydroxyl functional group were obtained and their activation to bear amine-reactive activated carbonate groups was established. These reactive nanogels could be functionalized with amine-containing drug such as doxorubicin. Drugs conjugated onto the nanogels through the acid sensitive carbamate group showed a pH dependent release. Thereafter, nanogels comprised of hydroxyl and maleimide functional groups were targeted so that post-activation of the hydroxyl groups, nanogels with amine and thiol reactivity could be obtained. For this purpose, a hydrophilic furan-protected maleimide-containing methacrylate monomer was synthesized. Unfortunately, incorporation of this monomer into nanogels was not very efficient.

Nonetheless, obtained nanogels were functionalized with thiol-containing fluorescent dye to demonstrate their functionalization. Due to challenges in incorporating the thiol-reactive maleimide group in high amounts within the nanogels, an alternative experimental protocol was investigated. Crosslinking of reactive hydrophilic copolymers instead of reactive monomers was pursued, as outlined in the subsequent chapter of this thesis.

## **4. MULTIFUNCTIONAL NANOGELS AS THERANOSTICS PLATFORMS: EXPLOITING REVERSIBLE AND NON- REVERSIBLE LINKAGES FOR TARGETING, IMAGING AND DRUG DELIVERY**

Adapted with permission from {Chambre, L., Degirmenci, A., Sanyal, R. and Sanyal, A., “Multifunctional Nanogels as Theranostic Platforms: Exploiting Reversible and Non-reversible Linkages for Targeting, Imaging and Drug Delivery”, *Bioconjugate Chemistry*, 2018, 29, 1885-1896.}

### **4.1. Introduction**

Nanocarriers engineered with the ability to simultaneously detect as well as treat diseases are expanding the versatility of therapeutic platforms available for nanomedicine. Indeed, the field of nanotheranostics has attracted a lot of interest since it offers the possibility of delivering the drug while simultaneously monitoring its localized delivery and therapeutic response. Among the various available theranostic platforms as discussed below, polymer-based nanomaterials, due to their excellent biocompatibility, degradability, and structural and compositional versatility are promising building blocks for construction of multi-functional theranostic agents [102,103].

To date, numerous nanosized delivery vehicles have been studied for theranostic purposes [104,105]. For example, chemotherapeutic agents have been conjugated onto magnetic nanoparticles since these particles enable magnetic resonance imaging, as well as onto gold nanoparticles and quantum dots (QDs), because of intrinsic fluorescence of these nano particles [106-110].

While these materials have been extensively studied, their inorganic or metallic nature has raised concern about their toxicity and their excretion from the body [109]. Oftentimes these materials are coated with polymers to increase their biocompatibility and make them suitable for biological applications. Also, the polymeric coating enables attachment of targeting groups and therapeutic agents on an otherwise inert scaffold with limited room for chemical modifications.

As an alternative, polymeric nanomaterial such as hyperbranched polymers, and nanogels offer an inherently biocompatible platform that can be readily rendered multi-functional [111,112]. In this regard, polymer-based carriers have been widely studied for cancer therapy and offer several advantages such as enhanced efficacy, prolonged circulation half-life, and sustained or triggered drug release [113-116]. Due to their size range in tens of nanometers, polymeric nanoparticles are also able to accumulate at specific disease sites through passive targeting via the enhanced permeability and retention effect (EPR) [117-119]. Additionally, internalization in cancer cells can be further enhanced through active targeting by the incorporation of targeting ligands specific for an overexpressed receptor [115,120-125].

Recent years have witnessed the extension of polymeric nanoparticles beyond simple delivery vehicles through incorporation of clinically relevant imaging modalities such as magnetic resonance imaging (MRI), positron emission tomography (PET), and fluorescent agents [126]. Over the past decade, nanogels have been evaluated for applications such as drug delivery, tissue engineering, protein encapsulation and release, and bioimaging [30-33]. Their high degree of stability and facile dispersibility makes them attractive delivery platforms. Furthermore, the ability to fabricate nanogels with diverse chemical compositions allows incorporation of various functional groups to enable covalent modifications with various molecules of interest such as drugs, biomolecules, and imaging agents.

Nanogels can be obtained either through an in situ simultaneous polymerization and cross-linking of hydrophilic monomers, or via cross-linking of hydrophilic copolymers containing reactive functional groups with appropriate cross-linkers [37, 92].

The latter approach offers increased versatility since a wide range of well-defined compositionally diverse copolymers can be synthesized using various controlled polymerization techniques. In order to obtain cross-linked gels with their sizes in the nanometric regime, surfactants are often needed, which can be difficult to completely remove after gel formation and can eventually display toxicity.

In order to obtain nanogels with good control through cross-linking of preformed copolymers, efficient crosslinking methods should be used. Since the advent of “click chemistry”, efficient transformations such as the azide–alkyne cycloaddition, and nucleophilic and radical thiol–ene reactions have been employed for effective cross-linking to obtain bulk hydrogels, microgels, and nanogels [63,127-132]. As an attractive alternative to employing surfactants, self-assembly of amphiphilic random copolymers can also serve as a facile approach to form stable aggregates in aqueous solutions that can be cross-linked later on. As a seminal contribution, Thayumanavan and co-workers reported synthesis of nanogels by exploiting the lower critical solution temperature (LCST) driven self-assembly of thermoresponsive copolymers. Polymer were heated above their LCST to form stable aggregates that were then cross-linked using the thiol–disulfide exchange reaction provide nanogels able to hold hydrophobic cargo and transport them into cells [133-134]. In another example, Oh and coworkers obtained nanogels using a disulfide based cross-linking of PEGMEMA grafted cellulose polymers [135]. Using similar temperature-induced self-assembly of thermoresponsive copolymers, our group reported synthesis of nanogels which were amenable to functionalization using the thiol–maleimide conjugation [37].

Survey of nanogels fabricated to date reveals that while most of these platforms are efficiently fabricated using click-type reactions, their subsequent functionalizations are mostly limited to nonreversible conjugations by subsequent utilization of the reactions used for cross-linking. Design and synthesis of nanogels with different reactive groups that would enable their modification through nonreversible as well as reversible degradable conjugations will expand their methods of multi-functionalization. While the nonreversible conjugation can be harnessed for robust attachment of imaging and targeting agents, the degradable linkers can be used for conjugation of drugs that can be transported as stable conjugates to the disease site and then released after cellular internalization.

In order to obtain effective theranostic platforms, nanogels should be readily functionalizable in an effective manner under mild conditions. Amine and thiol functional groups are among the most commonly employed functional groups for conjugations. The thiol–maleimide conjugation reaction proceeds with very high efficiencies under mild reaction conditions, oftentimes without the need for an additional catalyst. Due to its mild reaction conditions and high efficiency, a maleimide group is widely used for thiol conjugation [69,74,136,137]. Until recently, the utilization of this thiol reactive group in polymeric materials was limited since the electron deficient double bond of the maleimide unit is consumed during polymerization. Synthetic strategies which utilize the protection of the maleimide group through the Diels–Alder reaction with furan during the polymerization, followed by its unmasking via the retro Diels–Alder reaction, allows one to circumvent this problem. In recent years, this methodology has been used to synthesize several water-soluble thiol-reactive copolymers [138-145]. The robust nature of the thiol–maleimide conjugate makes it ideal for conjugation of targeting as well as imaging agents to polymeric constructs.

The conjugation of therapeutic agents to polymeric carriers should be through linkages stable enough to avoid premature release of drug during transport but be labile under certain conditions such as high pH or reducing conditions encountered upon reaching tumor tissues or upon cellular internalization [146,147]. Esters, carbamates, and certain amide linkages are among the most utilized for drug conjugation. Among these, the carbamate linker allows slow release of covalently attached molecules, but is more stable than ester, yet more easily hydrolyzable than amides [148-150]. Amine-containing drugs such as doxorubicin can be readily conjugated through carbamate linkages using activated carbonate functional groups as reactive handles [85].

Hence, nanogels containing both thiol-reactive maleimide and amine-reactive activated carbonate units would be attractive drug delivery vehicles since they can be conjugated through both nonreversible and reversible linkages. In this study, doxorubicin (DOX), a commonly used chemotherapeutic agent, is employed, but the platform developed is suitable for any amine group containing drug.

In this work, we disclose the design and synthesis of poly(ethylene glycol) (PEG) based nanogels amenable to facile multi-functionalization. Utilization of thiol–maleimide and carbamate chemistry yields a construct capable of drug delivery via active targeting, with additional possibility of incorporating an imaging agent (Figure 4.1). Copolymers containing maleimide, hydroxyl, and PEG groups as side chains were synthesized using reversible addition–fragmentation chain transfer (RAFT) polymerization. Nanogels were obtained through thermoresponsive self-assembly of these copolymers into nanoaggregates, followed by subsequent cross-linking via thiol-maleimide click reaction between dithiol based crosslinker and maleimide groups on the copolymers. The crosslinked nanogels were functionalized with thiol or maleimide bearing dye, conjugated with a drug through carbamate linkage and finally conjugated with a thiol-containing peptide based I ligand to increase selectivity of the construct. In particular, to achieve imaging and drug release via active targeting, the nanogels were modified with the chemotherapeutic drug doxorubicin and cRGDfC peptide, a targeting group with affinity for integrin receptors overexpressed in many cancer cells [151].

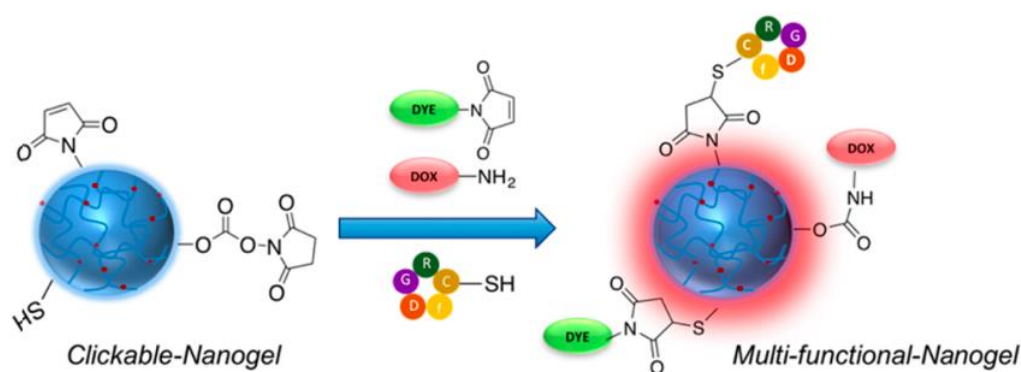


Figure 4.1. Schematic illustration of multi-functionalization of nanogels.

## 4.2. Experimental

### 4.2.1. Materials

Poly(ethylene glycol) methyl ether methacrylate ( $M_n = 300 \text{ g mol}^{-1}$ , PEGMEMA, 99%, SigmaAldrich) and 2-hydroxyethyl methacrylate (HEMA, 98%) are passed through basic alumina column to remove inhibitor. 2,2'- (Ethylenedioxy)diethanethiol, (95%), triethylamine (>99%, Merck), N,N'-disuccinimidyl carbonate (DSC, >95%), Nethylmaleimide (98%, Alfa Aesar), 2-mercaptoethanol (>99%, Merck), 5,5'-dithiobis (2-nitrobenzoic acid) (DTNB, >98%), tris-HCl (>99%), 2,2'-azobis(2-methylpropionitrile) (AIBN), and 4-cyano-4-(phenylcarbonothioylthio)pentanoic acid (RAFT CTA, >97%) were from Sigma-Aldrich unless otherwise stated and used as received. The cyanine5 maleimide (Cy5 maleimide) was procured from Lumiprobe. The dialysis bags (Spectra/Por Biotech Regenerated Cellulose Dialysis Membranes, MWCO 3.5 kDa) were purchased from Spectrum Laboratories. BODIPY-SH, furan-protected maleimide-containing monomer, and cyclic peptide cRGDfC were synthesized according to the literature [37,99,150]. Column chromatography was performed using Silicagel-60 (43–60  $\mu\text{m}$ ) and thin layer chromatography was performed by using silica gel plates (Kiesel gel 60 F254, 0.2 mm, Merck). Pierce BCA (bicinchoninic acid) Protein Assay Kit was used for peptide assay (Thermo Fischer Scientific). Human breast adenocarcinoma MDA-MB-231 cell line were obtained from ATCC (Virginia, US). The cells were maintained in RPMI-1640 culture medium (Roswell Park Memorial Institute) (Gibco, Invitrogen) supplemented with 10% fetal bovine serum (FBS) (Lonza), 100 U/mL penicillin, 100 g/mL streptomycin, 0.25 g/mL, 5% CO<sub>2</sub>, and 95% relative humidity. DAPI and Cell Counting Kit-8 (CCK-8) were obtained from Sigma-Aldrich.

### 4.2.2. Methods

NMR spectra were recorded using a 400 MHz Bruker spectrometer at 25 °C. Measurements were taken in deuterated chloroform (CDCl<sub>3</sub>). The molecular weights of the copolymers were estimated by gel permeation chromatography (GPC, Shimadzu).

Using a PSS-SDV column (Gram linear, length/ID  $8 \times 300$  mm,  $10 \mu\text{m}$  particle size) calibrated with poly(methyl methacrylate) standards (1–175 kDa) using a refractive-index detector. Dimethylacetamide (DMAC) was used as eluent at a flow rate of  $1 \text{ mL min}^{-1}$  at  $30 \text{ }^\circ\text{C}$ . Fourier transform infrared (FTIR) spectra were obtained using a Thermo Scientific Nicolet 380 FT-IR spectrometer. UV–visible spectra were collected on a Varian Cary 100 Scan UV–vis spectrophotometer. Fluorescence spectra were collected on a Varian Cary Eclipse spectrophotometer. Hydrodynamic radii of nanogels and polymers were determined from  $1 \text{ mg/mL}$  samples filtrated via  $0.2 \mu\text{m}$  cellulose acetate membrane using an off-line dynamic light scattering analysis (DLS, Malvern, Zetasizer Nano ZS). Molecular weights of nanogels were determined using static light scattering (SLS, Malvern, ZetasizerNano ZS). A  $dn/dc$  value ( $0.136 \text{ mL/g}$ ) for linear PEG was used as an approximation. Images of nanogels were obtained using a LVEM5 electron microscope system (DeLong America) in transmission electron microscopy (TEM) mode. Cell viability results of cytotoxicity experiments were determined via measuring the absorbance of 96-well plates at  $450 \text{ nm}$  using Multiscan FC Microplate Photometer from Thermo Scientific equipped with a quartz halogen light source of excitation wavelength range  $340\text{--}850 \text{ nm}$  with excitation filters installed at  $405$ ,  $450$ , and  $620 \text{ nm}$ . Cell internalization experiments were performed with Zeiss Observer Z1 fluorescence microscope connected to AxioCam MRc5 using a Zeiss filter set 38 (excitation BP  $470/40$ , emission BP  $525/50$ ) for imaging the cells and Zeiss filter set 49 (excitation G365, emission BP  $455/50$ ) was used for imaging DAPI stained nuclei. Images were processed to visualize cell nuclei and morphology using Zeiss AxioVision software. Statistical relevance of data analysis was carried out using ANOVA followed with Tukey's Multiple Comparison Test in GraphPad Prism Software.

#### **4.2.3. Synthesis of Furan-Protected Maleimide-Containing Copolymer**

Furan-protected maleimide-containing methacrylate (FuMaMA) monomer ( $63 \text{ mg}$ ,  $0.216 \text{ mmol}$ ), HEMA ( $56 \text{ mg}$ ,  $0.430 \text{ mmol}$ ), PEGMEMA ( $450 \text{ mg}$ ,  $1.5 \text{ mmol}$ ), RAFT CTA ( $4 \text{ mg}$ ,  $0.0143 \text{ mmol}$ ), and AIBN ( $0.50 \text{ mg}$ ,  $0.003 \text{ mmol}$ ) were dissolved in DMF ( $2 \text{ mL}$ ) and placed in a sealed round-bottom flask equipped with a magnetic stir bar. The reaction mixture was purged with  $\text{N}_2$  for  $15 \text{ min}$  and stirred at  $70 \text{ }^\circ\text{C}$  for  $24 \text{ h}$ . After the reaction, the unreacted monomers were removed by dialysis against methanol (MWCO  $3.5 \text{ kDa}$ ).

The obtained polymer was dried *in vacuo* and characterized using GPC and  $^1\text{H}$  NMR. Conversion = 79%,  $M_{n,\text{theo}} = 39765 \text{ g}\cdot\text{mol}^{-1}$ ,  $M_{n,\text{GPC}} = 30300 \text{ g}\cdot\text{mol}^{-1}$ ,  $M_w/M_n = 1.5$  relative to PMMA. The ratio of incorporated monomers in the copolymer was determined from  $^1\text{H}$  NMR spectrum as [FuMaMA]:[HEMA]:[PEGMEMA] = 1:2.2:4.9.  $^1\text{H}$  NMR ( $\text{CDCl}_3$ ,  $\delta$ ) 6.52 (s, 2H,  $\text{CH}_2\text{CH}$ ), 5.27 (s, 2H, CH bridgehead protons), 4.02 (s, 2H,  $\text{OCH}_2$  ester protons of PEGMEMA), 3.81 (s, 2H,  $\text{OCH}_2$  of HEMA), 3.75–3.42 (m, 4H,  $\text{OCH}_2$  of PEGMEMA and  $\text{NH}_2$ ), 3.39 (s, 3H,  $\text{OCH}_3$  of PEGMEMA), 2.92 (s, 2H,  $\text{CH}-\text{CH}$ , bridge protons), 2.11–0.56 (m, 7H,  $\text{NCH}_2\text{CH}_2\text{CH}_2\text{O}$ ,  $\text{CH}_2$ , and  $\text{CH}_3$  protons along polymer backbone).

#### 4.2.4. Activation of Maleimide Groups of Copolymer via the Retro Diels–Alder Reaction.

The copolymer (450 mg) was dissolved in anhydrous toluene and heated for 8 h at  $110^\circ\text{C}$  to obtain the thiol-reactive maleimide containing copolymer (420 mg, 93% yield). Complete removal of the oxabicyclic group was confirmed by  $^1\text{H}$  NMR analysis. The ratio of incorporated monomers was determined from the  $^1\text{H}$  NMR spectrum as [FuMaMA]:[HEMA]:[PEGMEMA] = 1:2.4:5.04.  $^1\text{H}$  NMR ( $\text{CDCl}_3$ ,  $\delta$  ppm) 6.78 (s, 2H,  $\text{CH}_2\text{CH}$ ), 4.03 (s, 2H,  $\text{OCH}_2$  ester protons of PEGMEMA), 3.77 (s, 2H,  $\text{OCH}_2$  of HEMA), 3.73–3.51 (m, 4H,  $\text{OCH}_2$  of PEGMEMA and  $\text{NCH}_2$ ), 3.37 (s, 3H,  $\text{OCH}_3$  of PEGMEMA), 2.21–0.62 (m, 7H,  $\text{NCH}_2\text{CH}_2\text{CH}_2\text{O}$ ,  $\text{CH}_2$ , and  $\text{CH}_3$  protons along polymer backbone).

#### 4.2.5. Synthesis of Nanogels.

In a round-bottom flask, copolymer (10 mg) was dissolved in water (1.9 mL) and heated at  $70^\circ\text{C}$  for 10 min. After 10 min, an aqueous solution of 2,2'-(ethylenedioxy)diethanethiol (0.09 mL, 16.6 mM) was added into the polymer solution. The solution was centrifuged at 7000 rpm for 25 min to remove the non-cross-linked copolymer to obtain nanogels (NG-OH) (7.6 mg, 76% yield).

#### 4.2.6. NHS Activation of Nanogel.

For the activation of the hydroxyl group, nanogels (**NG-OH**) were dispersed in THF (5 mg/mL). DSC (4.25 mg, 0.0165 mmol) and Et<sub>3</sub>N (0.006 mmol) were added into nanogel solution and the solution was stirred at rt for 24 h. After the reaction, solution was centrifuged at 7000 rpm for 25 min to yield amine-reactive nanogels (**NG-NHS**). Precipitated nanogels were redispersed in THF and centrifuged to remove unreacted reagents.

#### 4.2.7. Conjugation of DOX to NHS Nanogels.

NHS activated nanogels were dissolved in THF (5 mg/mL) and doxorubicin hydrochloride (9.6 mg, 0.0165 mmol) and Et<sub>3</sub>N (0.022 mmol) were added to this solution and the reaction mixture was stirred at 0 °C for 3 h. After the reaction, any unconjugated DOX was removed by dialysis against methanol (MWCO 3500) to obtain **NG-DOX**.

#### 4.2.8. Conjugation of BODIPY-SH to Nanogels.

For the conjugation of the dye BODIPY-SH, nanogels were dispersed in THF (1 mg/mL). BODIPY-SH (0.1 mg, 0.22 μmol) and Et<sub>3</sub>N (0.22 μmol) were added into the nanogel solution and stirred at room temperature for 24 h. After the reaction, the nanogels (**NG-DOX-BODIPY**) were centrifuged at 7000 rpm for 25 min. Precipitated nanogels were redispersed in THF and centrifuged. The process was repeated until all free dye was removed, as confirmed from the UV-vis spectrum of the supernatant.

#### 4.2.9. Conjugation of N-Ethyl Maleimide to Nanogels.

Nanogels (1 mg/mL) were dispersed in THF and *N*-ethylmaleimide (125 μg, 1 μmol) was introduced into the nanogel solution and the reaction was stirred for 24 h at room temperature. For removal of excess *N*-ethylmaleimide, nanogels were centrifuged at 7000 rpm for 25 min and dispersed in water.

#### 4.2.10. Conjugation of 2-Mercaptoethanol to Nanogels.

Nanogels conjugated with *N*-ethylmaleimide (1 mg/mL) were dispersed in degassed H<sub>2</sub>O and 2-mercaptoethanol (23 µg, 0.3 µmol) was added to the solution and stirred for 24 h at room temperature under nitrogen atmosphere. Nanogels were precipitated by centrifugation at 7000 rpm. Ellman's analysis was performed to determine the amount of unreacted thiol in the solution.

#### 4.2.11. Conjugation of cRGDfC to Nanogels.

To the nanogel (**NG-DOX**) solution (1 mL, 5 mg/mL) in water was added cRGDfC (400 µg, 0.690 µmol) and the reaction was stirred for 24 h at room temperature. For removal of the excess peptide, centrifuge and dialysis were used. After purification of the nanogels (**NG-DOX-RGD**), 100 µL of the sample was mixed with 2 mL BCA working reagent. The blue mixture was incubated for 30 min at 60 °C. After 30 min the blue mixture turned purple and its absorbance was measured at 562 nm via UV spectroscopy.

#### 4.2.12. Conjugation of Cy5 Maleimide to Nanogels.

To the nanogel (**NG-DOX-RGD**) solution (1 mL, 5 mg/mL) in degassed THF, Cy5 maleimide (25 µg, 0.039 µmol) was added and the reaction was stirred for 24 h at rt. Excess dye was removed by centrifugation at 7000 rpm for 25 min to obtain **NG-DOX-RGD-CY5**. The process was repeated until no more free Cy5 could be observed in the supernatant by fluorescence spectroscopy. Conjugation of Cy5 dye was confirmed using fluorescence spectroscopy.

#### 4.2.13. Release of Doxorubicin.

Doxorubicin conjugated nanogels (**NG-DOX**, 10 mg) were incubated in acetate buffer (pH 5.4) or phosphate buffered saline (PBS, pH 7.4) solutions (2 mL) in a dialysis bag (MWCO: 3.5 kDa). The dialysis bags were placed in a 25 mL release medium at 37 °C under 100 rpm oscillation. An aliquot of solution outside the dialysis bag was removed at predetermined time intervals and replaced with the same volume of fresh buffer.

The amount of released drug was determined spectrophotometrically using the absorbance of doxorubicin at 488 nm with the help of a calibration curve.

#### **4.2.14. Cytotoxicity Experiments with L929 Fibroblast Cells.**

Cytotoxicity of the nanogels were investigated via CCK-8 viability assay on L929 fibroblast cells. Cells (5000 cells/well) were seeded on a 96-well plate as triplicates in culture medium (100  $\mu$ L) and incubated at 37 °C for 24 h for cells to grow and adhere completely. Nanogel dispersions with different DOX concentrations (1.0–0.001 mg/ mL) were prepared in PBS (pH 7.4) and added to the cell media and the cells were incubated at 37 °C for 48 h. Solutions were removed and the cells were washed with PBS ( $2 \times 100 \mu$ L). The cells were incubated with CCK-8 reagent bearing media for 3 h. After the incubation, the absorbance values at 450 nm were measured via microplate reader. Results were gained by GraphPad prism software using nonlinear regression mode.

#### **4.2.15. Cytotoxicity Experiments with MDA-MB-231 Cells.**

Cytotoxic activity of the nanogels was investigated via CCK-8 viability assay on MDA-MB-231 human breast adenocarcinoma cell line. MDA-MB-231 cells (5000 cells/well) were seeded in a 96-well plate in 100  $\mu$ L RPMI supplemented with 10% fetal bovine serum (FBS) and incubated at 37 °C for 24 h for cells to adhere completely. Nanogel dispersions with different DOX concentrations ( $10^{-5}$ – $10^{-12}$  M) were prepared in RPMI and cell adhered plates were treated with nanogel dispersions at 37 °C for 48 h. After the incubation, nanogel solutions were removed from wells and the cells were washed with PBS (100  $\mu$ L) three times. CCK-8 solution (10%, 70  $\mu$ L) was added to each well and after incubation for 3 h, absorbance values at 450 nm were measured using a microplate reader. Results were obtained by GraphPad prism software using in nonlinear regression mode.

#### 4.2.16. Internalization Experiments.

For the cellular internalization experiment, MDA-MB-231 adenocarcinoma cells (50,000 cells/ well) were seeded in 12-well plate as triplicates in 1 mL culture media. The cells were incubated at 37 °C for 24 h. One of the plates were treated with the nanogels (0.5 mg/mL) conjugated to only doxorubicin whereas the other one was treated with the nanogel (0.5 mg/mL) conjugated to both doxorubicin and cRGDfC. After addition of the nanogels, cellular media were removed at several time points (3, 6, and 24 h). Following the removal of the nanogels, cells were washed with PBS (500 µL) and then DAPI (5 mg/mL) containing PBS were added to the plates. Cells were incubated at 37 °C for 20 min for nuclei staining. Cells were imaged using Zeiss Observer Z1 fluorescence microscope.

### 4.3. Results and Discussion

#### 4.3.1. Synthesis of Reactive Copolymers.

The synthesis of maleimide and hydroxyl group containing hydrophilic copolymer was accomplished using RAFT polymerization of a PEGbased methacrylate monomer (PEGMEMA), a furan-protected maleimide-containing methacrylate (FuMaMA) monomer, and a hydroxyl group containing methacrylate (HEMA) monomer. Briefly, FuMaMA was polymerized with commercially available PEGMEMA ( $M_n = 300 \text{ g mol}^{-1}$ ) at 70 °C using RAFT polymerization. The PEG based monomer was selected in order to obtain hydrophilic polymers with antibiofouling and thermoresponsive characteristics. A **poly(PEGMEMA-co-FuMaMA-co-HEMA)** copolymer was synthesized using a 7:1:3.5 feed ratio of PEGMEMA to FuMaMA to HEMA to furnish copolymer with similar monomer ratio ( $M_n = 30 \text{ kDa}$ ,  $PDI = 1.5$ ). The copolymer was heated to 110 °C to remove the furan protecting group to yield a thiol-reactive maleimide containing copolymer **poly(PEGMEMA-co-MaMA-co-HEMA)**.

The amount of monomer incorporation and complete unmasking of the maleimide unit in the copolymer via the retro Diels–Alder reaction were verified by using  $^1\text{H}$  NMR spectroscopy. The appearance of a new peak at 6.71 ppm and complete disappearance of peaks at 5.25 and 6.21 ppm in the  $^1\text{H}$  NMR spectrum revealed successful cycloreversion (Figure 4.2b). It was observed by UV–vis spectroscopy that the dithioester end group at the end of the polymer chain remained preserved during deprotection of the maleimide group (Figure 4.3).

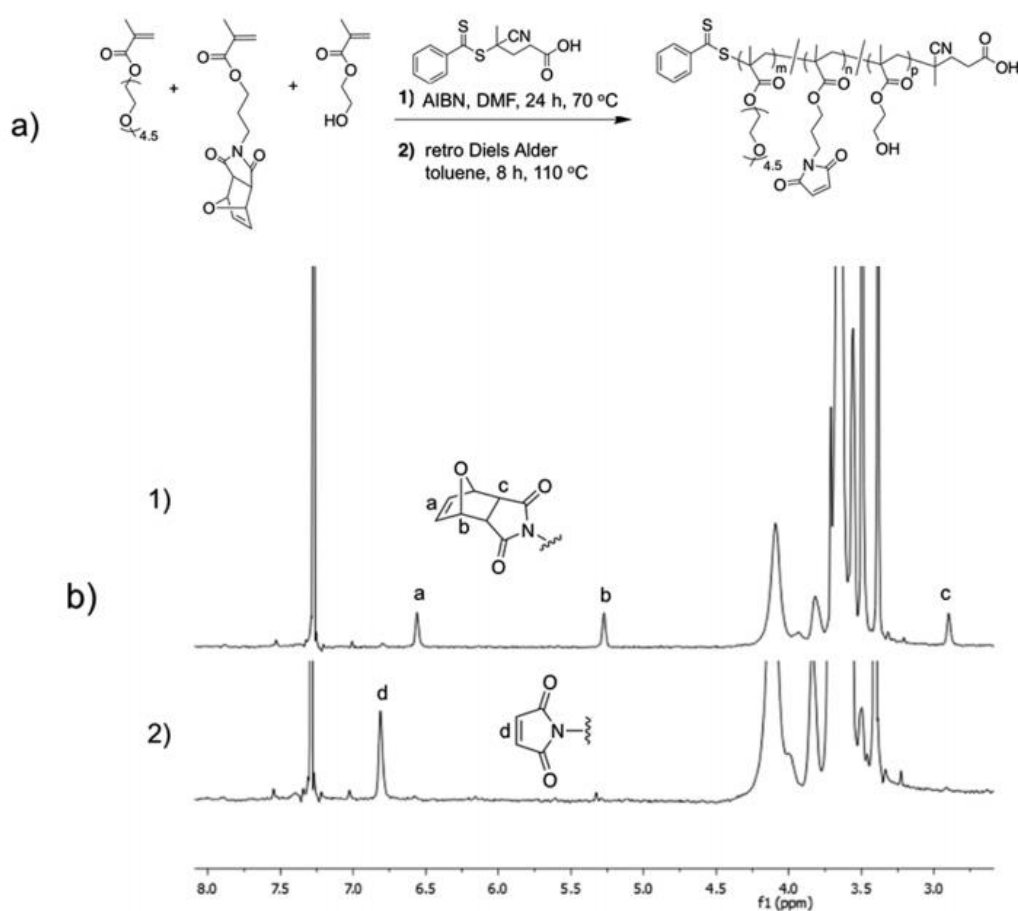


Figure 4.2. (a) Synthesis of copolymer poly(PEGMEMA-co-MaMA-co-HEMA);  $^1\text{H}$  NMR spectra of (1) poly(PEGMEMA-co-FuMaMA-co-HEMA) and (2) poly(PEGMEMA-co-MaMA-co-HEMA).

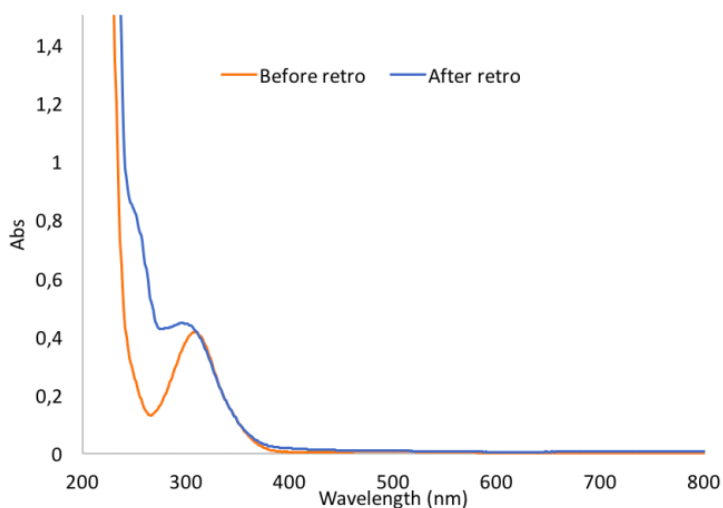


Figure 4.3. UV of the polymer before and after retro Diels-Alder reaction.

#### 4.3.2. Synthesis of Multi-Functionalizable Nanogels

The next step involves the self-assembly of these thiol-reactive copolymers into nanogels through cross-linking using dithiol- containing cross-linkers. It is well-established that PEGMEMA- based hydrophilic copolymers form stable nanosized aggregates above their LCST in aqueous media (Figure 4.4) [101]. A two-step protocol was followed to obtain cross-linked nanogels: first, the copolymers were assembled into nano- aggregates by heating the copolymer above its LCST in aqueous media, followed by their cross-linking via the thiol- maleimide “click” reaction [102,151,152]. To determine the LCST of the copolymer, transmittance of an aqueous solution of copolymer was measured at 600 nm at every 5 °C intervals between 30 and 80 °C. The LCST of copolymer **poly(PEGMEMA-co-MaMA- co-HEMA)** was determined around 70 °C based on the change in transmittance with increase in temperature (Figure 4.4c). The size of the aggregates in the turbid solution was determined using dynamic light scattering (DLS) as 88 nm at 70 °C, while a size of around 10 nm was obtained for the nearly transparent copolymer solution at room temperature (Figure 4.4b).

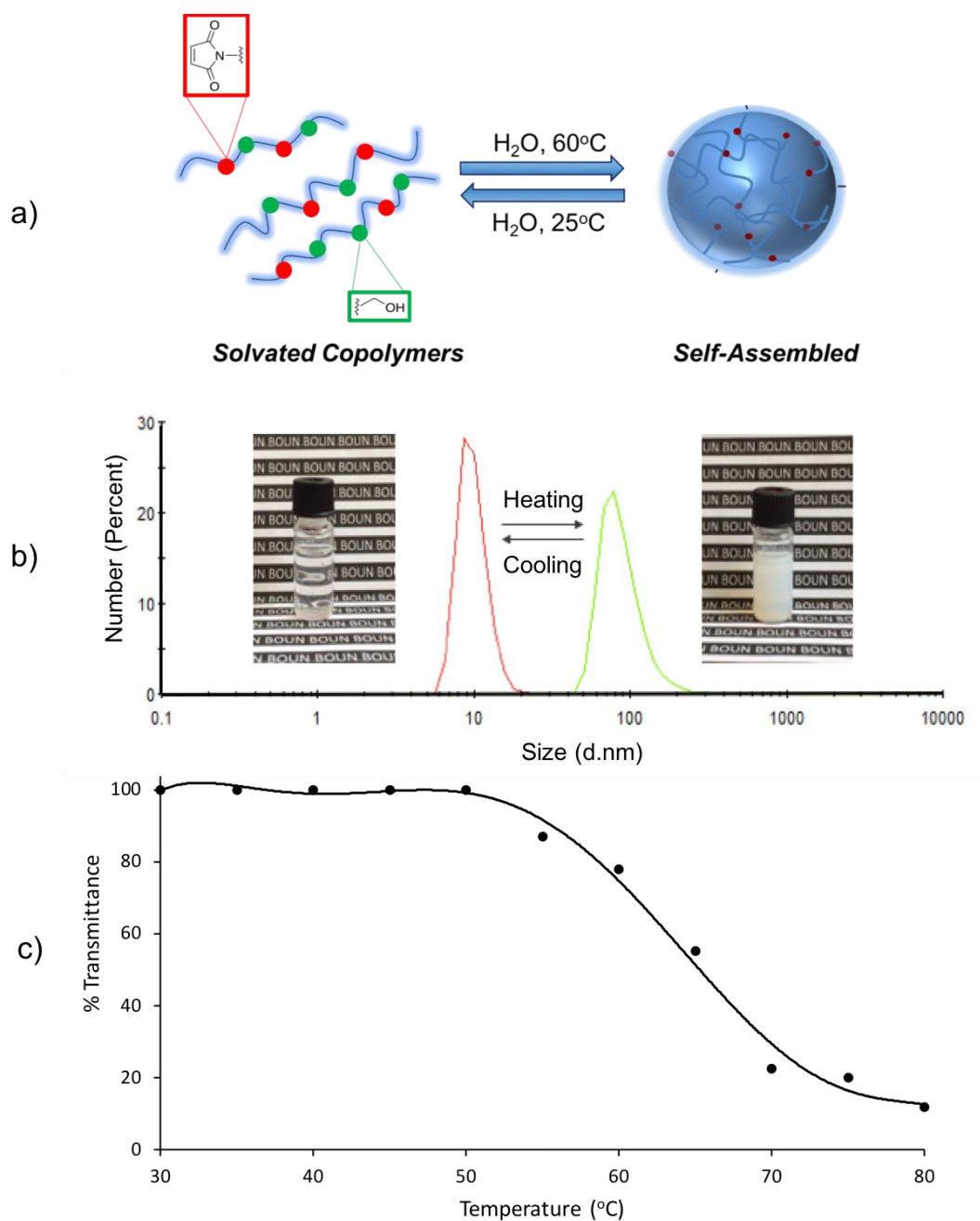


Figure 4.4. (a) Aggregation of copolymer in aqueous solution above its LCST. (b) Change in hydrodynamic size as determined by DLS at 25 and 70 °C. (c) Change in % transmittance of copolymer poly(PEGMEMA-co-MaMA-co-HEMA) solution at 600nm with temperature.

To synthesize the nanogels (**NG-OH**), the copolymer was dissolved in H<sub>2</sub>O and heated to 70 °C whereby the clear solution became turbid due to aggregation of copolymers. After formation of the aggregates, the water-soluble dithiol 2,2'-(ethylenedioxy)diethanethiol was added to this suspension with a maleimide to thiol molar ratio of 4:1. Normally, while the aqueous polymer solution was clear at room temperature, it became turbid upon heating to 70 °C. This self-assembly and formation of turbidity was reversible for polymer; however, the solution maintained its turbidity at room temperature after the gelation reaction. Nanogels were characterized by using DLS and TEM. Hydrodynamic diameter of the nanogel **NG-OH** in water was determined as 92 nm using DLS and  $34 \pm 9$  nm using TEM (Figure 4.5). DLS size is larger than that determined from TEM since nanogels are in their hydrated form. From static light scattering measurements, it was estimated that the nanogels have a molecular weight of  $8.6 \times 10^6$  Da (Figure 4.6).

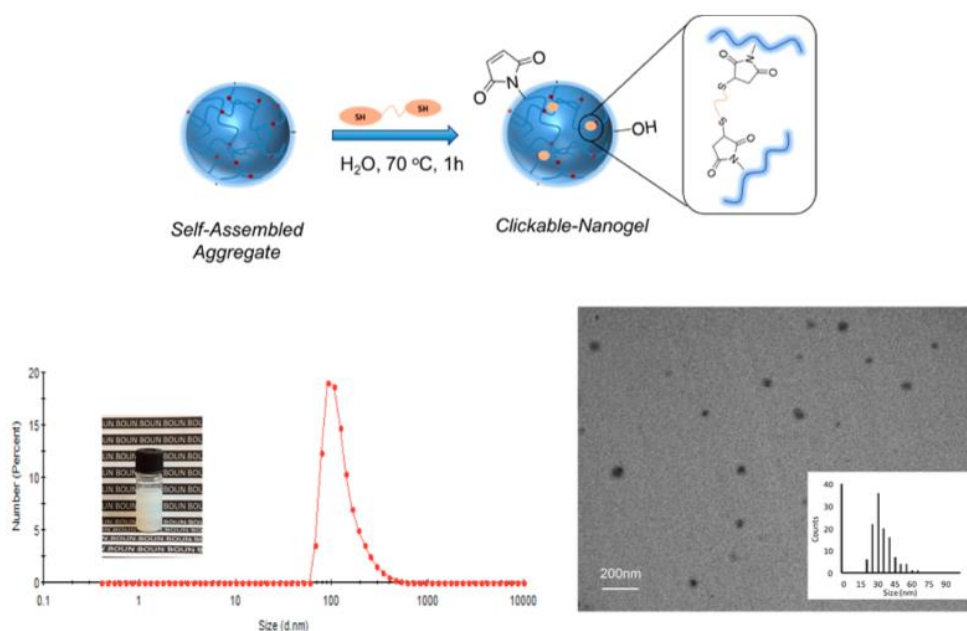


Figure 4.5. Schematic presentation of gelation reaction of copolymer poly(PEGMEMA-co-MaMA-co-HEMA), hydrodynamic size of nanogel at 25 °C using DLS and TEM.

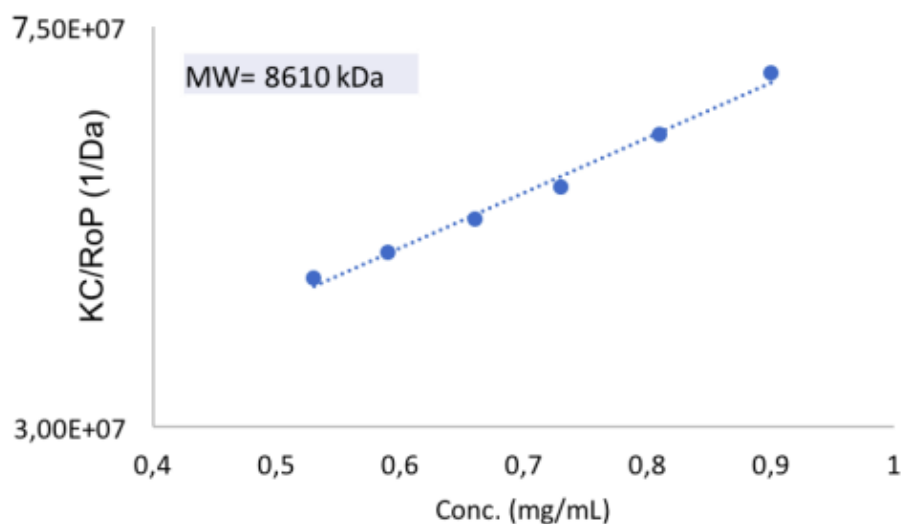


Figure 4.6. Molecular weight of the nanogels determined using static light scattering.

#### 4.3.3. Functionalization of Nanogels.

These nanogels possess three reactive functional groups for further modifications: the hydroxyl groups, the unreacted maleimide groups, and the residual thiol groups from the cross-linker. To determine the amount of maleimide consumed during the nanogel formation, a solution containing a known amount of 2-mercaptoethanol was added to the polymer before cross-linking. Thereafter, the decrease in the amount of thiol in the polymer solution was analyzed using Ellman's assay. This provides total maleimide content before cross-linking. The same procedure was repeated for N-ethylmaleimide treated nanogels. Based upon the decrease in thiol content before and after cross-linking, it was concluded that approximately 35% of the maleimide units on copolymers react during nanogel formation and 0.106  $\mu\text{mol}/\text{mg}$  are available for reaction. It should be noted that these are approximate since diffusion barriers probably limit access of thiols to all maleimide groups in nanogels.

**4.3.3.1. Conjugation of NHS to Nanogels.** Prior to further modification, hydroxyl group in the nanogels were activated using N, N'-disuccinimidyl carbonate to obtain activated carbonate groups for facile reaction with amine-containing molecules. Activation of the hydroxyls was performed in THF at room temperature in the presence of Et<sub>3</sub>N. The FTIR spectra of the nanogels prior to and after the reaction revealed the formation of new carbonate carbonyl bond stretches around 1724 cm<sup>-1</sup> originating from the NHS-carbonate group (Figure 4.7).

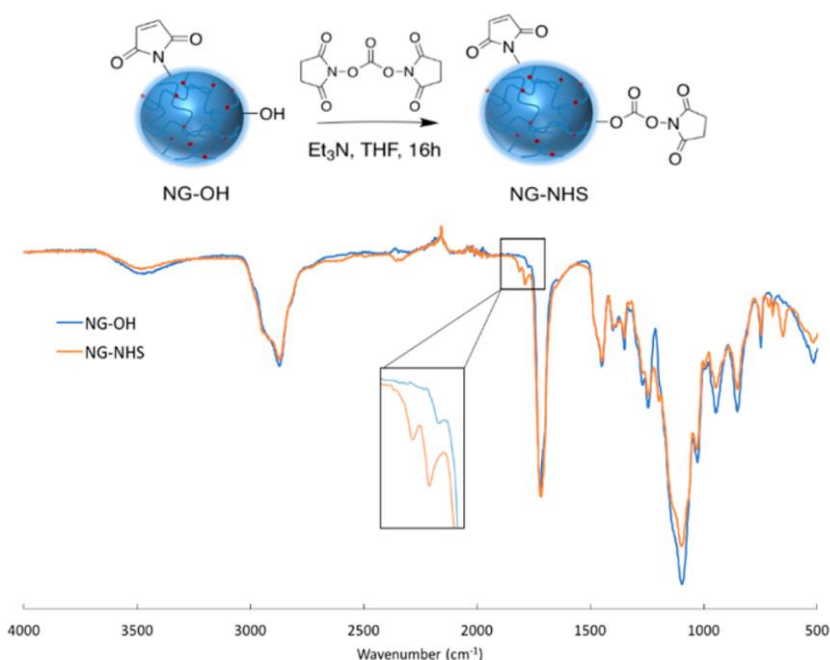


Figure 4.7. Illustration of activation and FTIR spectra of NG-OH and NG-NHS nanogels.

**4.3.3.2. Conjugation of DOX to Nanogels.** NHS-activated nanogels (**NG-NHS**) were conjugated with doxorubicin through carbamate linkages to yield dox-conjugated nanogels (**NG-DOX**). The reaction was carried out in THF at 0 °C for 3 h. The residual drug was removed via dialysis. In order to calculate the total amount of conjugated dox, UV spectroscopy was used, and intensity at 485 nm was recorded, and with the help of a calibration curve, the amount of conjugated dox was determined as 0.08 mg DOX/mg nanogel (27.6 μmol/mg). As a control, the same procedure was repeated with non-activated nanogels and no observable peak at 485 nm could be detected (Figure 4.8b).

During the activation and drug conjugation, no significant change in size or aggregation of nanogels occurred, as confirmed using DLS. Additionally, FTIR spectrum was recorded and compared with the spectrum of **NG-NHS**, and complete disappearance of carbonyl stretches belonging to the NHS moiety was observed (Figure 4.8c).

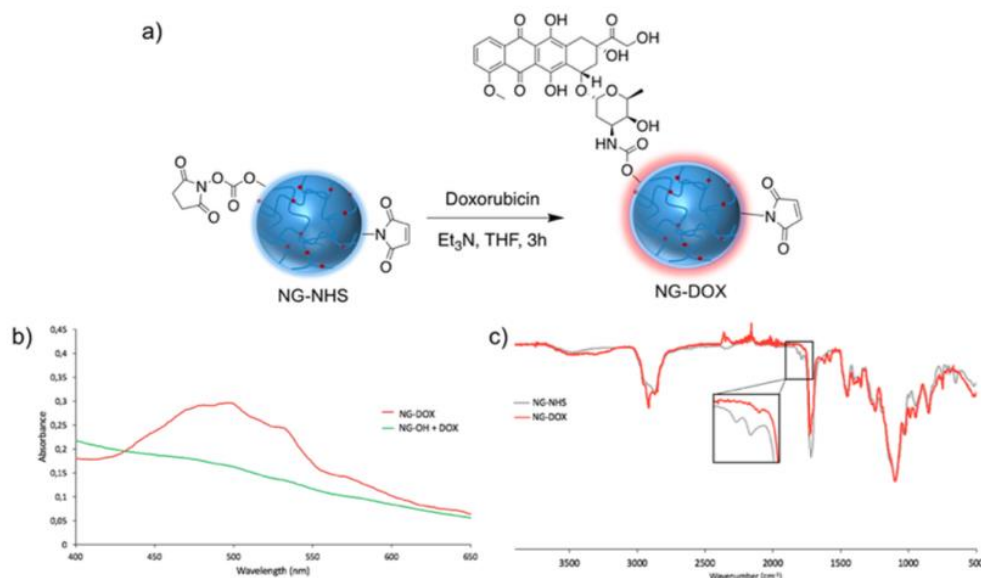


Figure 4.8. (a) Attachment of drug to NG-NHS nanogels. (b) UV-vis spectra of NG-DOX and NG-OH+DOX control experiment and (c) FTIR spectra of NG-NHS and NG-DOX nanogels.

**4.3.3.3. Conjugation of BODIPY-SH to Nanogels.** To demonstrate the presence of maleimide functional group left within the **NG-DOX** nanogels, a thiol-bearing hydrophobic dye, BODIPY-SH, was used for conjugation. The dye was synthesized using a previously reported procedure [37]. Conjugation of the dye to the nanogels was carried out in THF because the dye was insoluble in water. Unreacted BODIPY dye was removed via dialysis and UV spectra of nanogels were recorded, where an additional peak from BODIPY could be observed at 525 nm (Figure 4.9). Using UV-vis spectroscopy, the amount of dye conjugated to the nanogels was calculated as 5.2 nmol/mg nanogels using a calibration curve of the free dye.

To confirm that the dye was covalently bonded through thiol-maleimide coupling and not by encapsulation, a BODIPY dye (BODIPY-Br) was used for conjugation with a second batch of the nanogel. After the reaction of the nanogel with either BODIPY-SH or BODIPY-Br, nanogels were washed repeatedly with THF to remove any unbound dye and dispersed in water. The nanogels treated with BODIPY-Br did not show any absorbance in their UV spectrum, as well as not fluorescing under UV-illumination, as opposed to the nanogels treated with BODIPY-SH which exhibited strong absorbance and green fluorescence (Figure 4.10).

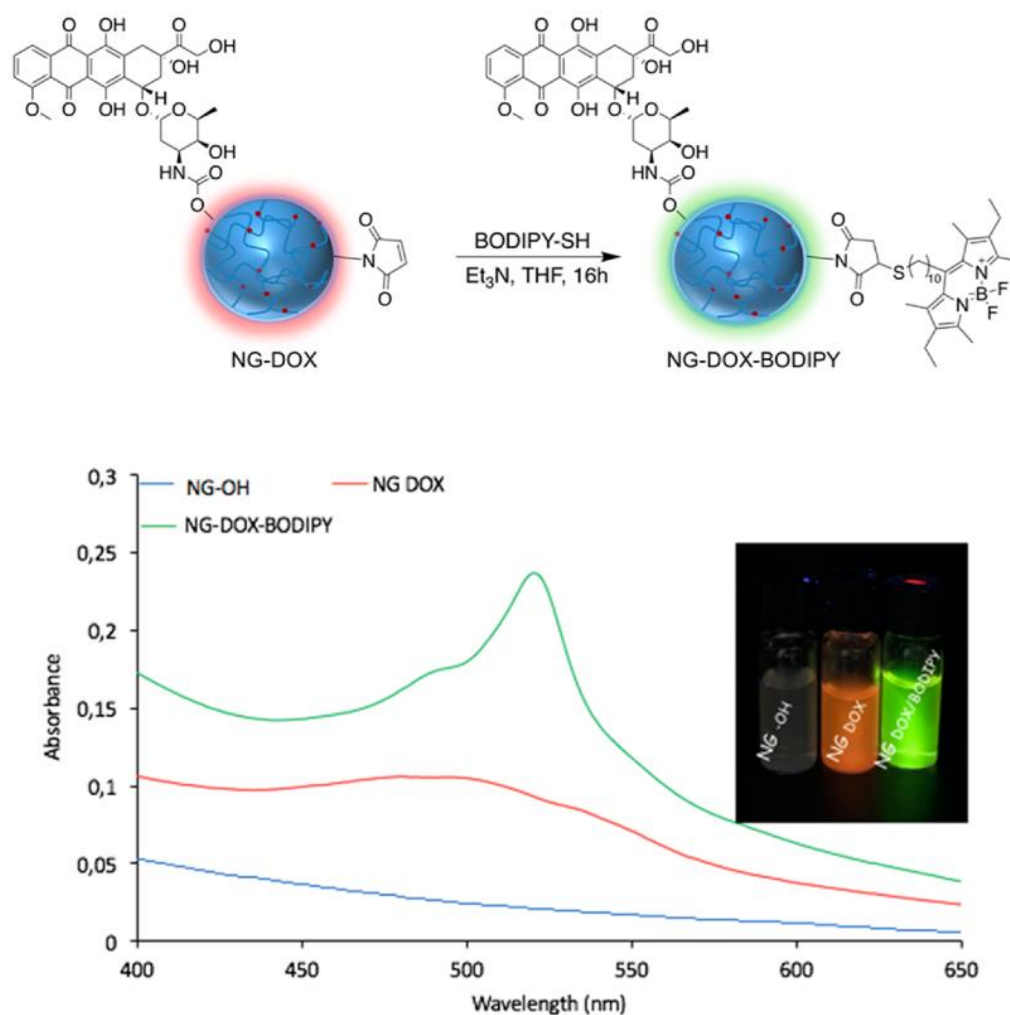


Figure 4.9. Attachment of BODIPY-SH to NG-DOX, UV spectra, and photograph under UV illumination of nanogel solutions after treatment with DOX and BODIPY-SH.

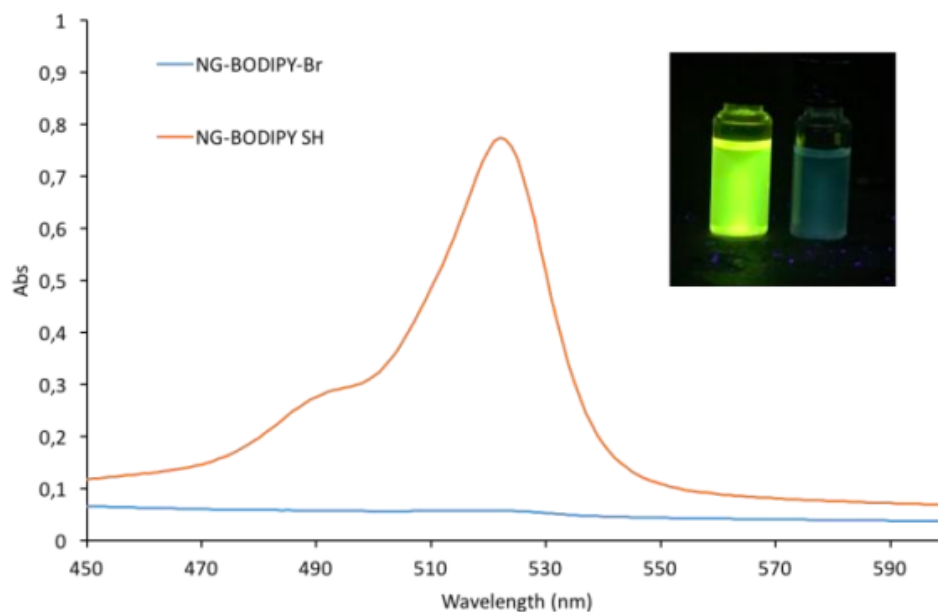


Figure 4.10. UV spectra and UV images of nanogel solution after treatment with Bodipy-SH (left) and Bodipy-Br (right).

**4.3.3.4. Conjugation of cRGDfC to Nanogels.** To show the multi-functionalizability of these nanogels and increase their selectivity, the maleimide groups were conjugated with a cyclic peptide bearing a free thiol, cRGDfC (**NG-DOX-RGD**, Figure 4.11). Due to the hydrophilic nature of the cRGDfC, the reaction was done in aqueous media at room temperature. The residual peptide was removed via dialysis. In order to calculate the total amount of conjugated cRGDfC, BCA Assay was used. The nanogel samples were incubated in the BCA working reagent for 30 min at 60 °C. After incubation, absorbance of the solution was measured using UV spectroscopy at 562 nm. Calibration curve of BSA standard was used to calculate the amount of cRGDfC in nanogels (0.098  $\mu\text{mol}/\text{mg}$  NG). In addition, BCA assay was performed on the fractions during the removal of cRGDfC via dialysis to confirm that all unbound peptide was removed.

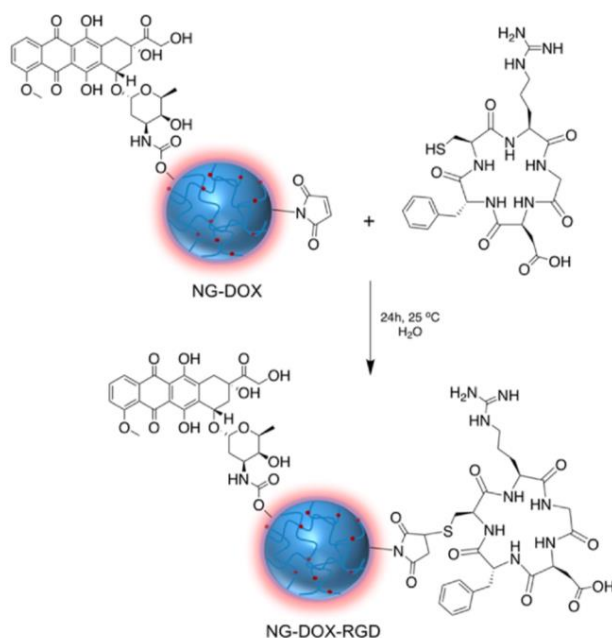


Figure 4.11. Conjugation of cyclic peptide cRGDfC to NG-DOX nanogel.

4.3.3.5. Conjugation of Cy5 Maleimide Dye to Nanogels. Finally, to show that the nanogels can be further functionalized, the thiol groups were conjugated with a maleimide-containing Cy5 dye to obtain nanogels functionalized with doxorubicin, peptide, and fluorescent dye (**NG-DOX-rGD-Cy5**, Figure 4.12). Prior to the reaction, Ellman's assay was performed on the nanogels to confirm that free SH groups available for conjugation were present. A thiol content of 0.025  $\mu\text{mol}/\text{mg}$  of nanogels was obtained. After conjugation, nonconjugated dye was removed via centrifugation, as confirmed from fluorescence spectroscopy of the supernatant solution. To confirm that the dye was covalently attached to the nanogel, a control experiment was done by treating the nanogel where all the free thiols were quenched using *N*-ethylmaleimide prior to treatment with the maleimide-containing Cy5 dye. As expected, no emission was observed for the control nanogels (Figure 4.12), thus suggesting that the residual thiol groups on the nanogels were enabling the dye attachment through nucleophilic thiol-maleimide addition.

As the amount of unreacted thiol is minimal, it was not possible to observe any signal for the dye using UV spectroscopy, hence the use of fluorescence spectroscopy.

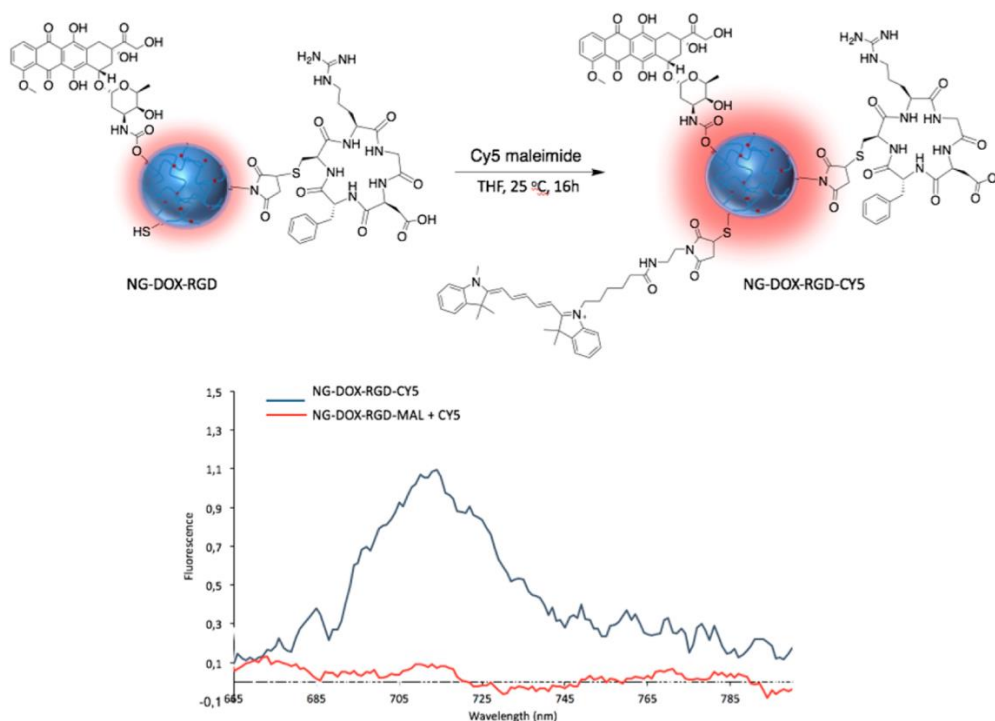


Figure 4.12. Conjugation of Cy5 maleimide to NG-DOX-RGD nanogels. Fluorescence spectra of NG-DOX-RGD-CY5 and control nanogels

#### 4.3.4. Drug Release Experiments.

To show the pH-sensitive nature of the carbamate linker in the nanogels, **NG-DOX** solutions were placed in dialysis bag (3.5 kDa cutoff) and immersed in 25 mL PBS buffer (pH = 7.4), and separately in an acetate buffer (pH = 5.4). At certain time intervals, a buffer aliquot was analyzed with fluorescence spectroscopy to measure the amount of released DOX.

As expected, a slow release of drug was observed at neutral pH ( $5.8 \pm 1.0\%$  over 30 days) since the drug is conjugated through a relatively stable, yet hydrolyzable carbamate linker, whereas a higher drug release was observed at lower pH ( $17.6 \pm 1.4\%$  over 30 days) due to enhanced degradation of the carbamate group in acidic medium (Figure 4.13).

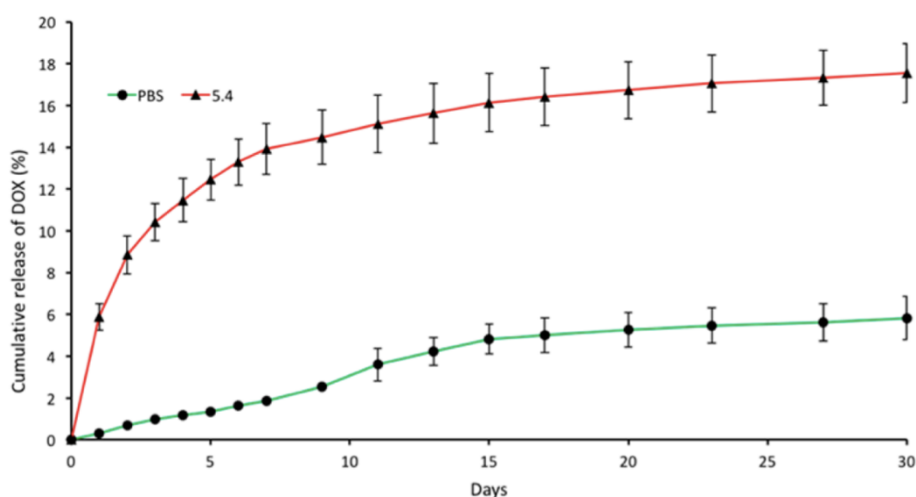


Figure 4.13. Cumulative release of doxorubicin from NG-DOX at pH 7.4 and pH 5.4.

#### 4.3.5. *In Vitro* Experiments.

In order for utilization of the nanogels as a theranostic platform, they should be nontoxic. To investigate their biocompatibility, L929 fibroblast cells were treated with nanogels (NG-NHS). Cells were incubated in 96-well plates and treated with nanogels for 48 h at 37 °C. CCK-8 assay was performed to determine cell viability. It was gratifying to observe that the nanogels did not show any appreciable cytotoxicity even at high concentrations (Figure 4.14). This high degree of biocompatibility could be expected due to the PEG-based matrix of these nanogels.

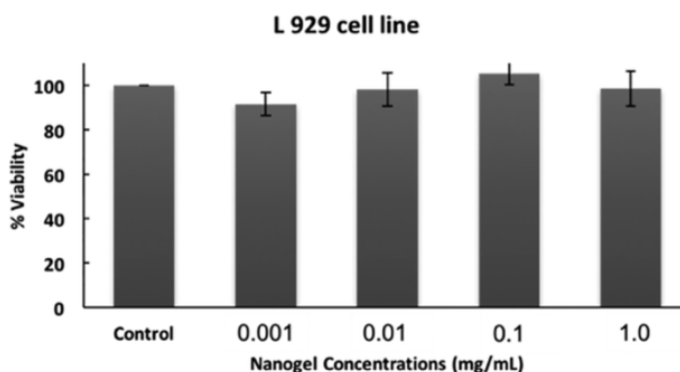


Figure 4.14. Cytotoxicity assay of NG-NHS on L 929 fibroblast cells.

#### 4.3.6. *In Vitro* Internalization Assays.

To investigate the cellular uptake of the Doxorubicin conjugated nanogels, adenocarcinoma MDA-MB-231 human breast cells were treated with the nanogels (**NG-DOX**). Inherent red fluorescence of doxorubicin enabled facile visualization of its internalization into the cells. To stain and visualize the nuclei of the cells, 4', 6-diamino-2-phenylindole (DAPI) was used due to its distinct blue fluorescence. Cultured cells were treated with nanogel samples (0.04 mg DOX/mL, 0.5 mg NG/mL) and incubated at 37 °C. Cells were treated with nanogels conjugated with doxorubicin (**NG-DOX**), and nanogels conjugated to both doxorubicin and cRGDfC (**NG-DOX-RGD**). The overexpressed integrin proteins on the surface of MDA-MB-231 cells make them a good target for the constructs carrying cRGDfC on their surface. Cellular uptake of the nanogels was screened at time points (3, 6, and 24 h) via fluorescence microscopy (Figure 4.15). From the micrographs, it could be clearly observed that the cells treated with nanogels containing the cyclic RGD group show higher fluorescence intensity as soon as 6 h, than the cells treated with nanogels lacking the targeting peptide group. To establish that it was indeed the binding on cyclic peptides on the nanogels with the cell receptors that led to enhanced internalization, control experiments where free cRGDfC peptide was used in excess to act as a competitor against the cRGDfC-containing nanogel was conducted. As expected, a level of internalization similar to the non-targeting group containing nanogel was observed.

The results suggested that the presence of the cyclic peptide based targeting group, cRGDfC, on these nanogels boosts their cellular internalization (Figure 4.15a). To further prove the enhanced internalization for the peptide-containing construct, normalized fluorescence intensity was obtained and as it can be observed the **NG-DOX-RGD** construct has a much higher intensity in 6 h compared to the other construct (Figure 4.15b).

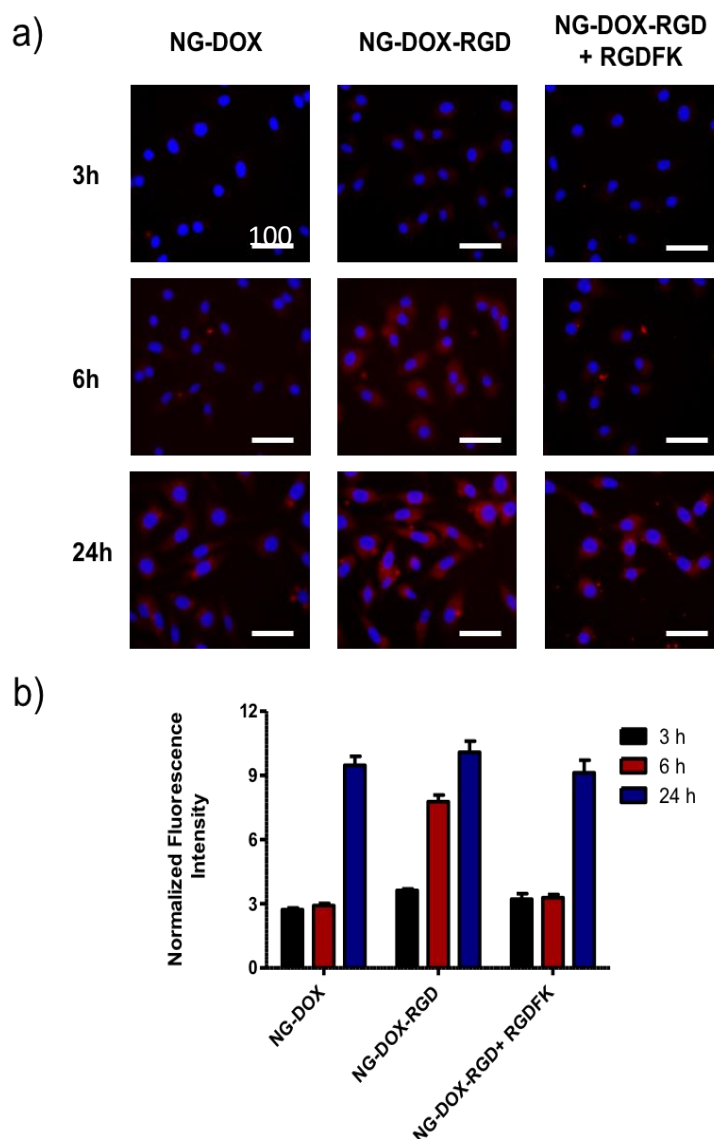
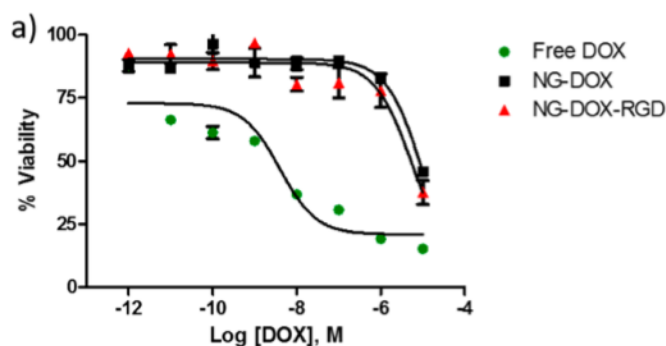


Figure 4.15. (a) Merged fluorescence images of MDA-MB-231 cells treated with nanogels NG-DOX, NG-DOX-RGD, and free cRGDfC and NG-DOX-RGD nanogels (NG-DOX-RGD + RGDFK). Cells were incubated at 37 °C for different time periods (3, 6, and 24 h). The scale bar is 100  $\mu$ m. (b) Normalized fluorescence intensity for NG-DOX, NG-DOX-RGD, and NG-DOX-RGD+RGDFK at 3, 6, and 24 h.

#### 4.3.7. In Vitro Cytotoxicity Assay of NG-DOX and NG-DOX-RGD Nanogels.

Cellular toxicity levels of **NG-DOX** and **NG-DOX-RGD** was investigated on cell lines overexpressing RGD recognizing integrins, namely, the MDA-MB-231 breast cancer cell lines. After 48 h continuous incubation, cell viabilities were determined using CCK-8 assay (Figure 4.16). It was observed that  $EC_{50}$  value of the RGD-containing construct (**NG-DOX-RGD**) was slightly lower than the RGD-depleted one (**NG-DOX**). Presumably, it is due to enhanced internalization of the peptide construct, as observed from the internalization experiment.



Constructs	$EC_{50}$ [M]
DOX	$3.98 \times 10^{-9}$
NG-DOX	$4.06 \times 10^{-5}$
NG-DOX-RGD	$5.49 \times 10^{-6}$

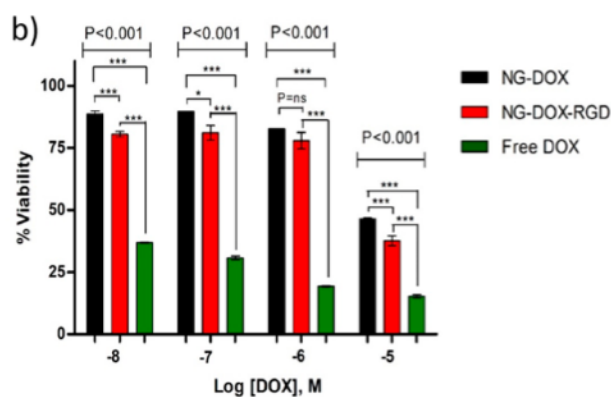


Figure 4.16. (a) In vitro toxicity of free DOX, NG-DOX, and NG-DOX-RGD on MDA-MB-231 breast cancer cells and (b) their histogram representation.

#### 4.4. Conclusions

In this part, fabrication and multi-functionalization of a biocompatible nanogel platform is disclosed. Copolymers containing thiol-reactive maleimide group, hydrogel group, and PEG-based side chains were synthesized using RAFT polymerization. The PEG grafts provide thermo-responsiveness to these polymers to yield nanosized aggregates upon heating to their LCST. The maleimide groups enable cross-linking of these aggregates in the presence of dithiol cross-linkers. Thus, fabricated nanogels can be treated with succinimidyl-dicarbonate to install *N*-hydroxysuccinimide group containing carbonates that enable conjugation of amine-containing drugs through acid labile carbamate linkages. It was demonstrated that the maleimide groups can be utilized to install thiol-containing cyclic peptides as targeting groups. Additionally, the residual thiol group from cross-linkers within the nanogels could be employed for conjugation of a maleimide-containing fluorescent dye. In vitro studies showed slightly enhanced cytotoxicity and cellular internalization for the targeting group containing constructs. Facile fabrication and functionalization of this novel multi-functionalizable nanogel platform should prove to be attractive for various theranostic applications.

## **5. A SURFACTANT-FREE DIRECT ACCESS TO PORPHYRIN-CROSSLINKED NANOGELS FOR PHOTODYNAMIC AND PHOTOTHERMAL THERAPY**

This chapter has been submitted for publication to *Bioconjugate Chemistry* 2018. {Chambre, L., Ekineker, G., Saw, W.S., Kiew, L.V., Chong, W. Y., Lee H. B., Chung, L. Y., Bretonnière, Y., Dumoulin, F., and Sanyal, A., “A Surfactant-free Direct Access to Porphyrin-crosslinked Nanogels for Photodynamic and Photothermal Therapy”}

### **5.1. Introduction**

Photodynamic therapy (PDT) has emerged as a safe and effective non-invasive method for the treatment of several types of cancer, infections and ophthalmology disorders [153]. The therapy relies on the production of cytotoxic species upon activation of a non-toxic light-sensitive dye called a photosensitizer (PS) by irradiation at an appropriate wavelength corresponding ideally to the absorption maxima of the PS. Upon absorption of one (monophotonic PDT) or two (biphotonic PDT) photons, the PS is first excited into its excited singlet state, then quickly relaxes into a more long-lived excited triplet state via the intersystem crossing. This PS in its excited triplet state can then transfer energy to molecular oxygen which is converted into singlet oxygen (Type II), or transfer an electron to produce other reactive oxygen species (ROS, Type I).

PDT is hence highly selective as cell death is spatially limited to regions subjected to irradiation, and even more if the PS can be targeted selectively to the cancerous cells [154]. In addition to skin cancers, advances in fiber optic technology enable illumination of internal organs, making this treatment suitable for a variety of internal organs cancers [155,156]. One of the common strategies to enhance the accumulation of the PS at the tumor site is based on their combination with or their incorporation into nanosized carriers [157-159].

Apart from increasing the solubility or bio-availability of the PS, nanosized drug delivery agents passively accumulate and are retained in the tumor via the enhanced permeability and retention effect (EPR) [11,12]. In addition to directly killing the cancer cells, antivascular PDT can also damage the tumor neovasculature, thus preventing cancer cells from receiving necessary nutrients. Vascular disrupting agents have been also combined with the photodynamic effect [160]. In the case of photoimmunotherapy, the immune system is activated to attack the tumor cells [161,162].

An ideal PS should fulfill several requirements such as possess ability to produce singlet oxygen efficiently and be non-toxic in the absence of light. Porphyrinoids are hence extremely suitable, and one of the first PS to be used was indeed a porphyrin, named Photofrin®, which is to date still the most prominent agent in clinical use, despite several drawbacks. It is an 18  $\pi$ -electron aromatic macrocycle that exhibits a characteristic optical spectrum with a strong  $\pi$ - $\pi^*$  transition around 400 nm (Soret band) and four additional Q bands in the visible region. Second-generation photosensitizers are well-defined structures with a porphyrinoid molecular basis. PS of the third-generation are often nanoparticles combining several properties and are now widely developed. Photosensitizing porphyrinoids with amphiphilic properties have been shown to be effective against cancers, microbial infections and, most recently, autoimmune skin disorders [163,164].

Several photosensitizers, in addition to generation of ROS, can also generate photothermal heating when the de-excitation is non-radiative [165-168]. Photothermal therapy (PTT) increases the local temperature of the cancerous cells above a threshold leading to cell death. Aggregated porphyrinoids, such as in the porphosome technology are suitable PTT agents [169]. Hence, some PS can exhibit dual photodynamic and photothermal effects.

However, PSs have frequent drawbacks such as low solubility in water and non-specific distribution after intravenous injection [170-172]. Due to their large aromatic structures, they tend to aggregate under physiological conditions, resulting in a self-quenching of the electronic events allowing singlet oxygen generation (SOG).

Thus, even in the case of water-soluble PSs, the selective accumulation at malignant site is not high enough for clinical use [173]. In this regard, the incorporation of PSs into water-dispersable nanocarriers can enhance the solubility of PSs, as well as the selectivity of the treatment by efficient cellular internalization [174-178]. The carriers must have minimal internal toxicity, possess tumor selectivity and adequate retention ability.

There are numerous candidates such as liposomes, micelles, nanoparticles, and nanogels that satisfy the abovementioned requirements [179-183]. Among these, nanogels possess several desirable characteristics such as tunability of size, stability, high loading capacity and formation of stable conjugates through non-covalent or covalent interactions and thus qualifies for an efficient drug delivery platform [87,184].

Hydrophilic nanogels can be engineered through either polymerization of hydrophilic monomers or chemical crosslinking of hydrophilic polymers using emulsion or inverse emulsion systems [90,185,186]. When non-amphiphilic polymers are used for nanogel synthesis, surfactants are often necessary to stabilize the nanosized emulsion required for the formation of crosslinked nanogel [187]. Unfortunately, removal of surfactants from the crosslinked materials is quite difficult, and often exhaustive washing is unable to completely remove them, inducing undesirable toxicity during biological applications. The choice of crosslinking reaction is also crucial since it should be effective and contributory to the environment needed for nanogels formation with good control over size and polydispersity. To date, several of the 'click' reactions such as the azide-alkyne cycloaddition, and nucleophilic and radical thiol-ene reactions have been employed to obtain crosslinked materials such as bulk hydrogels, microgels, as well as nanogels [64,127-131]. Click chemistry is also known as a powerful widely used synthetic tool in the synthesis of porphyrinoids [188].

To circumvent the use of surfactants, nanogels can be prepared via covalent cross-linking of amphiphilic polymers that undergo self-assembly to form nanosized aggregates [189-191]. One such strategy employs crosslinking of thermosensitive polymers that assemble to nanosized aggregates upon heating them above their lower critical solution temperature (LCST).

In a recent study, we reported that copolymers comprised of PEG and maleimide groups as side chains, self-assemble into nanosized aggregates that can be crosslinked using dithiol-based crosslinkers to provide stable nanogels [37,192]. One can envision that utilization of a functional molecule as a crosslinker will integrate them into the obtained nanogels during their formation, and thus impart their functional attributes to the construct. Using PS as crosslinkers would yield photosensitizing nanogels in a single step, where insertion of the PS into the nanogels serves the dual role of a crosslinker and the photoactive agent. To test this strategy, we chose a tetravalent porphyrin-based PS as a model crosslinker to enable direct access to photosensitizing nanogels suitable for PDT and/or PTT.

In this study, we report a novel strategy for direct synthesis of porphyrin-crosslinked nanogels using the self-assembly and *in situ* crosslinking of thermoresponsive copolymers. PEG-methacrylate based copolymers containing reactive azide groups as side chains were assembled into nanosized aggregates and crosslinked with a tetra-alkynyl Zn porphyrin, using the copper(I)-catalyzed azide-alkyne cycloaddition reaction. Nanogels containing varying amount of the porphyrin were prepared and characterized. Overall, a versatile and modular approach to fabricate PS-crosslinked nanogels was established (Figure 5.1). These nano-objects are expected to exhibit photodynamic and/or photothermal properties, depending on the aggregation of the embedded porphyrins. Their photophysical properties were measured and their cellular toxicity and ability to kill cancer cells in both PDT and PTT modes were demonstrated.

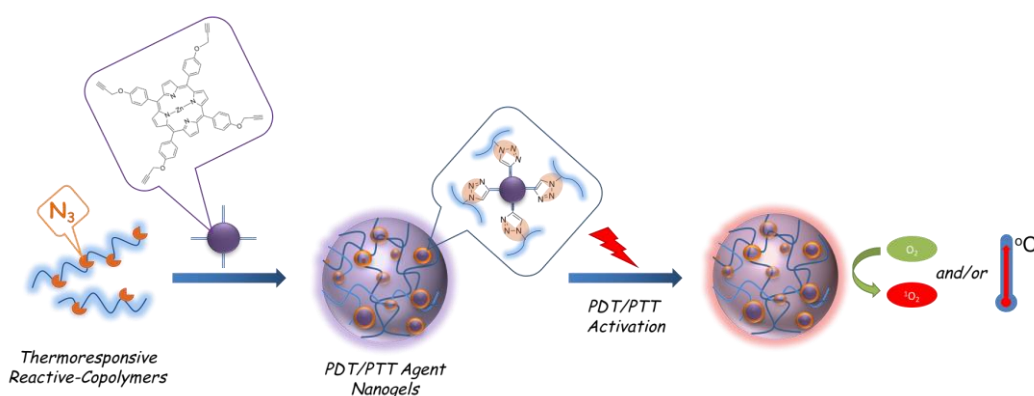


Figure 5.1. Synthesis and photo-induced singlet oxygen generation and photothermal heating of the porphyrin-crosslinked nanogels.

## 5.2. Experimental

### 5.2.1. Materials

*Chemicals.* Poly(ethylene glycol) methyl ether methacrylate ( $M_n = 300 \text{ gmol}^{-1}$ , PEGMEMA, 99%),  $\text{CuSO}_4$  and sodium ascorbate (NaAsc), 2,2'-azobis(2-methylpropionitrile) (AIBN), 4-cyano-4-(phenylcarbonothioylthio)pentanoic acid (CTA, >97%), were purchased from Sigma-Aldrich unless otherwise stated and used as received. The dialysis bags (Spectra/Por Biotech Regenerated Cellulose Dialysis Membranes, MWCO 3.5 and 40 kDa) were purchased from Spectrum Laboratories. Azidohexyl methacrylate (AHMA) was synthesized according to literature [193]. 5,10,15,20-Tetrakis(4'-propargyloxyphenyl)-Zn(II)-porphyrin was synthesized according to literature [192]. PEGMEMA monomer was passed through basic alumina column to remove inhibitor. Column chromatography was performed using Silicagel-60 (43-60  $\mu\text{m}$ ) and thin layer chromatography was performed by using silica gel plates (Kieselgel 60 F254, 0.2 mm, Merck).

*Instrumentation.* NMR spectra were recorded using a 400 MHz Bruker spectrometer at 25 °C. Measurements were taken in deuterated chloroform ( $\text{CDCl}_3$ ). The molecular weights of the copolymers were estimated by gel permeation chromatography (GPC) using a PSS-SDV column (Gram linear, length/ID 8  $\times$  300 mm, 10  $\mu\text{m}$  particle size) calibrated with poly(methyl methacrylate) standards (1–175 kDa) using a refractive-index detector. Dimethylacetamide (DMAC) was used as eluent at a flow rate of 1  $\text{mL min}^{-1}$  at 30 °C. Hydrodynamic radii of nanogels and polymers were determined from 1 mg/mL samples using an off-line dynamic light scattering analysis (DLS, Malvern, Zetasizer Nano ZS). Images of nanogels were obtained using a LVEM5 electron microscope system (Delong America) on transmission electron microscopy (TEM) mode.

### 5.2.2. Preparation of azido-containing copolymer.

Azidohexyl methacrylate (AHMA) monomer (34 mg, 0.167 mmol), PEGMEMA (200 mg, 0.667 mmol), RAFT CTA (4 mg, 0.0143 mmol) and AIBN (0.40 mg, 0.003 mmol) were dissolved in DMF (0.5 mL) and placed in a sealed round-bottom flask equipped with a magnetic stir bar. The reaction mixture was purged with N<sub>2</sub> for 15 min and stirred at 70 °C for 24 h. After the reaction, the unreacted monomers were removed by dialysis against methanol (MWCO 3.5 kDa). The obtained polymer was dried under *vacuo* and characterized using GPC and <sup>1</sup>H NMR. Conversion = 85%,  $M_{n,theo} = 16840 \text{ g}\cdot\text{mol}^{-1}$ ,  $M_{n,GPC} = 14000 \text{ g}\cdot\text{mol}^{-1}$ ,  $M_w/M_n = 1.3$  relative to PMMA. The ratio of incorporated monomers in the copolymer was determined from <sup>1</sup>H NMR spectrum as [AHMA]:[PEGMEMA] = 1:4. <sup>1</sup>H NMR (CDCl<sub>3</sub>, δ) 4.02 (s, 2H, OCH<sub>2</sub> ester protons of PEGMEMA), 3.75 – 3.42 (m, 4H, OCH<sub>2</sub> of PEGMEMA), 3.41 (s, 3H, OCH<sub>3</sub> of PEGMEMA), 3.34 (s, 2H, N<sub>3</sub>CH<sub>2</sub> of AHMA), 2.11 – 0.56 (m, 7H, NCH<sub>2</sub> CH<sub>2</sub> CH<sub>2</sub>O, CH<sub>2</sub> and CH<sub>3</sub> protons along the polymer backbone).

### 5.2.3. Preparation of the nanogels.

In a conical flask, copolymer (5 mg, 0.33 μmol) was dissolved in water (2 mL) and heated at 70 °C for 10 min. After 10 min, was added an aqueous solution of tetra-propargyl porphyrin (1.6 mg, 1.78 μmol) in acetone (200 μL). Then a solution of sodium ascorbate (NaAsc, 0.140 mg, 0.707 μmol) and CuSO<sub>4</sub> (0.018 mg, 0.072 μmol) was added to the polymer and porphyrin mixture. The solution was left to react for 2 hours and purified via dialysis (40 kD) in ethanol to remove non-crosslinked polymer and porphyrin to obtain the nanogel **NG-A** (4.35 mg, 84 %). The same experiment was repeated with different amounts of the tetra-alkynyl porphyrin linker (0.8 mg and 0.4 mg) to obtain **NG-B** and **NG-C** respectively with similar yields (87% and 79%). Several batches of nanogels with high level of consistency were prepared using the abovementioned protocol.

### 5.2.4. Photophysics and photochemistry.

*Electronic absorption.* UV-visible spectra were collected on a Varian Cary 100 Scan UV-vis spectrophotometer or a JASCO V670 spectrometer.

*Fluorescence.* Fluorescence spectra of the nanogels were collected on a Varian Cary Eclipse spectrophotometer at room temperature using a 1 cm pathlength rectangular quartz cuvette. The emission and excitation slit width are 5 nm. Spectra were reference-corrected for both the excitation source light intensity variation (lamp and grating) and the emission spectral response (detector and grating). The porphyrin emission spectra were measured with excitation at 425 nm. The quantum yields of phosphorescence  $\Phi_F$  were determined in ethanol using zinc tetraphenylporphyrin (ZnTPP) as the reference ( $\Phi_F = 0.031$  in ethanol) [195].

*Singlet oxygen generation.* Singlet oxygen was detected directly by recording its phosphorescence emission at 1275 nm using a Horiba–Jobin Yvon Fluorolog-3 spectrofluorimeter equipped with an AsGa detector. The  $^1\text{O}_2$  emission spectra were measured with excitation at 425 nm. The quantum yields of singlet oxygen generation  $\Phi_\Delta$  were determined in ethanol using phenalenone as the reference ( $\Phi_\Delta = 0.95$  in ethanol) [196]. Phosphorescence spectra were recorded at room-temperature.

### 5.2.5. *In vitro* studies.

*Materials and cell lines.* Human breast adenocarcinoma MDA-MB-231 cell lines were obtained from ATCC (Virginia, US). The cells were maintained in Dulbecco's Modified Eagle's Medium culture medium (DMEM) supplemented with 10% fetal bovine serum (FBS) (Gibco, Thermo Fisher Scientific, Massachusetts, US), 5%  $\text{CO}_2$ , and 95% relative humidity. ProLong Gold Antifade Mountant with 4',6-diamidino-2-phenylindole (DAPI) was obtained from Thermo Fisher Scientific (Massachusetts, US). 3-(4,5-Dimethylthiazol-2-yl)-2,5-diphenyl tetrazolium bromide (MTT) and phosphate-buffered saline (PBS) were purchased from Sigma-Aldrich Co. (Missouri, US). Dimethyl sulfoxide was supplied by Merck Millipore (Massachusetts, USA).

*Dark and phototoxicity evaluation.* For dark cytotoxicity test without laser treatment, the MDA-MB-231 cell line was grown and maintained in complete DMEM at 37 °C in a 5%  $\text{CO}_2$  humidified chamber. MDA-MB-231 cells were seeded in 96-well plates at  $1 \times 10^4$  cells/well and were incubated overnight for cell adherence before nanogel samples were introduced. **NG-A** diluted in complete DMEM were added to the cells to give final concentrations ranging from 0.004 to 0.024 mg/ml.

The cells were then incubated for 24 hours at 37 °C in 5% CO<sub>2</sub>. The cell viability was assessed using MTT assay. Ten microliters of MTT (5 mg/ml in PBS) was added to each well and incubated for 4 h, followed by carefully removal of the spent culture medium with MTT and replaced with 100 µl of DMSO to dissolve the purple formazan crystals. The optical density of each well was then measured at 570 nm using a microplate reader (Infinite M200 PRO, Tecan, Männedorf, Switzerland). The viability of the cells in response to the treatment of **NG-A** was calculated as a percentage (%) of cell viability = (OD treated/OD control) × 100. The dark cytotoxicity test procedure was repeated for **NG-C** with concentration ranging from 0.008 to 0.024 mg/ml.

For phototoxicity evaluation, MDA-MB-231 cells in 96-well plates were treated with **NG-A and NG-C** at concentrations ranging from 0.004 to 0.024 mg/ml and followed by incubation for 2 hours at 37 °C with 5% CO<sub>2</sub> and 95% humidified atmosphere. Thereafter, the cells were irradiated with a blue laser diode (450 nm, 0.4 W.cm<sup>2</sup>) (PLTB450B, Osram, Munich, Germany) for 5 minutes. To ensure the entire surface area in each well was equally irradiated during the process; the diameter of laser beam was increased from 4 mm to 7 mm using a Plano-Convex lens (KBC031, Newport Corporation, California, US) and the laser power was adjusted accordingly to maintain the laser intensity. Laser irradiation was conducted separately on each well and the surrounding wells were masked by black-colored paper to prevent light spillage. After the laser treatment, cell viability was assessed via MTT assay. The phototoxicity evaluation procedure was repeated with a red laser diode (635 nm) at a power intensity of 1 W.cm<sup>2</sup> (HL 63193, Oclaro, California, US).

*Cellular internalization.* MDA-MB-231 cells (3×10<sup>5</sup> cells/well) were seeded on glass cover slips (22×22 mm), placed in 6 wells plate. The cells were then incubated with complete DMEM overnight at 37 °C in a 5% CO<sub>2</sub> humidified chamber. The cells were treated with **NG-A** (0.012 mg/ml) for 2 hours at 37 °C. After treatment, free **NG-A** were removed and the cells were rinsed twice with cold phosphate buffer saline (PBS). The cells were then fixed with 4% paraformaldehyde on a glass coverslip for 10 min at 37 °C and rinsed twice again with PBS. Fixed cells on glass coverslips were mounted on glass slides with Prolong Gold Antifade Mountant with DAPI. Cellular uptake of the nanogels was observed with a confocal laser scanning microscope using a 63 × oil immersion objective (Leica TCS SP5 II, Leica Microsystem, Wetzlar, Mannheim, Germany).

The DAPI dye was excited using a 405 nm diode laser and had its emission detected between 414 and 481 nm on the photomultiplier tube (PMT), while the **NG-A** was excited using a 458 nm argon laser and had their emissions detected 590–730 nm on the PMT detector. All scans were performed in an independent sequential mode to ensure no spectral overlap during acquisitions. Images were captured using the Leica LAS-AF image capture software. The cellular internalization study was repeated under identical experimental procedure with **NG-C** (0.024 mg/ml).

#### **5.2.6. Photothermal properties of nanogels.**

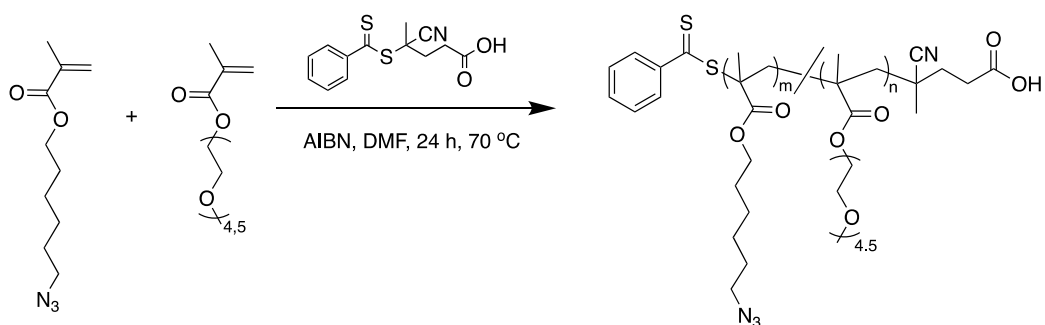
Transient bulk temperature profiles of nanogels were obtained using a red laser diode of 635 nm ( $1 \text{ W.cm}^{-2}$ ) and a blue laser diode of 450 nm ( $0.4 \text{ W.cm}^{-2}$ ) respectively. The nanogels at 0.012 and 0.024 mg/ml were suspended in complete DMEM and underwent laser irradiation for a maximum of 5 minutes. The temperature changes of the suspension were monitored using a thermocouple (Type T, Omega Engineering, Connecticut, US) with the probe positioned at the center of the suspension. All measurements were carried out at an initial temperature of 26 °C and the temperature changes of the suspension were recorded over the period of laser irradiation using a data logger (HH127, Omega Engineering, Connecticut, US).

### **5.3. Results and Discussion**

#### **5.3.1. Synthesis of reactive azide-functionalized copolymers.**

The synthesis of an azide-containing hydrophilic thermoresponsive copolymer was accomplished using reversible addition-fragmentation chain transfer (RAFT) polymerization of PEG-based methacrylate monomer (PEGMEMA) and an azide-containing methacrylate (AHMA) monomer (Scheme 5.1). Hydrophilic copolymers with pendant ethylene glycol chains were chosen since they possess thermoresponsive characteristics and are known to assemble into nanosized aggregates above their LCST.

In order to achieve facile crosslinking, a poly(PEGMEMA-co-AHMA) copolymer with several pendant azide groups was synthesized using a 4:1 feed ratio of PEGMEMA to AHMA to furnish a copolymer with similar monomer ratio (4:1) and mono-modal and narrow polydispersity index ( $M_n=14$  kDa,  $PDI=1.3$ ). The chemical composition and purity of the obtained polymer was confirmed using  $^1H$  NMR spectroscopy (Figure 5.2).



Scheme 5.1. Synthesis of copolymer poly(PEGMEMA-co-AHMA).

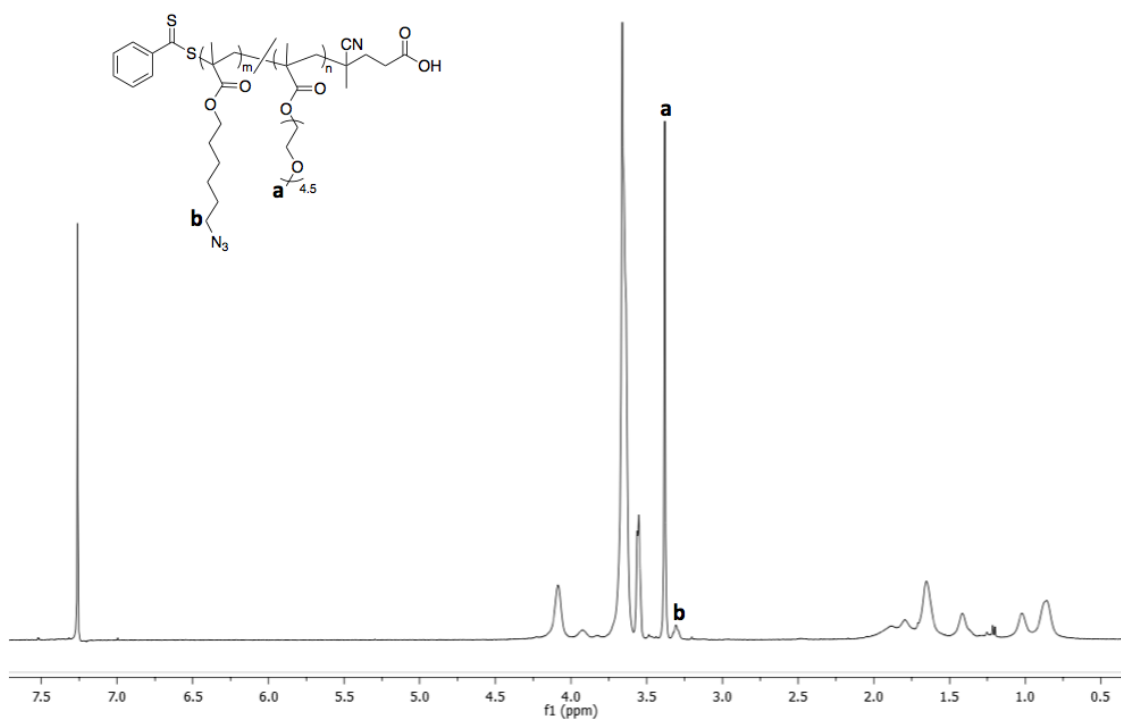


Figure 5.2.  $^1H$  NMR of copolymer poly(PEGMEMA-co-AHMA).

### 5.3.2. Synthesis of porphyrin-crosslinked nanogels.

A two-step procedure was followed to obtain crosslinked nanogels: first, the copolymers were heated above their LCST to obtain nanosized aggregates in aqueous media, followed by their crosslinking via Cu(I)-catalyzed azide-alkyne cycloaddition in the presence of the tetra-alkynyl Zn porphyrin. While the aqueous solution containing the copolymer was nearly transparent at room temperature, the solution turned turbid upon heating (Figure 5.3).

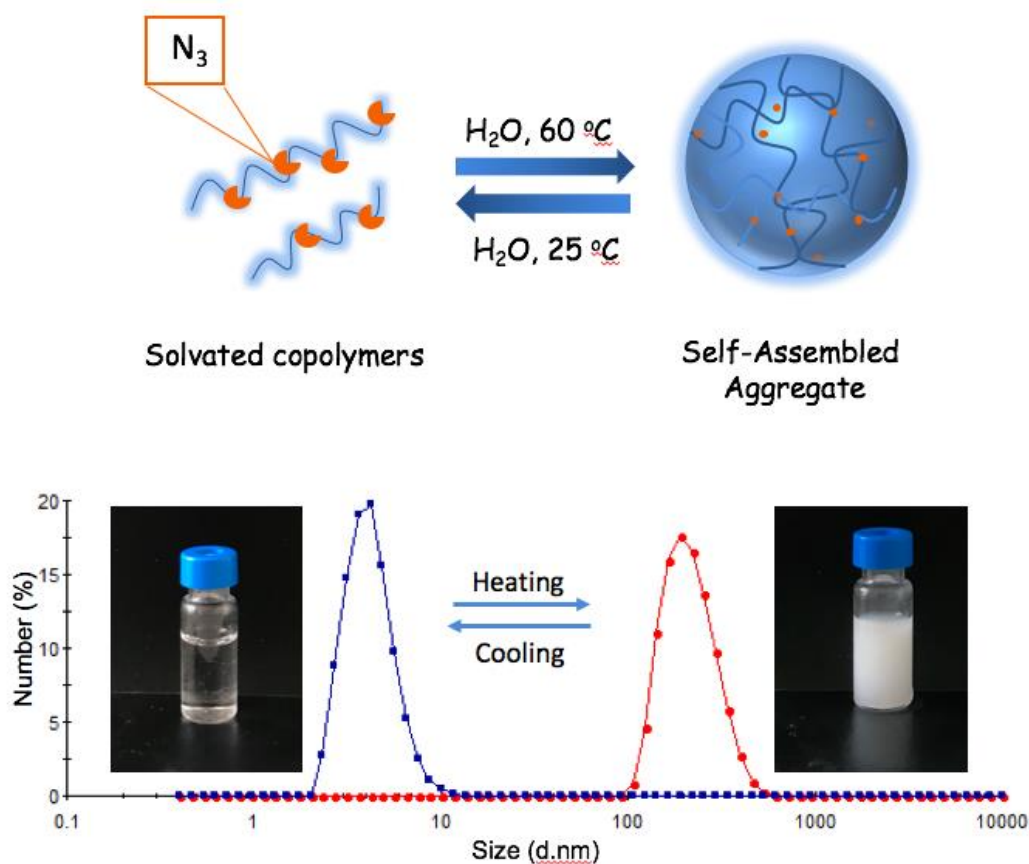


Figure 5.3 Aggregation of copolymers in aqueous solution above its LCST and change in hydrodynamic size as determined by DLS at 25 and 70 °C.

Size analysis using DLS showed that while an average size of 4 nm was obtained for the copolymer solution at room temperature, the size of the aggregates in the turbid solution was determined as 218 nm at 70 °C. Upon cooling to room temperature, the turbid solution regained its transparency and did not show presence of any aggregates. The next step involved fixing the aggregate as stable nanogels through crosslinking.

After formation of the aggregates in aqueous media, the tetra-alkynyl Zn porphyrin dissolved in minimal amount of acetone is added into the solution, followed by addition of mixture of the CuSO<sub>4</sub>/NaAsc catalyst system. No loss of turbidity takes place during these additions, and turbidity remained observed upon and after cooling the reaction to room temperature after the crosslinking. No crosslinking was observed when the catalyst system was not introduced into the reaction mixture, and upon cooling a clear solution with precipitated porphyrin was obtained. Obtained nanogels were purified using dialysis in ethanol to remove any unreacted copolymer and residual porphyrin. Thereafter, nanogels were obtained as dispersion in aqueous media by finally dialyzing against water.

Hydrodynamic diameter of the nanogel **NG-A** in water was determined as 111 nm using DLS. Analysis using TEM under dry conditions on a carbon film coated copper grid revealed a slightly lower size of  $77 \pm 16.9$  nm, probably due to shrinkage of the nanogels upon drying (Figure 5.4). It was evident through visual inspection that the porphyrin was well-dispersed in aqueous media upon conjugation to the nanogels, since addition of an acetone solution of porphyrin to aqueous media resulted in precipitation (Figure 5.4b).

Using this methodology, three sets of nanogels (**NG-A**, **NG-B** and **NG-C**) with varying amount of porphyrin were prepared by adjusting the ratio of alkyne to azide groups as 1:2, 1:4 and 1:8, respectively. Consequently, **NG-A** has the highest porphyrin content while **NG-C** has the lowest. No significant change in DLS size could be observed upon changing the crosslinker ratio (Figure 5.4b), which can be expected since the size of the self-assembled aggregates prior to crosslinking are similar.

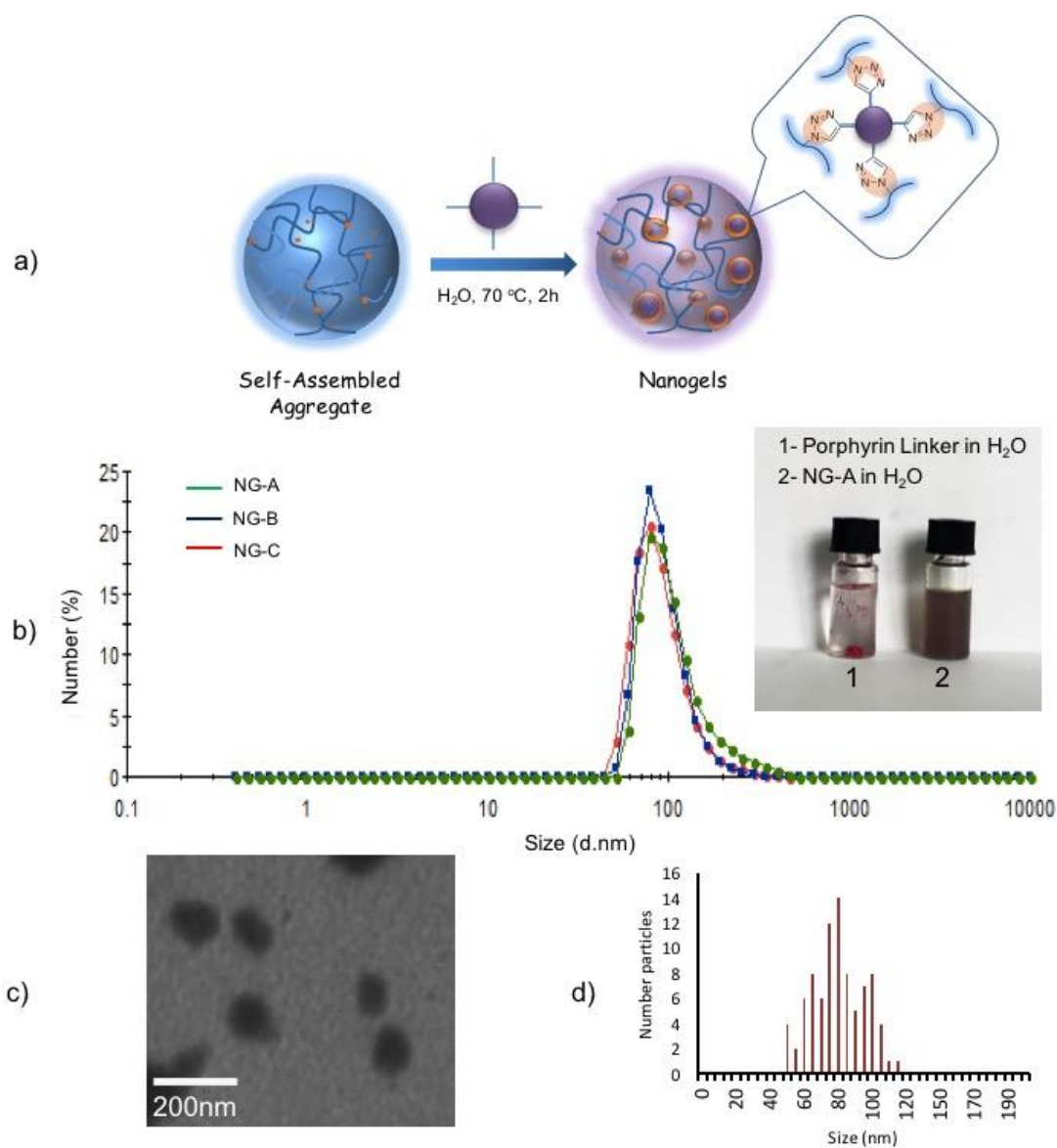


Figure 5.4. a) Schematic presentation of gelation. b) Hydrodynamic size of **NG-A**, **NG-B** and **NG-C** at 25 °C using DLS. c) Size of nanogel **NG-A** using TEM. d) Size distribution of **NG-A** from TEM analysis.

### 5.3.3. Photophysics and photochemistry.

All the photophysical and photochemical data of the three nanogels have been measured in ethanol and are summarized in Table 5.1. The general shape of the electronic absorption spectra (Figure 5.5) is not significantly modified by the porphyrin content of each nanogel and all the band maximum absorption remain the same independently from the porphyrin ratio. Fluorescence emission spectra also have all the same maxima, and fluorescence quantum yields are all similar to those of the reference ZnTPP, without being affected by the their inclusion into the nanogel or the loading ratio.

The generation of singlet oxygen was measured at five different concentrations of nanogels, with excitation at 425 nm. Phenalenone was used as the reference ( $\Phi_{\Delta} = 0.95$ ) [196]. The SOG quantum yield values are consistent with the respective porphyrin content of the nanogels, with a linear trend. **NG-A** which has four times the amount of porphyrin compared to **NG-C** exhibits a two-fold SOG quantum yield value compared to those of **NG-C**, the value for **NG-B** being in between as expected.

Table 5.1. UV-vis, fluorescence and singlet oxygen generation values of the nanogels

Nanogel	Porphyrin relative ratio	$\lambda_{\text{abs}}$ (nm)	$\lambda_{\text{em}}$ (nm)	$\Phi_{\text{F}}$	$\Phi_{\Delta}$
<b>NG-A</b>	2	425, 570, 607	615, 647	3	42
<b>NG-B</b>	1	425, 570, 607	615, 647	3	30
<b>NG-C</b>	0.5	425, 570, 607	615, 647	3	21

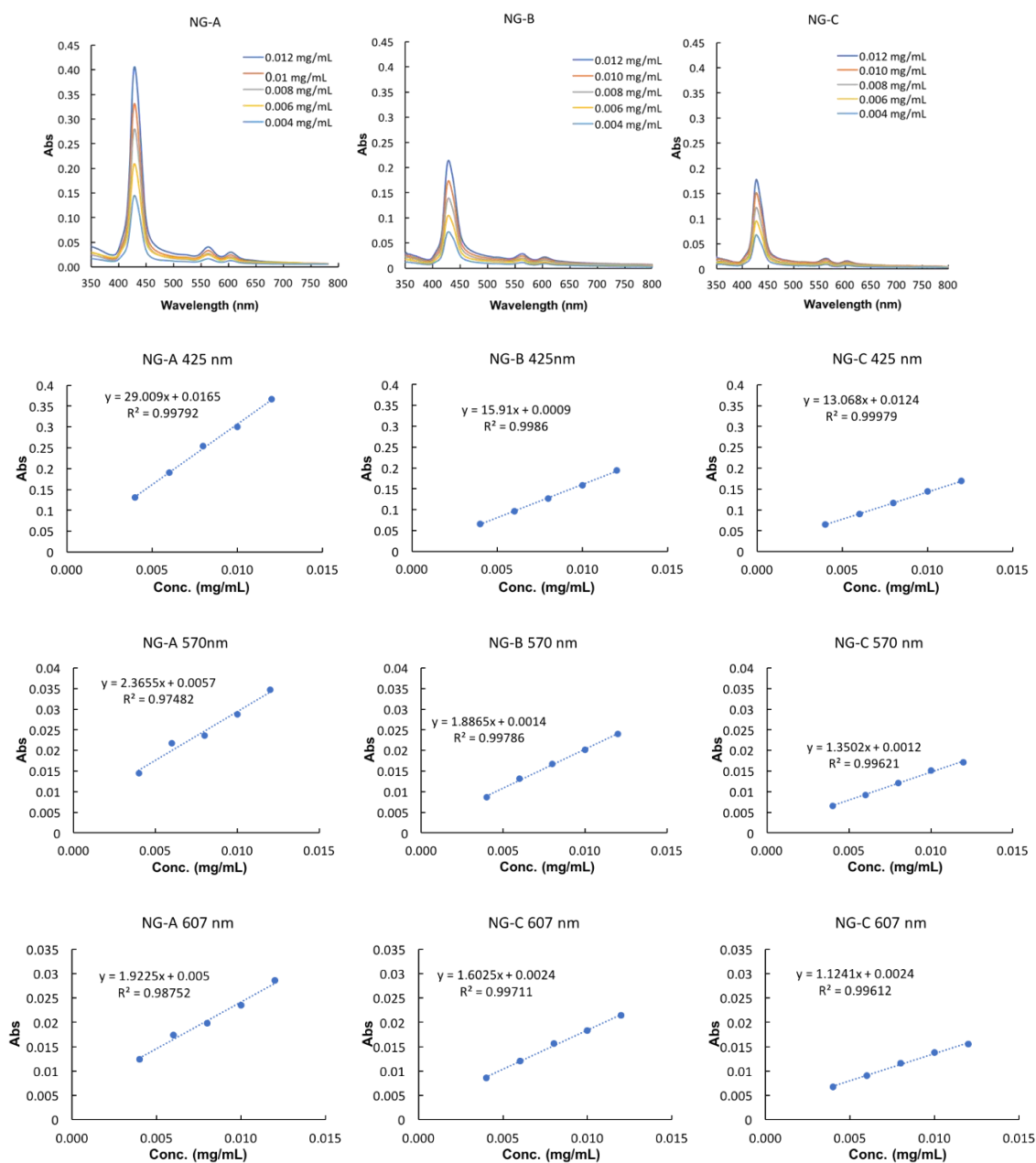


Figure 5.5. UV-visible spectra of NG-A, NG-B and NG-C in ethanol and plots of the absorbance at 425, 570 and 607 nm vs concentration.

*In vitro dark and phototoxicity.* Having established that the nanogels can generate singlet oxygen, the toxicity of NG-A and NG-C (with the highest and lowest amount of porphyrin) against human breast adenocarcinoma MDA-MB-231 cells was tested to ascertain their toxicity with and without irradiation.

MDA-MB-231 cells were incubated with **NG-A** and **NG-C** nanogels and the dark and phototoxicity was analyzed using the MTT assay (Figure 5.6).

For phototoxicity testing, two different irradiation wavelengths were used to excite the nanogels. First excitation was with a blue laser diode at 450 nm with a  $0.4 \text{ W.cm}^{-2}$  weak energy intensity, allowed by the intense B band absorption of the porphyrin. Second excitation was with a red laser diode at 635 nm at a stronger energy intensity ( $1 \text{ W.cm}^{-2}$ ) to compensate for the less intense absorption at this wavelength. Irradiation at longer wavelengths has the dual advantage of being able to penetrate more deeply into the tissues and to avoid the excitation of endogenous chromophores.

As porphyrins in close proximity to one another are likely to exhibit also photothermal properties, the well-known example being porphysomes<sup>17</sup>, the temperature variations of nanogels solutions irradiated at the same conditions ( $0.4 \text{ W.cm}^{-2}$  at 450 nm and  $1 \text{ W.cm}^{-2}$  at 635 nm) were also recorded (Figure 5.7) [169]. As blue light in particular is known to reduce the viability of eukaryotic cells, the effect of laser irradiation at these wavelengths and energy intensities in the absence of nanogels were first experimentally confirmed to not damage the MDA-MB-231 cells (Figure 5.8) [197].

Without laser irradiation, high cell viability ( $\geq 90\%$ ) was observed for both **NG-A** and **NG-C** treated cells (Figure 5.6A). Upon irradiation at 450 nm,  $\text{IC}_{50}$  values of cells treated with **NG-A** and **NG-C** were  $0.011$  and  $0.023 \text{ mg.mL}^{-1}$  respectively (Figure 5.6B), with a concurrent slight increase in bulk temperature ( $1.1\text{-}1.4 \text{ }^\circ\text{C}$  and  $3.6\text{-}4.0 \text{ }^\circ\text{C}$  for **NG-A** and **NG-C**, respectively, Figure 5.7A) compared to the medium irradiated in the absence of nanogels. The photo-induced cell death observed here can hence be attributed to primarily from photodynamic action. The respective  $\text{IC}_{50}$  values of **NG-A** and **NG-C** are consistent with the four-fold lower amount of porphyrin in **NG-C** than in **NG-A** at equal concentration of nanogels.

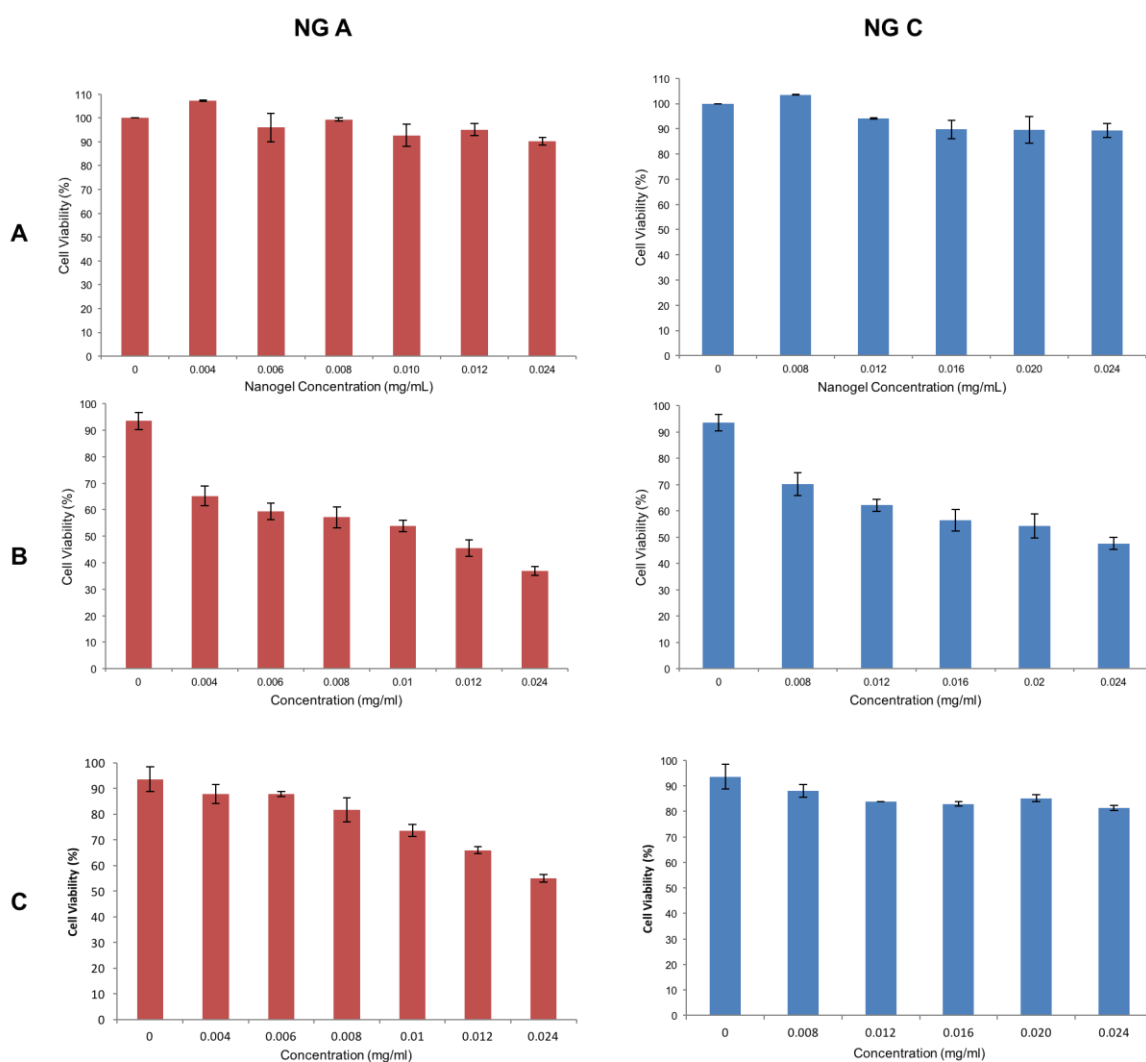


Figure 5.6. Cell viability of MDA-MB-231 after (A) 24 h of incubation in the dark, (B) laser irradiation at 450 nm,  $0.4 \text{ W.cm}^{-2}$  and (C) laser irradiation at 635 nm,  $1 \text{ W.cm}^{-2}$ .

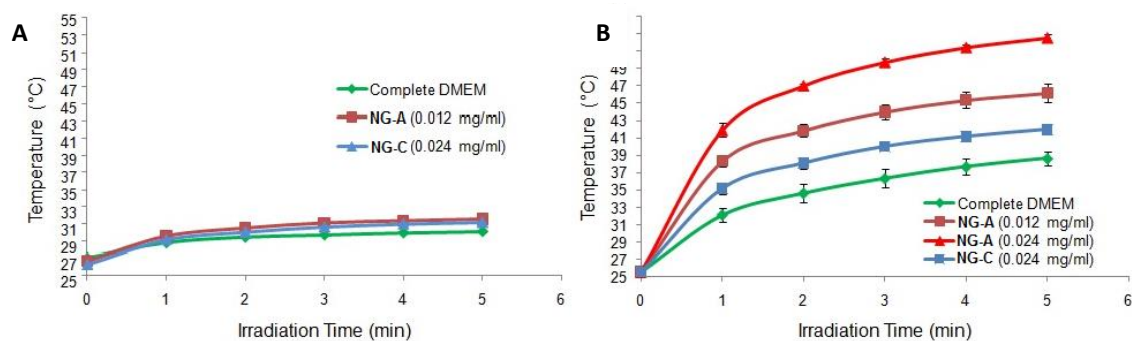


Figure 5.7. Transient bulk temperature profile of NG-A and NG-C dispersions in DMEM under laser irradiation at (A) 450 nm ( $0.4 \text{ W.cm}^{-2}$ ), (B) 635 nm ( $1 \text{ W.cm}^{-2}$ ).

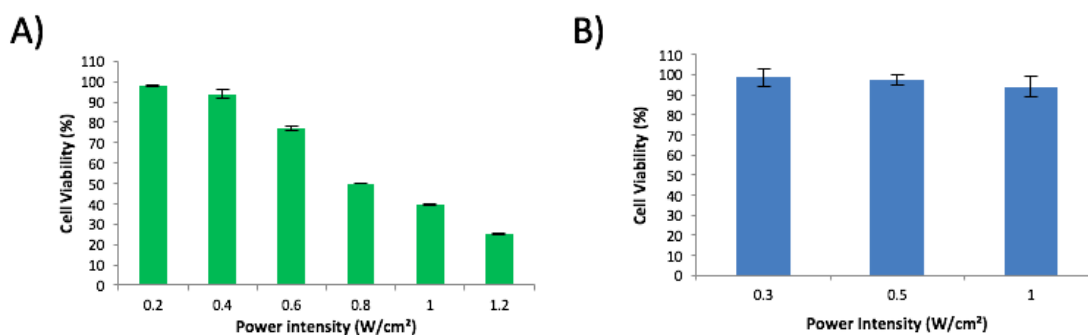


Figure 5.8. Effect of laser irradiation on MDA-MB-231 cells at (A) 435nm and (B) 650nm.

Notable differences were observed when irradiating at 635 nm (Figure 5.6C and 5B). In terms of cell viability, **NG-A** displayed higher phototoxicity than **NG-C** ( $\approx 65\%$  vs  $>80\%$  cell viability respectively at 0.24 mg/ml, Figure 4C). In terms of temperature elevation, both **NG-A** and **NG-C** exhibited higher bulk temperature increase than the control (DMEM without nanogels), but to a larger extent for **NG-A** (0.012 mg/mL) which produced a higher temperature elevation of  $7.5 \text{ }^\circ\text{C}$  compared to **NG-C** (0.024 mg/mL) which induced a lower temperature increase of  $3.3 \text{ }^\circ\text{C}$  (Figure 5.6B). The total amounts of porphyrin present are the same for these two conditions (**NG-A** at 0.012 mg/mL and **NG-C** at 0.024 mg/mL), except the macrocycles are closer to each other in **NG-A** than in **NG-C**.

This is consistent with the principles of photothermal induction, where heat generation is maximized when the photosensitizers are close to each other as their de-excitation due to non-radiative processes is greater than the emission of fluorescence, phosphorescence or the generation of singlet oxygen. In the same excitation conditions, **NG-A** at 0.024 mg/mL could even induce a temperature increase of 13.6 °C. Photo-induced cell death observed upon irradiation at 635 nm can therefore be attributed to a mixed photodynamic and photothermal effect.

#### 5.3.4. Cellular Internalization

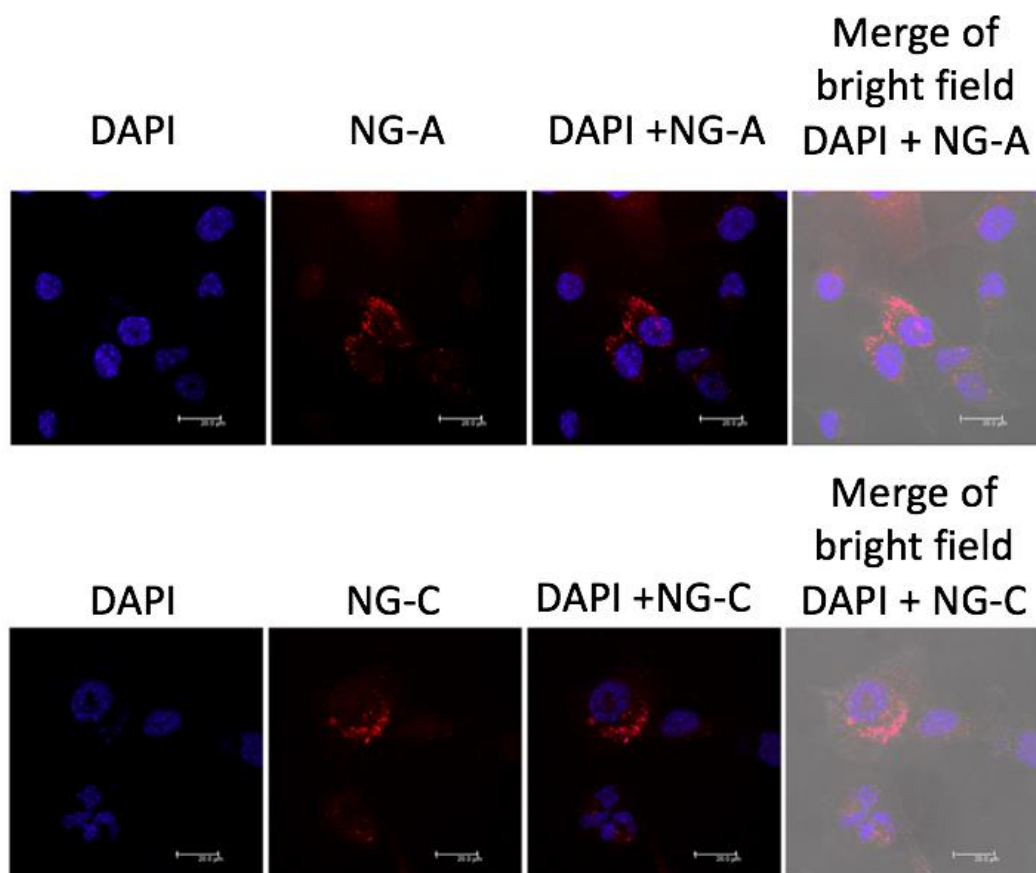


Figure 5.9. Cellular internalization of nanogels **NG-A** and **NG-C**. Corresponding bright field images merged with fluorescence images were included for clarity. The scale bars correspond to 20  $\mu\text{m}$ .

Cellular uptake of **NG-A** and **NG-C** by MDA-MB-231 cells was determined and analyzed using confocal microscopy. Images of cells treated with **NG-A** and **NG-C** respectively co-stained with a nucleus-specific probe (DAPI) were captured and minimal fluorescence overlaps between nanogel samples (red fluorescence) and DAPI (blue fluorescence) were observed (Figure 5.9). This result suggests that **NG-A** and **NG-C** were internalized into cytoplasm; however both nanogel samples were not localized in nucleus after 2 hours of incubation. Our finding is consistent with other report indicating that only nanoparticles with size  $\leq 6$  nm were able to enter cell nucleus [198].

#### 5.4. Conclusions

Porphyrin-crosslinked nanogels as PDT and PTT agents were obtained in a single step through crosslinking of nanosized self-assembled aggregates of thermoresponsive copolymers. Tetra-propargyl porphyrin based crosslinkers were used to obtain nanogels through the copper-catalyzed azide-alkyne cycloaddition reaction under surfactant free conditions. The obtained nanogels were readily dispersible in aqueous media and solubilized compared to the otherwise hydrophobic porphyrin moiety. Varying the amount of porphyrin based crosslinker during nanogel formation allows for tunability of the amount of PDT/PTT agent incorporated into the nanogel.

Thus obtained porphyrin containing nanogels preserved the photophysical characteristics of the porphyrin, and were able to generate singlet oxygen under UV-irradiation. The nanogels could also be heated through irradiation at longer wavelengths to provide photothermal heating. Biological experiments demonstrated that the porphyrin containing nanogels were able to induce cancer cell death when illuminated at short and long wavelengths and were observed to accumulate in the cytoplasm region of the cells. Due to the modular nature of the fabrication of porphyrin-crosslinked nanogels, the strategy will be extended to integrate other PDT and PTT photosensitizers, such as phthalocyanine

## **6. STIMULI-RESPONSIVE ANTIBIOTIC RELEASING CRYOGELS**

### **6.1. Introduction**

Advances in controlled drug release systems and devices have addressed many of the challenges encountered in traditional drug delivery. Both spatial and temporal control over drug administration helps address issues like undesirable toxicity and overdosing that leads to complications like development of resistance toward treatment [7,120,148,199]. Development of resistance toward therapeutic agent is a widespread problem in many diseases, and has especially emerged as a major hurdle in combating bacterial infections [25,200,201].

While utilization of local administration of antibiotics in cases like wound healing circumvents issues like systemic toxicity to a large extent, control over release of drug is an important criterion to maintain effective concentration of therapeutic agent over prolonged period as well as to reduce the over-dosage of antibiotic administered. To address this issue, stimuli responsive systems where on-demand release can be triggered have been focus of recent research [14]. To date, several drug releasing systems where stimuli such as UV-irradiation, magnetic, redox, pH, enzymatic and thermal cues have been employed to trigger release have in reported [40,192,202-205]. In most formulations the drug is either encapsulated or covalently integrated into a polymeric matrix which is responsive to the abovementioned external stimuli. Utilization of heat as an external trigger has been widely used due to simplicity in its application [206]. Local application of heat to a specific material leads to either physical or chemical changes in the matrix, which in turn affects the release of therapeutic agent stored in the matrix either through physical or chemical interactions.

Lately, local application of heat in a more precise and convenient manner has been done through photothermal heating [207]. This allows utilization of a source like near infrared irradiation to induce heating of a photothermally active material. In particular crosslinked polymeric systems such as hydrogels, have been embedded with photothermal materials like gold nanorods, organic chromophores like thiophenes and indocyanines, and lately carbon based materials such as graphene oxide [208-212]. In particular, graphene based materials have gained a lot of popularity because of their facile availability when compared to the other alternatives which require expensive chemicals and are more labor intensive. Graphene oxide and their derivatives have been used to fabricate drug delivery platforms either as discrete nanocarriers or have been incorporated into composite nanomaterials [213-215]. Hydrogels integrated with graphene oxide and its derivatives have been used for photothermally triggered release of anti-cancer drugs and proteins [59, 216, 217].

A survey of literature shows that while graphene oxide sheets and surface coatings have been used to combat bacterial infections, a hydrogel interface where release of an antibiotic can be triggered through exposure to NIR has yet to be explored. We envisioned that a graphene oxide embedded hydrogel interface where release of encapsulated and/or covalently bound antibiotics can be triggered through photothermal heating would be an effective on-demand dosing platform. While thermal heating will promote the release of encapsulated antibiotic through enhanced diffusion, a thermally cleavage bond will enable a control over the release of the conjugated antibiotic through specific cleavage of bonds.

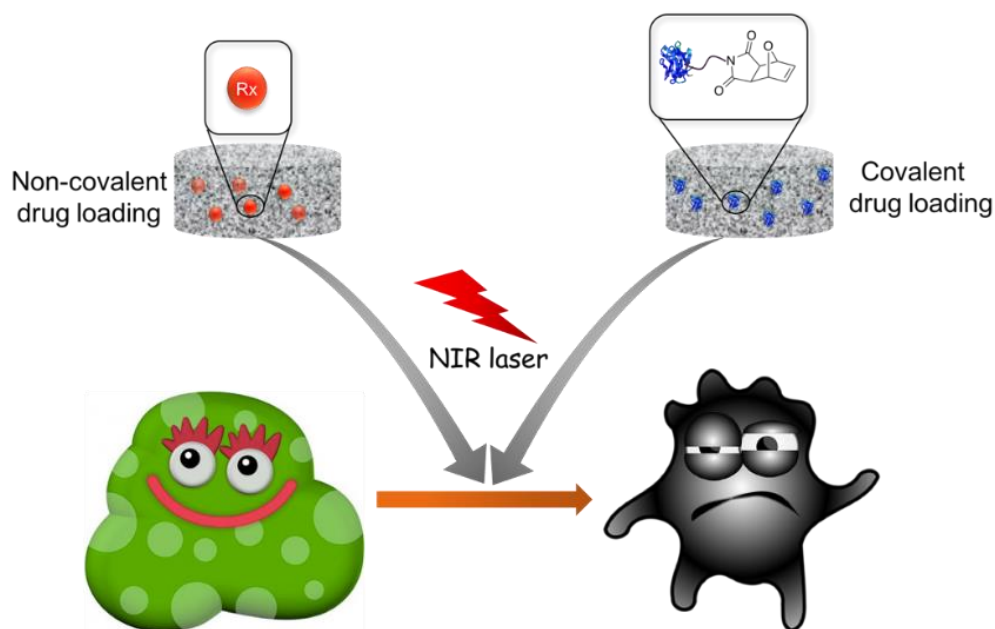
The retro Diels-Alder cycloreversion reaction has been widely explored as a thermally cleavable trigger [142-144]. In particular, the Diels-Alder *endo*-cycloadduct obtained through reaction of a furan and maleimide containing units at low temperatures undergoes cycloreversion triggered fragmentation at moderately low temperatures [218]. While the furan-maleimide dyad has been extensively explored to fabricate self-healing materials, this reaction has been utilized in recent years for fabrication of crosslinked hydrogel materials at room temperature in a reagent free manner [219-221]. While the Diels-Alder reaction has been employed for the formation of the hydrogel itself, utilization of furan as a handle to release therapeutically active agents from polymeric materials is rare.

Vieyres *et al.* reported dendrimers containing furan group at their periphery, where lipoic acid drugs were conjugated and released upon heating from ambient to physiological temperatures [222]. A seminal contribution which reports utilization of the Diels-Alder cycloreversion to release peptides was reported by Bowman and coworkers. They fabricated crosslinked hydrogels using the thiol-Michael addition reaction and used pendant maleimide units to integrate peptides through a furan linkage, where release of the peptide in a temperature dependent manner was observed [55]. In another example Bowman and coworkers reported attachment of furan-containing dexamethasone to maleimide containing hydrogels and demonstrated heat induced release of drug over time [68]. Coupling of photothermal heating with the retro DA-reaction has been reported by Niidome and coworkers. The authors demonstrated that a PEG chain coating attached onto gold nanorods through a furan-maleimide adduct could be removed with NIR irradiation mediated cleavage of the cycloadduct. One can expect that fabrication of release systems using cheaper and readily available graphene based materials will be pragmatic [223]. The recognition that the *endo*-cycloadduct furnishes an easily activable trigger is evident from other recent reports by Hawker and Fujigaya who incorporate this motif for functionalization of polymers [224,225].

While traditionally hydrogels have been extensively explored as drug release systems and scaffolds for biomolecular and cellular scaffolds, in recent years, focus has shifted to utilization of the macroporous member of the hydrogel family, often referred to as cryogels [226]. The higher porosity of cryogels addresses several of the challenges in traditional hydrogels related to transport of bio-molecules which limit extent of matrix functionalization and accessibility, as well as release of conjugated payloads. In a recent study we demonstrated that the superior performance of cryogels over traditional hydrogels for conjugation and release of anti-cancer drugs [85].

Compared to hydrogels, cryogels exhibited better release of drugs, presumable due to the higher porosity and swellability of these materials which allows for better transport of medium into their interiors. It can be envisioned that fabrication of a rGO-containing cryogel containing furan groups in the matrix will provide a system capable of acting as an anti-bacterial depot where drugs can be either encapsulated or conjugated to release them in a controlled fashion in the presence of a photothermal trigger.

Herein, we report fabrication of photothermally addressable cryogels consisting of an rGO-embedded matrix comprised of hydrophilic poly(ethylene glycol) and hydrophobic furfuryl groups. The furfuryl groups serve the dual role of providing hydrophobic groups for delivering hydrophobic pockets, as well as under covalent conjugation with maleimide-containing therapeutically active agents such as antimicrobial peptides (AMPs). While the system performed as expected for release of conventional antibiotic like Ampicillin, the study reveals that integration of rGO inside the cryogels hindered the release of AMPs. To circumvent this problem, a bilayer device structure where the furan-containing cryogel was supported on a rGO-coated surface was employed. It was demonstrated that while passive release of conjugated dyes and peptides to the cryogel was minimal, enhanced active-release was observed under NIR irradiation. It was demonstrated that while the cryogel scaffolds were non-toxic towards HeLa, cryogels loaded with encapsulated antibiotic such as ampicillin or conjugated AMPs were active against *E. Coli* and *S. Aureus* bacteria strains, respectively (Scheme 6.1).



Scheme 6.1. Schematic illustration of the irradiation of antibacterial loaded cryogels for the killing of bacteria triggered by near infrared laser.

## 6.2. Experimental

### 6.2.1. Materials

Ampicillin was purchased from Sigma-Aldrich (Darmstadt, Germany) and used as received. Poly(ethylene glycol) methyl ether methacrylate (PEGMEMA,  $M_n = 300 \text{ gmol}^{-1}$ ), poly(ethylene glycol) dimethacrylate (PEGDMA,  $M_n = 550 \text{ gmol}^{-1}$ ), and furfuryl methacrylate (FuMA) were obtained from Sigma Aldrich and purified by filtering through activated aluminum oxide column prior to use. 2,2-dimethoxy-2-phenylacetophenone (DMPA), and *N*-(5-fluoresceinyl)maleimide were purchased from Sigma Aldrich. BM(PEG)2 (1,8-bismaleimido-diethyleneglycol) was obtained from Thermo Fisher. Solvents were obtained from Merck and used as received without further purification unless otherwise noted. All gelation reactions were performed at 365 nm using a UV Lamp with a 100W spot bulb at a distance of 10 cm. Anti-microbial peptide (RWRWRWC-NH<sub>2</sub>) was synthesized by Aleksandra Loczechin and used as such. Kapton® HN polyimide foils with a thickness of 125  $\mu\text{m}$  were obtained from DuPont™ and graphene oxide was purchased from Graphenea, Spain. Graphene oxide was reduced according to literature procedure [59] Cytotoxicity and anti-bacterial assays were done according to literature protocols [227].

### 6.2.2. Fabrication of Cryogels.

A mixture of all monomers and crosslinkers at desirable ratios was prepared in 1,4-dioxane. Gelation was undertaken at -13 °C under UV irradiation exposure. After 1 h, cryogels were thawed at room temperature and washed with 1,4-dioxane followed by water to remove any unreacted monomers. The cryogels were dried under vacuum to yield spongy materials.

### 6.2.3. Synthesis of Maleimide-conjugated Peptide.

The linker BM(PEG)<sub>2</sub> (0.81 mg, 2.62  $\mu$ mol) and peptide RWRWRWC-NH<sub>2</sub> (1mg, 0.871  $\mu$ mol) are mixed together in DMF. Progress of reaction was followed using LCMS and upon completion of reaction, the peptide was precipitated in cold ether and centrifuged to obtain the desired peptide-maleimide.

### 6.2.4. Synthesis of rGO Loaded Furan-containing Cryogels

The method for cryogel preparation was followed with additional introduction of rGO. Mixtures were sonicated to achieve maximum possible homogeneity. The cryogels were dried in *vacuo* and black crosslinked materials were obtained.

### 6.2.5. Preparation of Kapton/rGO flexible patch

Kapton foils (10  $\times$  10 mm<sup>2</sup>) were cleaned with acetone in an ultrasonic water bath for 30 min, followed with isopropanol for 10 min and then dried under a nitrogen flow. The cleaned Kapton foils were modified with rGO by drop-casting (100  $\mu$ L) three times, followed by drying at room temperature for several hours.

### 6.2.6. Swelling of cryogels

Swelling studies were done by cutting small piece of dried cryogel and placing it in a beaker containing distilled/deionized water at room temperature. At regular time interval, the cryogel samples were weighed after removing excess water and the percentage of water uptake was calculated using the following equation:

$$\text{Swelling \%} = (W_{\text{wet}} - W_{\text{dry}}) / W_{\text{dry}} * 100$$

where  $W_{\text{wet}}$  and  $W_{\text{dry}}$  are the weights of the cryogels in their swollen and dried states, respectively.

### 6.2.7. Antibiotic loading

6.2.7.1. Non-covalent integration of ampicillin. The cryogels were loaded with ampicillin by mixing the cryogel with ampicillin solution containing varying amounts of the drug under shaking for 12 h at 4°C. The concentration of antibiotic loaded onto the gel was determined using HPLC analysis.

#### 6.2.7.2. Diels-Alder Reaction of Maleimide-contain Dye and Peptide.

*Conjugation of N-(5-Fluoresceinyl) maleimide.* A solution of dye in PBS was prepared and loaded with the cryogel CG-40 and let to react for 24h at room temperature. Any unbound dye was washed with PBS. Solution of PBS was analyzed by fluorescence to ensure total removal of the dye.

*Conjugation of Maleimide-containing Antibacterial Peptide.* Aqueous solution of the peptide-maleimide was prepared and loaded with the cryogels CG-40 at different concentrations of peptide and let to react for 24h at room temperature. Any unbound peptide was washed with water. Wash solution was analyzed by UV-vis spectroscopy to ensure total removal of free peptide.

### 6.2.8. Quantification of loading and release

*High-performance liquid chromatography (HPLC) for quantification of AMP loading and release.* The concentration of ampicillin loaded onto **CGrGO-40** was determined by an HPLC system (Shimadzu, Tokyo, Japan) equipped with a 5 µm C<sub>4</sub> QS Uptisphere<sup>®</sup> 300 Å, 250 mm × 4.6 mm column heated to 40 °C. The mobile phase consisted of a mixture of eluent A (trifluoroacetic acid 0.1% in water) and eluent B (trifluoroacetic acid 0.1 % in acetonitrile) at a flow rate of 1 mL/min. The samples were injected at a volume of 40 µL and the detection wavelength was 227 nm. A calibration curve of a series of ampicillin solutions of different concentrations was used to determine the concentration of ampicillin remaining in the supernatant solution used for loading, allowing the determination of the ampicillin concentration in **CG-rGO**.

The concentration of aliquot removed at different time interval were measured using the same parameters as above to determine the amount and % of ampicillin released.

*Fluorescent plate reader for quantification of dye loading and release.* The concentration of dye loaded onto **CGrGO-40** was determined by a plate reader. First a calibration curve of a series of dye solutions of different concentrations was generated. The concentrations of dye remaining in the supernatant used for loading and wash solutions were measured, allowing the determination of the dye concentration in **CGrGO**. The concentration of aliquot removed at different time interval during the photothermal and passive release were measured using the same parameters as above to determine the amount and % of dye released.

### **6.2.9. Photothermal release studies**

Antibiotic release experiments were performed in 1 mL PBS buffer. The cryogels were irradiated with a continuous mode laser with an output light at 980 nm ( $1\text{ W cm}^{-2}$ ) for various time intervals (1-60 min). Thermal images were captured by an infrared camera. The amount of antibiotic released was evaluated by HPLC. The quantity of dye released was determined using fluorescence spectroscopy.

### **6.2.10. Characterization**

UV–visible spectra were collected on a Varian Cary 100 Scan UV–vis spectrophotometer.  $^1\text{H}$  NMR and  $^{13}\text{C}$  NMR spectra were obtained using a Bruker 400 MHz spectrometer. Optical images of cell lines were recorded using a 10× magnification inverted microscope (Nikon Eclipse TS100, Japan) Scanning electron microscope (SEM) was performed to characterize the morphologies of cryogels using an ESEM-FEG/EDAX Philips XL-30 (Philips, Eindhoven, The Netherlands) instrument operating at 10 kV.

## 6.3. Results and Discussion

### 6.3.1. Fabrication of rGO loaded furan-modified cryogels

A series of rGO-containing maleimide reactive cryogels (**CGrGO-0–CGrGO-40**, Table 6.1) were fabricated using varying amounts of poly(ethylene glycol) methyl ether methacrylate (PEGMEMA) and furfuryl methacrylate (FuMA) monomer and aqueous dispersion of rGO (2.0 wt. %). The synthesis of cryogel was performed at  $-13\text{ }^{\circ}\text{C}$  under UV irradiation (365 nm) in the presence of 2,2-dimethoxy-2-phenylacetophenone (DMPA) and poly(ethylene glycol) dimethacrylate (PEGDMA) as a cross-linker (Figure 6.1). In order to compare the result with rGO-depleted cryogel, the same procedure was repeated without any addition of reduced graphene oxide to obtain CG with different percentage of Furan.

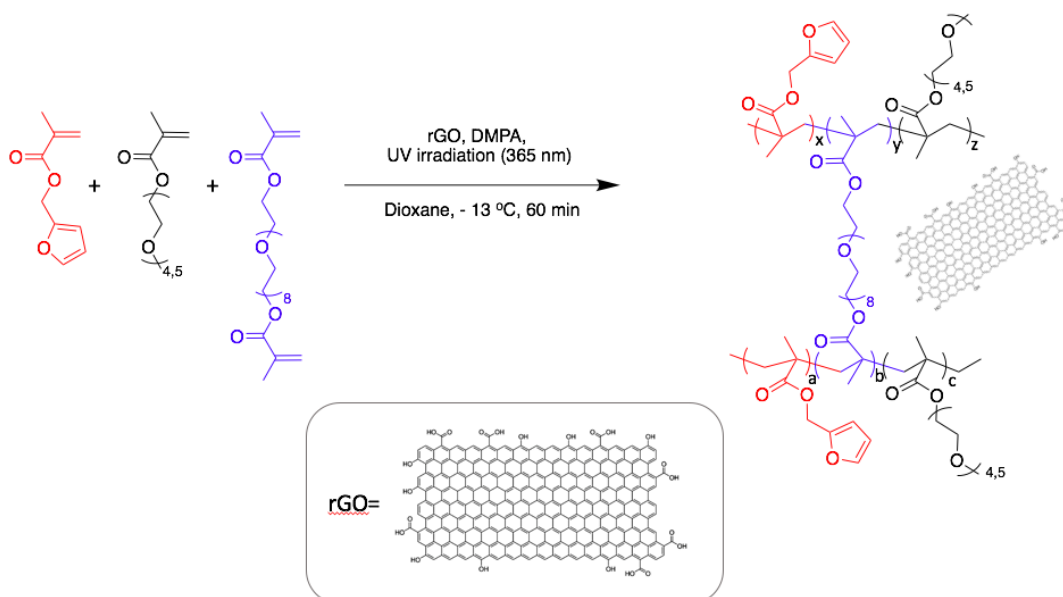


Figure 6.1. Illustration of fabrication of furan-containing rGO embedded cryogels.

Table 6.1. Composition and conversion of cryogels fabricated via photo-crosslinking.

Entry	Cryogel	[FuMA]: [PEGMEMA]	Gel Content (%)
1	CGrGO-0	0:100	89
2	CGrGO-10	10:90	89
3	CGrGO-20	20:80	85
4	CGrGO-30	30:70	86
5	CGrGO-40	40:60	93

The swelling profiles of the cryogels were studied by tracking their water uptake as a function of time until the cryogels reached constant weight which occurred within a few minutes (Figure 6.2a). Generally, all cryogels showed a decrease in swelling with increasing hydrophobic monomer content. The same procedure was repeated with cryogels without any reduced graphene oxide, denoted as CG hereafter (Figure 6.2b). It was observed that their swelling was much higher (e.g. 1122% swelling for **CG** vs 468% for **CGrGO**). It can be concluded from these results that the use of rGO renders the cryogels more hydrophobic and decrease overall water uptake.

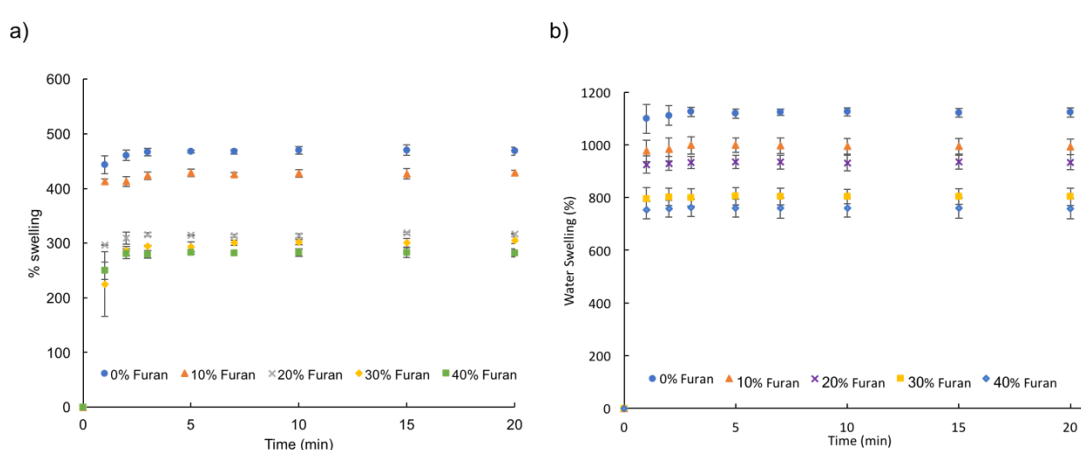


Figure 6.2. Water uptake of cryogels containing varying amounts of furan (a) with rGO and (b) without rGO in water at 24 °C.

The morphology of the resulting **CG-rGO** was investigated using scanning electron microscopy (SEM). Figure 6.3 shows the formation of pores around 10  $\mu\text{m}$  for the **CG-rGO** and 25  $\mu\text{m}$  for **CG**. Presumably, it is the small pores and more dense structure of the rGO-containing cryogels compared to the cryogels devoid of rGO that reduces the overall water uptake.



Figure 6.3. Hydrogel samples prepared using similar amount of monomers and SEM images of cryogels with (left) and without (right) embedded rGO.

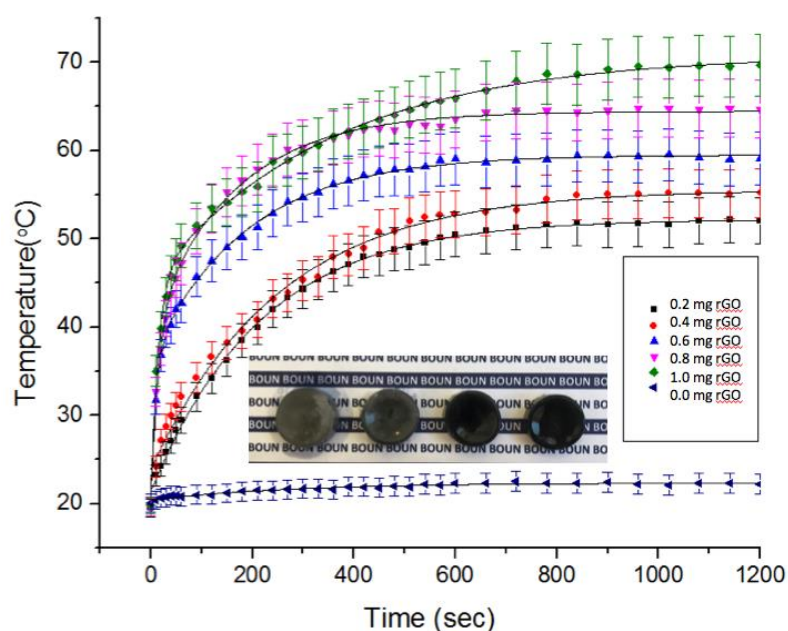


Figure 6.4. Photothermal heating curves of cryogels with different amount of rGO when immersed in PBS (0.1 M, pH 7.4) and exposed to laser light of 980 nm for 10 min at  $1\text{W cm}^{-2}$ .

Thereafter, the photothermal properties of the **CGrGO** cryogels were explored (Figure 6.4). Irradiation of **CGrGO** (30 mg/mL in PBS) with a continuous wave laser at 980 nm at  $1 \text{ Wcm}^{-2}$  for 20 min resulted in a surface temperature of about  $70 \pm 3 \text{ }^\circ\text{C}$ . The same experiment was repeated with cryogels containing different amount of rGO, and it was observed that the lower the amount of rGO, the lower was the increase in temperature.

### 6.3.2. Loading of anti-bacterial compounds

Loading of the anti-bacterial (antibiotic and peptide) can be achieved via two ways; they can be loaded by simply immersing the gel into aqueous solution of ampicillin in water at  $4 \text{ }^\circ\text{C}$  for 24h, or it can be achieved via Diels-Alder reaction between the furan inside the cryogels and a maleimide containing peptide or dye. Both antibiotics and peptide contain aromatic, thus promoting their interaction with rGO through  $\pi$ - $\pi$  stacking.

6.3.2.1. Loading via absorption. The loading capacity of **CGrGO** cryogels for ampicillin was evaluated by determining the concentration of the antibiotic in solution before and after loading using HPLC. It was observed that the initial concentrations of loading is proportional to the amount loaded inside the cryogels (Figure 6.5). Using solution concentration of  $800 \text{ } \mu\text{g mL}^{-1}$  of the antibiotics resulted in the loading of about  $114 \text{ } \mu\text{g mL}^{-1}$  (14 %) for ampicillin.

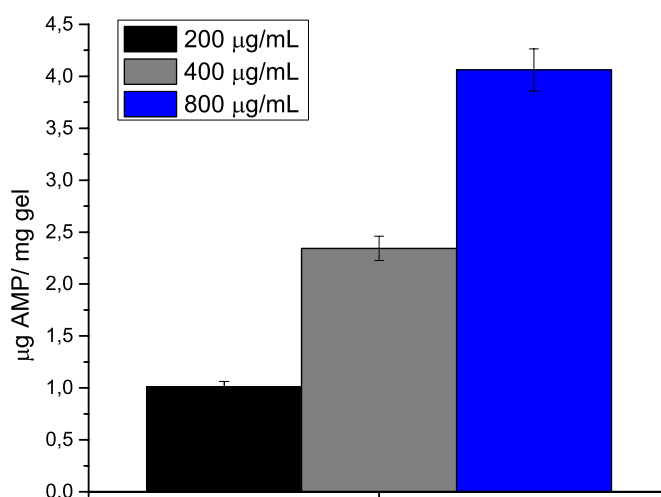


Figure 6.5. Loading capacity of cryogel with different concentrations of Ampicillin.

**6.3.3.2. Loading via Diels-Alder reaction.** The loading of maleimide-containing molecules was evaluated by determining the concentration of the peptide or dye in solution before and after loading using HPLC or fluorescence spectroscopy. To demonstrate the presence of furan, a maleimide containing dye, *N*-fluorescein maleimide was loaded onto the cryogel by immersing the gel in a solution of dye at room temperature for 24h. After thorough washing, the amount of unbounded dye was determined using fluorescence spectroscopy to yield a binding efficiency of 39%. To also prove that the dye was indeed covalently bonded to the furan moiety and not entrapped, a furan-depleted cryogel was loaded with the same amount of dye as the furan cryogel. It was determined by fluorescence microscopy, that indeed no dye was left inside the gel after washing (Figure 6.6).

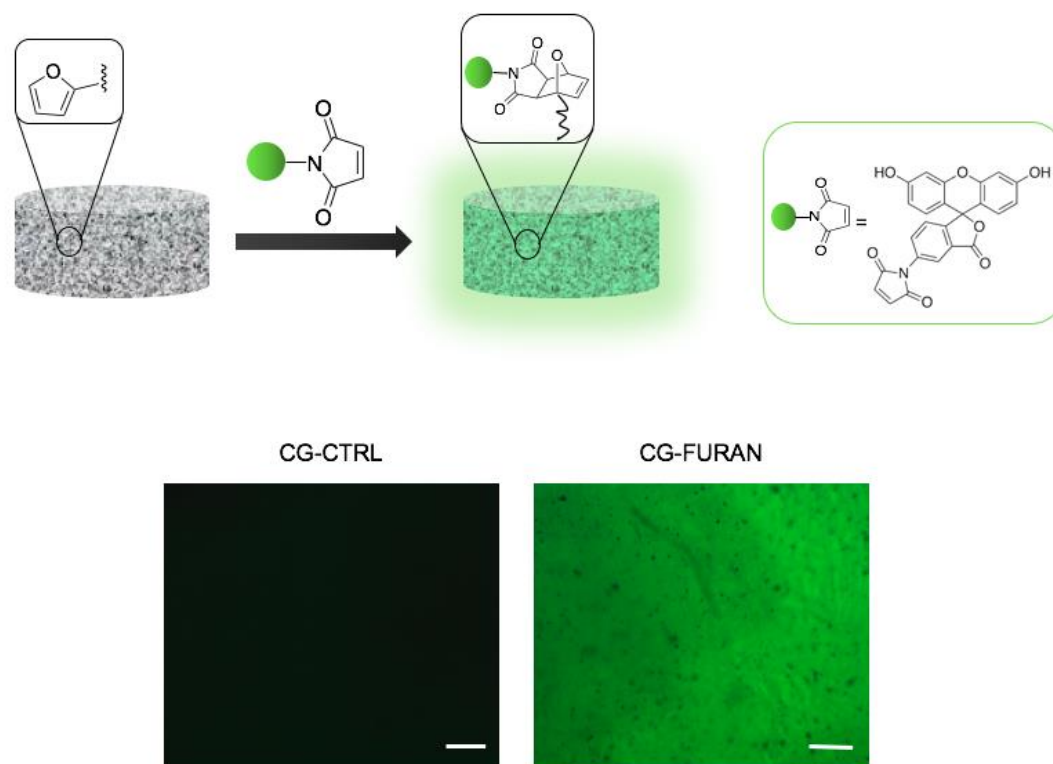


Figure 6.6. Schematic representation of dye loading and microscopy images of CGrGO-0 (control) and CGrGO-40 (CG-Furan) after treatment with maleimide dye.

One of the pipelines in the development of successful antimicrobial therapy focuses on use of specific antimicrobial peptides. Local delivery of newly developed therapeutic agents which would not permit development of bacterial resistance represents an attractive option in improved antimicrobial therapy. It seems that antimicrobial peptides, associated with appropriate delivery system of nanosize range, could serve this purpose. For that purpose, a maleimide modified anti-microbial peptide containing three tryptophan and three arginine units was used. The same loading procedure as for the dye was repeated with maleimide-containing peptide. From the determination of unbound peptide it was deduced that peptides could be conjugated with an efficiency of 33%.

### 6.3.3. Release of antibiotic

Subsequently, we explored the photothermal properties of the **CGrGO** cryogel to trigger the release of the drug. Figure 6.8 shows the release profiles for ampicillin upon irradiating **CGrGO** loaded with ampicillin ( $114 \mu\text{g mL}^{-1}$ ) with NIR light. Using a laser power density of  $1 \text{ W cm}^{-2}$  results in a total release of  $55.9 \mu\text{g mL}^{-1}$  ampicillin ( $\approx 49\%$  of loaded antibiotic).

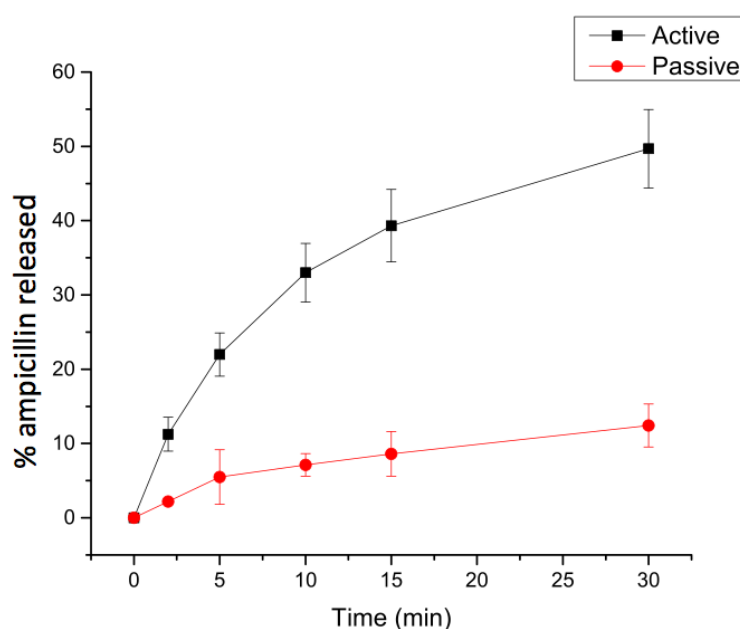


Figure 6.7. Release of ampicillin in using active and at passive ( $24^{\circ}\text{C}$ ) modes.

The released antibiotic concentration are much larger than the minimum inhibitory concentration of ampicillin for Gram-negative *E. coli* K12 ( $10 \mu\text{g mL}^{-1}$ ). To show the effect of the laser combined with rGO, the ‘passive’ release was also measured, and only 12% ( $13 \mu\text{g mL}^{-1}$ ) of loaded ampicillin was released after 30 min.

#### 6.3.4. Release of Peptide from Cryogels.

The equilibrium of the Diels–Alder reaction is thermally controlled; elevated temperatures induce the reverse reaction and the reformation of maleimide and furan moieties, whereas lower temperatures favors adduct formation. If peptide or dye release from the cryogel is governed by a DA/rDA mechanism, exposing the polymer networks to different temperatures should dramatically influence the rate and quantity of material released from the network.

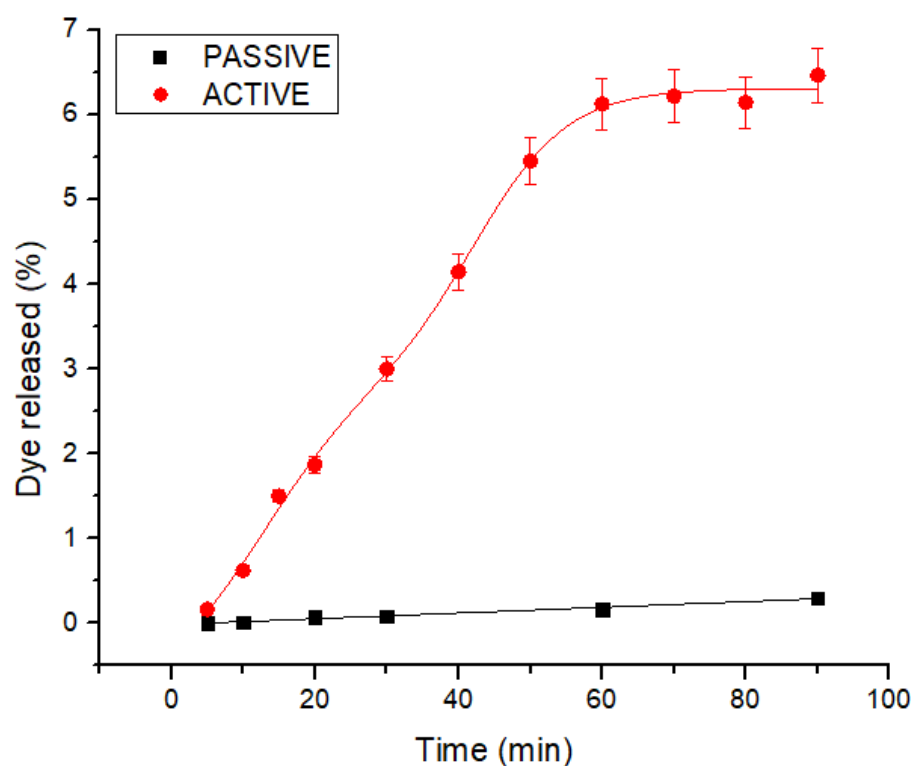


Figure 6.8. Release of fluorescein maleimide dye via retro Diels Alder from CG-rGO in % using laser (active) and at 37 °C (passive).

Increasing the temperature at which the release studies were conducted resulted in an increase in the amount of the peptide and dye release from the cryogel networks (Figure 6.9). Using a laser power of  $1 \text{ W cm}^{-2}$ , the gel conjugated with *N*-fluorescein maleimide was irradiated and it was deduced that only 6% of dye was released after 90 minutes compared to 0.6% released at  $37 \text{ }^\circ\text{C}$  without irradiation.

Interestingly, repeating the same experiment with the **CGrGO-40** loaded with peptide, it was observed that no peptide was released from the gel, whether at  $37 \text{ }^\circ\text{C}$  or using the NIR laser ( $65\text{-}70 \text{ }^\circ\text{C}$ ). It was assumed that this is probably due to strong  $\pi$ - $\pi$  stacking between the peptide and the rGO inside the gel preventing release of any peptide or dye.

In order to circumvent this issue, the maleimide containing constructs were loaded inside rGO depleted cryogel **CG-40** to prevent any  $\pi$ - $\pi$  interactions. Furthermore, to render this system photothermal, a rGO-covered kapton patch was used on top of the cryogel **CG-40** loaded with either the dye or the peptide. The choice of Kapton as a patch material is based on some of its interesting physico-chemical properties. Highly aromatic polyimide resins such as Kapton have high thermal stability ( $> 300 \text{ }^\circ\text{C}$ ), a high glass transition temperature ( $T_g > 200 \text{ }^\circ\text{C}$ ), proven chemical resistance as well as excellent flexibility and adhesive properties [199,205]. As illustrated in Figure 6.10, significantly different profiles were obtained for the two temperatures evaluated, with the peptide releasing almost thirty times more rapidly at  $70 \text{ }^\circ\text{C}$  compared to the release at  $37 \text{ }^\circ\text{C}$ .

The higher release rate observed at elevated temperatures corresponds to an increased reverse rate in the rDA reaction relative to the forward reaction. Using such construct allowed for a much higher release of dye, 28 % using NIR and 1.4% at  $37 \text{ }^\circ\text{C}$ . The same procedure was therefore repeated for the anti-microbial peptide and it was deduced that about 41% of the conjugated peptide was released after 60 min of laser compared to 4% release at  $37 \text{ }^\circ\text{C}$ .

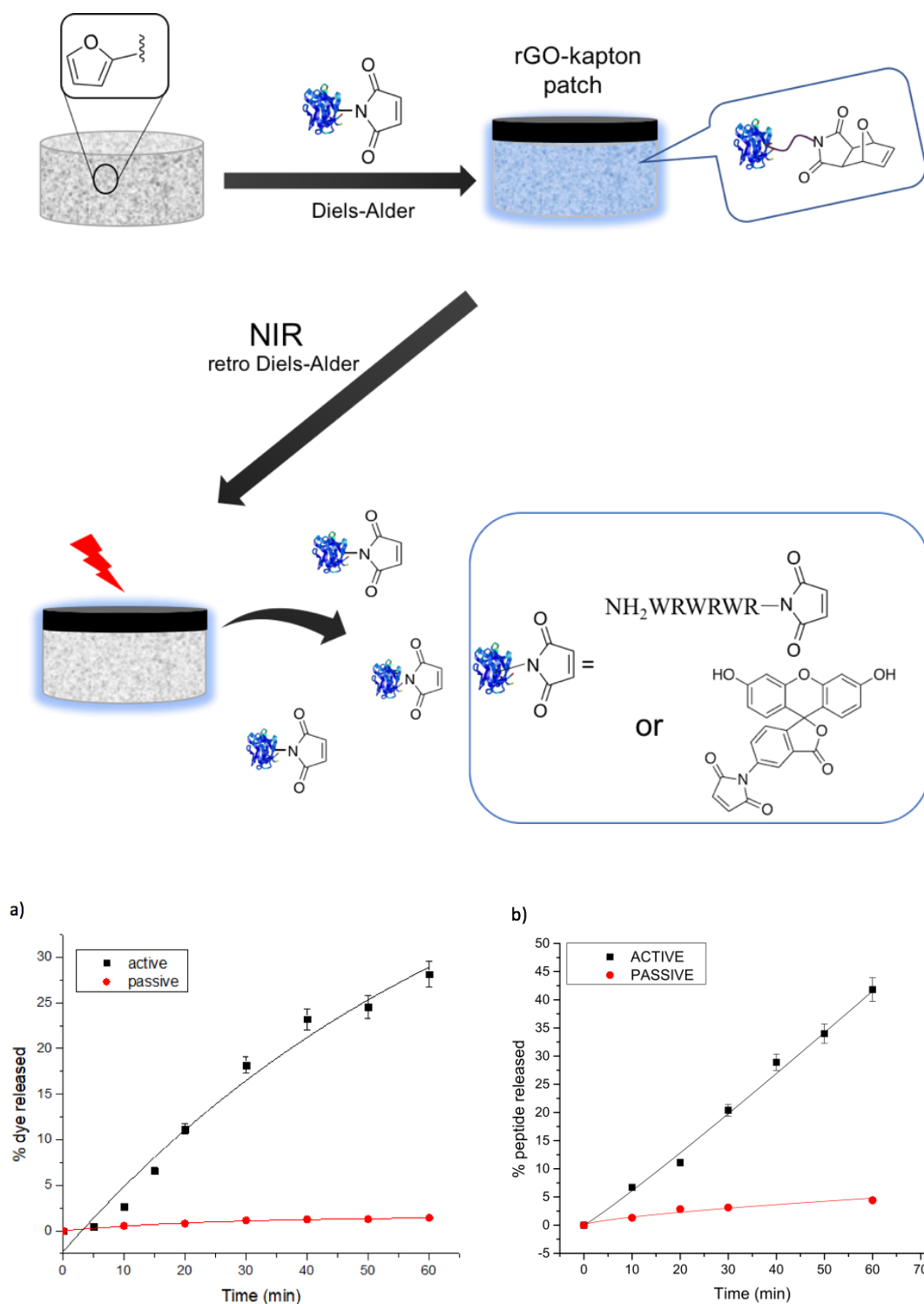


Figure 6.9. Schematic representation of loading and release of maleimide containing construct using DA-rDA mechanism. a) Release of the fluorescein maleimide dye and b) anti-microbial peptide at 37 °C (passive) and at 70 °C (active) using NIR laser.

### 6.3.5. In vitro tests

In order to utilize the cryogel as a wound healing platform, they should be nontoxic. To investigate their biocompatibility, HeLa cells were treated with different set of cryogels. Cells were incubated in 12-well plates and treated with cryogels for 48 h at 37 °C. CCK-8 assay was performed to determine cell viability. It was satisfying to observe that the cryogels did not show any cytotoxicity (Figure 6.11). This high degree of biocompatibility could be expected due to the PEG-based matrix of these cryogels.

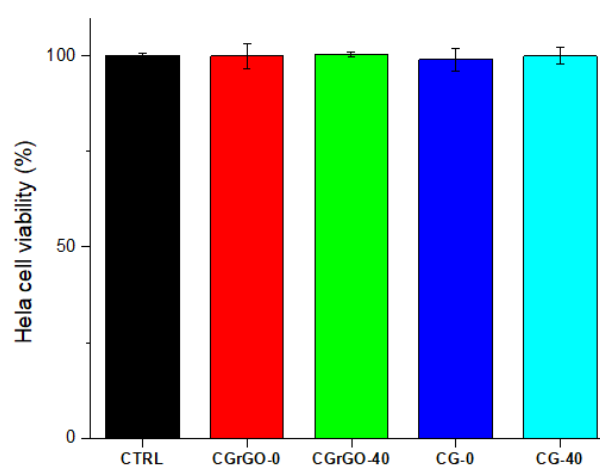


Figure 6.10. Cells viability of HeLa after 24h incubation with CGrGO (0-40% furan) and CG (0-40% furan)

### 6.3.6. Activity of released antibiotic and anti-microbial peptide

Following photothermal triggered ampicillin release, its antibiotic efficiency was determined by determining the titer of viable bacteria able to grow. Figure 6.12a shows the bacteria viability based on the change in OD<sub>600</sub> values upon incubation of *E. coli* K12 with different ampicillin released samples using 1 W cm<sup>-2</sup>. Bacteria were all killed after 10 min irradiation, with a released concentration of ampicillin of 34 µg/mL.

The same procedure was repeated to trigger the release of the peptide via retro Diels-Alder reaction, its antibiotic efficiency was determined by determining the titer of viable bacteria able to grow. Figure 6.12b shows the bacteria viability based on the change in OD<sub>600</sub> values upon incubation of *S. Aureus* with different peptide released samples using 1 W cm<sup>-2</sup>. Bacteria growth was inhibited by 75% after irradiation of 10 and 20 min, as the amount of peptide released was lower or close to the MIC value (16 µg/mL), after 30 min, no bacteria are left at a higher concentration of release peptide (40 µg/mL).

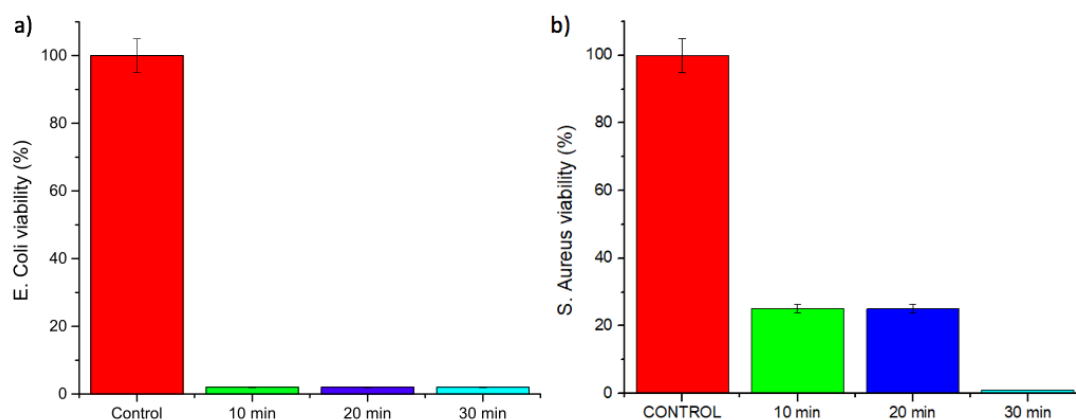


Figure 6.11. a) Bacteria *E.coli* viability in %, b) Bacteria *S. aureus* viability in % upon treatment with antibiotics released from cryogels.

#### 6.4. Conclusion

As a conclusion, cryogels were fabricated using photo-polymerization leading to a rGO-embedded matrix comprised of hydrophilic poly(ethylene glycol) and hydrophobic furfuryl groups. Furfuryl groups were incorporated as a control over the hydrophobicity as well as a handle for Diels-Alder conjugation. An antibiotics, ampicillin was loaded inside the matrix via adsorption, while a maleimide-containing anti-microbial peptide was conjugated via the Diels-Alder reaction. It was demonstrated that while passive release of conjugated dyes and peptides to the cryogel was minimal, enhanced active-release was observed under NIR.

While 100 % of *E. Coli* bacteria were eradicated after 10 min of NIR irradiation on the ampicillin loaded cryogels, no release of peptide from the matrix could be observed due to the strong  $\pi$ - $\pi$  interactions between the anti-microbial peptide and the rGO. Hence, a new device model was constructed where rGO-depleted cryogels were interfaced with a NIR responsive construct. A Kapton patch modified with rGO was placed onto the surface of the furan cryogel functionalized with the peptide. After 10 min of irradiation, 75% of the gram positive bacteria, *S. Aureus*, was eradicated using NIR, while 100% was eradicated after 30 min. Moreover, the cryogel scaffolds were non-toxic towards HeLa cells and had no anti-microbial activity prior to loading of antibiotics. It can be envisioned that the facile fabrication and modular nature of the construct reported here provides a platform that can be adapted for on-demand delivery of various drugs for combating different diseases.

## 7. THIOL-REACTIVE MACROPOROUS CRYOGELS FOR BIOMOLECULAR IMMOBILIZATION

### 7.1. Introduction

Macroporous polymeric gels, namely cryogels are novel polymer materials with sponge-like porous microstructures prepared via cryo-polymerization of gel-forming monomers under frozen conditions. As explained in the previous chapter, cryogelation method is one of the most versatile techniques used in the last few decades for modeling the porous structure of polymer gels [75,226]. This simple technology commonly requires only one cycle of freezing-defrosting of the reagent/polymer solution, and allows production of materials of varying morphology, mechanical properties and permeability [228,229]. Cryogels have been used in a wide range of applications, including tissue engineering, as cell scaffolds, in bioreactors, materials for biological and chemical separations, and as adsorbents in biomedical and environmental applications [230-233].

Apart from applications like drug loading as described in the previous chapter, cryogels can be used as a support for proteins and cellular materials. For example, cryogels have been used for developing biomaterial-based vaccination system where minimal extracorporeal manipulation can localize and maintain transferred cells to a specific microenvironment. For example, Bencherif and coworkers developed an injectable cryogel-based whole-cell cancer vaccines, using cryogels that were fabricated with alginate containing covalently coupled RGD peptides with the aim of enhancing tumor cell attachment through integrin binding [234].

Previously, Sanyal and coworkers used photo-polymerization to fabricate thiol reactive functionalizable PEG-containing hydrogels for bio-immobilization [136]. Bulk and micropatterned hydrogels with varying amounts of maleimide functional groups were obtained by photo-polymerization utilizing a protected maleimide group and PEG diacrylate as a cross-linker.

After deprotection of the maleimide, the hydrogel patterns were decorated with fluorescent thiol-containing dye, and a thiol-containing biotin ligand via Michael addition. The really strong affinity of Streptavidin to biotin allowed its immobilization onto biotinylated hydrogel patterns to achieve facile bio-immobilization [136]. In order to enhance the absorptivity of the materials with a high capacity toward a target compound, cryogels are a great option as they provide large interconnected pores and ensures a larger surface area compared to hydrogels for the attachment of biologically active ligands [235-237]. Sandeman et al. successfully fabricated cryogels containing epoxy and hydroxyls functionals group for the covalent immobilization of *B. anthracis* exotoxin specific antibodies PANG and Valortim® for the removal of anthrax protective antigen from PBS [238].

In another example, Bereli and coworkers fabricated super-macroporous cryogels for the purification of lysozyme from egg white by molecular imprinting. Purification of lysozyme from egg white was monitored by determining the lysozyme activity using *Micrococcus lysodeikticus* as substrate and the purity of the desorbed lysozyme was about 94% [239]. Moreover the cryogel could be used several times without decreasing the adsorption capacity significantly. Likewise, Roque et al. designed a separation technique made of biodegradable polymer for the purification of Adenoviruses that are an important platform in the field of vaccine development and gene therapy [240-242].

As of today, a wide choice of chromatographic platform are available, but they remain expensive as well as they have low surface accessibility, rendering the binding affinity of the viruses or large molecules mediocre [243,244]. Using cryogel as a chromatographic tool provides a highly porous and robust platform, thus allowing fast separation through convection of large biomolecule at low pressure, and decreasing the shear force exerted as well as the degradation of the biomolecule of interest [245,247].

In this study, we report the fabrication of maleimide containing cryogels using photopolymerization that can be used for protein immobilization. The macroporous cryogels were successfully functionalized via Michael addition reaction between the maleimide present on the cryogels with thiol containing protein such as bovine serum albumin.

These cryogels were also functionalized with a ligand, biotin-thiol, used for the immobilization of the protein streptavidin. Furthermore, it was established that the degree of immobilization onto such polymeric constructs can be adjusted by modifying the amount of reactive functional groups in the gel (Figure 7.1).

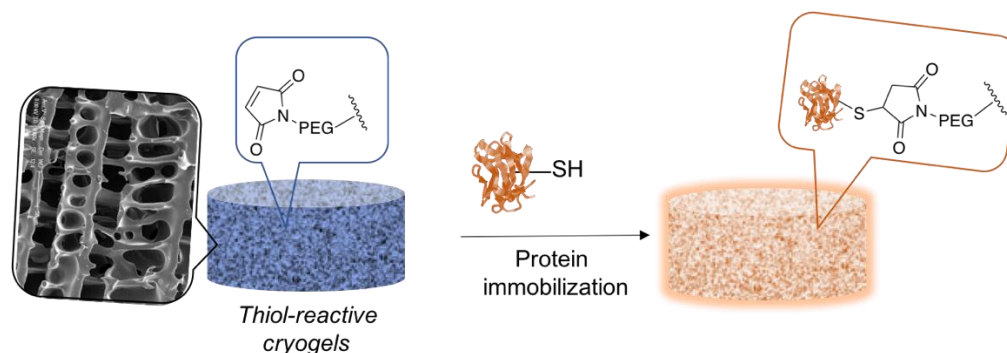


Figure 7.1. Schematic representation of protein immobilization onto maleimide bearing microporous cryogels.

## 7.2. Experimental

### 7.2.1. Materials

The furan-protected maleimide-containing methacrylate monomer (FuMaMA) and Biotin thiol (Biotin-SH) were synthesized according to literature [98,248]. Poly(ethylene glycol) methyl ether methacrylate (PEGMEMA,  $M_n = 300 \text{ g mol}^{-1}$ ), poly(ethylene glycol) dimethacrylate (PEGDMA,  $M_n = 550 \text{ g mol}^{-1}$ ), were obtained from Sigma Aldrich and purified by filtering through activated aluminum oxide column prior to use. 2, 2-dimethoxy-2-phenylacetophenone (DMPA), Albumin–fluorescein isothiocyanate conjugate (FITC-BSA), Poly(ethylene glycol) methacrylate ( $M_n = 360 \text{ g mol}^{-1}$ , PEGMA, 99%) and 4-aminobutyric acid were purchased from Sigma Aldrich. Rhodamine conjugated streptavidin (TRITC-streptavidin) was obtained from Pierce and used as received. PEGFuMaMA monomer was synthesized according to the procedure given in Chapter 3, p.26. Column chromatography was performed using silica gel 60 (43–60 nm, Merck).

Thin layer chromatography was performed using silica gel plates (Kieselgel 60 F254, 0.2 mm, Merck).

### **7.2.2. Methods**

All gelation reactions were performed at 365 nm using a UV Lamp with a 100W spot bulb at a distance of 10 cm. NMR spectra were recorded using a 400 MHz Bruker spectrometer at 25 °C. Measurements were taken in deuterated chloroform (CDCl<sub>3</sub>). Fourier transform infrared (FTIR) spectra were obtained using a Thermo Scientific Nicolet 380 FT-IR spectrometer. To characterize the cryogel morphology, scanning electron microscopy (SEM) was performed with an ESEM- FEG/EDAX Philips XL-30 (Philips, Eindhoven, The Netherlands) instrument operating at 10 kV. The attachment of FITC-BSA and TRITC-streptavidin onto the cryogels was confirmed using a fluorescence microscope (HBO100 ZEISS Fluorescence Microscopy, Carl Zeiss Canada Ltd., Canada).

### **7.2.3. Fabrication of Photopolymerized Cryogels.**

Cryogel precursors were prepared by mixing PEGMEMA, PEGDMA cross-linker, and DMPA at appropriate desired ratios in dioxane with varying feed of the PEGFuMaMA monomer. The monomers mixture was placed under UV source at a distance of 10 cm at -13 °C. After 60 min, obtained cryogels were washed with dioxane and rinsed thoroughly with water and dried under vacuum. The furan-protected maleimide groups in cryogels were activated to thiol-reactive unprotected maleimide form via the retro-DA reaction by placing in a vacuum oven at 110 °C for 2 h.

### **7.2.4. Swelling Study of Bulk Hydrogel.**

Swelling profiles were done by cutting small piece of dried cryogel and placing it in a beaker containing distilled/deionized water at room temperature.

At regular time interval, the cryogel samples were weighed after removing excess water and the percentage of water uptake was calculated using the following equation:

$$\text{swelling \%} = (W_{\text{wet}} - W_{\text{dry}}) / W_{\text{wet}} * 100$$

where  $W_{\text{wet}}$  = weight of the cryogel in swollen state and  $W_{\text{dry}}$  = weight of the cryogel in dry state.

#### **7.2.5. Functionalization of Cryogels with FITC-BSA.**

Maleimide containing cryogels were soaked in a solution of green-fluorescent Bovine Serum Albumin (BSA), conjugated with FITC (0.03 mg/mL in PBS) at room temperature. After 12 hours, the gels were washed thoroughly with PBS to remove any unbound FITC-BSA. As a control experiment, FITC-BSA dye was added to a cryogel sample depleted of maleimide monomer as well as a sample with protected maleimide to ascertain minimal non-specific interactions as well as absence of entrapment of the protein in the gel.

#### **7.2.6. Biotinylation of the Cryogels**

Samples of maleimide-containing cryogels were soaked in a solution of biotin-thiol (MeOH/THF 1:1) for 12 h at room temperature. After 12 h, the gels were rinsed thoroughly with the same solvent mixture to remove any unreacted biotin-thiol.

#### **7.2.7. Immobilization of Streptavidin onto the Biotinylated Cryogels.**

A solution of TRITC- Streptavidin (1  $\mu\text{g/mL}$  in PBS) was added directly onto the previously swollen cryogels. After immobilization of streptavidin for 15 min, cryogels were washed thoroughly with PBS and then analyzed using fluorescence microscopy. A biotin-depleted cryogel was used as control to show minimum non-specific interactions when biotin is not present.

### 7.3. Results and Discussion

#### 7.3.1. Synthesis of hydrophilic maleimide monomer

Our group previously synthesized a furan-protected maleimide-containing monomer, namely FuMaMA [26]. Due to its short carbon chain, this monomer was hydrophobic, and this limits its utilization in presence of organic solvent. In order to obtain a hydrophilic monomer, with a longer chain, this monomer was modified with a PEG chain. To do so, a furan-protected maleimide functionalized with a carboxylic acid (FuMaCOOH) was used. The acid was then coupled with PEG 360 through esterification using EDC and DMAP in DCM to obtain the hydrophilic FuMaPEGMA monomer in 67% yield. Fabrication of Thiol-reactive Cryogels (Figure 3.10).

Cryogels containing different amounts of furan-protected maleimide monomer were fabricated via photopolymerization of the PEGFuMaMA monomer with PEGMEMA ( $M_n = 300 \text{ g mol}^{-1}$ ), a PEG-diacrylate cross-linker in the presence of DMPA as a photoinitiator (Figure 7.2). The PEG-based hydrophilic monomer was chosen to obtain anti-biofouling cryogels to lower any nonspecific interactions of biomolecules with the matrix of the cryogel. Cryogels **CG-PEGFuMa10**, **CG-PEGFuMa20**, and **CG-PEGFuMa30** enclosing 10, 20, and 30 mol % of the furan protected monomer PEGFuMaMA were synthesized. As a control platform, cryogel **CG-CTRL**, depleted of any activated maleimide group, was also prepared. Cryogels were obtained with high yields ca. 90%, with porous morphology and rapid swelling profiles indicating high water uptake (Figure 7.3 and Table 7.1).

Table 7.1. Photopolymerization of cryogels in presence of PEGFuMaMA

Cryogel	PEGFuMaMA % (mole)	Swelling (%)	Gel content (%)
CG-PEGFuMa10	10	370	93
CG-PEGFuMa20	20	338	86
CG-PEGFuMa30	30	326	88

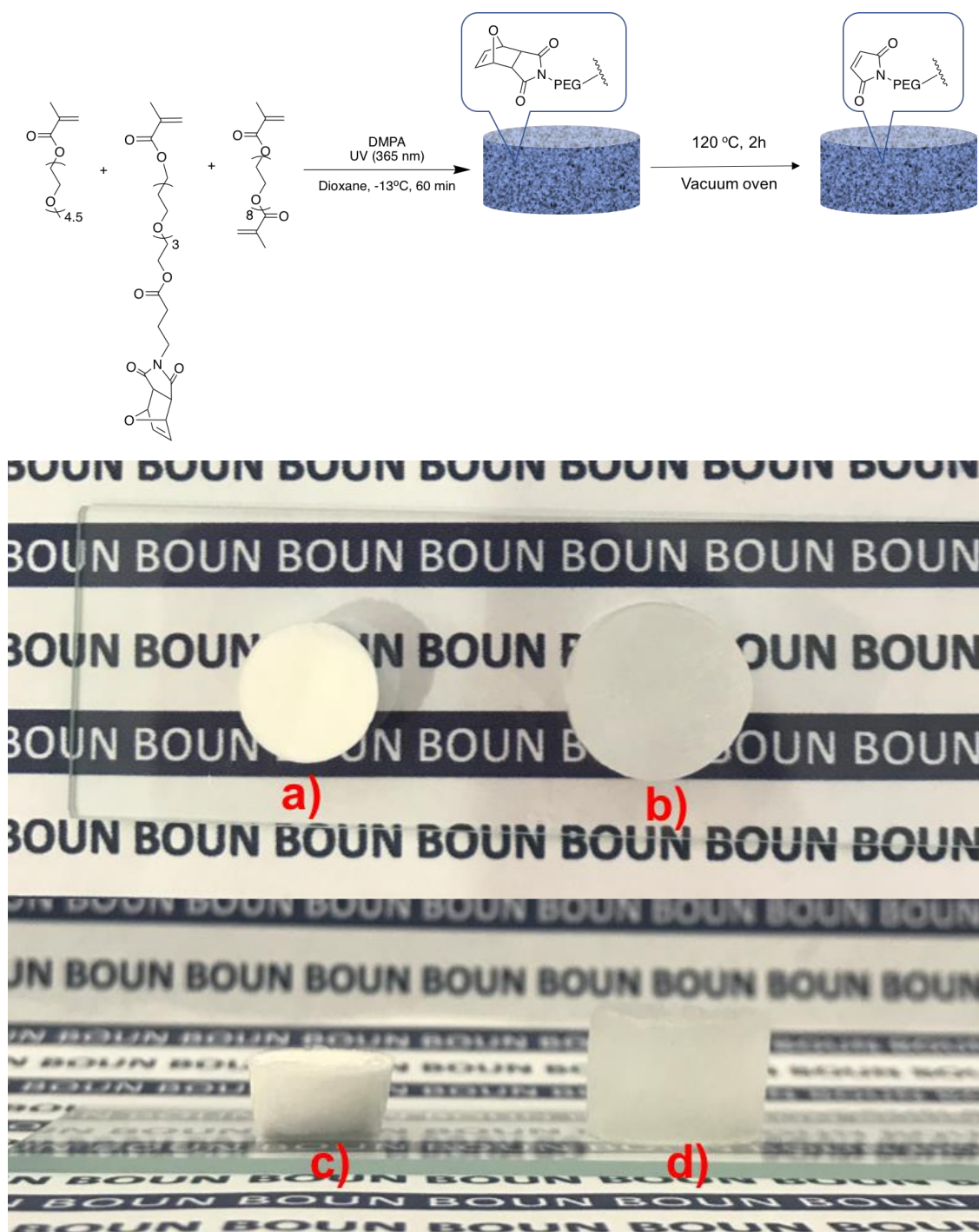


Figure 7.2. Schematic representation for the fabrication of thiol-reactive microporous cryogel, and a) top view of dry cryogel, b) top view of wet cryogel, c) side view of dry cryogel and d) side view of wet cryogel.

The FTIR spectra showed the expected C=O stretching band belonging to ester groups at  $\sim 1727\text{ cm}^{-1}$  for all cryogels. In addition, the spectra revealed the presence of the out-of-phase C=O stretching vibration at  $\sim 1700\text{ cm}^{-1}$  corresponding to cyclic imides due to furan protected maleimide units of maleimide inside the cryogels (Figure 7.3c). In addition, weak band at  $\sim 1773\text{ cm}^{-1}$  assigned to the in-phase C=O stretching vibration of maleimide units was also observed.

From the swelling studies it was observed that as the concentration of the PEGFuMaMA monomer increases, the final equilibrium swelling of the hydrogels reduces. This can be attributed to the relatively hydrophobic nature of the maleimide cyclo-adduct unit. For example, the swelling of **CG-PEGFuMa10** reached 370% after 2 min, while the swelling ratios were 338% and 326% for **CG-PEGFuMa20** and **CG-PEGFuMa30** respectively (Figure 7.3b).

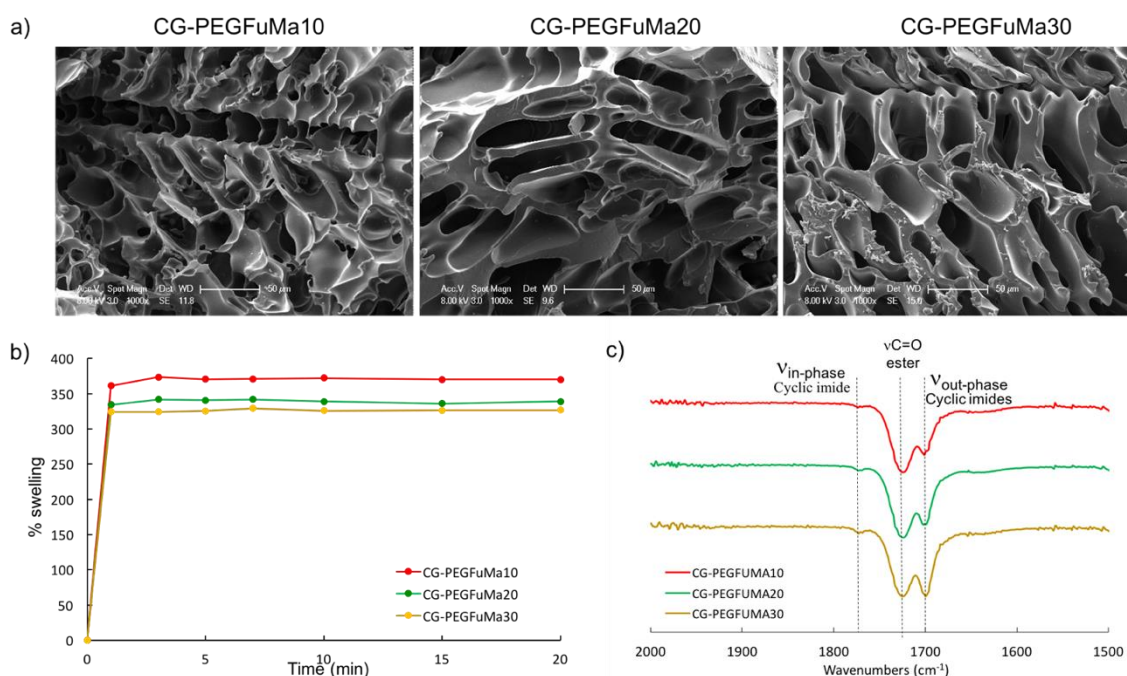


Figure 7.3. Comparison of a) morphology from SEM images, b) swelling profile, and c) FTIR spectra of cryogels.

### 7.3.2. Functionalization of Cryogels via Thiol–Ene Conjugation.

The efficiency of functionalization of these cryogels was investigated by conjugation of a thiol containing fluorescent protein, namely, BSA-FITC (Figure 7.4). As a control, the latent cryogels (**CG-PEGFuMa**) that were not activated via retro Diels–Alder reaction were exposed to that same protein, as well as a cryogel devoid of the maleimide monomer (**CG-CTRL**). As expected, from fluorescence microscopy analysis it was deduced that the non-activated as well as maleimide depleted cryogels did not show any significant fluorescence (Figure 7.4 b and c).

Alternatively, cryogels that were activated by retro Diels/Alder cycloreversion reaction to contain the thiol-reactive maleimide group were successfully functionalized via nucleophilic Michael addition reaction and exhibited fluorescence considerably high fluorescence. To investigate if the proximity of the maleimide group to the cryogel matrix played any role, a comparison was made for cryogels obtained using the hydrophobic maleimide monomer and PEG-based maleimide monomer. It was observed that when bioconjugation of FITC-BSA was performed under similar conditions, higher amount of protein immobilization was observed for the cryogel formulated using the PEG-based maleimide (Figure 7.4). Furthermore, cryogels with increasing ratio of activated maleimide (**CG-PEGMa10**, **CG- PEGMa 20** and **CG- PEGMa 30**) were reacted with FITC-BSA and an increase in fluorescence could be observed for the cryogel with an increase of maleimide group within the gels (Figure 7.5). These results demonstrate that the amount of proteins that can be immobilized on these cryogels can be controlled using the amount of thiol-reactive maleimide groups present in their matrix.

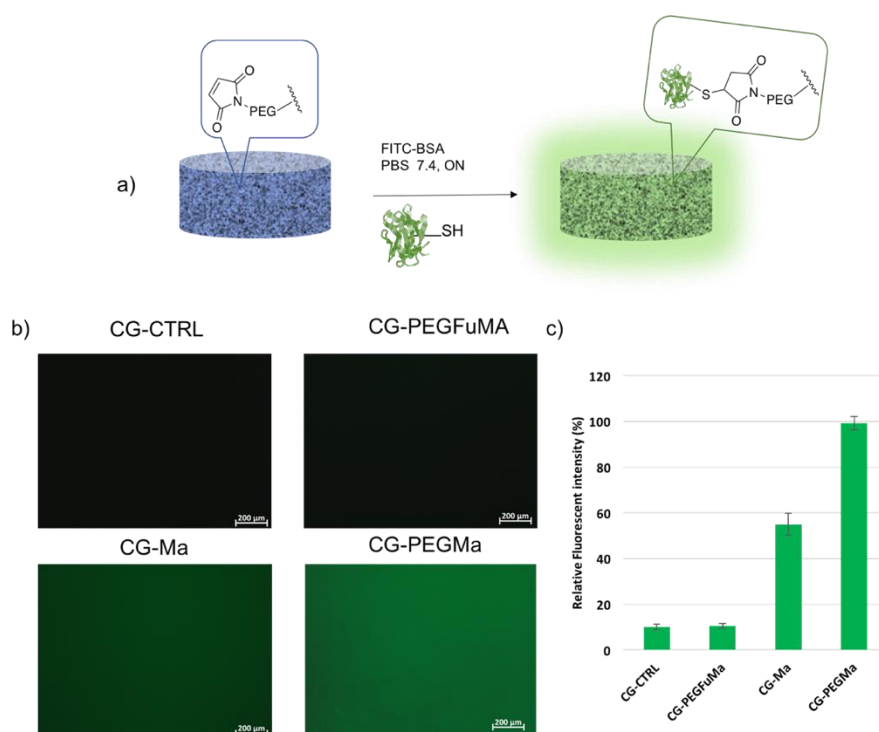


Figure 7.4. a) Functionalization of crygel with FITC-BSA, b) Fluorescence images of crygels after functionalization, c) relative fluorescence intensities of the crygels after functionalization with FITC-BSA.

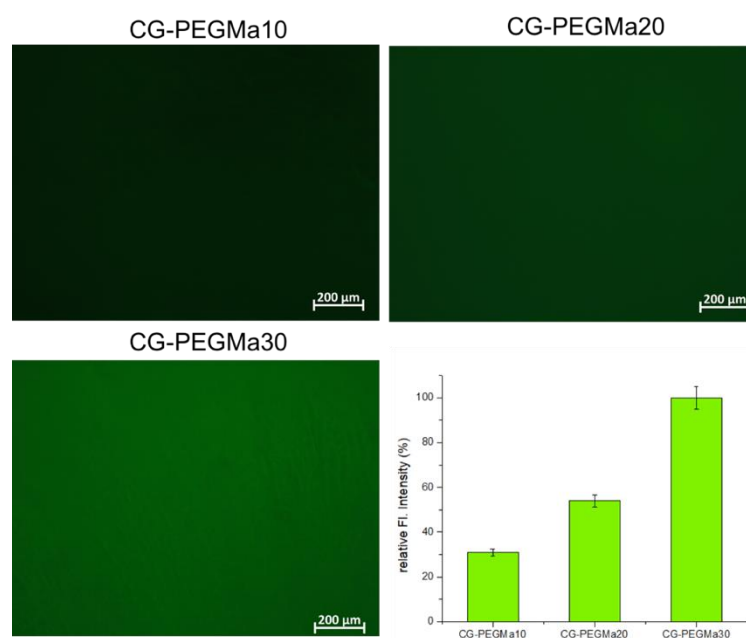


Figure 7.5. Fluorescence images and relative fluorescent intensities of crygels after their functionalization with FITC-BSA.

### 7.3.3. Functionalization of Cryogels with Biotin-thiol and Immobilization of Streptavidin.

Biotin and streptavidin are known to possess one of the strongest non-covalent biological interactions, and in addition to their great interactions, the binding of streptavidin to biotin have the advantages of being highly specific, rapid and unaffected by change of pH or temperature making them widely used as a model system for protein-ligand interactions [249,250]. To demonstrate the applicability of the cryogels as platform for biomolecular immobilizations, a fluorescently labelled protein, namely, TRITC-streptavidin, was immobilized on a cryogel functionalized with a biotin-thiol (Figure 7.6).

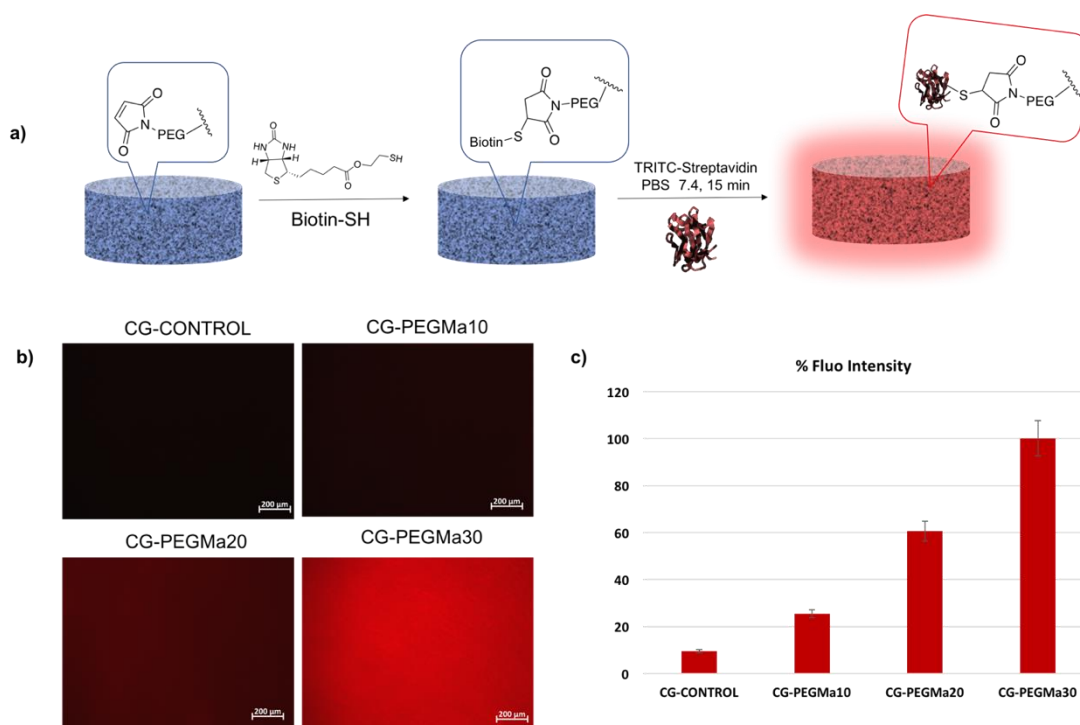


Figure 7.6. a) Biotinylation of the cryogels, followed by immobilization of TRITC-streptavidin, b) fluorescence microscopy images of TRITC-streptavidin immobilized cryogels and c) relative fluorescence intensities of cryogels after protein immobilization.

All cryogels (**CG-PEGMa10**, **CG-PEGMa20** and **CG-PEGMa30**) containing the thiol-reactive maleimide groups were incubated in equal amount of thiol-containing biotin solution. An aqueous solution of TRITC-streptavidin was added onto the biotinylated cryogels and after thoroughly rinsing off any unreacted streptavidin from the gel, cryogels were analyzed with fluorescence microscopy. The cryogel (**GC-control**) which is not biotinylated was also treated with TRITC-streptavidin. As expected, no significant fluorescence was seen due to minimal interactions of streptavidin with the anti-biofouling matrix of the cryogel (Figure 7.6b). An increase in fluorescence intensity could also be observed while using cryogels with increasing amount of maleimide groups, thus demonstrating their tunability as a biomolecular immobilization platform (Figure 7.6).

#### 7.4. Conclusion

In conclusion, thiol-reactive maleimide group containing macroporous cryogels were fabricated using photopolymerization of a masked maleimide group containing monomer. The maleimide group were subsequently activated to their thiol reactive form using the retro Diels-Alder reaction. Thereafter, the cryogels were functionalized using a thiol-containing BSA protein, and it was demonstrated that the cryogels fabricated using hydrophilic maleimide monomer showed higher loading. Cryogels were also biotinylated and successful immobilization of the protein TRITC-streptavidin was performed. The extent of protein immobilization could be controlled by varying the amount of thiol-reactive group within the cryogels. It can be envisioned that the facile fabrication and conjugation and overall control over the extent of functionalization of these macroporous constructs will make them desirable scaffolds for many biomedical applications.

## 8. CONCLUSIONS

In this dissertation, we investigated the design and fabrication of crosslinked polymeric structures to render them suitable for various biomedical application such as drug delivery and protein immobilization.

In the first chapter of this thesis, background information about polymeric materials and their biomedical applications were presented. Additionally, the chapter provides an overview of the different types of crosslinked polymeric constructs utilized for drug delivery systems. An emphasis was made on nanogels and bulk hydrogels; their synthetic route were described as well as their utilizations in the biomedical field. The next three chapters described fabrication of novel nanogels as drug delivery systems. In particular, the second and third chapter reported novel functionalizable nanogels that were modified with a chemotherapeutic drug, doxorubicin and a dye to be utilized as theranostic platforms for the treatment of cancer tumor. Additionally, the nanogels studied in the fourth chapter were decorated with a targeting ligand and showed enhanced internalization in breast cancer cells. Moreover, the drug release profile were pH dependent emphasizing their potential as a suitable delivery agent for acidic cancerous tissues. In the fifth chapter, a novel concept of fabrication of porphyrin-comprising nanogel for potential utility in photodynamic and photothermal therapy was described. Successful singlet oxygen generation and toxicity of these nanogels against MDA-MB-231 breast cancer cells upon activation through irradiation at appropriate wavelengths was demonstrated.

In the last two chapters, macroporous cryogels are fabricated and utilized as antibacterial wound patch and bio-immobilization support owing to their great physical and mechanical properties. In the sixth chapter, thermo-responsive rGO-embedded cryogels were decorated with furan moieties and utilized as platform for antibiotic and anti-microbial peptide delivery in wound infections. The patches successfully eradicated *S. Aureus* and *E. Coli* bacteria. In the seventh and final chapter, novel cryogels containing a thiol-reactive maleimide groups were fabricated and protein like BSA and streptavidin were successfully immobilized onto the cryogels.

It was observed that the functional group density on these macroporous constructs could be effectively tailored by varying the feed ratio of monomers preceding the photopolymerization, which allows control over the extent of biomolecular immobilization.

In summary, in this dissertation, biocompatible and multifunctional crosslinked polymeric structures for various biomedical applications were prepared. Modification of the constructs were performed through incorporation of graphene based nanomaterials to make them thermoresponsive. Several types of efficient conjugation handles were also incorporated to enable successful attachment and release of diverse therapeutic agents. The constructs developed in this study bears potential to serve as attractive candidates for various drug delivery and theranostic applications, as well as serve as viable platforms for biomolecular immobilization and sensing.

## REFERENCES

1. World Health Organization, “Cancer”, <http://www.who.int/news-room/factsheets/detail/cancer>, accessed at August 2018.
2. D. A. LaVan, T. McGuire, and R. Langer, “Small-scale systems for in vivo drug delivery,” *Nature Biotechnology*, vol. 21, no. 10, pp. 1184–1191, 2003.
3. M. Ferrari, “Cancer nanotechnology: opportunities and challenges,” *Nature Reviews Cancer*, vol. 5, no. 3, pp. 161–171, 2005.
4. G. M. Whitesides, “The ‘right’ size in nanobiotechnology,” *Nature Biotechnology*, vol. 21, no. 10, pp. 1161–1165, 2003.
5. A. D. Bangham, M. M. Standish, and J. C. Watkins, “Diffusion of univalent ions across the lamellae of swollen phospholipids,” *Journal of Molecular Biology*, vol. 13, no. 1, pp. 238–IN27, 1965.
6. Z. Li, S. Tan, S. Li, Q. Shen, and K. Wang, “Cancer drug delivery in the nano era: An overview and perspectives,” *Oncology Reports*, vol. 38, no. 2, pp. 611–624, 2017.
7. R. Langer and J. Folkman, “Polymers for the sustained release of proteins and other macromolecules,” *Nature*, vol. 263, no. 5580, pp. 797–800, 1976.
8. V. Wagner, A. Dullaart, A.-K. Bock, and A. Zweck, “The emerging nanomedicine landscape,” *Nature Biotechnology*, vol. 24, no. 10, pp. 1211–1217, 2006.
9. P. Decuzzi, R. Pasqualini, W. Arap, and M. Ferrari, “Intravascular Delivery of Particulate Systems: Does Geometry Really Matter?,” *Pharmaceutical Research*, vol. 26, no. 1, pp. 235–243, 2009.

10. F. Gu, B. Teply and N. Mann, "Precise engineering of targeted nanoparticles by using self-assembled biointegrated block copolymers," *Proceedings of the National Academy of Sciences*, vol. 105, no. 7, pp. 2586–2591, 2008.
11. H. Maeda, K. Tsukigawa, and J. Fang, "A Retrospective 30 Years After Discovery of the Enhanced Permeability and Retention Effect of Solid Tumors: Next-Generation Chemotherapeutics and Photodynamic Therapy-Problems, Solutions, and Prospects," *Microcirculation*, vol. 23, no. 3, pp. 173–182, 2016.
12. H. Maeda, "The enhanced permeability and retention (EPR) effect in tumor vasculature: the key role of tumor-selective macromolecular drug targeting.," *Advances in enzyme regulation*, vol. 41, pp. 189–207, 2001.
13. Y. Lee and D. H. Thompson, "Stimuli-responsive liposomes for drug delivery," *Wiley Interdisciplinary Reviews: Nanomedicine and Nanobiotechnology*, vol. 9, no. 5, p. e1450, 2017.
14. R. B. Greenwald, Y. H. Choe, J. McGuire, and C. D. Conover, "Effective drug delivery by PEGylated drug conjugates," *Advanced Drug Delivery Reviews*, vol. 55, no. 2, pp. 217–250, 2003.
15. O. C. Farokhzad and R. Langer, "Impact of Nanotechnology on Drug Delivery," *ACS Nano*, vol. 3, no. 1, pp. 16–20, 2009
16. R. Duncan, "The dawning era of polymer therapeutics," *Nature Reviews Drug Discovery*, vol. 2, no. 5, pp. 347–360, 2003.
17. M. Janssen, G. Mihov, T. Welting, J. Thies, and P. Emans, "Drugs and polymers for delivery systems in OA joints: Clinical needs and opportunities," *Polymers*, vol. 6, no. 3, pp. 799–819, 2014.
18. K. Nawalany, B. Kozik, M. Kepczynski, S. Zapotoczny, M. Kumorek, M. Nowakowsak and B. Jachimaska, "Properties of Polyethylene Glycol Supported Tetraarylporphyrin in Aqueous Solution and Its Interaction with Liposomal Membranes," *The Journal of Physical Chemistry B*, vol. 112, no. 39, pp. 12231–12239, 2008.

19. G. Pasut and F. M. Veronese, "PEGylation for improving the effectiveness of therapeutic biomolecules.," *Drugs of today (Barcelona, Spain : 1998)*, vol. 45, no. 9, pp. 687–95, 2009.
20. J.-C. Olivier, "Drug transport to brain with targeted nanoparticles.," *NeuroRx : the journal of the American Society for Experimental NeuroTherapeutics*, vol. 2, no. 1, pp. 108–19, 2005.
21. V. P. Torchilin, "Recent advances with liposomes as pharmaceutical carriers," *Nature Reviews Drug Discovery*, vol. 4, no. 2, pp. 145–160, 2005.
22. M. J. Roberts, M. D. Bentley, and J. M. Harris, "Chemistry for peptide and protein PEGylation.," *Advanced drug delivery reviews*, vol. 54, no. 4, pp. 459–76, 2002.
23. R. Duncan, "Polymer conjugates as anticancer nanomedicines," *Nature Reviews Cancer*, vol. 6, no. 9, pp. 688–701, 2006.
24. M. J. Vicent, L. Dieudonné, R. J. Carbajo, and A. Pineda-Lucena, "Polymer conjugates as therapeutics: future trends, challenges and opportunities," *Expert Opinion on Drug Delivery*, vol. 5, no. 5, pp. 593–614, 2008.
25. A. S. Fauci, "Infectious Diseases: Considerations for the 21st Century," *Clinical Infectious Diseases*, vol. 32, no. 5, pp. 675–685, 2001.
26. M.-H. Xiong, Y. Bao, X.-Z. Yang, Y.-H. Zhu, and J. Wang, "Delivery of antibiotics with polymeric particles," *Advanced Drug Delivery Reviews*, vol. 78, pp. 63–76, 2014.
27. F. Wu, G. Meng, J. He, Y. Wu, F. Wu, and Z. Gu, "Antibiotic-Loaded Chitosan Hydrogel with Superior Dual Functions: Antibacterial Efficacy and Osteoblastic Cell Responses," *ACS Applied Materials & Interfaces*, vol. 6, no. 13, pp. 10005–10013, 2014.
28. B. Boonkaew, P. M. Barber, S. Rengpipat, P. Supaphol, M. Kempf, and J. He, "Development and characterization of a novel antimicrobial, sterile hydrogel dressing for burn wounds: Single-step production with gamma irradiation creates silver nanoparticles and radical polymerization," *J Pharm Sci*, vol. 103, 2014.

29. J. Hoque, B. Bhattacharjee, R. G. Prakash, K. Paramanandham, and J. Haldar, "Dual Function Injectable Hydrogel for Controlled Release of Antibiotic and Local Antibacterial Therapy," *Biomacromolecules*, vol. 19, no. 2, pp. 267–278, 2018.
30. J. Lux, A. G. White, M. Chan, C. J. Anderson, and A. Almutairi, "Nanogels from Metal-Chelating Crosslinkers as Versatile Platforms Applied to Copper-64 PET Imaging of Tumors and Metastases," *Theranostics*, vol. 5, no. 3, pp. 277–288, 2015.
31. D. C. González-Toro, J.-H. Ryu, R. T. Chacko, J. Zhuang, and S. Thayumanavan, "Concurrent Binding and Delivery of Proteins and Lipophilic Small Molecules Using Polymeric Nanogels," *Journal of the American Chemical Society*, vol. 134, no. 16, pp. 6964–6967, 2012.
32. Y. Hashimoto, S. Mukai, S. Sawada, Y. Sasaki, and K. Akiyoshi, "Nanogel tectonic porous gel loading biologics, nanocarriers, and cells for advanced scaffold," *Biomaterials*, vol. 37, pp. 107–115, 2015.
33. E. A. Murphy, B. K. Majeti, R. Mukthavaram, L. M. Acevedo, L. A. Barnes, and D. A. Cheresh, "Targeted nanogels: a versatile platform for drug delivery to tumors.," *Molecular cancer therapeutics*, vol. 10, no. 6, pp. 972–82, 2011.
34. Y. Zhang, H. Huang, F. Zhou, Z. Wu, L. Yuan, D. Li and H. Chen, "A surface decorated with diblock copolymer for biomolecular conjugation," *Soft Matter*, vol. 6, no. 12, p. 2616, 2010.
35. C. Boyer, M. R. Whittaker, M. Luzon, and T. P. Davis, "Design and Synthesis of Dual Thermoresponsive and Antifouling Hybrid Polymer/Gold Nanoparticles," *Macromolecules*, vol. 42, no. 18, pp. 6917–6926, 2009.
36. I. Neamtu, A. G. Rusu, A. Diaconu, L. Elena, N. Aurica, and P. Chiriac, "Drug Delivery Basic concepts and recent advances in nanogels as carriers for medical applications," *Drug Delivery*, vol. 4, pp. 539-557, 2017.

37. B. Aktan, L. Chambre, R. Sanyal, and A. Sanyal, "'Clickable' Nanogels via Thermally Driven Self-Assembly of Polymers: Facile Access to Targeted Imaging Platforms using Thiol–Maleimide Conjugation," *Biomacromolecules*, vol. 18, no. 2, pp. 490–497, 2017.
38. M. J. Joralemon, , R. K. O'Reilly, C. J. Hawker, K. L. Wooley, "Shell Click-Crosslinked (SCC) Nanoparticles: A New Methodology for Synthesis and Orthogonal Functionalization," *Journal of American Chemical Society*, vol. 127, pp. 16892-16899, 2005.
39. H. Wu, H. Jin, C. Wang, Z. Zhang, H. Ruan, L. Sun, C. Yang, Y. Li, W. Qin, C and C. Wang, "Synergistic Cisplatin/Doxorubicin Combination Chemotherapy for Multidrug-Resistant Cancer via Polymeric Nanogels Targeting Delivery," *ACS Applied Materials & Interfaces*, vol. 9, no. 11, pp. 9426–9436, 2017.
40. S. Ahadian, R.B. Sadeghian, S. Salehi, S. Ostravidov, H. Bae, M. Ramalingam and A. Khademhosseini, "Bioconjugated Hydrogels for Tissue Engineering and Regenerative Medicine," *Bioconjugate Chemistry*, vol. 26, no. 10, pp. 1984–2001, 2015.
41. N. A. Peppas, J. Z. Hilt, A. Khademhosseini, and R. Langer, "Hydrogels in Biology and Medicine: From Molecular Principles to Bionanotechnology," *Advanced Materials*, vol. 18, no. 11, pp. 1345–1360, 2006.
42. B. D. Ratner, A. S. Hoffman, "Synthetic Hydrogels for Biomedical Applications," pp. 1–36, 1976.
43. A. S. Hoffman, "Hydrogels for biomedical applications.," *Advanced drug delivery reviews*, vol. 54, no. 1, pp. 3–12, 2002.
44. M. Sepantafar, H. Baharvand, R. Maheronnaghsh, H. Mohammadi, F. Radmanesh, M. Hasani-Sadrabadi and M. Ebrahimi, "Engineered Hydrogels in Cancer Therapy and Diagnosis." *Trends in biotechnology*, vol. 35, no. 11, pp. 1074–1087, 2017.

45. R. Censi, Vermonden T, van Steenbergen MJ, Deschout H, Braeckmans K, De Smedt SC, van Nostrum CF, di Martino P, Hennink WE, “Photopolymerized thermosensitive hydrogels for tailorable diffusion-controlled protein delivery,” *Journal of Controlled Release*, vol. 140, no. 3, pp. 230–236, 2009.
46. X. J. Loh, S. H. Goh, and J. Li, “Hydrolytic degradation and protein release studies of thermogelling polyurethane copolymers consisting of poly[(R)-3-hydroxybutyrate], poly(ethylene glycol), and poly(propylene glycol),” *Biomaterials*, vol. 28, no. 28, pp. 4113–4123, 2007.
47. M. Eroğlu, S. Irmak, A. Acar, and E. B. Denkbaş, “Design and evaluation of a mucoadhesive therapeutic agent delivery system for postoperative chemotherapy in superficial bladder cancer.,” *International journal of pharmaceutics*, vol. 235, no. 1–2, pp. 51–9, 2002.
48. J. B. Wolinsky, Y. L. Colson, and M. W. Grinstaff, “Local drug delivery strategies for cancer treatment: Gels, nanoparticles, polymeric films, rods, and wafers,” *Journal of Controlled Release*, vol. 159, no. 1, pp. 14–26, 2012.
49. W. Hennink and C. van Nostrum, “Novel crosslinking methods to design hydrogels,” *Advanced Drug Delivery Reviews*, vol. 54, no. 1, pp. 13–36, 2002.
50. D. A. Ossipov and J. Hilborn, “Poly(vinyl alcohol)-Based Hydrogels Formed by ‘Click Chemistry’,” *Macromolecules*, vol. 39, pp. 1709-1718, 2006.
51. M. Malkoch, N. Gupta, L. Mespouille, P. Dubois, A.F. Mason, J. L. Hedrick, Q. Liao, C. W. Frank, K. Kingsbury and C. J. Hawker, Craig, “Synthesis of well-defined hydrogel networks using Click chemistry,” *Chemical Communications*, vol. 0, no. 26, p. 2774, 2006.
52. M. Wei, Y. Gao, X. Li, and M. J. Serpe, “Stimuli-responsive polymers and their applications,” *Polymer Chemistry*, vol. 8, no. 1, pp. 127–143, 2017.

53. T. Yoshida, "Stimuli-sensitive polymers for drug delivery and diagnostic systems interacting with biosurfaces," *Switchable and Responsive Surfaces and Materials for Biomedical Applications*, pp. 235–258, 2015.
54. I. Altinbasak, R. Sanyal, and A. Sanyal, "Best of both worlds: Diels–Alder chemistry towards fabrication of redox-responsive degradable hydrogels for protein release," *RSC Advances*, vol. 6, no. 78, pp. 74757–74764, 2016.
55. K. C. Koehler, D. L. Alge, K. S. Anseth, and C. N. Bowman, "A Diels-Alder modulated approach to control and sustain the release of dexamethasone and induce osteogenic differentiation of human mesenchymal stem cells.," *Biomaterials*, vol. 34, no. 16, pp. 4150–8, 2013.
56. M. Hammad, V. Nica, and R. Hempelmann, "On-command controlled drug release by diels-Alder reaction using Bi-magnetic core/shell nano-carriers," *Colloids and Surfaces B: Biointerfaces*, vol. 150, pp. 15–22, 2017.
57. A. Castonguay *et al.*, "Thermosensitive dendrimer formulation for drug delivery at physiologically relevant temperatures," *Chemical Communications*, vol. 47, no. 44, p. 12146, 2011.
58. M. Arslan, D. Aydin, A. Degirmenci, A. Sanyal, and R. Sanyal, "Embedding Well-Defined Responsive Hydrogels with Nanocontainers: Tunable Materials from Telechelic Polymers and Cyclodextrins," *ACS Omega*, vol. 2, no. 10, pp. 6658–6667, 2017.
59. F. Teodorescu *et al.*, "Photothermally triggered on-demand insulin release from reduced graphene oxide modified hydrogels," *Journal of Controlled Release*, vol. 246, pp. 164–173, 2017.
60. J. Tavakoli, Y. Tang, "Hydrogel Based Sensors for Biomedical Applications: An Updated Review," *Polymers*, vol. 9, no. 364, 2017.

61. N. A. Peppas and D. S. Van Blarcom, "Hydrogel-based biosensors and sensing devices for drug delivery," *Journal of Controlled Release*, vol. 240, pp. 142–150, 2016.
62. S. Kaga, T. N. Gevrek, A. Sanyal, and R. Sanyal, "Synthesis and functionalization of dendron-polymer conjugate based hydrogels via sequential thiol-ene 'click' reactions," *Journal of Polymer Science Part A: Polymer Chemistry*, vol. 54, no. 7, pp. 926–934, 2016.
63. S. Yigit, R. Sanyal, and A. Sanyal, "Fabrication and Functionalization of Hydrogels through 'Click' Chemistry," *Chemistry - An Asian Journal*, vol. 6, no. 10, pp. 2648–2659, 2011.
64. C. A. DeForest, B. D. Polizzotti, and K. S. Anseth, "Sequential click reactions for synthesizing and patterning three-dimensional cell microenvironments," *Nature Materials*, vol. 8, no. 8, pp. 659–664, 2009.
65. V. Crescenzi, L. Cornelio, C. Di Meo, S. Nardecchia, and R. Lamanna, "Novel Hydrogels via Click Chemistry: Synthesis and Potential Biomedical Applications," *Biomacromolecules*, vol. 8, no. 6, pp. 1844–1850, 2007.
66. P. Caliceti *et al.*, "Controlled release of biomolecules from temperature-sensitive hydrogels prepared by radiation polymerization.," *Journal of controlled release : official journal of the Controlled Release Society*, vol. 75, no. 1–2, pp. 173–81, 2001.
67. R. Gheneim, C. Perez-Berumen, A. Gandini, "Diels–Alder Reactions with Novel Polymeric Dienes and Dienophiles: Synthesis of Reversibly Cross-Linked Elastomers," 2002.
68. K. C. Koehler, K. S. Anseth, and C. N. Bowman, "Diels–Alder Mediated Controlled Release from a Poly(ethylene glycol) Based Hydrogel," *Biomacromolecules*, vol. 14, no. 2, pp. 538–547, 2013.
69. H. Tan, J. P. Rubin, and K. G. Marra, "Direct Synthesis of Biodegradable Polysaccharide Derivative Hydrogels Through Aqueous Diels-Alder Chemistry." *Macromol. Rapid Commun.*, vol. 32, 905–911, 2011.

70. R. Jin *et al.*, “Synthesis and characterization of hyaluronic acid–poly(ethylene glycol) hydrogels via Michael addition: An injectable biomaterial for cartilage repair,” *Acta Biomaterialia*, vol. 6, no. 6, pp. 1968–1977, 2010.
71. M. Arslan, T. N. Gevrek, A. Sanyal, and R. Sanyal, “Cyclodextrin mediated polymer coupling via thiol–maleimide conjugation: facile access to functionalizable hydrogels,” *RSC Adv.*, vol. 4, no. 101, pp. 57834–57841, 2014.
72. L. Beria, T. N. Gevrek, A. Erdog, R. Sanyal, D. Pasini, and A. Sanyal, “‘Clickable’ hydrogels for all: facile fabrication and functionalization,” *Biomater. Sci.*, vol. 2, no. 1, pp. 67–75, 2014.
73. P. Matteini, F. Tatini, L. Cavigli, S. Ottaviano, G. Ghini, and R. Pini, “Graphene as a photothermal switch for controlled drug release,” *Nanoscale*, vol. 6, no. 14, p. 7947, 2014.
74. J. Conde, N. Oliva, M. Atilano, H. S. Song, and N. Artzi, “Self-assembled RNA–triple-helix hydrogel scaffold for microRNA modulation in the tumour microenvironment,” *Nature Materials*, vol. 15, no. 3, pp. 353–363, 2016.
75. J. Conde, N. Oliva, Y. Zhang, and N. Artzi, “Local triple-combination therapy results in tumour regression and prevents recurrence in a colon cancer model,” *Nature Materials*, vol. 15, no. 10, pp. 1128–1138, 2016.
76. W. Li, K. Dong, J. Ren, and X. Qu, “A  $\beta$ -Lactamase-Imprinted Responsive Hydrogel for the Treatment of Antibiotic-Resistant Bacteria,” *Angewandte Chemie International Edition*, vol. 55, no. 28, pp. 8049–8053, 2016.
77. D. Ciolacu, C. Rudaz, M. Vasilescu, and T. Budtova, “Physically and chemically cross-linked cellulose cryogels: Structure, properties and application for controlled release,” *Carbohydrate Polymers*, vol. 151, pp. 392–400, 2016.
78. V. M. Gun’ko, I. N. Savina, and S. V. Mikhalovsky, “Cryogels: Morphological, structural and adsorption characterisation,” *Advances in Colloid and Interface Science*, vol. 187–188, pp. 1–46, 2013.

79. A. Regand and H. D. Goff, "Structure and ice recrystallization in frozen stabilized ice cream model systems," *Food Hydrocolloids*, vol. 17, no. 1, pp. 95–102, 2003.
80. D. Josic, A. Buchacher, and A. Jungbauer, "Monoliths as stationary phases for separation of proteins and polynucleotides and enzymatic conversion," *Journal of Chromatography B: Biomedical Sciences and Applications*, vol. 752, no. 2, pp. 191–205, 2001.
81. I. N. Savina, G. C. Ingavle, A. B. Cundy, and S. V. Mikhalovsky, "A simple method for the production of large volume 3D macroporous hydrogels for advanced biotechnological, medical and environmental applications," *Scientific Reports*, vol. 6, no. 1, p. 21154, 2016.
82. S. A. Bencherif, T. M. Braschler, and P. Renaud, "Advances in the design of macroporous polymer scaffolds for potential applications in dentistry," *Journal of Periodontal & Implant Science*, vol. 43, no. 6, p. 251, 2013.
83. T. M. A. Henderson, K. Ladewig, D. N. Haylock, K. M. McLean, and A. J. O'Connor, "Cryogels for biomedical applications," *Journal of Materials Chemistry B*, vol. 1, no. 21, p. 2682, 2013.
84. D. Aydin, M. Arslan, A. Sanyal, and R. Sanyal, "Hooked on Cryogels: A Carbamate Linker Based Depot for Slow Drug Release," *Bioconjugate Chemistry*, vol. 28, no. 5, pp. 1443–1451, 2017.
85. F. Sultana, Manirujjaman, Imran-Ul-Haque, M. Arafat, and S. Sharmin, "An overview of nanogel drug delivery system," *Journal of Applied Pharmaceutical Science*, vol. 3, no. 8 SUPPL, pp. 95–105, 2013.
86. J. K. Oh, R. Drumright, D. J. Siegwart, and K. Matyjaszewski, "The development of microgels/nanogels for drug delivery applications," *Progress in Polymer Science*, vol. 33, no. 4, pp. 448–477, 2008.

87. J. K. Oh, C. Tang, H. Gao, N. V. Tsarevsky, and K. Matyjaszewski, "Inverse Miniemulsion ATRP: A New Method for Synthesis and Functionalization of Well-Defined Water-Soluble/Cross-Linked Polymeric Particles," *Journal of the American Chemical Society*, vol. 128, no. 16, pp. 5578–5584, 2006.
88. M. Hellmund, H. Zhou, O. Samsonova, P. Welker, T. Kissel, and R. Haag, "Functionalized Polyglycerol Amine Nanogels as Nanocarriers for DNA," *Macromolecular Bioscience*, vol. 14, no. 9, pp. 1215–1221, 2014.
89. J. K. Oh *et al.*, "Biodegradable Nanogels Prepared by Atom Transfer Radical Polymerization as Potential Drug Delivery Carriers: Synthesis, Biodegradation, in Vitro Release, and Bioconjugation," 2007.
90. S. Singh, J. Blöbbaum, M. Möller, and A. Pich, "Biohybrid nanogels by crosslinking of ovalbumin with reactive star-PEGs in W/O emulsions," *Journal of Polymer Science Part A: Polymer Chemistry*, vol. 50, no. 20, pp. 4288–4299, 2012.
91. W. Shen, Y. Chang, G. Liu, H. Wang, A. Cao, and Z. An, "Biocompatible, Antifouling, and Thermosensitive Core–Shell Nanogels Synthesized by RAFT Aqueous Dispersion Polymerization," *Macromolecules*, vol. 44, no. 8, pp. 2524–2530, 2011.
92. N. J. Warren and S. P. Armes, "Polymerization-Induced Self-Assembly of Block Copolymer Nano-objects via RAFT Aqueous Dispersion Polymerization," *Journal of the American Chemical Society*, vol. 136, no. 29, pp. 10174–10185, 2014.
93. S. Sugihara, A. Blanazs, S. P. Armes, A. J. Ryan, and A. L. Lewis, "Aqueous Dispersion Polymerization: A New Paradigm for in Situ Block Copolymer Self-Assembly in Concentrated Solution," *Journal of the American Chemical Society*, vol. 133, no. 39, pp. 15707–15713, 2011.
94. A. Blanazs *et al.*, "Sterilizable Gels from Thermoresponsive Block Copolymer Worms," *Journal of the American Chemical Society*, vol. 134, no. 23, pp. 9741–9748, 2012.

95. V. J. Cunningham, M. J. Derry, L. A. Fielding, O. M. Musa, and S. P. Armes, "RAFT Aqueous Dispersion Polymerization of N-(2-(Methacryloyloxy)ethyl)pyrrolidone: A Convenient Low Viscosity Route to High Molecular Weight Water-Soluble Copolymers."
96. A. Blanz, J. Madsen, G. Battaglia, A. J. Ryan, and S. P. Armes, "Mechanistic Insights for Block Copolymer Morphologies: How Do Worms Form Vesicles?," *Journal of the American Chemical Society*, vol. 133, no. 41, pp. 16581–16587, 2011.
97. J. Yeow, J. Xu, and C. Boyer, "Polymerization-Induced Self-Assembly Using Visible Light Mediated Photoinduced Electron Transfer–Reversible Addition–Fragmentation Chain Transfer Polymerization," *ACS Macro Letters*, vol. 4, no. 9, pp. 984–990, 2015.
98. T. Dispinar, R. Sanyal, and A. Sanyal, "A Diels-Alder/retro Diels-Alder strategy to synthesize polymers bearing maleimide side chains," *Journal of Polymer Science Part A: Polymer Chemistry*, vol. 45, no. 20, pp. 4545–4551, 2007.
99. Heather D. Maynard, and Sheldon Y. Okada, and R. H. Grubbs\*, "Synthesis of Norbornenyl Polymers with Bioactive Oligopeptides by Ring-Opening Metathesis Polymerization" *Macromolecules*, vol. 33, pp.6239-6248, 2000.
100. J. F. Lutz, "Polymerization of oligo(ethylene glycol) (meth)acrylates: Toward new generations of smart biocompatible materials," *Journal of Polymer Science, Part A: Polymer Chemistry*, vol. 46, no. 11, pp. 3459–3470, 2008.
101. D. P. Nair *et al.*, "The Thiol-Michael Addition Click Reaction: A Powerful and Widely Used Tool in Materials Chemistry," *Chemistry of Materials*, vol. 26, no. 1, pp. 724–744, 2014.
102. C. Clawson, L. Ton, S. Aryal, V. Fu, S. Esener, and L. Zhang, "Synthesis and characterization of lipid-polymer hybrid nanoparticles with ph-triggered poly(ethylene glycol) shedding," *Langmuir*, vol. 27, no. 17, pp. 10556–10561, 2011.
103. C.-M. J. Hu *et al.*, "Half-antibody functionalized lipid-polymer hybrid nanoparticles for targeted drug delivery to carcinoembryonic antigen presenting pancreatic cancer cells.," *Molecular pharmaceuticals*, vol. 7, no. 3, pp. 914–20, 2010.

104. Jacob D. Gibson, A. Bishnu P. Khanal, and E. R. Zubarev\*, "Paclitaxel-Functionalized Gold Nanoparticles," *Journal of the American Chemical Society*, vol. 129, no. 37, pp. 11653–11661, 2007.
105. Xiao *et al.*, "Gold Nanorods Conjugated with Doxorubicin and cRGD for Combined Anticancer Drug Delivery and PET Imaging," *Theranostics*, vol. 2, no. 8, pp. 757–768, 2012.
106. N. Kohler, C. Sun, A. Fichtenholtz, J. Gunn, C. Fang, and M. Zhang, "Methotrexate-Immobilized Poly(ethylene glycol) Magnetic Nanoparticles for MR Imaging and Drug Delivery," *Small*, vol. 2, no. 6, pp. 785–792, 2006.
107. M. K. Yu, J. Park, and S. Jon, "Targeting strategies for multifunctional nanoparticles in cancer imaging and therapy.," *Theranostics*, vol. 2, no. 1, pp. 3–44, 2012.
108. V. Bagalkot *et al.*, "Quantum Dot–Aptamer Conjugates for Synchronous Cancer Imaging, Therapy, and Sensing of Drug Delivery Based on Bi-Fluorescence Resonance Energy Transfer," *Nano Letters*, vol. 7, no. 10, pp. 3065–3070, 2007.
109. R. Kumar, A. Kulkarni, D. K. Nagesha, and S. Sridhar, "In vitro evaluation of theranostic polymeric micelles for imaging and drug delivery in cancer.," *Theranostics*, vol. 2, no. 7, pp. 714–22, 2012.
110. K.-T. Yong *et al.*, "Preparation of Quantum Dot/Drug Nanoparticle Formulations for Traceable Targeted Delivery and Therapy," *Theranostics*, vol. 2, no. 7, pp. 681–694, 2012.
111. H. Bahadar, F. Maqbool, K. Niaz, and M. Abdollahi, "Toxicity of Nanoparticles and an Overview of Current Experimental Models.," *Iranian biomedical journal*, vol. 20, no. 1, pp. 1–11, 2016.
112. B. E. Rolfe *et al.*, "Multimodal Polymer Nanoparticles with Combined <sup>19</sup>F Magnetic Resonance and Optical Detection for Tunable, Targeted, Multimodal Imaging in Vivo."
113. A. K. Pearce *et al.*, "Development of a polymer theranostic for prostate cancer," *Polym. Chem.*, vol. 5, no. 24, pp. 6932–6942, 2014.

114. R. H. Fang *et al.*, “Lipid-insertion enables targeting functionalization of erythrocyte membrane-cloaked nanoparticles,” *Nanoscale*, vol. 5, no. 19, pp. 8884–8888, 2013.
115. R. A. Petros and J. M. DeSimone, “Strategies in the design of nanoparticles for therapeutic applications,” *Nature Reviews Drug Discovery*, vol. 9, no. 8, pp. 615–627, 2010.
116. A. Z. Wang, R. Langer, and O. C. Farokhzad, “Nanoparticle Delivery of Cancer Drugs,” *Annual Review of Medicine*, vol. 63, no. 1, pp. 185–198, 2012.
117. H. Maeda, J. Wu, T. Sawa, Y. Matsumura, and K. Hori, “Tumor vascular permeability and the EPR effect in macromolecular therapeutics: a review.,” *Journal of controlled release : official journal of the Controlled Release Society*, vol. 65, no. 1–2, pp. 271–84, 2000.
118. Y. Matsumura and H. Maeda, “A new concept for macromolecular therapeutics in cancer chemotherapy: mechanism of tumorotropic accumulation of proteins and the antitumor agent smancs.,” *Cancer research*, vol. 46, no. 12 Pt 1, pp. 6387–92, 1986.
119. O. C. Farokhzad and R. Langer, “Impact of Nanotechnology on Drug Delivery,” *ACS Nano*, vol. 3, no. 1, pp. 16–20, 2009.
120. B. P. Timko *et al.*, “Advances in Drug Delivery,” *Annual Review of Materials Research*, vol. 41, no. 1, pp. 1–20, 2011.
121. C. Ju *et al.*, “Sequential Intra-Intercellular Nanoparticle Delivery System for Deep Tumor Penetration,” *Angewandte Chemie International Edition*, vol. 53, no. 24, pp. 6253–6258, 2014.
122. W. Chen, K. Achazi, B. Schade, and R. Haag, “Charge-conversional and reduction-sensitive poly(vinyl alcohol) nanogels for enhanced cell uptake and efficient intracellular doxorubicin release,” *Journal of Controlled Release*, vol. 205, pp. 15–24, 2015.
123. K. Raghupathi, L. Li, J. Ventura, M. Jennings, and S. Thayumanavan, “pH responsive soft nanoclusters with size and charge variation features,” *Polym. Chem.*, vol. 5, no. 5, pp. 1737–1742, 2014.

124. X. Chen *et al.*, “Dual responsive supramolecular nanogels for intracellular drug delivery,” *Chemical Communications*, vol. 50, no. 29, p. 3789, 2014.
125. T. Krasia-Christoforou and T. K. Georgiou, “Polymeric theranostics: using polymer-based systems for simultaneous imaging and therapy,” *Journal of Materials Chemistry B*, vol. 1, no. 24, p. 3002, 2013.
126. M. Arslan, T. N. Gevrek, R. Sanyal, and A. Sanyal, “Fabrication of poly(ethylene glycol)-based cyclodextrin containing hydrogels via thiol-ene click reaction,” *European Polymer Journal*, vol. 62, pp. 426–434, 2015.
127. V. Truong, I. Blakey, and A. K. Whittaker, “Hydrophilic and Amphiphilic Polyethylene Glycol-Based Hydrogels with Tunable Degradability Prepared by ‘Click’ Chemistry,” *Biomacromolecules*, vol. 13, no. 12, pp. 4012–4021, 2012.
128. S. M. Hodgson, S. A. McNelles, L. Abdullahu, I. A. Marozas, K. S. Anseth, and A. Adronov, “Reproducible Dendronized PEG Hydrogels via SPAAC Cross-Linking,” *Biomacromolecules*, vol. 18, no. 12, pp. 4054–4059, 2017.
129. J. D. McCall and K. S. Anseth, “Thiol–Ene Photopolymerizations Provide a Facile Method To Encapsulate Proteins and Maintain Their Bioactivity,” *Biomacromolecules*, vol. 13, no. 8, pp. 2410–2417, 2012
130. R. J. Ono *et al.*, “Biodegradable Strain-Promoted Click Hydrogels for Encapsulation of Drug-Loaded Nanoparticles and Sustained Release of Therapeutics.”
131. Y. Wen and J. K. Oh, “Recent Strategies to Develop Polysaccharide-Based Nanomaterials for Biomedical Applications,” *Macromolecular Rapid Communications*, vol. 35, no. 21, p. n/a-n/a, 2014.
132. J.-H. Ryu, S. Bickerton, J. Zhuang, and S. Thayumanavan, “Ligand-Decorated Nanogels: Fast One-Pot Synthesis and Cellular Targeting,” *Biomacromolecules*, vol. 13, no. 5, pp. 1515–1522, 2012.

133. J.-H. Ryu, R. T. Chacko, S. Jiwanich, S. Bickerton, R. P. Babu, and S. Thayumanavan, "Self-Cross-Linked Polymer Nanogels: A Versatile Nanoscopic Drug Delivery Platform," *Journal of the American Chemical Society*, vol. 132, no. 48, pp. 17227–17235, 2010.
134. K. Rahimian, Y. Wen, and J. K. Oh, "Redox-responsive cellulose-based thermoresponsive grafted copolymers and in-situ disulfide crosslinked nanogels," *Polymer*, vol. 72, pp. 387–394, 2015.
135. C. Subramani *et al.*, "Direct Fabrication of Functional and Biofunctional Nanostructures Through Reactive Imprinting," *Advanced Materials*, vol. 23, no. 28, pp. 3165–3169, 2011.
136. E. J. Park, T. N. Gevrek, R. Sanyal, and A. Sanyal, "Indispensable Platforms for Bioimmobilization: Maleimide-Based Thiol Reactive Hydrogels," *Bioconjugate Chemistry*, vol. 25, no. 11, pp. 2004–2011, 2014.
137. M. Arslan *et al.*, "Bioinspired Anchorable Thiol-Reactive Polymers: Synthesis and Applications Toward Surface Functionalization of Magnetic Nanoparticles," *Macromolecules*, vol. 47, no. 15, pp. 5124–5134, 2014.
138. O. Gok, H. Durmaz, E. S. Ozdes, G. Hizal, U. Tunca, and A. Sanyal, "Maleimide-based thiol reactive multiarm star polymers via Diels-Alder/retro Diels-Alder strategy," *Journal of Polymer Science Part A: Polymer Chemistry*, vol. 48, no. 12, pp. 2546–2556, 2010.
139. O. Gok, I. Kosif, T. Dispinar, T. N. Gevrek, R. Sanyal, and A. Sanyal, "Design and Synthesis of Water-Soluble Multifunctionalizable Thiol-Reactive Polymeric Supports for Cellular Targeting."
140. G. Hizal, U. Tunca, and A. Sanyal, "Discrete macromolecular constructs via the Diels-Alder 'Click' reaction," *Journal of Polymer Science Part A: Polymer Chemistry*, vol. 49, no. 19, p. n/a-n/a, 2011.

141. S. Onbulak, S. Tempelaar, R. J. Pounder, O. Gok, R. Sanyal, A. P. Dove and A. Sanyal, "Synthesis and Functionalization of Thiol-Reactive Biodegradable Polymers," *Macromolecules*, vol. 45, no. 3, pp. 1715–1722, 2012.
142. A. Sanyal, "Diels-Alder Cycloaddition-Cycloreversion: A Powerful Combo in Materials Design," *Macromolecular Chemistry and Physics*, vol. 211, no. 13, pp. 1417–1425, 2010.
143. G. Mantovani, F. Lecolley, L. Tao, D.M. Haddleton, J. Clerx, J. J. L. M. Cornelissen and K. Velonia., "Design and Synthesis of N-Maleimido-Functionalized Hydrophilic Polymers via Copper-Mediated Living Radical Polymerization: A Suitable Alternative to PEGylation Chemistry," *Journal of American Chemical Society*, vol. 127, pp.2966-2973, 2005.
144. Y. Oz and A. Sanyal, "The Taming of the Maleimide: Fabrication of Maleimide-Containing 'Clickable' Polymeric Materials," *The Chemical Record*, vol. 18, no. 6, pp. 570–586, 2018.
145. C. C. Lee *et al.*, "A single dose of doxorubicin-functionalized bow-tie dendrimer cures mice bearing C-26 colon carcinomas," *Proceedings of the National Academy of Sciences*, vol. 103, no. 45, pp. 16649–16654, 2006.
146. S. Thatte, K. Datar, and R. M. Ottenbrite, "Perspectives On: Polymeric Drugs and Drug Delivery Systems," *Journal of Bioactive and Compatible Polymers*, vol. 20, no. 6, pp. 585–601, 2005.
147. M. Zovko, B. Zorc, P. Novak, P. Tepeš, B. Cetina-Čižmek, and M. Horvat, "Macromolecular prodrugs," *International Journal of Pharmaceutics*, vol. 285, no. 1–2, pp. 35–41, 2004.
148. R. B. Greenwald, Y. H. Choe, J. McGuire, and C. D. Conover, "Effective drug delivery by PEGylated drug conjugates," *Advanced Drug Delivery Reviews*, vol. 55, no. 2, pp. 217–250, 2003.

149. G. Digilio *et al.*, “NMR structure of two novel polyethylene glycol conjugates of the human growth hormone-releasing factor, hGRF(1-29)-NH<sub>2</sub>,” *Journal of the American Chemical Society*, vol. 125, no. 12, pp. 3458–3470, 2003.
150. C. F. McCusker, P. J. Kocienski, F. T. Boyle, and A. G. Schätzlein, “Solid-phase synthesis of c(RGDfK) derivatives: on-resin cyclisation and lysine functionalisation.,” *Bioorganic & medicinal chemistry letters*, vol. 12, no. 4, pp. 547–9, 2002.
151. C. E. Hoyle and C. N. Bowman, “Thiol-Ene Click Chemistry,” *Angewandte Chemie International Edition*, vol. 49, no. 9, pp. 1540–1573, 2010.
152. W. Xi, T. F. Scott, C. J. Kloxin, and C. N. Bowman, “Click Chemistry: Click Chemistry in Materials Science),” *Advanced Functional Materials*, vol. 24, no. 18, pp. 2566–2566, 2014.
153. D. E. J. G. J. Dolmans, D. Fukumura, and R. K. Jain, “Photodynamic therapy for cancer,” *Nature Reviews Cancer*, vol. 3, no. 5, pp. 380–387, 2003.
154. D. W. C. Hunt, “Rostaporfin (Miravant Medical Technologies).,” *IDrugs: the investigational drugs journal*, vol. 5, no. 2, pp. 180–6, 2002.
155. S. K. Powers and J. Tony Brown, “Light dosimetry in brain tissue: An in vivo model applicable to photodynamic therapy,” *Lasers in Surgery and Medicine*, vol. 6, no. 3, pp. 318–322, 1986.
156. A. Shinde, S. M. Perinchery, and V. M. Murukeshan, “A targeted illumination optical fiber probe for high resolution fluorescence imaging and optical switching,” *Scientific Reports*, vol. 7, p. 45654, 2017.
157. S. S. Lucky, K. C. Soo, and Y. Zhang, “Nanoparticles in Photodynamic Therapy,” *Chemical Reviews*, vol. 115, no. 4, pp. 1990–2042, 2015.
158. F. Moret and E. Reddi, “Strategies for optimizing the delivery to tumors of macrocyclic photosensitizers used in photodynamic therapy (PDT),” *Journal of Porphyrins and Phthalocyanines*, vol. 21, no. 4–6, pp. 239–256, 2017.

159. A. Srivatsan, J. R. Missert, S. K. Upadhyay, and R. K. Pandey, "Porphyrin-based photosensitizers and the corresponding multifunctional nanoplatforams for cancer-imaging and phototherapy," *Journal of Porphyrins and Phthalocyanines*, vol. 19, no. 1–3, pp. 109–134, 2015.
160. S. Tuncel *et al.*, "Assessing the Dual Activity of a Chalcone–Phthalocyanine Conjugate: Design, Synthesis, and Antivasular and Photodynamic Properties," *Molecular Pharmaceutics*, vol. 10, no. 10, pp. 3706–3716, 2013.
161. S. K. Sharma, P. Mroz, T. Dai, Y.-Y. Huang, T. G. St Denis, and M. R. Hamblin, "Photodynamic Therapy for Cancer and for Infections: What Is the Difference?," *Israel journal of chemistry*, vol. 52, no. 8–9, pp. 691–705, 2012.
162. M. Olivo, R. Bhuvaneswari, S. S. Lucky, N. Dendukuri, and P. Soo-Ping Thong, "Targeted Therapy of Cancer Using Photodynamic Therapy in Combination with Multi-faceted Anti-Tumor Modalities," *Pharmaceutics*, vol. 3, no. 5, pp. 1507–1529, 2010.
163. K. Han, Z. Ma, and H. Han, "Functional peptide-based nanoparticles for photodynamic therapy," *Journal of Materials Chemistry B*, vol. 6, no. 1, pp. 25–38, 2018.
164. N. Malatesti, I. Munitic, and I. Jurak, "Porphyrin-based cationic amphiphilic photosensitizers as potential anticancer, antimicrobial and immunosuppressive agents.," *Biophysical reviews*, vol. 9, no. 2, pp. 149–168, 2017.
165. J.-Y. Kim, W. Il Choi, M. Kim, and G. Tae, "Tumor-targeting nanogel that can function independently for both photodynamic and photothermal therapy and its synergy from the procedure of PDT followed by PTT," *Journal of Controlled Release*, vol. 171, no. 2, pp. 113–121, 2013.
166. K. Deng, Z. Hou, X. Deng, P. Yang, C. Li, and J. Lin, "Enhanced Antitumor Efficacy by 808 nm Laser-Induced Synergistic Photothermal and Photodynamic Therapy Based on a Indocyanine-Green-Attached  $W_{18}O_{49}$  Nanostructure," *Advanced Functional Materials*, vol. 25, no. 47, pp. 7280–7290, 2015.

167. J. Han *et al.*, “Single-layer MoS<sub>2</sub> nanosheet grafted upconversion nanoparticles for near-infrared fluorescence imaging-guided deep tissue cancer phototherapy,” *Nanoscale*, vol. 8, no. 15, pp. 7861–7865, 2016.
168. J. Han, W. Park, S. Park, and K. Na, “Photosensitizer-Conjugated Hyaluronic Acid-Shielded Polydopamine Nanoparticles for Targeted Photomediated Tumor Therapy,” *ACS Applied Materials & Interfaces*, vol. 8, no. 12, pp. 7739–7747, 2016.
169. E. Huynh and G. Zheng, “Porphysome nanotechnology: A paradigm shift in lipid-based supramolecular structures,” *Nano Today*, vol. 9, no. 2, pp. 212–222, 2014.
170. D. J. Lee *et al.*, “Photodynamic tumor therapy of nanoparticles with chlorin e6 sown in poly(ethylene glycol) forester,” *J. Mater. Chem. B*, vol. 3, no. 23, pp. 4690–4697, 2015.
171. K. S. Lam *et al.*, “Abstract 4508: Novel multifunctional nanocarriers for drug delivery, photodynamic therapy, sonodynamic therapy, MRI and PET imaging.,” *Cancer Research*, vol. 73, no. 8 Supplement, 2014.
172. A. Vaidya, Y. Sun, T. Ke, E.-K. Jeong, and Z.-R. Lu, “Contrast enhanced MRI-guided photodynamic therapy for site-specific cancer treatment,” *Magnetic Resonance in Medicine*, vol. 56, no. 4, pp. 761–767, 2006.
173. Y. N. Konan, R. Gurny, and E. Allémann, “State of the art in the delivery of photosensitizers for photodynamic therapy,” *Journal of Photochemistry and Photobiology B: Biology*, vol. 66, no. 2, pp. 89–106, 2002.
174. L. V. Kiew *et al.*, “Near-infrared activatable phthalocyanine-poly-L-glutamic acid conjugate: increased cellular uptake and light–dark toxicity ratio toward an effective photodynamic cancer therapy,” *Nanomedicine: Nanotechnology, Biology and Medicine*, vol. 13, no. 4, pp. 1447–1458, 2017.
175. M. Asadian-Birjand, J. Bergueiro, S. Wedepohl, and M. Calderón, “Near Infrared Dye Conjugated Nanogels for Combined Photodynamic and Photothermal Therapies,” *Macromolecular Bioscience*, vol. 16, no. 10, pp. 1432–1441, 2016.

176. S. Belali *et al.*, “Synthesis and Characterization of Temperature-Sensitive and Chemically Cross-Linked Poly(*N*-isopropylacrylamide)/Photosensitizer Hydrogels for Applications in Photodynamic Therapy,” *Biomacromolecules*, vol. 19, no. 5, pp. 1592–1601, 2018.
177. X. Huang, I. H. El-Sayed, W. Qian, and M. A. El-Sayed, “Cancer Cell Imaging and Photothermal Therapy in the Near-Infrared Region by Using Gold Nanorods,” *Journal of the American Chemical Society*, vol. 128, no. 6, pp. 2115–2120, 2006.
178. B. Pucelik, I. Gürol, V. Ahsen, F. Dumoulin, and J. M. Dąbrowski, “Fluorination of phthalocyanine substituents: Improved photoproperties and enhanced photodynamic efficacy after optimal micellar formulations,” *European Journal of Medicinal Chemistry*, vol. 124, pp. 284–298, 2016.
179. H. Nakamura *et al.*, “Micelles of zinc protoporphyrin conjugated to N-(2-hydroxypropyl)methacrylamide (HPMA) copolymer for imaging and light-induced antitumor effects in vivo,” *Journal of Controlled Release*, vol. 165, no. 3, pp. 191–198, 2013.
180. D. Peer, J. M. Karp, S. Hong, O. C. Farokhzad, R. Margalit, and R. Langer, “Nanocarriers as an emerging platform for cancer therapy,” *Nature Nanotechnology*, vol. 2, no. 12, pp. 751–760, 2007.
181. M. Elsabahy, G. S. Heo, S.-M. Lim, G. Sun, and K. L. Wooley, “Polymeric Nanostructures for Imaging and Therapy,” *Chemical Reviews*, vol. 115, no. 19, pp. 10967–11011, 2015.
182. C. Mauriello-Jimenez *et al.*, “Porphyrin- or phthalocyanine-bridged silsesquioxane nanoparticles for two-photon photodynamic therapy or photoacoustic imaging,” *Nanoscale*, vol. 9, no. 43, pp. 16622–16626, 2017.
183. R. T. Chacko, J. Ventura, J. Zhuang, and S. Thayumanavan, “Polymer nanogels: A versatile nanoscopic drug delivery platform,” *Advanced Drug Delivery Reviews*, vol. 64, no. 9, pp. 836–851, 2012.

184. K. Landfester, "Miniemulsion Polymerization and the Structure of Polymer and Hybrid Nanoparticles," *Angewandte Chemie International Edition*, vol. 48, no. 25, pp. 4488–4507, 2009.
185. M. Antonietti and K. Landfester, "Polyreactions in miniemulsions," *Progress in Polymer Science*, vol. 27, no. 4, pp. 689–757, 2002.
186. G.-D. Fu, H. Jiang, F. Yao, L.-Q. Xu, J. Ling, and E.-T. Kang, "Preparation of Fluorescent Organometallic Porphyrin Complex Nanogels of Controlled Molecular Structure via Reverse-Emulsion Click Chemistry," *Macromolecular Rapid Communications*, vol. 33, no. 18, pp. 1523–1527, 2012.
187. J. F. Lovell *et al.*, "Porphyrin-Cross-Linked Hydrogel for Fluorescence-Guided Monitoring and Surgical Resection," *Biomacromolecules*, vol. 12, no. 9, pp. 3115–3118, 2011.
188. F. Dumoulin and V. Ahsen, "Click chemistry: the emerging role of the azide-alkyne Huisgen dipolar addition in the preparation of substituted tetrapyrrolic derivatives," *Journal of Porphyrins and Phthalocyanines*, vol. 15, no. 07n08, pp. 481–504, 2011.
189. E. Akiyama, N. Morimoto, P. Kujawa, Y. Ozawa, F. M. Winnik, and K. Akiyoshi, "Self-Assembled Nanogels of Cholesteryl-Modified Polysaccharides: Effect of the Polysaccharide Structure on Their Association Characteristics in the Dilute and Semidilute Regimes," *Biomacromolecules*, vol. 8, no. 8, pp. 2366–2373, 2007.
190. J.-H. Ryu, S. Jiwanich, R. Chacko, S. Bickerton, and S. Thayumanavan, "Surface-Functionalizable Polymer Nanogels with Facile Hydrophobic Guest Encapsulation Capabilities," *Journal of the American Chemical Society*, vol. 132, no. 24, pp. 8246–8247, 2010.
191. Jung Kwon Oh *et al.*, "Biodegradable Nanogels Prepared by Atom Transfer Radical Polymerization as Potential Drug Delivery Carriers: Synthesis, Biodegradation, in Vitro Release, and Bioconjugation," 2007.

192. L. Chambre, A. Degirmenci, R. Sanyal, and A. Sanyal, "Multi-Functional Nanogels as Theranostic Platforms: Exploiting Reversible and Nonreversible Linkages for Targeting, Imaging, and Drug Delivery," *Bioconjugate Chemistry*, vol. 29, no. 6, pp. 1885–1896, 2018.
193. N. Cengiz, H. Kabadayiglu, and R. Sanyal, "Orthogonally functionalizable copolymers based on a novel reactive carbonate monomer," *Journal of Polymer Science Part A: Polymer Chemistry*, vol. 48, no. 21, pp. 4737–4746, 2010.
194. Yu Liu, Chen-Feng Ke, Heng-Yi Zhang, and Jie Cui, and F. Ding, "Complexation-Induced Transition of Nanorod to Network Aggregates: Alternate Porphyrin and Cyclodextrin Arrays," 2007.
195. M. Ghosh, A. K. Mora, S. Nath, A. K. Chandra, A. Hajra, and S. Sinha, "Photophysics of Soret-excited free base tetraphenylporphyrin and its zinc analog in solution," *Spectrochimica Acta Part A: Molecular and Biomolecular Spectroscopy*, vol. 116, pp. 466–472, 2013.
196. R. Schmidt, C. Tanielian, R. Dunsbach, and C. Wolff, "Phenalenone, a universal reference compound for the determination of quantum yields of singlet oxygen O<sub>2</sub>(<sup>1</sup>Δ<sub>g</sub>) sensitization," *Journal of Photochemistry and Photobiology A: Chemistry*, vol. 79, no. 1–2, pp. 11–17, 1994.
197. S. L. Hopkins *et al.*, "An in vitro cell irradiation protocol for testing photopharmaceuticals and the effect of blue, green, and red light on human cancer cell lines," *Photochemical & Photobiological Sciences*, vol. 15, no. 5, pp. 644–653, 2016.
198. S. Huo *et al.*, "Ultrasmall gold nanoparticles as carriers for nucleus-based gene therapy due to size-dependent nuclear entry.," *ACS nano*, vol. 8, no. 6, pp. 5852–62, 2014.
199. J. B. Wolinsky, Y. L. Colson, and M. W. Grinstaff, "Local drug delivery strategies for cancer treatment: Gels, nanoparticles, polymeric films, rods, and wafers," *Journal of Controlled Release*, vol. 159, no. 1, pp. 14–26, 2012.

200. P. Basnet and N. Skalko-Basnet, "Nanodelivery Systems for Improved Topical Antimicrobial Therapy," *Current Pharmaceutical Design*, vol. 19, no. 41, pp. 7237–7243, 2013.
201. C. Li *et al.*, "Flexible Nanoholey Patches for Antibiotic-Free Treatments of Skin Infections," *ACS Applied Materials & Interfaces*, vol. 9, no. 42, pp. 36665–36674, 2017.
202. T. Jing, L. Fu, L. Liu, and L. Yan, "A reduction-responsive polypeptide nanogel encapsulating NIR photosensitizer for imaging guided photodynamic therapy," *Polymer Chemistry*, vol. 7, no. 4, pp. 951–957, 2016.
203. M. Fang, J. Long, W. Zhao, L. Wang, and G. Chen, "pH-Responsive Chitosan-Mediated Graphene Dispersions," *Langmuir*, vol. 26, no. 22, pp. 16771–16774, 2010.
204. M. K. Jaiswal *et al.*, "Thermoresponsive Magnetic Hydrogels as Theranostic Nanoconstructs," *ACS Applied Materials & Interfaces*, vol. 6, no. 9, pp. 6237–6247, 2014.
205. S. K. Rastogi *et al.*, "Enhanced Release of Molecules upon Ultraviolet (UV) Light Irradiation from Photoresponsive Hydrogels Prepared from Bifunctional Azobenzene and Four-Arm Poly(ethylene glycol)," *ACS Applied Materials & Interfaces*, p. acsami.6b16183, 2017.
206. S. Szunerits and R. Boukherroub, "Antibacterial activity of graphene-based materials," *Journal of Materials Chemistry B*, vol. 4, no. 43, pp. 6892–6912, 2016.
207. F. Teodorescu *et al.*, "Transdermal skin patch based on reduced graphene oxide: A new approach for photothermal triggered permeation of ondansetron across porcine skin," *Journal of Controlled Release*, vol. 245, pp. 137–146, 2017.
208. D. Mawad *et al.*, "Electroconductive Hydrogel Based on Functional Poly(Ethylenedioxy Thiophene)," *Chemistry of Materials*, vol. 28, no. 17, pp. 6080–6088, 2016.

209. J. Yang, M.-H. Yao, R.-M. Jin, D.-H. Zhao, Y.-D. Zhao, and B. Liu, "Polypeptide-Engineered Hydrogel Coated Gold Nanorods for Targeted Drug Delivery and Chemophothermal Therapy," *ACS Biomaterials Science & Engineering*, vol. 3, no. 10, pp. 2391–2398, 2017.
210. H. Jin *et al.*, "Melittin-Containing Hybrid Peptide Hydrogels for Enhanced Photothermal Therapy of Glioblastoma," *ACS Applied Materials & Interfaces*, vol. 9, no. 31, pp. 25755–25766, 2017.
211. E. Caló and V. V. Khutoryanskiy, "Biomedical applications of hydrogels: A review of patents and commercial products," *European Polymer Journal*, vol. 65, pp. 252–267, 2015.
212. G. Chang, S. Li, F. Huang, X. Zhang, Y. Shen, and A. Xie, "Multifunctional Reduced Graphene Oxide Hydrogel as Drug Carrier for Localized and Synergic Photothermal/Photodynamics/Chemo Therapy," *Journal of Materials Science & Technology*, vol. 32, no. 8, pp. 753–762, 2016.
213. Y. Oz, A. Barras, R. Sanyal, R. Boukherroub, S. Szunerits, and A. Sanyal, "Functionalization of Reduced Graphene Oxide via Thiol–Maleimide 'Click' Chemistry: Facile Fabrication of Targeted Drug Delivery Vehicles," *ACS Applied Materials & Interfaces*, vol. 9, no. 39, pp. 34194–34203, 2017.
214. J. T. Robinson *et al.*, "Ultrasmall Reduced Graphene Oxide with High Near-Infrared Absorbance for Photothermal Therapy," *Journal of the American Chemical Society*, vol. 133, no. 17, pp. 6825–6831, 2011.
215. S. Goenka, V. Sant, and S. Sant, "Graphene-based nanomaterials for drug delivery and tissue engineering," *Journal of Controlled Release*, vol. 173, pp. 75–88, 2014.
216. Y. Fong, C.-H. Chen, and J.-P. Chen, "Intratumoral Delivery of Doxorubicin on Folate-Conjugated Graphene Oxide by In-Situ Forming Thermo-Sensitive Hydrogel for Breast Cancer Therapy," *Nanomaterials*, vol. 7, no. 11, p. 388, 2017.

217. C. Fiorica, N. Mauro, G. Pitarresi, C. Scialabba, F. S. Palumbo, and G. Giammona, “Double-Network-Structured Graphene Oxide-Containing Nanogels as Photothermal Agents for the Treatment of Colorectal Cancer,” *Biomacromolecules*, vol. 18, no. 3, pp. 1010–1018, 2017.
218. A. Gandini, “The furan/maleimide Diels–Alder reaction: A versatile click–unclick tool in macromolecular synthesis,” *Progress in Polymer Science*, vol. 38, no. 1, pp. 1–29, 2013.
219. T. Ma, X. Gao, H. Dong, H. He, and X. Cao, “High-throughput generation of hyaluronic acid microgels via microfluidics-assisted enzymatic crosslinking and/or Diels–Alder click chemistry for cell encapsulation and delivery,” *Applied Materials Today*, vol. 9, pp. 49–59, 2017.
220. X. Chen *et al.*, “A Thermally Re-mendable Cross-Linked Polymeric Material,” *Science*, vol. 295, no. 5560, pp. 1698–1702, 2002.
221. C. M. Nimmo, S. C. Owen, and M. S. Shoichet, “Diels–Alder Click Cross-Linked Hyaluronic Acid Hydrogels for Tissue Engineering,” *Biomacromolecules*, vol. 12, no. 3, pp. 824–830, 2011.
222. A. Vieyres, T. Lam, R. Gillet, G. Franc, A. Castonguay, and A. Kakkar, “Combined CuI-catalysed alkyne–azide cycloaddition and furan–maleimide Diels–Alder ‘click’ chemistry approach to thermoresponsive dendrimers,” *Chemical Communications*, vol. 46, no. 11, p. 1875, 2010.
223. S. Yamashita, H. Fukushima, Y. Niidome, T. Mori, Y. Katayama, and T. Niidome, “Controlled-Release System Mediated by a Retro Diels–Alder Reaction Induced by the Photothermal Effect of Gold Nanorods,” *Langmuir*, vol. 27, no. 23, pp. 14621–14626, 2011.
224. E. H. Discekici, A. H. St. Amant, S. N. Nguyen, I.-H. Lee, C. J. Hawker, and J. Read de Alaniz, “Endo and Exo Diels–Alder Adducts: Temperature-Tunable Building Blocks for Selective Chemical Functionalization,” *Journal of the American Chemical Society*, vol. 140, no. 15, pp. 5009–5013, 2018.

225. Y. Nagai, Y. Tsutsumi, N. Nakashima, and T. Fujigaya, "Synthesis of Single-Walled Carbon Nanotubes Coated with Thiol-Reactive Gel via Emulsion Polymerization," *Journal of the American Chemical Society*, vol. 140, no. 27, pp. 8544–8550, 2018.
226. F. M. Plieva, I. Y. Galaev, and B. Mattiasson, "Macroporous gels prepared at subzero temperatures as novel materials for chromatography of particulate-containing fluids and cell culture applications," *Journal of Separation Science*, vol. 30, no. 11, pp. 1657–1671, 2007.
227. R. Jijie, A. Barras, J. Bouckaert, N. Dumitrascu, S. Szunerits, and R. Boukherroub, "Enhanced antibacterial activity of carbon dots functionalized with ampicillin combined with visible light triggered photodynamic effects," *Colloids and Surfaces B: Biointerfaces*, vol. 170, pp. 347–354, 2018.
228. I. N. Savina *et al.*, "Porous structure and water state in cross-linked polymer and protein cryo-hydrogels," *Soft Matter*, vol. 7, no. 9, p. 4276, 2011.
229. B. Gyarmati, E. Zsuzsanna Mészár, L. Kiss, M. A. Deli, K. László, and A. Szilágyi, "Supermacroporous chemically cross-linked poly(aspartic acid) hydrogels," *ACTA BIOMATERIALIA*, 2015.
230. T. M. A. Henderson, K. Ladewig, D. N. Haylock, K. M. McLean, and A. J. O'Connor, "Cryogels for biomedical applications," *Journal of Materials Chemistry B*, vol. 1, no. 21, p. 2682, 2013.
231. F. M. Plieva, I. Y. Galaev, W. Noppe, and B. Mattiasson, "Cryogel applications in microbiology," *Trends in Microbiology*, vol. 16, no. 11, pp. 543–551, 2008.
232. V. I. Lozinsky, "Polymeric cryogels as a new family of macroporous and supermacroporous materials for biotechnological purposes," 2008.
233. V. I. Lozinsky, I. Y. Galaev, F. M. Plieva, I. N. Savina, H. Jungvid, and B. Mattiasson, "Polymeric cryogels as promising materials of biotechnological interest," *Trends in Biotechnology*, vol. 21, no. 10, pp. 445–451, 2003.
234. S. A. Bencherif *et al.*, "Injectable cryogel-based whole-cell cancer vaccines," *Nature Communications*, vol. 6, no. 1, p. 7556, 2015.

235. P. Öncel, K. Çetin, A. A. Topçu, H. Yavuz, and A. Denizli, "Molecularly imprinted cryogel membranes for mitomycin C delivery," *Journal of Biomaterials Science, Polymer Edition*, vol. 28, no. 6, pp. 519–531, 2017.
236. V. Weber, I. Linsberger, M. Hauner, A. Leistner, A. Leistner, and D. Falkenhagen, "Neutral Styrene Divinylbenzene Copolymers for Adsorption of Toxins in Liver Failure," *Biomacromolecules*, vol. 9, no. 4, pp. 1322–1328, 2008.
237. H. Sun, B. Ge, S. Liu, and H. Chen, "Preparation of nitrocellulose (NC) immuno-affinity membrane for purification of rAPC antibody," *Journal of Separation Science*, vol. 31, no. 6–7, pp. 1201–1206, 2008.
238. G. Baydemir, N. Bereli, M. Andaç, R. Say, I. Y. Galaev, and A. Denizli, "Bilirubin recognition via molecularly imprinted supermacroporous cryogels," *Colloids and Surfaces B: Biointerfaces*, vol. 68, no. 1, pp. 33–38, 2009.
239. N. Bereli, M. Andaç, G. Baydemir, R. Say, I. Y. Galaev, and A. Denizli, "Protein recognition via ion-coordinated molecularly imprinted supermacroporous cryogels," *Journal of Chromatography A*, vol. 1190, no. 1–2, pp. 18–26, 2008.
240. G. C. Ingavle *et al.*, "Affinity binding of antibodies to supermacroporous cryogel adsorbents with immobilized protein A for removal of anthrax toxin protective antigen," *Biomaterials*, vol. 50, pp. 140–153, 2015.
241. C. S. M. Fernandes *et al.*, "Biobased monoliths for adenovirus purification," *ACS Applied Materials and Interfaces*, vol. 7, no. 12, pp. 6605–6612, 2015.
242. S. L. Ginn, I. E. Alexander, M. L. Edelstein, M. R. Abedi, and J. Wixon, "Gene therapy clinical trials worldwide to 2012 - an update," *The Journal of Gene Medicine*, vol. 15, no. 2, pp. 65–77, 2013.
243. N. Tatsis and H. C. J. Ertl, "Adenoviruses as vaccine vectors," *Molecular Therapy*, vol. 10, no. 4, pp. 616–629, 2004.

244. E. Burova and E. Ioffe, "Chromatographic purification of recombinant adenoviral and adeno-associated viral vectors: methods and implications," *Gene Therapy*, vol. 12, no. S1, pp. S5–S17, 2005.
245. C. Peixoto, T. B. Ferreira, M. F. Q. Sousa, M. J. T. Carrondo, and P. M. Alves, "Towards purification of adenoviral vectors based on membrane technology," *Biotechnology Progress*, vol. 24, no. 6, pp. 1290–1296, 2008.
246. A. Podgornik, S. Yamamoto, M. Peterka, and N. L. Krajnc, "Fast separation of large biomolecules using short monolithic columns," *Journal of Chromatography B*, vol. 927, pp. 80–89, 2013.
247. E. Uliyanchenko, S. Van Der Wal, and P. J. Schoenmakers, "Deformation and degradation of polymers in ultra-high-pressure liquid chromatography," *Journal of Chromatography A*, vol. 1218, pp. 6930–6942, 2011.
248. T.-L. To, K. F. Medzihradzky, A. L. Burlingame, W. F. DeGrado, H. Jo, and X. Shu, "Photoactivatable protein labeling by singlet oxygen mediated reactions," *Bioorganic & Medicinal Chemistry Letters*, vol. 26, no. 14, pp. 3359–3363, 2016.
249. P. S. Stayton *et al.*, "Streptavidin-biotin binding energetics," *Biomolecular Engineering*, vol. 16, no. 1–4, pp. 39–44, 1999.
250. C. E. Chivers, A. L. Koner, E. D. Lowe, and M. Howarth, "How the biotin–streptavidin interaction was made even stronger: investigation via crystallography and a chimaeric tetramer," *Biochemical Journal*, vol. 435, no. 1, pp. 55–63, 2011

## **9. APPENDIX A: COPYRIGHT NOTICES**

Copyrights belonging to figures and chapters which were taken from literature articles can be found here.

[Oncol Rep.](#) 2017 Aug; 38(2): 611–624.

Published online 2017 Jun 14. doi: [10.3892/or.2017.5718](https://doi.org/10.3892/or.2017.5718)

PMCID: PMC5562049

PMID: [28627697](https://pubmed.ncbi.nlm.nih.gov/28627697/)

## Cancer drug delivery in the nano era: An overview and perspectives

Zhen Li,<sup>1,2</sup> Shirui Tan,<sup>3</sup> Shuan Li,<sup>1</sup> Qiang Shen,<sup>4</sup> and Kunhua Wang<sup>1,2</sup>

[Author information](#) ► [Article notes](#) ► [Copyright and License information](#) ▼ [Disclaimer](#)

[Copyright](#) : © Li et al.

This is an open access article distributed under the terms of the [Creative Commons Attribution-NonCommercial-NoDerivs License](#), which permits use and distribution in any medium, provided the original work is properly cited, the use is non-commercial and no modifications or adaptations are made.

Figure A.1. Copyright of [6]



RightsLink®

Home

Account  
info

Help



**Title:** Stimuli-responsive liposomes for drug delivery  
**Author:** Y. Lee, D.H. Thompson  
**Publication:** Wiley Interdisciplinary Reviews - Nanomedicine and Nanobiotechnology  
**Publisher:** John Wiley and Sons  
**Date:** Feb 15, 2017  
 Copyright © 2017, John Wiley and Sons

Logged in as:  
 LAURA CHAMBRE  
 Account #:  
 3001287341  
 LOGOUT

### Order Completed

Thank you for your order.

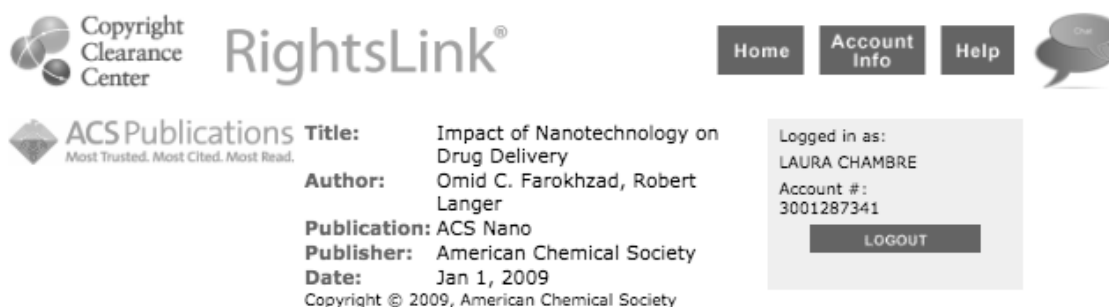
This Agreement between VADISTANBUL ("You") and John Wiley and Sons ("John Wiley and Sons") consists of your license details and the terms and conditions provided by John Wiley and Sons and Copyright Clearance Center.

Your confirmation email will contain your order number for future reference.

#### [printable details](#)

License Number	4358730609055
License date	May 30, 2018
Licensed Content Publisher	John Wiley and Sons
Licensed Content Publication	Wiley Interdisciplinary Reviews - Nanomedicine and Nanobiotechnology
Licensed Content Title	Stimuli-responsive liposomes for drug delivery
Licensed Content Author	Y. Lee, D.H. Thompson
Licensed Content Date	Feb 15, 2017
Licensed Content Volume	9
Licensed Content Issue	5
Licensed Content Pages	40
Type of use	Dissertation/Thesis
Requestor type	University/Academic
Format	Print and electronic
Portion	Figure/table
Number of figures/tables	1
Original Wiley figure/table number(s)	figure 2
Will you be translating?	No
Title of your thesis / dissertation	Polymeric Materials for Delivery of Chemotherapeutic and Antibacterial Agents*
Expected completion date	Aug 2018
Expected size (number of pages)	200

Figure A.2. Copyright license of [13]



Copyright Clearance Center RightsLink®

Home Account Info Help

ACS Publications **Title:** Impact of Nanotechnology on Drug Delivery  
**Author:** Omid C. Farokhzad, Robert Langer  
**Publication:** ACS Nano  
**Publisher:** American Chemical Society  
**Date:** Jan 1, 2009  
 Copyright © 2009, American Chemical Society

Logged in as:  
 LAURA CHAMBRE  
 Account #:  
 3001287341  
 LOGOUT

**PERMISSION/LICENSE IS GRANTED FOR YOUR ORDER AT NO CHARGE**

This type of permission/license, instead of the standard Terms & Conditions, is sent to you because no fee is being charged for your order. Please note the following:

- Permission is granted for your request in both print and electronic formats, and translations.
- If figures and/or tables were requested, they may be adapted or used in part.
- Please print this page for your records and send a copy of it to your publisher/graduate school.
- Appropriate credit for the requested material should be given as follows: "Reprinted (adapted) with permission from (COMPLETE REFERENCE CITATION). Copyright (YEAR) American Chemical Society." Insert appropriate information in place of the capitalized words.
- One-time permission is granted only for the use specified in your request. No additional uses are granted (such as derivative works or other editions). For any other uses, please submit a new request.

If credit is given to another source for the material you requested, permission must be obtained from that source.

BACK

CLOSE WINDOW

Copyright © 2018 Copyright Clearance Center, Inc. All Rights Reserved. [Privacy statement](#). [Terms and Conditions](#).  
 Comments? We would like to hear from you. E-mail us at [customer-care@copyright.com](mailto:customer-care@copyright.com)

Figure A.3. Copyright License of [15].

## Drugs and Polymers for Delivery Systems in OA Joints: Clinical Needs and Opportunities

Maarten Janssen <sup>1</sup> ✉, George Mihov <sup>2</sup> ✉, Tim Welting <sup>1</sup> ✉, Jens Thies <sup>2</sup> ✉ and Pieter Emans <sup>1,\*</sup> ✉

<sup>1</sup> Department of Orthopaedic Surgery, Maastricht University Medical Center, P. Debyelaan 25, 6229 HX Maastricht, the Netherlands

<sup>2</sup> DSM Biomedical, Koestraat 1, 6167 RA Geleen, the Netherlands

\* Author to whom correspondence should be addressed.

Received: 31 January 2014 / Revised: 2 March 2014 / Accepted: 3 March 2014 / Published: 13 March 2014

(This article belongs to the Special Issue Polymers for Drug Delivery)

[View Full-Text](#) | [Download PDF](#) (454 KB, uploaded 13 March 2014) | [Browse Figures](#)

### Abstract

Osteoarthritis (OA) is a big burden of disease worldwide and one of the most common causes of disability in the adult population. Currently applied therapies consist of physical therapy, oral medication, intra-articular injections, and surgical interventions, with the main goal being to reduce pain and improve function and quality of life. Intra-articular (IA) administration of drugs has potential benefits in OA treatment because it minimizes systemic bioavailability and side effects associated with oral administration of drugs without compromising the therapeutic effect in the joint. However, IA drug residence time is short and there is a clinical need for a vehicle that is able to provide a sustained release long enough for IA therapy to fulfill its promise. This review summarizes the use of different polymeric systems and the incorporated drugs for IA drug delivery in the osteoarthritic joint with a primary focus on clinical needs and opportunities. [View Full-Text](#)

**Keywords:** osteoarthritis; drug delivery systems; DMOAD

### ▼ Figures

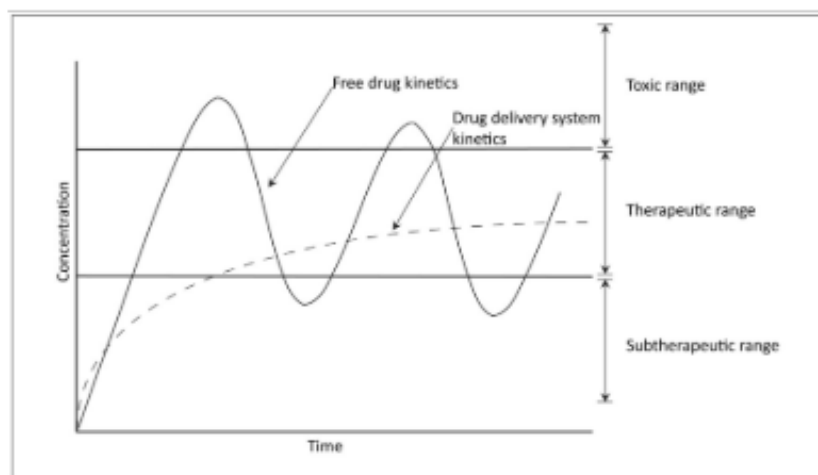


Figure 1

This is an open access article distributed under the Creative Commons Attribution License (CC BY 3.0).

Figure A.4. Copyright License of [17].



RightsLink®

Home

Account  
Info

Help



**Title:** Delivery of antibiotics with polymeric particles  
**Author:** Meng-Hua Xiong, Yan Bao, Xian-Zhu Yang, Yan-Hua Zhu, Jun Wang  
**Publication:** Advanced Drug Delivery Reviews  
**Publisher:** Elsevier  
**Date:** 30 November 2014  
 Copyright © 2014 Elsevier B.V. All rights reserved.

Logged in as:  
 LAURA CHAMBRE  
 Account #:  
 3001287341

LOGOUT

### Review Order

Please review the order details and the associated [terms and conditions](#).

No royalties will be charged for this reuse request although you are required to obtain a license and comply with the license terms and conditions. To obtain the license, click the Accept button below.

Licensed Content Publisher	Elsevier
Licensed Content Publication	Advanced Drug Delivery Reviews
Licensed Content Title	Delivery of antibiotics with polymeric particles
Licensed Content Author	Meng-Hua Xiong, Yan Bao, Xian-Zhu Yang, Yan-Hua Zhu, Jun Wang
Licensed Content Date	30 November 2014
Licensed Content Volume	78
Licensed Content Issue	n/a
Licensed Content Pages	14
Type of Use	reuse in a thesis/dissertation
Portion	figures/tables/illustrations
Number of figures/tables/illustrations	1
Format	both print and electronic
Are you the author of this Elsevier article?	No
Will you be translating?	No
Original figure numbers	1
Title of your thesis/dissertation	Polymeric Materials for Delivery of Chemotherapeutic and Antibacterial Agents"
Expected completion date	Aug 2018
Estimated size (number of pages)	200

Figure A.5. Copyright license of [26].



**Copyright Clearance Center**

# RightsLink®

[Home](#)
[Create Account](#)
[Help](#)




**ACS Publications**  
Most Trusted. Most Cited. Most Read.

**Title:** Dual Function Injectable Hydrogel for Controlled Release of Antibiotic and Local Antibacterial Therapy

**Author:** Jiaul Hoque, Brinta Bhattacharjee, Relekar G. Prakash, et al

**Publication:** Biomacromolecules

**Publisher:** American Chemical Society

**Date:** Feb 1, 2018

Copyright © 2018, American Chemical Society

**LOGIN**

If you're a [copyright.com](#) user, you can login to RightsLink using your [copyright.com](#) credentials. Already a [RightsLink](#) user or want to [learn more?](#)

**PERMISSION/LICENSE IS GRANTED FOR YOUR ORDER AT NO CHARGE**

This type of permission/license, instead of the standard Terms & Conditions, is sent to you because no fee is being charged for your order. Please note the following:

- Permission is granted for your request in both print and electronic formats, and translations.
- If figures and/or tables were requested, they may be adapted or used in part.
- Please print this page for your records and send a copy of it to your publisher/graduate school.
- Appropriate credit for the requested material should be given as follows: "Reprinted (adapted) with permission from (COMPLETE REFERENCE CITATION). Copyright (YEAR) American Chemical Society." Insert appropriate information in place of the capitalized words.
- One-time permission is granted only for the use specified in your request. No additional uses are granted (such as derivative works or other editions). For any other uses, please submit a new request.

If credit is given to another source for the material you requested, permission must be obtained from that source.

BACK

CLOSE WINDOW

Copyright © 2018 [Copyright Clearance Center, Inc.](#) All Rights Reserved. [Privacy statement](#). [Terms and Conditions](#). Comments? We would like to hear from you. E-mail us at [customer-care@copyright.com](mailto:customer-care@copyright.com)

Figure A.6. Copyright license of [29].

Journal  
**Drug Delivery** >  
Volume 24, 2017 - Issue 1

Enter keywords, authors, DOI etc.

4244  
Views  
22  
CrossRef citations  
0  
Altmetric

Review

## Basic concepts and recent advances in nanogels as carriers for medical applications

Iordana Neamtu, Alina Gabriela Rusu, Alina Diaconu, Loredana Elena Nita & Aurica P. Chiriac ✉  
Pages 539-557 | Received 07 Nov 2016, Accepted 20 Dec 2016, Published online: 09 Feb 2017

Download citation <https://doi.org/10.1080/10717544.2016.1276232> [Check for updates](#)

[Full Article](#) [Figures & data](#) [References](#) [Citations](#) [Metrics](#) [Licensing](#) [PDF](#)

© 2017 The Author(s). Published by Informa UK Limited, trading as Taylor & Francis Group.

This is an Open Access article distributed under the terms of the Creative Commons Attribution License (<http://creativecommons.org/licenses/by/4.0/>), which permits unrestricted use, distribution, and reproduction in any medium, provided the original work is properly cited.

People also

Review  
A novel str  
achieve eff  
drug deliv  
cells as car

Figure A.7. Copyright license of [36].



Copyright Clearance Center RightsLink®

Home Account Info Help

ACS Publications **Title:** "Clickable" Nanogels via Thermally Driven Self-Assembly of Polymers: Facile Access to Targeted Imaging Platforms using Thiol-Maleimide Conjugation

**Author:** Bugra Aktan, Laura Chambre, Rana Sanyal, et al

**Publication:** Biomacromolecules

**Publisher:** American Chemical Society

**Date:** Feb 1, 2017

Copyright © 2017, American Chemical Society

Logged in as:  
LAURA CHAMBRE  
Account #:  
3001287341  
LOGOUT

**PERMISSION/LICENSE IS GRANTED FOR YOUR ORDER AT NO CHARGE**

This type of permission/license, instead of the standard Terms & Conditions, is sent to you because no fee is being charged for your order. Please note the following:

- Permission is granted for your request in both print and electronic formats, and translations.
- If figures and/or tables were requested, they may be adapted or used in part.
- Please print this page for your records and send a copy of it to your publisher/graduate school.
- Appropriate credit for the requested material should be given as follows: "Reprinted (adapted) with permission from (COMPLETE REFERENCE CITATION). Copyright (YEAR) American Chemical Society." Insert appropriate information in place of the capitalized words.
- One-time permission is granted only for the use specified in your request. No additional uses are granted (such as derivative works or other editions). For any other uses, please submit a new request.

If credit is given to another source for the material you requested, permission must be obtained from that source.

Figure A.8. Copyright license of [37].



RightsLink®

Home

Account Info

Help



ACS Publications  
Most Trusted. Most Cited. Most Read.

**Title:** Shell Click-Crosslinked (SCC) Nanoparticles: A New Methodology for Synthesis and Orthogonal Functionalization  
**Author:** Maisie J. Joralemon, Rachel K. O'Reilly, Craig J. Hawker, et al  
**Publication:** Journal of the American Chemical Society  
**Publisher:** American Chemical Society  
**Date:** Dec 1, 2005  
Copyright © 2005, American Chemical Society

Logged in as:  
LAURA CHAMBRE  
Account #:  
3001287341

LOGOUT

**PERMISSION/LICENSE IS GRANTED FOR YOUR ORDER AT NO CHARGE**

This type of permission/license, instead of the standard Terms & Conditions, is sent to you because no fee is being charged for your order. Please note the following:

- Permission is granted for your request in both print and electronic formats, and translations.
- If figures and/or tables were requested, they may be adapted or used in part.
- Please print this page for your records and send a copy of it to your publisher/graduate school.
- Appropriate credit for the requested material should be given as follows: "Reprinted (adapted) with permission from (COMPLETE REFERENCE CITATION). Copyright (YEAR) American Chemical Society." Insert appropriate information in place of the capitalized words.
- One-time permission is granted only for the use specified in your request. No additional uses are granted (such as derivative works or other editions). For any other uses, please submit a new request.

If credit is given to another source for the material you requested, permission must be obtained from that source.

Figure A.9. Copyright license of [38].



RightsLink®

Home

Account  
Info

Help

ACS Publications  
Most Trusted. Most Cited. Most Read.

**Title:** Synergistic Cisplatin/Doxorubicin Combination Chemotherapy for Multidrug-Resistant Cancer via Polymeric Nanogels Targeting Delivery

**Author:** Haiqiu Wu, Haojie Jin, Cun Wang, et al

**Publication:** Applied Materials

**Publisher:** American Chemical Society

**Date:** Mar 1, 2017

Copyright © 2017, American Chemical Society

Logged in as:

LAURA CHAMBRE

Account #:

3001287341

#### PERMISSION/LICENSE IS GRANTED FOR YOUR ORDER AT NO CHARGE

This type of permission/license, instead of the standard Terms & Conditions, is sent to you because no fee is being charged for your order. Please note the following:

- Permission is granted for your request in both print and electronic formats, and translations.
- If figures and/or tables were requested, they may be adapted or used in part.
- Please print this page for your records and send a copy of it to your publisher/graduate school.
- Appropriate credit for the requested material should be given as follows: "Reprinted (adapted) with permission from (COMPLETE REFERENCE CITATION). Copyright (YEAR) American Chemical Society." Insert appropriate information in place of the capitalized words.
- One-time permission is granted only for the use specified in your request. No additional uses are granted (such as derivative works or other editions). For any other uses, please submit a new request.

If credit is given to another source for the material you requested, permission must be obtained from that source.

Figure A.10. Copyright license of [39].



RightsLink®

Home

Account  
Info

Help



**Title:** Photothermally triggered on-demand insulin release from reduced graphene oxide modified hydrogels

**Author:** Florina Teodorescu, Yavuz Oz, Gurvan Quéniat, Amar Abderrahmani, Catherine Foulon, Marie Lecoeur, Rana Sanyal, Amitav Sanyal, Rabah Boukherroub, Sabine Szunerits

**Publication:** Journal of Controlled Release

**Publisher:** Elsevier

**Date:** 28 January 2017

© 2016 Elsevier B.V. All rights reserved.

Logged in as:  
LAURA CHAMBRE  
Account #:  
3001287341

LOGOUT

### Review Order

Please review the order details and the associated [terms and conditions](#).

No royalties will be charged for this reuse request although you are required to obtain a license and comply with the license terms and conditions. To obtain the license, click the Accept button below.

Licensed Content Publisher	Elsevier
Licensed Content Publication	Journal of Controlled Release
Licensed Content Title	Photothermally triggered on-demand insulin release from reduced graphene oxide modified hydrogels
Licensed Content Author	Florina Teodorescu, Yavuz Oz, Gurvan Quéniat, Amar Abderrahmani, Catherine Foulon, Marie Lecoeur, Rana Sanyal, Amitav Sanyal, Rabah Boukherroub, Sabine Szunerits
Licensed Content Date	28 January 2017
Licensed Content Volume	246
Licensed Content Issue	n/a
Licensed Content Pages	10
Type of Use	reuse in a thesis/dissertation
Portion	figures/tables/illustrations
Number of figures/tables/illustrations	1
Format	both print and electronic
Are you the author of this Elsevier article?	No
Will you be translating?	No
Original figure numbers	1
Title of your thesis/dissertation	Polymeric Materials for Delivery of Chemotherapeutic and Antibacterial Agents"
Expected completion date	Aug 2018
Estimated size (number of pages)	200

Figure A.11. Copyright license of [59].

*J Periodontal Implant Sci.* 2013 Dec; 43(6): 251–261.  
Published online 2013 Dec 31. doi: [10.5051/jpis.2013.43.6.251](https://doi.org/10.5051/jpis.2013.43.6.251)

PMCID: PMC3891856  
PMID: [24455437](https://pubmed.ncbi.nlm.nih.gov/24455437/)

## Advances in the design of macroporous polymer scaffolds for potential applications in dentistry

[Sidi A. Bencherif](#)<sup>1,2</sup> [Thomas M. Braschler](#)<sup>1,3</sup> [Philippe Renaud](#)<sup>3</sup>

[Author information](#) ▶ [Article notes](#) ▶ [Copyright and License information](#) ▼; [Disclaimer](#)

Copyright © 2013 Korean Academy of Periodontology

This is an Open Access article distributed under the terms of the Creative Commons Attribution Non-Commercial License (<http://creativecommons.org/licenses/by-nc/3.0/>).

Figure A.12. Copyright license of [80].



The screenshot displays the RightsLink interface. At the top left is the Copyright Clearance Center logo. The main header features the RightsLink logo and navigation buttons for Home, Account Info, and Help. Below the header, the ACS Publications logo is visible with the tagline "Most Trusted. Most Cited. Most Read." The central area lists publication details: Title: Hooked on Cryogels: A Carbamate Linker Based Depot for Slow Drug Release; Author: Duygu Aydin, Mehmet Arslan, Amitav Sanyal, et al; Publication: Bioconjugate Chemistry; Publisher: American Chemical Society; Date: May 1, 2017. A copyright notice for 2017 American Chemical Society is at the bottom. On the right, a user is logged in as LAURA CHAMBRE with account number 3001287341, and a LOGOUT button is present.

**Copyright Clearance Center** RightsLink®

Home Account Info Help

**ACS Publications** Most Trusted. Most Cited. Most Read.

**Title:** Hooked on Cryogels: A Carbamate Linker Based Depot for Slow Drug Release

**Author:** Duygu Aydin, Mehmet Arslan, Amitav Sanyal, et al

**Publication:** Bioconjugate Chemistry

**Publisher:** American Chemical Society

**Date:** May 1, 2017

Copyright © 2017, American Chemical Society

Logged in as:  
LAURA CHAMBRE  
Account #:  
3001287341  
LOGOUT

#### PERMISSION/LICENSE IS GRANTED FOR YOUR ORDER AT NO CHARGE

This type of permission/license, instead of the standard Terms & Conditions, is sent to you because no fee is being charged for your order. Please note the following:

- Permission is granted for your request in both print and electronic formats, and translations.
- If figures and/or tables were requested, they may be adapted or used in part.
- Please print this page for your records and send a copy of it to your publisher/graduate school.
- Appropriate credit for the requested material should be given as follows: "Reprinted (adapted) with permission from (COMPLETE REFERENCE CITATION). Copyright (YEAR) American Chemical Society." Insert appropriate information in place of the capitalized words.
- One-time permission is granted only for the use specified in your request. No additional uses are granted (such as derivative works or other editions). For any other uses, please submit a new request.

Figure A.13. Copyright license of [84].



RightsLink®

Home

Account  
Info

Help



ACS Publications  
Most Trusted. Most Cited. Most Read.

**Title:** Multi-Functional Nanogels as  
Theranostic Platforms:  
Exploiting Reversible and  
Nonreversible Linkages for  
Targeting, Imaging, and Drug  
Delivery

**Author:** Laura Chambre, Aysun  
Degirmenci, Rana Sanyal, et al

**Publication:** Bioconjugate Chemistry

**Publisher:** American Chemical Society

**Date:** May 1, 2018

Copyright © 2018, American Chemical Society

Logged in as:  
LAURA CHAMBRE  
Account #:  
3001287341

LOGOUT

#### PERMISSION/LICENSE IS GRANTED FOR YOUR ORDER AT NO CHARGE

This type of permission/license, instead of the standard Terms & Conditions, is sent to you because no fee is being charged for your order. Please note the following:

- Permission is granted for your request in both print and electronic formats, and translations.
- If figures and/or tables were requested, they may be adapted or used in part.
- Please print this page for your records and send a copy of it to your publisher/graduate school.
- Appropriate credit for the requested material should be given as follows: "Reprinted (adapted) with permission from (COMPLETE REFERENCE CITATION). Copyright (YEAR) American Chemical Society." Insert appropriate information in place of the capitalized words.
- One-time permission is granted only for the use specified in your request. No additional uses are granted (such as derivative works or other editions). For any other uses, please submit a new request.

Figure A.14. Copyright license of [192].